UNIVERSITÀ DEGLI STUDI DI PADOVA

Dipartimento di Fisica e Astronomia "Galileo Galilei"

Master Degree in Astrophysics and Cosmology

Final Dissertation

Gravitational Relaxation and Kinetic Theory in Fuzzy Dark Matter

Thesis supervisor
Prof. Sabino Matarrese

Candidate
Rojin Bayati

Thesis co-supervisor
Prof. Matteo Viel

Academic Year 2024/25

Acknowledgments

I would like to express my deepest gratitude to my supervisors, Prof. Sabino Matarrese and Prof. Matteo Viel, for their invaluable guidance, insightful advice, and support throughout this research. Their expertise and encouragement have been instrumental in shaping this work.

A special thanks to Luca Teodori, whose patience, generosity, and insightful discussions have been a great source of support throughout this thesis. His help has been truly essential in my challenges along the way.

Finally, I extend my appreciation to all those who have contributed to this journey, directly or indirectly, through their encouragement and inspiration.

Abstract

Fuzzy Dark Matter (FDM), composed of ultra-light bosons with a de Broglie wavelength on galactic scales, presents an intriguing alternative to traditional Cold Dark Matter (CDM) models. On large scales, FDM behaves similarly to CDM, reproducing the observed large-scale structure of the universe. However, on scales comparable to its de Broglie wavelength, FDM exhibits wave-like density fluctuations that influence gravitational dynamics in ways that CDM does not.

Unlike CDM, which is modeled as a collection of collisionless, point-like particles, FDM wave-like nature leads to distinctive dynamical behaviors that could potentially resolve several outstanding challenges in cosmology and astrophysics. These include the nature of dark matter on galactic scales, the formation and suppression of small-scale structures, and the evolution of cosmic systems. Its predictions can be directly tested with observations in various astrophysical contexts, making FDM a compelling alternative to conventional dark matter models.

FDM wave-like nature introduces a unique relaxation process that influences the evolution of galaxies, stellar clusters, and other cosmic structures. In particular, FDM exhibits stochastic density fluctuations on the scale of the de Broglie wavelength that never damp. The gravitational field from these fluctuations diffuses stars and black holes from their orbits through phase space. We show that this relaxation process can be analyzed quantitatively with the same tools used to analyze classical two-body relaxation in an N-body system, and can be described by treating the FDM fluctuations as quasiparticles. Particularly, we study the dynamics of FDM halos using the Fokker-Planck equation to describe the statistical evolution of test particles in the fluctuating potential of a FDM halo. We derive the kinetic equations for FDM and solve them to analyze the evolution of velocity distributions.

One key consequence of FDM dynamics is the reduction of dynamical friction, which affects the motion of supermassive black holes and globular clusters. Unlike in CDM, where dynamical friction leads to the inward migration of these objects, FDM suppresses this effect, preventing their inspiral at smaller radii. This has significant implications for black hole mergers and the long-term evolution of dense stellar systems. Additionally, FDM fluctuations could cause heating and expansion in a stellar population. The fluctuations within FDM inject energy into galactic centers, which contrasts with the core-collapse behavior expected in collisionless dark matter models. On larger scales, FDM suppresses small-scale structures, which affects galaxy formation and halo evolution, potentially leading to different density profiles within dark matter halos.

A central aspect of this work is the kinetic modeling of FDM, incorporating the Schrödinger-Poisson and the Boltzmann–Nordheim–Uehling–Uhlenbeck (BNUU) formalisms. We examine how quantum fluctuations influence halo evolution and explore the implications of the Balescu-Lenard equation for long-term structure formation.

By investigating these astrophysical consequences of FDM, this thesis aims to improve our understanding of how fuzzy dark matter shapes the structure and evolution of the universe.

Contents

1 Introduction

Dark matter is one of the most profound mysteries in modern astrophysics and cosmology. Observational evidence, ranging from the rotation curves of galaxies (Rubin and Ford, 1970; Rubin et al., 1980) to the gravitational lensing of light (Zwicky, 1937; Clowe et al., 2004), and the anisotropies in the cosmic microwave background (Spergel et al., 2003), strongly suggests the existence of an unseen form of matter that interacts gravitationally but remains elusive to direct detection. This component, constituting approximately 27% of the universe's energy density, plays a pivotal role in shaping the large-scale structure of the cosmos (Peebles, 1982) and driving the evolution of galaxies and clusters. Despite its ubiquity, the exact nature of dark matter remains unknown, leading to the development of various theoretical models that attempt to explain its fundamental nature. While the standard paradigm assumes that dark matter is collisionless and cold, alternative candidates have been proposed, spanning a wide range of masses and interaction properties. The proposed mass range for dark matter candidates spans an enormous range, from ultra-light bosons with masses around $\sim 10^{-22}$ eV (Hu et al., 2000) to primordial black holes with masses up to $\sim 10 M_\odot$ (Bird et al., 2016; Garcia-Bellido and Morales, 2017; Sasaki et al., 2018; Jedamzik, 2020).

One of the most well-known candidates is the Weakly Interacting Massive Particle (WIMP), predicted by extensions of the Standard Model such as supersymmetry (G. Jungman and Griest, 1996; G. Bertone and Silk, 2005). WIMPs are relatively heavy, with masses ranging from about 10 GeV to a few TeV, and interact only through gravity and the weak nuclear force. Their expected relic abundance through thermal freeze-out naturally aligns with the observed dark matter density. Despite extensive searches no confirmed signals have been observed.

Another possible candidate is the axion, originally proposed to solve the strong CP problem in quantum chromodynamics (Peccei and Quinn, 1977; Weinberg, 1978). Axions are extremely light particles, with masses between 10^{-6} eV and 10^{-3} eV, and interact very weakly with normal matter. Experimental searches aim to detect axions through photon conversion in strong magnetic fields (Aja et al., 2022; Pandey et al., 2024).

Sterile neutrinos are another hypothesis, representing a type of neutrino that does not interact via the weak nuclear force, unlike ordinary neutrinos. If they exist, they could have masses in the keV range and contribute to dark matter in the form of warm dark matter, which exhibits intermediate behavior between cold dark matter and hot neutrino-like dark matter (Abazajian et al., 2001).

Another alternative to particle-based dark matter candidates is primordial black holes (PBHs), which are hypothetical black holes that may have formed in the early universe due to high-density fluctuations (Carr and Hawking, 1974). Although observational data from microlensing surveys (Alcock et al., 2000; Niikura et al., 2019; Griest et al., 2014; Tisserand et al., 2007) and CMB measurements (Carr et al., 2010) place constraints on the abundance of lower-mass PBHs, they still allow a small fraction of dark matter to consist of low-mass PBHs, particularly in the mass range between $10^{-16}\,M_\odot$ and $10^{-6}\,M_\odot$ (Katz et al., 2018; Ballesteros et al., 2020; Escrivà et al., 2024) without violating observational limits.

Moreover, there exists a type of dark matter models known as wave dark matter, which consists of extremely light bosonic particles, so light that they behave more like waves than individual particles on galactic scales (Hu et al., 2000; Schive et al., 2014a). With masses around 10^{-22} eV or lower, these particles create wave-like effects that can influence the structure of galaxies, forming solitonic cores in halos (Schive et al., 2014a) and suppressing small-scale structure formation compared to cold dark matter (Hui et al., 2017). Unlike collisionless cold dark matter, which behaves like a collection of tiny, fast-moving particles, wave dark matter is better described as a wave with astrophysical scale wavelength and can form interference patterns in its density distribution.

Each of these dark matter candidates leads to different predictions from imprints on large scale structure formation to other astrophysical observables. Researchers are actively working to detect or rule out these possibilities using a combination of experiments, astrophysical observations, and computer simulations.

1.1 Light Dark Matter

Light dark matter consists of particles with very light masses. This feature brings the potential to explain several unresolved issues in cosmology and astrophysics such as the formation of structures, and the evolution of cosmic systems.

1.1.1 Wave-like Behavior of Light Dark Matter

When dark matter particles are extremely light, their wave-like nature becomes significant on astrophysical scales. This wave-particle duality is quantified by the de Broglie wavelength, which is inversely proportional to a particle's momentum. Mathematically, the de Broglie wavelength is given by

$$\lambda_{\mathrm{dB}} = \frac{h}{mv}, \tag{1.1}$$

where m and v are the particle's mass and the velocity dispersion of the galactic halo respectively. As the above equation suggests, this wavelength becomes particularly significant for particles with extremely small masses. In a system with number density n, if the de Broglie wavelength exceeds the typical inter-particle separation $d = \left(\frac{1}{n}\right)^{1/3}$, the system behaves as a wave-like medium rather than a collection of individual particles

$$\lambda_{\mathrm{dB}} > \left(\frac{1}{n}\right)^{1/3}. \tag{1.2}$$

Rearranging this condition, we obtain,

$$n > \left(\frac{1}{\lambda_{\mathrm{dB}}}\right)^{3}, \tag{1.3}$$

or equivalently, expressing the de Broglie wavelength in terms of mass and velocity,

$$n > \left(\frac{mv}{h}\right)^{3}. \tag{1.4}$$

This implies that wave-like behavior emerges when the number density is sufficiently high or the particle mass is sufficiently low. Specifically, it can be shown that this criterion is satisfied when $m \lesssim 30$ eV. In a galaxy like the Milky Way, the average number of particles occupying a volume of λ_{dB}^3 is

$$N_{\mathrm{dB}} \sim \left(\frac{34\,\mathrm{eV}}{m}\right)^{4} \left(\frac{250\ \mathrm{km/h}}{v}\right)^{3}. \tag{1.5}$$

Then for $m \ll 30$ eV, N_{dB} is so large that the set of particles is best described by classical waves. Here, we emphasize classical, since large occupancy implies negligible quantum fluctuations (Hui, 2021).

1.1.2 Mass Range and Theoretical Motivation

As noted by Hui (2021) the possible mass range for light dark matter particles is quite broad, with experimental efforts primarily focusing on the quantum chromodynamics (QCD) axion, with a mass of approximately 10^{-6} eV or lower (Graham et al., 2015; Marsh, 2016; Sikivie, 2020), as a well-motivated candidate.

String theory predicts a large number of axion-like particles (ALPs) spanning a broad mass spectrum (Svrcek and Witten, 2006; Arvanitaki et al., 2010; Halverson et al., 2017; Bachlechner et al., 2019), some of which could be considered as dark matter candidates (Svrcek and Witten, 2006; Arvanitaki et al., 2010; Halverson et al., 2017; Bachlechner et al., 2019). At the extreme low-mass of the spectrum lies the possibility of an ALP with mass around

$$10^{-22}\ \text{eV} \lesssim m \lesssim 10^{-20}\ \text{eV}, \tag{1.6}$$

with a relic abundance that naturally aligns the observed dark matter density. This mass range is particularly interesting because it is constrained by astrophysical observations and cosmological considerations. Particles lighter than 10^{-22} eV have de Broglie wavelengths comparable to or larger than the sizes of galaxies, leading to excessive suppression of small-scale structure formation, which is inconsistent with observations of Lyman-α forests and dwarf galaxies (Marsh, 2016; Hui et al., 2017).

For masses above 10^{-20} eV, the wave-like effects no longer significantly impact structure formation (Hui et al., 2017). In particular, Lyman-α constraints suggest that ultra-light dark matter with $m \gtrsim 10^{-20}$ eV would be indistinguishable from cold dark matter (CDM), thus losing its advantage in addressing small-scale structure problems (Nori et al., 2021).

More generally, ultra-light dark matter in this mass range is often referred to as fuzzy dark matter (FDM) which is going to be the main focus in this thesis. Originally proposed by Hu et al. (2000) to address small-scale structure issues in CDM cosmology (Spergel and Steinhardt, 2000), FDM features a large de Broglie wavelength that modifies structure formation and yields distinct astrophysical signatures.

1.1.3 Distinction Between FDM and Other Light Dark Matter Candidates

Various light dark matter candidates exhibit wave-like properties, but their astrophysical implications are mass-dependent. For FDM with a mass of $m \sim 10^{-22}$ eV, the large de Broglie wavelength induces quantum pressure effects, resulting in cored density profiles instead of the cuspy ones predicted by CDM (Hu et al., 2000; Sikivie, 2009).

In contrast, heavier ALPs with masses in the range 10^{-5} eV $\lesssim m \lesssim 10^{-3}$ eV have shorter wavelengths, making them relevant for laboratory axion searches (Raffelt, 1996). The QCD axion, with a mass around 10^{-6} eV, is motivated by the strong CP problem in QCD, with ongoing direct detection efforts. Interestingly, despite these differences even at these smaller scales, such masses can produce significant astrophysical consequences, such as the formation of solitons or effects near black holes. Despite their differences, the fundamental wave dynamics remains consistent across this mass spectrum (Schive et al., 2014a; Cardoso et al., 2016).

1.1.4 Observational Motivation

Now let us delve into the properties of FDM in more detail. As mentioned earlier, FDM is composed of bosons with extremely small masses, typically $m_{\mathrm{b}} \sim 10^{21} - 10^{22}$ eV (e.g., Hu et al. (2000); Hui et al. (2017)). In particular, the corresponding de Broglie wavelength at velocity v is

$$\lambda_{\mathrm{dB}} = \frac{h}{mv} \simeq 1.2\,\mathrm{kpc}\left(\frac{10^{-22}\,\mathrm{eV}}{m_{\mathrm{b}}}\right)\left(\frac{100\,\mathrm{km\ s^{-1}}}{v}\right). \tag{1.7}$$

This wavelength is comparable to galaxy scales at a typical galaxy velocity v (Hu et al., 2000; Marsh, 2016; Hui et al., 2017).

The wave-like behavior of FDM is evident in interference patterns that give rise to stochastic density fluctuations on the scale of the de Broglie wavelength. These fluctuations are a direct consequence of the superposition of the wave functions of the FDM particles. Notably, these density fluctuations are persistent and never damp, distinguishing FDM from traditional CDM models whose small-scale density fluctuations gradually damp through phase mixing (Bar-Or et al., 2021).

The gravitational field generated by FDM fluctuations has significant dynamical implications, as it interacts with both baryonic structures such as stars, globular clusters, and black holes-and the FDM waves themselves. These interactions lead to scattering processes that further shape the evolution of the system on both small and large scales.

Cosmological models based on CDM have successfully explained many key features of the universe, including the cosmic microwave background (Planck Collaboration et al., 2020), the large-scale structures (Eisenstein et al., 2005; Alam and others , eBOSS Collaboration), galaxy clustering (Peebles, 1980), the Lyman-α forest (Viel et al., 2013), and the matter power spectrum (Tegmark and others , SDSS Collaboration).

Despite these successes, CDM struggles to accurately predict the properties of small-scale structures, such as the number of observed dwarf galaxies and the steepness of dark matter density profiles in the central regions of galaxies (e.g., Weinberg et al. (2015); Bullock and Boylan-Kolchin (2017)). Particularly, the *core-cusp* problem is a significant issue in CDM models. CDM simulations predict a steep central density profile, known as the cusp, where the density increases dramatically toward the center of dark matter halos. This is at odds with observational data, which suggests that many low-mass galaxies have relatively flat or core-like profiles in their dark matter distribution (Famaey and McGaugh, 2012) The FDM, because of its quantum pressure, softens the central density of halos, leading to the formation of a core instead of a cusp. This quantum pressure counteracts gravitational collapse in the center, resulting in a more diffuse density distribution that matches observations of low-mass galaxies more closely (Hu et al., 2000; Hui et al., 2017). To elaborate more, CDM's overconcentration problem predicts that small galaxies, such as dwarf galaxies, should have highly concentrated dark matter halos, with very high dark matter densities (Navarro et al., 1997b). However, many dwarf galaxies are observed to have lower central densities than predicted by CDM models. FDM addresses this by leading to less concentrated and more diffuse halos for low-mass galaxies, which results in a better agreement with the observed central densities of these galaxies (Schive et al., 2014b).

Another one of the challenges that CDM faces is the *missing satellite problem*. High-resolution simulations predict a large number of small dark matter subhalos around the Milky Way (Klypin et al., 1999) and other large galaxies. These subhalos should host dwarf galaxies, leading to a higher number of observed satellites. The actual number of observed dwarf satellite galaxies around the Milky Way and Andromeda is much lower than expected (Bullock and Boylan-Kolchin, 2017). On the other hand, FDM's smooth, wave-like nature suppresses the formation of small-scale structures in the early universe, which results in fewer small satellites around larger galaxies, providing a better match to observed satellite galaxy counts (Hui et al., 2017).

Overall, the formation and evolution of small-scale structures provide a key distinction between CDM and FDM. In CDM, dark matter halos undergo frequent mergers, leading to the formation of subhalos, small dark matter clumps that contribute to galaxy halo substructure (Springel et al., 2001). While this hierarchical structure formation is broadly consistent with observations, it presents some tensions, such as the overabundance of predicted dwarf-sized halos compared to observed galaxies. Additionally, CDM predicts that small-scale fluctuations collapse at very high redshifts (e.g., $z \gtrsim 10$), leading to the early formation of galaxies and dark matter halos (Peebles, 1982).

In contrast, the wave-like nature of FDM suppresses small-scale fluctuations, preventing the formation of subhalos below a characteristic scale and leading to smoother, more uniform halos (Schive et al., 2014a). This suppression delays the formation of low-mass halos and results in a smoother evolution of large-scale structure (Hui et al., 2017). Such effects could help resolve discrepancies in the abundance and distribution of small galaxies while providing a more stable framework for cosmic structure formation (Seife et al., 2020). Additionally, FDM's suppression of early small-scale structures may offer a better match to high-redshift observations, potentially addressing tensions in early cosmic structure formation.

These discrepancies could either stem from our incomplete understanding of baryonic physics on small scales or from deviations in the nature of dark matter from the assumptions underlying CDM. FDM offers an intriguing alternative that reconciles many of these issues. On scales much larger than the de Broglie wavelength, FDM behaves similarly to CDM, thereby retaining its ability to explain large-scale structure and the cosmic microwave background. However, on smaller scales, FDM exhibits markedly different behavior.

1.1.5 Constraints on FDM Mass

Several studies have placed constraints on the mass dark matter particles, The Lyman-α forest power spectrum requires masses $m_\mathrm{b} \lesssim$ a few $\times 10^{-21}$ eV to be excluded (Kobayashi et al., 2017; Nori et al., 2019) to avoid excessive suppression of small-scale structures (Viel et al., 2013; Armengaud et al., 2017; Irsìc et al., 2017). In particular, the Lyman-α forest, which probes the matter distribution through absorption features in quasar spectra, places these tight limits on the mass of dark matter particles. If dark matter were too light, it would smooth out the power spectrum, inconsistent with the observed small-scale features (Viel et al., 2013; Nori et al., 2021). This would imply that FDM behaves similarly to CDM on small scales.

However, these constraints have limitations: They often rely on assumptions, such as a uniform ionizing background, which may oversimplify the conditions in the universe; alternative FDM models, such as those discussed by Leong et al. (2018), can have weaker mass constraints; and the dynamical processes associated with FDM remain relevant even if the particle mass does not significantly influence small-scale structure (Bar-Or et al., 2019).

One might wonder if the mass of dark matter particles could be even smaller than 10^{-23} eV. In principle, it is possible, but only if the particle constitutes a small fraction of dark matter. As the mass of dark matter particles decreases, their de Broglie wavelength increases, leading to significant quantum pressure that prevents the collapse of dark matter into dense structures, such as dwarf galaxies. This issue arises because quantum pressure opposes gravitational clumping, which is necessary for the formation of these galaxies (Hu et al., 2000).

Moreover, the behavior of dark matter on large scales, as observed in the CMB and large-scale structure surveys, imposes $m_{\rm b} \gtrsim 10^{-22}$s. Light dark matter would fail to reproduce the observed galaxy clustering (Hlozek et al., 2015).

As the mass approaches the present-day Hubble constant ($m \sim 10^{-33}$ eV), the field evolves so slowly that it behaves as dark energy rather than dark matter (Hlozek et al., 2015). Thus, the transition from dark matter to dark energy appears continuous with decreasing mass.

1.1.6 The Bosonic Nature of FDM

A fundamental assumption of FDM and ultralight dark matter models is their bosonic nature, which carries significant implications. First, Bose-Einstein statistics permits large numbers of bosons to occupy the same quantum state, resulting in collective wave behavior.

Second, the Pauli exclusion principle, which applies to fermions, prevents fermionic dark matter from forming extended wave-like structures (Tremaine and Gunn, 1979). Specifically, the pressure that fermions experience due to the Pauli exclusion principle opposes gravitational collapse. When attempting to compress fermionic dark matter, the particles resist further compression into dense regions because doing so would violate the Pauli exclusion principle (Chavanis, 2011). In essence, fermions counteract clumping and tend to spread out over a larger volume, preventing the formation of compact, extended structures.

Lastly, quantum pressure plays a crucial role in stabilizing solitonic cores and inhibiting gravitational collapse at small scales (Sikivie, 2009). Thus, the bosonic nature of light dark matter shapes dark matter halo structures and dynamics in different ways than CDM.

1.2 Stellar System Dynamics in the Presence of FDM

Stellar systems, such as globular and nuclear star clusters, elliptical and spiral galaxies, and their surrounding dark matter haloes, are fundamental components of the large-scale structure of the universe. These systems are made up of vast numbers of self-gravitating objects, primarily stars, whose motion and gravitational interactions determine the system's overall behavior and evolution. A common approach in studying the dynamics of stellar systems is to model them as a gas of stars, applying methods from equilibrium thermodynamics and two-body collision theory. In this simplified framework, stars follow individual orbits and their interactions, dominated by gravity, lead to collective system-wide behavior.

However, this classical approach has limitations when applied to self-gravitating systems. Unlike gases of particles with weak interactions, gravitational forces lead to continuous, non-linear perturbations, which prevent the system from ever reaching a true equilibrium state. Instead, the system is in a constant state of dynamical evolution. This breakdown of equilibrium-based descriptions reveals the need for a more sophisticated kinetic theory that accounts for the complex, long-range interactions between the objects within the system. In this view, the orbits of individual stars are not static but evolve over time due to both direct gravitational interactions and the larger-scale mass distribution of the galaxy and its dark matter halo (Hamilton and Fouvry, 2024).

In the context of FDM, these ideas take on additional complexity. FDM, with its characteristic properties such as the de Broglie wavelength associated with each particle, introduces a wave mechanical nature to the dark matter distribution. In contrast to the classical treatment of stellar systems, FDM can lead to smoother, less clumpy dark matter profiles that affect the evolution of stellar systems. The interactions between the stars and the fuzzy dark matter halo can modify the gravitational potential in ways that differ from those seen in systems dominated by more conventional, collisionless dark matter. The interplay between the gravitational relaxation of stars and the dynamical effects of FDM offers a unique perspective on the evolution of these systems, influencing their structure and the timescales over which they evolve.

1.2.1 Evolution of Stellar Systems

In a stellar system, the term *encounter* is used to denote the gravitational perturbation of the orbit of one star by another. The cumulative effect of such encounters drives the evolution of stellar systems, altering their energy distribution, phase-space structure, and long-term dynamics. Several relaxation mechanisms contribute to this evolution, leading to the redistribution of energy and momentum within the system. Below, we summarize the key processes:

Two-Body Relaxation: Relaxation in a stellar system primarily arises from weak, cumulative gravitational encounters between stars (Chandrasekhar, 1943). These interactions cause individual stars to gradually deviate from their initial orbits due to phase-space diffusion. Over time, this leads to the redistribution of kinetic energy and angular momentum, increasing the system's entropy. The characteristic timescale for this process, known as the *relaxation time*, depends on the number of stars, their velocities, and the system's density. In globular clusters, two-body relaxation can lead to mass segregation and even core collapse (Binney and Tremaine, 2008), while in galaxies, the process is too slow to play a dominant role.

Violent Relaxation: In contrast to two-body relaxation, *violent relaxation* occurs on a much shorter timescale during the early phases of a system's formation (Lynden-Bell, 1967). When a self-gravitating system undergoes a rapid potential change—such as during a merger or collapse—the phase-space distribution of stars is significantly altered before individual encounters become important. This results in a rapid redistribution of energy and the establishment of a quasi-equilibrium state within a few dynamical timescales. Unlike collisional relaxation, violent relaxation does not lead to a steady-state Maxwellian velocity distribution but instead leaves the system with a memory of its initial conditions.

Resonant Relaxation: In stellar systems dominated by a central massive object, such as galactic nuclei, two-body relaxation is inefficient due to the near-Keplerian nature of stellar orbits. Instead, *resonant relaxation* becomes the dominant mechanism (Rauch and Tremaine, 1996). In this regime, angular momentum transfer is enhanced because the torques exerted by stars on each other persist over long timescales. This process leads to faster relaxation of orbital orientations compared to energy relaxation and is particularly relevant in the vicinity of supermassive black holes (Alexander, 2017; Merritt, 2013).

Equipartition: Encounters within a stellar system promote the redistribution of kinetic energy among stars of varying masses. While heavier stars tend to lose energy and sink deeper into the gravitational potential, lighter stars gain energy and diffuse outward. This process is analogous to thermal equipartition in gases but is not always fully achieved in stellar systems (Spitzer, 1969). For example, in multi-mass clusters, Spitzer instability can prevent global equipartition if the most massive stars dominate the energy distribution (Trenti and van der Marel, 2013).

Escape and Tidal Effects: Encounters can provide some stars with enough energy to escape the system, leading to gradual *evaporation* (Hénon, 1961). This process is closely linked to the relaxation timescale and is particularly important in open clusters. However, in globular clusters and galactic nuclei, external tidal fields also play a significant role in mass loss. Tidal stripping due to the host galaxy (Gnedin, 1999) and disk shocking from passages through the galactic plane accelerate the escape process, influencing the long-term survival of stellar systems (Baumgardt and Makino, 2003).

Binary Interactions and Energy Regulation: Binary stars play a crucial role in regulating the energy of stellar systems. Hard binaries (those with binding energy much greater than the typical kinetic energy of stars) act as an energy source, transferring energy to passing stars and preventing core collapse (Heggie, 1975). This process, governed by Heggie's Law (*hard binaries get harder*), is an essential heating mechanism in dense clusters, especially post-core collapse (Fregeau, 2004). Additionally, interactions with primordial binaries influence cluster evolution by redistributing energy through frequent dynamical encounters (Giersz, 2008).

These relaxation mechanisms collectively shape the evolution of stellar systems, influencing their structure, lifetime, and observational properties. The interplay between collisional and collisionless processes determines the system's long-term fate, particularly in environments ranging from star clusters to galactic nuclei. Understanding these processes provides insight into the life cycles of stellar systems and their long-term stability. In the following, we will focus on the process of relaxation and how it can affect the stellar system in general.

1.2.2 Gravitational Relaxation

As mentioned earlier, the interactions between particles (such as stars or dark matter components) that result in changes to their individual trajectories and velocities are referred to as encounters in self-gravitating systems. These interactions are typically gravitational, though in some contexts, other forces might play a role.

In classical systems, such encounters generally occur due to two-body or multi-body interactions, where the gravitational attraction between objects causes them to exchange energy and momentum (Binney and Tremaine, 2008; Stefano Ruffo, 2017). Over long periods, these interactions lead to a system's tendency to evolve toward a state of statistical equilibrium, where the energy and momentum are distributed more uniformly among the particles. Consequently, the orbits of stars or other constituents within the system become altered, leading to a redistribution of energy across the system. This process is essential for the evolution of stellar systems and plays a key role in their long-term dynamical state. *N-body relaxation* describes the gradual redistribution of energy and momentum through gravitational interactions among the constituents in classical systems (Binney and Tremaine, 2008). These encounters, driven by long-range forces, lead to changes in individual orbits and contribute to the overall dynamical evolution of the system.

In stellar dynamics, the term *diffusion* describes the stochastic transfer of energy as stars experience successive encounters that gradually modify their velocities and positions.

The diffusion rate depends on the encounter frequency and the strength of gravitational interactions. Over time, this process drives the system toward relaxation, where the velocity distribution becomes more uniform. The characteristic timescale for significant diffusion, known as the *relaxation timescale*, is determined by the system's size, density, and interaction dynamics. Diffusion plays a crucial role in the redistribution of energy across large-scale systems, shaping the evolution of galaxies, clusters, and other self-gravitating structures (Binney and Tremaine, 2008).

Hui et al. (2017) proposed a remarkable analogy for FDM dynamics: the fluctuating gravitational force arising from an FDM field of mean density ρ is equivalent to that produced by a classical N-body system composed of quasiparticles. These quasiparticles possess an effective mass $m_{\text{eff}} \sim \rho\lambda^3$. The gravitational interactions are now mediated by fluctuations in the FDM field, giving the system's evolution an additional layer of complexity.

Relaxation processes in FDM systems are central to understanding their dynamic evolution and astrophysical implications. The wave-like nature of FDM introduces mechanisms of interaction among quasiparticles, stars, and massive objects, leading to outcomes that differ significantly from traditional collisionless dark matter[1] models (Hui et al., 2017; Hamilton and Fouvry, 2024):

1. Formation and Growth of a Central Soliton: The relaxation between quasiparticles within an FDM halo plays a pivotal role in the development of a central Bose-Einstein condensate (BEC) or soliton. This soliton forms as a result of quantum pressure counteracting gravitational collapse in the innermost regions of the halo (Schive et al., 2014a; Hui et al., 2017). Over time, energy redistribution through wave interference and relaxation processes allows the soliton to grow in mass and stabilize. The soliton serves as a dense, coherent core, surrounded by a halo of less-dense wave interference patterns. This dual structure is a hallmark of FDM halos and has been observed in numerical simulations (Schive et al., 2014a; Yifan Liu, 2020). The soliton's growth reflects the ongoing relaxation within the quasiparticle population, balancing gravitational attraction with quantum pressure.

2. Heating and Expansion of Stellar Systems: Relaxation between FDM quasiparticles and macroscopic objects such as stars can drive significant changes in the stellar system's structure. As quasiparticles interact with stars, energy is transferred, leading to the heating of the stellar system. This energy transfer can cause stars to move to higher-energy orbits, resulting in an overall expansion of the stellar distribution. The process continues as the system evolves toward equipartition, a state where the kinetic energy of stars aligns with that of the quasiparticles (Binney and Tremaine, 2008; Y. Farhi, 2020). This interplay impacts the morphology and dynamics of galaxies, potentially influencing the size and velocity dispersion profiles of stellar components in FDM-dominated environments.

3. Stalling of Massive Object Inspiral: Massive objects such as black holes or globular clusters embedded in FDM halos interact dynamically with both baryonic matter and the quasiparticles. While dynamical friction - a drag force arising from the gravitational wake of perturbed matter - would typically cause such massive objects

[1] Note that, as stated by Hamilton and Fouvry (2024), *collisional* refers to a model of dark matter involving a finite cross-section for two dark matter particles to annihilate, in contrast with standard *collisionless* dark matter, which has no such cross-section i.e. no self-interaction.

to spiral inward toward the galactic center, relaxation processes with FDM quasiparticles can counteract this motion (HongSheng Zhao, 2000). As the quasiparticles transfer energy and momentum to the massive object, the inspiral is stalled, preventing the object from reaching the galaxy's core. This interaction modifies the predicted central density profiles and dynamical behavior of massive objects in FDM systems. The relaxation-induced stalling can have profound implications for the coevolution of supermassive black holes and their host galaxies, as well as for the long-term stability of globular cluster systems (Hui et al., 2017; Y. Farhi, 2020).

1.3 Structure of This Thesis

In the following, we introduce the kinetic theory and the fundamental equations governing the evolution of the phase-space distribution function. We then examine the physics of the relaxation process in detail, including its characteristic timescale. In Chapter 3, we derive the equations governing gravitational relaxation across different scenarios, focusing specifically on the diffusion coefficients for each case.

In Chapter 4, we extend these calculations to the context of FDM, generalizing the kinetic equation to incorporate dynamical friction. Chapter 5 presents two distinct approaches to deriving the kinetic equation, offering complementary perspectives on the formalism.

Chapter 6 explores the boundary between scales where gravitational forces dominate, potentially leading to instabilities—and those where counteracting forces provide stability, including a discussion of the generalized Jeans scale. In Chapter 7, we analyze the astrophysical consequences of relaxation processes in FDM halos and their impact on the dynamics of astrophysical systems.

Finally, in Chapter 8, we summarize our findings and present concluding remarks.

2 Kinetic Theory and Relaxation Dynamics

Kinetic theory provides a framework for understanding the collective behavior of particles in a system, such as their velocities and positions. In classical systems, such as stellar systems or dark matter halos, the particles may interact through gravitational forces or, in some cases, via other forces. These interactions lead to changes in macroscopic behaviors like temperature, pressure, and velocity distributions (Binney and Tremaine, 2008; Chandrasekhar, 1943).

2.1 Foundations of Kinetic Theory in Gravitational Systems

Kinetic theory plays an essential role in understanding the behavior of stars, dark matter particles, and baryonic matter in self-gravitating systems such as galaxies, star clusters, and dark matter halos. Unlike traditional kinetic theory, which focuses on systems where particles interact through direct collisions, self-gravitating systems are dominated by long-range gravitational interactions. In these systems, particles don't collide directly but instead influence each other through gravity. Despite this difference, the principles of transport processes—such as diffusion and energy redistribution—are analogous to those found in collisional systems. These processes govern how energy and momentum are transferred within the system, ultimately leading to relaxation and describing the statistical distribution of velocities, positions, and energies of the system's constituents.

In classical stellar dynamics, the system of stars in a galaxy can be modeled as a collection of particles moving under the influence of mutual gravitational attraction. Relaxation occurs when stars undergo a series of close encounters, gradually redistributing their energy and momentum, ultimately leading the system toward a state of statistical equilibrium.

The phase space distribution $F(\mathbf{r}, \mathbf{v}, t)$ gives the number of stars per unit phase space (position $\mathbf{r}$ and velocity $\mathbf{v}$) at time t. The evolution of this distribution function is governed by the collisionless Boltzmann equation (CBE)

$$\frac{\partial F}{\partial t} + \mathbf{v} \cdot \nabla_r F + \mathbf{f_g} \cdot \nabla_v F = 0, \tag{2.1}$$

where $\mathbf{f_g}$ represents the gravitational force per mass acting on the particles. The gravitational force per mass on a star at position $\mathbf{r}$ is given by

$$\mathbf{f_g} = -\nabla\Phi(\mathbf{r}), \tag{2.2}$$

where $\Phi(\mathbf{r})$ is the gravitational potential due to the mass distribution of the galaxy or star cluster.

The CBE equation demonstrates that distribution function evolves over time, primarily due to gravitational interactions between the stars. The equilibrium state is typically reached when the distribution function stabilizes, meaning that no further redistribution of energy occurs.

In self-gravitating systems, the gravitational potential plays a crucial role in shaping the velocity distribution of particles. For example, in spherical systems such as globular clusters or elliptical galaxies, the velocity distribution of stars can be described by a Maxwell-Boltzmann distribution in equilibrium, but modified by the gravitational potential. The velocity dispersion in such systems is related to the mass distribution through the virial theorem. As relaxation progresses, the system's velocity dispersion becomes more uniform, and the stellar distribution approaches a steady state. The virial theorem that relates the system's kinetic and potential energies, and it is given by

$$2\langle T\rangle = -\langle U\rangle, \tag{2.3}$$

where T is the kinetic energy, and U is the potential energy. The virial theorem gives a useful constraint on the overall dynamical state of the system and helps relate the mass distribution to the velocity distribution.

2.2 The Kinetic Framework of Fuzzy Dark Matter

In the case of fuzzy dark matter, the application of kinetic theory is more complex. For CDM, particles are assumed to have negligible velocity dispersion at the present epoch, leading to structures like halos that are nearly collisionless. This means that cold dark matter particles do not undergo significant self-scattering or collisions that would lead to energy dissipation or thermalization. However, for FDM, the particles exhibit wave-like interference effects that changes the dynamics of the halo (Hu et al., 2000).

As shown by Hui et al. (2017), the presence of wave effects in FDM modifies the kinetic theory in several ways. In particular, the gravitational interactions among FDM particles are mediated by the fluctuations in the FDM field. These fluctuations give rise to a quantum pressure that counteracts gravitational collapse, leading to the formation of a soliton in the center of FDM halos. This soliton is a dense, coherent structure that forms as a result of relaxation and wave interference effects, marking a key difference between FDM and traditional collisionless dark matter models (Schive et al., 2014a).

FDM particles are described by a field $\psi(\mathbf{r}, t)$, which obeys the Schrödinger-Poisson system

$$i\hbar\frac{\partial\psi}{\partial t} = -\frac{\hbar^2}{2m}\nabla^2\psi + m\Phi\psi. \tag{2.4}$$

$$\nabla^2\Phi = 4\pi G m|\psi|^2. \tag{2.5}$$

The field ψ introduces wave-like behavior, and the dynamics of the system are influenced by the quantum pressure in addition to the gravitational force. The quantum pressure arises from the Madelung (1926) transformation and the superfluid treatment (see Appendix A.2) and can be expressed as

$$Q = -\frac{\hbar^2}{2m_{\text{eff}}}\frac{\Delta\sqrt{\rho}}{\sqrt{\rho}}, \tag{2.6}$$

where m_{eff} is the effective mass of the FDM particle and is related to the mean density ρ of the FDM field as

$$m_{\text{eff}} \sim \rho\lambda^3, \tag{2.7}$$

where λ is the de Broglie wavelength associated with the FDM particle.

Moreover, FDM halos experience different relaxation dynamics than CDM halos. While CDM halos undergo N-body relaxation driven by gravitational interactions, FDM halos experience a different relaxation, where wave-like behavior leads to the gradual redistribution of energy across the system. This process is slower than N-body relaxation but plays a critical role in shaping the final structure of the halo expected to consist of a central soliton surrounded by a diffuse distribution of dark matter (Schive et al., 2014a).

The interactions between FDM particles and baryonic matter also impact the evolution of stellar systems in FDM-dominated environments. As FDM particles interact with stars, they can transfer energy, causing the stars to move to higher-energy orbits. This process can lead to the heating and expansion of the stellar system, impacting the overall structure and morphology of the galaxy. The system tends toward equipartition, where the kinetic energy of the stars aligns with that of the FDM particles. The rate of energy transfer between stars and FDM particles can be written as

$$\frac{dE_{\text{stars}}}{dt} = \langle \dot{E}_{\text{FDM}} \rangle, \tag{2.8}$$

where E_{stars} is the total energy of the stellar system, and $\langle \dot{E}_{\text{FDM}} \rangle$ is the average rate of energy transfer from FDM particles to stars.

Finally, the interaction between massive objects (such as black holes or globular clusters) and FDM particles modifies the expected behavior of these objects. In particular, the dynamical friction that would normally cause such objects to spiral toward the center of a galaxy is counteracted by relaxation with FDM particles. The interaction between the massive object and FDM particles leads to a reduction in the drag force, effectively stalling the inspiral of the object. The modified drag force F_{drag} in the presence of FDM particles can be written as

$$F_{\text{drag}} \sim \frac{GM_{\text{object}} m_{\text{eff}}}{r^2} \cdot \left(\frac{\sigma_{\text{FDM}}}{\sigma_{\text{object}}} \right), \tag{2.9}$$

where M_{object} is the mass of the massive object, and r is the distance from the center of the galaxy. σ_{FDM} and σ_{object} are the velocity dispersions of the FDM particles and the massive object, respectively (Vogelsberger et al., 2014).

In a nutshell, kinetic theory provides a comprehensive framework to describe the dynamics of both stellar and gravitational systems. The relaxation processes, whether driven by gravitational interactions in CDM or wave-like behavior in FDM, are crucial in determining the equilibrium properties of these systems, influencing their evolution over time.

2.3 Gravitational Encounters and Relaxation Processes

In stellar systems such as star clusters or galaxies, each star is subject to fluctuating forces from encounters with its neighbors. Therefore, a smooth gravitational potential approximation does not hold here, as individual stellar encounters gradually disrupt the stability of the original orbits. These encounters, though weak, impart small, random perturbations to the velocities of stars, causing them to diffuse in phase space over time. This process leads to a progressive loss of memory of their original trajectories, ultimately resulting in stars finding themselves on entirely unrelated orbits.

The characteristic timescale over which this occurs is known as the relaxation time t_{relax}. The value of t_{relax} depends on several factors, including the density and velocities of stars, the size of the system, and the range of interaction strengths. Over timescales that exceed t_{relax}, the cumulative effects of many such encounters dominate the evolution of the system, rendering the smooth gravitational potential approximation invalid, necessitating a shift from the smooth gravitational potential approximation to one that accounts for the discreteness of stars and their collective gravitational interactions. This transition is not only crucial for understanding the long-term behavior of stellar systems, such as the redistribution of energy in star clusters, but also extends to other astrophysical systems, including FDM halos.

In the context of FDM, relaxation processes lead to similar phase-space diffusion and dynamical evolution. The fluctuating gravitational force from an FDM field with mean density ρ is argued to resemble that of a classical N-body system, where the system is composed of quasiparticles with an effective mass $m_{\text{eff}} \sim \rho\lambda^3$ (Hui et al., 2017). As we shall see in this section, the relaxation time tends to be higher for lighter particles.

In plausible CDM models, the particle mass m is typically very small, and due to the weak interactions between CDM particles (often assumed to be non-interacting or only weakly interacting), the relaxation time far exceeds the age of the universe (Bar-Or et al., 2019), rendering dark halos effectively collisionless. However, in FDM models due to quantum fluctuations, the effective mass of the quasiparticles is sufficiently large that can influence the halo's structure, causing it to undergo more significant relaxation compared to CDM halos over shorter timescales.

This relaxation drives various astrophysical phenomena: between quasiparticles, it can lead to the formation and growth of a central Bose–Einstein condensate or soliton (though this process is not explored here). Relaxation between quasiparticles and macroscopic objects like stars can heat the stellar system, causing it to expand as it evolves toward equipartition with the quasiparticles. Furthermore, relaxation between quasiparticles and massive objects, such as black holes or globular clusters, can trigger the inspiral of these objects toward the galaxy's center, an effect counteracting dynamical friction from baryonic and dark matter (Bar-Or et al., 2019).

2.3.1 Estimating the Perturbation from Stellar Encounters

The goal here is to explore when we can approximate a galaxy composed of N identical stars of mass m as a smooth density distribution and gravitational field. Let us take a subject star and try to estimate the difference between the actual velocity of it after an interval of motion across the galaxy and the velocity that it would have had if the mass of the other stars were smoothly distributed. Since the gravitational field is not fully smooth, the star diffuses from its original orbit in phase space and finds a wholly new unrelated orbit. Relaxation time t_{relax} determines the time it takes the star to lose its memory of its original orbit. After the relaxation time the system's gravitational field can no longer be approximated as smooth, as the cumulative effects of stellar interactions introduce significant deviations from a uniform potential.

As a result of this diffusion from the original orbit, entropy increases, and the system becomes less sensitive to initial conditions. The relaxation process drives the stellar system to form a small, dense core with a large, low-density halo.

Consider a second star (the field star) at a distance b from the subject star. We want to estimate the change in velocity δv that the encounter imparts to the subject star. Assuming that $|\delta v|/v \ll 1$ that the field star remains stationary during the encounter, δv is perpendicular to v, since the accelerations parallel to v average to zero.We approximate the field star's trajectory as a straight-line path and integrate the perpendicular force, $F_\perp$ along this trajectory.

$$F_\perp = \frac{Gm^2}{b^2+x^2}\cos\theta = \frac{Gm^2 b}{(b^2+x^2)^{3/2}} = \frac{Gm^2}{b^2}\left[1+\left(\frac{vt}{b}\right)^2\right]^{-3/2}. \tag{2.10}$$

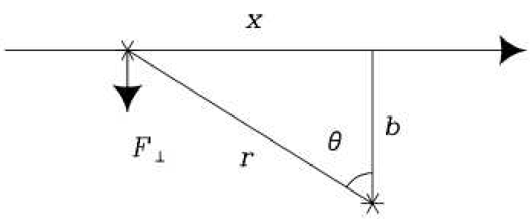

Figure 2.1: Field star approaches the subject star at speed v and impact parameter b. We estimate the resulting impulse to the subject star by approximating the field star's trajectory as a straight line (Binney and Tremaine, 2008).

From Newton's law

$$m\dot{v} = F \quad \text{so} \quad \delta v = \frac{1}{m}\int_{-\infty}^{\infty} dt\, F_{\perp}, \tag{2.11}$$

and we have

$$\delta v = \frac{Gm}{b^2}\int_{-\infty}^{\infty} \frac{dt}{[1+(vt/b)^2]^{3/2}} = \frac{Gm}{bv}\int_{-\infty}^{\infty}\frac{ds}{(1+s^2)^{3/2}} = \frac{2Gm}{bv}. \tag{2.12}$$

In words, δv is roughly equal to the acceleration at closest approach, Gm/b^2, multiplied by the duration of this acceleration $2b/v$. Clearly, this result is not precise as it suffers from our simplifications.

The surface density of field stars in the host galaxy is of order $N/\pi R^2$, where N is the number of stars and R is the galaxy's radius. Over a single crossing, the subject star experiences

$$\delta n = \frac{N}{R^2}2\pi b\, db = \frac{2N}{R^2} b\, db \tag{2.13}$$

encounters with impact parameters ranging from b to $b + db$. Each encounter produces a perturbation δv to the subject star's velocity. Because these small perturbations are randomly oriented in the plane perpendicular to $\mathbf{v}$, their mean value is zero, but their mean square is not. After one crossing, the mean-square velocity change is

$$\sum \delta v^2 \simeq \delta v^2 \delta n = \left(\frac{2Gm}{bv}\right)^2 \frac{2N}{R^2} b\, db. \tag{2.14}$$

Integrating the above equation over all impact parameters from $b_{\rm min}$ to $b_{\rm max}$, the mean-square velocity change per crossing is

$$\Delta v^2 \equiv \int_{b_{\rm min}}^{b_{\rm max}} \sum \delta v^2 \simeq 8N\left(\frac{Gm}{Rv}\right)^2 \log\Lambda, \tag{2.15}$$

where the factor

$$\ln\Lambda \equiv \ln\left(\frac{b_{\rm max}}{b_{\rm min}}\right) \tag{2.16}$$

is called the Coulomb logarithm accounting for the ratio between the maximum and minimum scales of the encounters. We will elaborate more on this topic later in this chapter.

2.3.2 Calculating the Relaxation Timescale

Encounters between the subject star and field stars cause a kind of diffusion of the subject star velocity that is distinct from the steady acceleration caused by the overall mass distribution in the stellar system. This diffusive process is sometimes called *two-body relaxation* since it arises from the cumulative effect of myriad two-body encounters between the subject star and passing field stars.

Relaxation time can be estimated from the number of encounters required to significantly change the velocity of the subject star. The typical speed σ of a field star is roughly that of a particle in a circular orbit at the edge of the galaxy,

$$\sigma^2 \approx \frac{GNm}{R}. \tag{2.17}$$

We can use the above relation to eliminate R from Δv

$$\frac{\Delta v^2}{\sigma^2} \approx \frac{8\log\Lambda}{N}. \tag{2.18}$$

If the subject star makes many crossings of the galaxy, the velocity will change by roughly Δv^2 at each crossing (Binney and Tremaine, 2008), so the number of crossings n_{relax} that is required for its velocity to change by of order itself is given by

$$n_{\mathrm{relax}} \simeq \frac{N}{8\log\Lambda}. \tag{2.19}$$

The relaxation time may be defined as $t_{\mathrm{relax}} = n_{\mathrm{relax}} t_{\mathrm{cross}}$, where $t_{\mathrm{cross}} = R/\sigma$ is the time it takes to cross the stellar system and is equal to the dynamical time, which is

$$t_{\mathrm{dyn}} = t_{\mathrm{cross}} = \frac{R}{\sigma} \tag{2.20}$$

Moreover, assuming the minimum impact parameter as the inter-star distance[2], meaning that $\Lambda \sim \frac{R}{n^{-1/3}} = N^{1/3}$, by equation (2.17), the final result is

$$t_{\mathrm{relax}} \simeq \frac{0.1N}{\log N} t_{\mathrm{cross}} \tag{2.21}$$

Now we can substitute the above relations in (2.21) and obtain

$$t_{\mathrm{relax}} \simeq \frac{\sigma^3 R^3}{G^2 m^2 \log N} \tag{2.22}$$

After one relaxation time, the cumulative small kicks from many encounters with passing stars have significantly changed the subject star's orbit from the one it would have had if the gravitational field had been smooth. In effect, after a relaxation time a star has lost its memory of its initial conditions. In galaxies with $N \approx 10^{11}$ stars and and typical crossing times of a few hundred dynamical times, stellar encounters are unimportant, except very near their centers. In a globular cluster however, where $N \approx 10^5$ and the crossing time $t_{\mathrm{cross}} \approx 1$ Myr, relaxation strongly influences the cluster structure during its lifetime of 10 Gyr.

[2] A more precise calculation is given in the next subsection

In all systems, the dynamics over timescales $\lesssim t_{\mathrm{relax}}$ is that of a collisionless system in which the constituent particles move under the influence of the gravitational field generated by a smooth mass distribution, rather than a collection of mass points. Non-baryonic dark matter is also collisionless, since both weak interactions and gravitational interactions between individual WIMPs are negligible in any galactic context (Binney and Tremaine, 2008).

For dark matter systems like FDM halos, similar processes of relaxation affect the distribution of matter and the overall dynamics, making it an important factor to consider in the evolution of such systems.

2.3.3 Fundamental Assumptions in Gravitational Relaxation

In out calculations, we assume a homogeneous system, for which we invoke the *Jeans swindle*, neglecting any acceleration due to the homogeneous average density Bar-Or et al. (2019). Jeans Swindle refers to the assumption that the gravitational potential is sourced only by fluctuations to this uniform background density (Binney and Tremaine, 1987, 2008; Ershkovich, 2011; Falco et al., 2013). In an infinite homogeneous gravitating system, any cosmic structure is affected by an inconsistency: due to the Poisson's equation, such an overdensity does not allow the system to be in equilibrium. A constant gravitational potential leads to a zero density (Jeans, 1929; Zeldovich and Novikov, 1971).

Dark matter halos are described as localized regions of excess matter density compared to the mean matter density of the Universe. At large distances from the halo center, the uniform background density dominates the overall density distribution (Tavio et al., 2008). In a more general context, the background density, the cosmological constant, and the effects of the Universe's expansion contribute to the gravitational potential. These contributions, however, effectively cancel each other out when properly accounted for. The Jeans Swindle involves neglecting the uniform background density to resolve an inconsistency in gravitational modeling. Falco et al. (2013) argues that if we fully account for the expansion of the Universe and the cosmological constant, the Jeans Swindle becomes unnecessary. This implies a more rigorous formalism that naturally resolves the inconsistency without discarding the background density.

This assumption, however, breaks down on scales larger than the Jeans length defined as the following

$$\lambda_J \sim \left(\frac{\sigma^2}{G\rho}\right)^{1/2}. \tag{2.23}$$

2.3.4 Encounter Scales and the Coulomb Logarithm

According to equation (2.16), the Coulomb logarithm is defined as the ratio the between the maximum and minimum encounter scales that dominate the relaxation time. For finite systems, the Jeans length is comparable to the system's radius R, as indicated by the virial theorem. At scales much larger than R, the density becomes negligible and the assumption of homogeneity no longer holds. Encounters on scales b with $r \ll b \ll R$ average to zero. Therefore, we set $b_{\mathrm{max}} \simeq \min(r, R)$, or in general, we can write it as $b_{\mathrm{max}} = f_1 R$ with f_1 being the uncertainty factor of order unity.

For classical N-body systems composed of point particles of mass m_p, the minimum scale of relevance is characterized by the impact parameter $b_{90} \equiv Gm_p/\sigma^2$ which corresponds to the distance at which a typical particle is deflected by $90°$. However, for impact parameters smaller than b_{90}, our assumption of a straight-line trajectory breaks down. Therefore, we set

$$b_{\rm min} = f_2\, b_{90} \tag{2.24}$$

where f_2 is another uncertainty factor of order unity. The Coulomb logarithm can then be expressed as

$$\ln \Lambda = \ln \left(\frac{R}{b_{90}}\right) + \ln \left(\frac{f_1}{f_2}\right), \tag{2.25}$$

where the second term accounts for the uncertainties. In most systems of interest, $R \gg b_{90}$; for example, in a typical elliptical galaxy, $R/b_{90} \gtrsim 10^{10}$ (Bar-Or et al., 2019). Hence, the fractional uncertainty in $\ln \Lambda$ arising from f_1 and f_2 is small, and we lose little accuracy by setting $f_2/f_1 = 1$ (Binney and Tremaine, 2008). Therefore for a classical system, the Coulomb factor is given as

$$\Lambda_{\rm cl} = \frac{R}{b_{90}} \tag{2.26}$$

In case of classical N-body systems composed of point particles, if the particles have a non-zero scale length ϵ, either due to representing star clusters or other subsystems of non-zero size, or due to artificial *softening*[3] for numerical accuracy, we set $b_{\rm min} \simeq \epsilon$. In this case, the softened Coulomb factor is defined as

$$\Lambda_{\rm soft} = \frac{b_{\rm max}}{\epsilon} \tag{2.27}$$

For FDM quasiparticles, the appropriate minimum scale is set to half the typical de Broglie angular wavelength

$$b_{\rm min} \simeq \frac{\lambda_\sigma}{2} = \frac{h}{2 m_b \sigma}, \tag{2.28}$$

and finally the FDM Coulomb factor can be written as (Bar-Or et al., 2019)

$$\Lambda_{\rm FDM} = \frac{2 b_{\rm max}}{\lambda_\sigma}. \tag{2.29}$$

In general, it is common to express the Coulomb factor in terms of the quantities used in equation (2.29), (2.27) and 2.26 rather than designating a precise value to it. This ambiguity stems from the fact that the exact value of $b_{\rm max}$ can not be determined in calculations for in an infinite homogeneous medium lacks boundaries or a well-defined maximum encounter scale. However, the uncertainty in the value of Λ is limited to a factor of order unity. This is considered a minor issue because such variations do not significantly affect calculations when $\Lambda \gg 1$, then the logarithm $\ln \Lambda$ changes very slowly with respect to Λ, so small variations in Λ have an even smaller impact on the results. This makes the precise determination of Λ less critical (Bar-Or et al., 2019).

[3]The force softening kernel is some function added to the force between particles to avoid the divergence of the integration of the force between them when the particles approach each other in close encounters, while keeping the Newton's laws unchanged. As a result of adding the softening kernel to the integration, the force exerted on a particle by another paticle at the same location is zero (Binney and Tremaine, 2008).

2.4 Fokker-Planck Equation

Under the influence of a smooth potential, the distribution function evolves according to the collisionless (i.e. for systems with dynamic timescales $\lesssim t_{\rm relax}$) Boltzmann equation $dF/dt = 0$ (see equation (2.1)), where the derivative is taken along the phase-space trajectory of a given star. In words, the flow through phase space of the probability fluid is incompressible; the phase-space density F of the fluid around a given star always remains the same. In contrast to flows of incompressible fluids such as water, the density will generally vary greatly from point to point in phase space; the density is constant as one follows the flow around a particular star but the density around different stars can be quite different. Therefore, for collisionless systems, where two-body encounters are negligible, the evolution of $P(\mathbf{v}, t)$ is instead governed by the collisionless Boltzmann equation.

On the other hand, when encounters are taken into account, the phase-space density around a star changes with time (Binney and Tremaine, 2008), and the system experiences a changing potential. In self-gravitating systems, encounters gradually drive the system towards equilibrium, making the Fokker-Planck formalism essential for understanding relaxation mechanisms. In this case, the potential can no longer be approximated with a smooth gravitational field $t > t_{\rm relax}$. The evolution of the probability density function $P(\mathbf{v}, t)$, which describes the probability distribution of velocities $\mathbf{v}$ of a test particle, can be derived under the following assumptions:
1. Stochastic Encounters: The particle's velocity changes due to random encounters with other particles, described by a transition probability $W(\mathbf{v} \to \mathbf{v} + \Delta\mathbf{v})$, which gives the probability per unit time of a velocity change $\Delta\mathbf{v}$.
2. Markovian Process: The transition probability depends only on the current velocity $\mathbf{v}$ and the velocity change $\Delta\mathbf{v}$, and not on the history of the system.
3. Small Velocity Changes: The changes in velocity $\Delta\mathbf{v}$ due to encounters are small, allowing for a Taylor expansion of the distribution function around $\mathbf{v}$.
4. Negligible Higher-Order Moments: Higher-order terms in the Taylor expansion and higher moments of $\Delta\mathbf{v}$ are small and can be neglected. This is equivalent to ignoring higher moments of the transition probability (e.g. Risken (1996)) and is usually a good assumption if the first and second moments of the transition probability are finite.

The probability density function $P(\mathbf{v}, t)$ evolves in time due to stochastic encounters, governed by the transition probability $W(\mathbf{v} \to \mathbf{v} + \Delta\mathbf{v})$, the probability per unit time of a velocity change $\Delta\mathbf{v}$ (Chandrasekhar, 1943). The evolution equation is

$$\frac{\partial P(\mathbf{v}, t)}{\partial t} = \int \left[W(\mathbf{v} - \Delta\mathbf{v} \to \mathbf{v}) P(\mathbf{v} - \Delta\mathbf{v}, t) - W(\mathbf{v} \to \mathbf{v} + \Delta\mathbf{v}) P(\mathbf{v}, t)\right] (\Delta\mathbf{v}). \quad (2.30)$$

Here, the first term accounts for subject stars transitioning into $\mathbf{v}$, and the second term accounts for the ones leaving $\mathbf{v}$.

For small velocity changes $\Delta\mathbf{v}$, expand $P(\mathbf{v} - \Delta\mathbf{v}, t)$ in a Taylor series around $\mathbf{v}$

$$P(\mathbf{v} - \Delta\mathbf{v}, t) \approx P(\mathbf{v}, t) - \Delta v_i \frac{\partial P}{\partial v_i} + \frac{1}{2} \Delta v_i \Delta v_j \frac{\partial^2 P}{\partial v_i \partial v_j} + \ldots \quad (2.31)$$

Substituting this expansion into the first term of the evolution equation gives

$$\int W(\mathbf{v}-\Delta\mathbf{v}\to\mathbf{v})P(\mathbf{v}-\Delta\mathbf{v},t)(\Delta\mathbf{v}) \approx \int W(\mathbf{v}\to\mathbf{v}+\Delta\mathbf{v}) \times \left[P(\mathbf{v},t) - \Delta v_i \frac{\partial P}{\partial v_i} + \frac{1}{2}\Delta v_i \Delta v_j \frac{\partial^2 P}{\partial v_i \partial v_j}\right](\Delta\mathbf{v}). \tag{2.32}$$

The moments of the transition probability $W(\mathbf{v}\to\mathbf{v}+\Delta\mathbf{v})$ known as the first and second-order diffusion coefficients are defined as

$$D_i = D[\Delta v_i] = \frac{\langle \Delta v_i(T)\rangle}{T} = \int \Delta v_i W(\mathbf{v}\to\mathbf{v}+\Delta\mathbf{v})(\Delta\mathbf{v}), \tag{2.33}$$

$$D_{ij} = D[\Delta v_i \Delta v_j] = \frac{\langle \Delta v_i(T)\Delta v_j(T)\rangle}{T} = \int \Delta v_i \Delta v_j W(\mathbf{v}\to\mathbf{v}+\Delta\mathbf{v})(\Delta\mathbf{v}). \tag{2.34}$$

where $\Delta v_i(T)$ is the change in velocity component i over time T. For small $\Delta\mathbf{v}$, higher-order moments are neglected.

Substitute the Taylor expansion and the definitions of D_i and D_{ij} into the evolution equation. The first term becomes

$$\int W(\mathbf{v}-\Delta\mathbf{v}\to\mathbf{v})P(\mathbf{v}-\Delta\mathbf{v},t)(\Delta\mathbf{v}) \approx P(\mathbf{v},t) - \frac{\partial P}{\partial v_i}D_i(\mathbf{v}) + \frac{1}{2}\frac{\partial^2 P}{\partial v_i \partial v_j}D_{ij}(\mathbf{v}). \tag{2.35}$$

Adding the second term (loss term)

$$-\int W(\mathbf{v}\to\mathbf{v}+\Delta\mathbf{v})P(\mathbf{v},t)(\Delta\mathbf{v}) \approx -P(\mathbf{v},t)\int W(\mathbf{v}\to\mathbf{v}+\Delta\mathbf{v})(\Delta\mathbf{v}) = -P(\mathbf{v},t). \tag{2.36}$$

Combining terms, the Fokker-Planck equation for $P(\mathbf{v},t)$ is

$$\frac{\partial P(\mathbf{v},t)}{\partial t} = -\frac{\partial}{\partial v_i}\left(D_i(\mathbf{v})P(\mathbf{v},t)\right) + \frac{\partial^2}{\partial v_i \partial v_j}\left(D_{ij}(\mathbf{v})P(\mathbf{v},t)\right). \tag{2.37}$$

The two terms on the right-hand side of equation (2.37) correspond to different physical effects. The first term represents systematic changes in velocity, often associated with friction or coherent forces. The function $D_i(\mathbf{v})$ is known as the first diffusion coefficient, which describes the deterministic drift of particles in velocity space.

The second term accounts for random fluctuations in velocity due to encounters with other particles. The second diffusion coefficient $D_{ij}(\mathbf{v})$ quantifies the stochastic changes in velocity, analogous to Brownian motion.

The Fokker-Planck equation provides a statistical description of relaxation due to weak, long-range encounters between stars or dark matter particles. These small-angle deflections accumulate over time, leading to diffusion in velocity space.

3 Diffusion Processes and Kinetic Relaxation

This chapter is dedicated to finding the correct form of the kinetic equation to describe the evolution of velocity distribution caused by diffusion processes. We begin by calculating the velocity diffusion coefficients for a test particle with zero mass, situated in a potential that undergoes stochastic fluctuations. These stochastic fluctuations drive changes in the velocity of the test particle, and the way these fluctuations are correlated in space and time determines how the test particle responds to them. We will study three main cases, including a potential with stochastic fluctuations, density fluctuations from an infinite homogeneous classical system of point-like particles and finally extended field particles which is a more complex scenario.

3.1 Diffusion by a Fluctuating Potential

Consider that a zero-mass test particle is under the influence of a potential with stochastic fluctuations and a spatial uniform average and stationary in time. We will restrict the calculations to the linear regime which for classical particles is equivalent to assuming that $\varepsilon \gg b_{90}$. Consider a time-dependent potential $\Phi(\mathbf{r}, t)$ with zero mean, $\langle \Phi(\mathbf{r}, t) \rangle = 0$, and stationary correlation function,

$$\langle \Phi(\mathbf{r}, t)\, \Phi(\mathbf{r}', t') \rangle = C_\Phi(\mathbf{r} - \mathbf{r}', t - t'); \tag{3.1}$$

here $\langle \cdot \rangle$ denotes an ensemble average, i.e., an average over all possible realizations of the potential. It is useful to write the potential in terms of its temporal and spatial Fourier transform, $\widehat{\Phi}(\mathbf{k}, \omega)$, defined by

$$\Phi(\mathbf{r}, t) = \iint \frac{\mathrm{d}\mathbf{k}\mathrm{d}\omega}{(2\pi)^4}\, \widehat{\Phi}(\mathbf{k}, \omega)\, \mathrm{e}^{\mathrm{i}\mathbf{k}\cdot\mathbf{r} - \mathrm{i}\omega t}. \tag{3.2}$$

The correlation function of $\widehat{\Phi}(\mathbf{k}, \omega)$ is given by

$$\langle \widehat{\Phi}(\mathbf{k}, \omega)\, \widehat{\Phi}^*(\mathbf{k}', \omega') \rangle = (2\pi)^4 \widehat{C}_\Phi(\mathbf{k}, \omega) \delta(\omega - \omega') \delta(\mathbf{k} - \mathbf{k}'), \tag{3.3}$$

where $\widehat{C}_\Phi(\mathbf{k}, \omega)$ is the temporal and spatial Fourier transform of the potential correlation function $C_\Phi(\mathbf{r}, t)$.

Given the potential in equation (3.2), the acceleration of the test particle is

$$\dot{\mathbf{v}}(\mathbf{r}, t) = -\nabla\Phi(\mathbf{r}, t) = -\mathrm{i} \iint \frac{\mathbf{k}\mathrm{d}\mathbf{k}\mathrm{d}\omega}{(2\pi)^4}\, \widehat{\Phi}(\mathbf{k}, \omega)\, \mathrm{e}^{\mathrm{i}\mathbf{k}\cdot\mathbf{r} - \mathrm{i}\omega t}, \tag{3.4}$$

and its change in velocity over time t is given by

$$\Delta\mathbf{v}(t) = \int_0^t \mathrm{d}s\, \dot{\mathbf{v}}[\mathbf{r}(s), s]. \tag{3.5}$$

As we assume that the mean force is zero, we can expand $\mathbf{r}(t)$ around the initial position and velocity,

$$\mathbf{r}(t) = \mathbf{r}_0 + \mathbf{v}_0 t + \int_0^t \mathrm{d}s\, (t - s)\, \dot{\mathbf{v}}(\mathbf{r}_0 + \mathbf{v}_0 s, s) + \cdots . \tag{3.6}$$

Thus, the change in velocity is given by the expression below

$$\begin{aligned}\Delta\mathbf{v}(t) = &-i \iint \frac{d\mathbf{k}\,d\omega}{(2\pi)^4}\,\widehat{\Phi}(\mathbf{k},\omega)\,e^{i\mathbf{k}\cdot\mathbf{r}_0}\int_0^t ds\,e^{i(\mathbf{k}\cdot\mathbf{v}_0-\omega)s}\\ &+ i\iint \frac{d\mathbf{k}\,d\omega}{(2\pi)^4}\iint \frac{d\mathbf{k}'\,d\omega'}{(2\pi)^4}\,\mathbf{k}\cdot\mathbf{k}'\,\widehat{\Phi}(\mathbf{k},\omega)\,\widehat{\Phi}^*(\mathbf{k}',\omega')\,e^{i(\mathbf{k}-\mathbf{k}')\cdot\mathbf{r}_0}\\ &\times\int_0^t ds\,e^{i(\mathbf{k}\cdot\mathbf{v}_0-\omega)s}\int_0^s ds'\,(s-s')\,e^{-i(\mathbf{k}'\cdot\mathbf{v}_0-\omega')s'},\end{aligned} \tag{3.7}$$

The goal is to derive the diffusion coefficients $D[\Delta v_i] = \frac{\langle\Delta v_i(T)\rangle}{T}$ and $D[\Delta v_i \Delta v_j] = [\frac{\langle\Delta v_i(T)\Delta v_j(T)\rangle}{T}]$.

First we try to workout $\Delta v_i(T)$ and $\Delta v_i(T)\Delta v_j(T)$ so we can calculate their averages during a certain time period. For such an encounter we have (see appendix A.3)[4]

$$\Delta v_i = \sum_{k=1}^{3}(\Delta\mathbf{v}\cdot\hat{\mathbf{e}}'_k)(\hat{\mathbf{e}}_i\cdot\hat{\mathbf{e}}'_k), \tag{3.8}$$

$$\Delta v_i \Delta v_j = \sum_{k,l=1}^{3}(\Delta\mathbf{v}\cdot\hat{\mathbf{e}}'_k)(\Delta\mathbf{v}\cdot\hat{\mathbf{e}}'_l)(\hat{\mathbf{e}}_i\cdot\hat{\mathbf{e}}'_k)(\hat{\mathbf{e}}_j\cdot\hat{\mathbf{e}}'_l). \tag{3.9}$$

Since the potential has zero mean, the average of the first term in the expression for $\Delta\mathbf{v}$ will be zero and as result, for the $i-th$ component of the velocity change we will have

$$\begin{aligned}\langle\Delta v_i(T)\rangle = &\, i\iint \frac{d\mathbf{k}\,d\omega}{(2\pi)^4}\sum_{j=1}^{3}(\hat{\mathbf{e}}_i\cdot\hat{\mathbf{e}}'_j)(\mathbf{k}\cdot\hat{\mathbf{e}}'_j)\iint\frac{d\mathbf{k}'\,d\omega'}{(2\pi)^4}\,(\mathbf{k})\cdot(\mathbf{k}')\\ &\times\langle\widehat{\Phi}(\mathbf{k},\omega)\,\widehat{\Phi}^*(\mathbf{k}',\omega')\rangle e^{i(\mathbf{k}-\mathbf{k}')\cdot\mathbf{r}_0}\int_0^T ds\,e^{i(\mathbf{k}\cdot\mathbf{v}_0-\omega)s}\int_0^T ds'\,(s-s')\,e^{-i(\mathbf{k}'\cdot\mathbf{v}_0-\omega')s'}\end{aligned} \tag{3.10}$$

Furthermore, we can now use the correlation function given below

$$\left\langle\widehat{\Phi}(\mathbf{k},\omega)\widehat{\Phi}^*(\mathbf{k}',\omega')\right\rangle = (2\pi)^4\widehat{C}_\Phi(\mathbf{k},\omega)\,\delta(\omega-\omega')\,\delta(\mathbf{k}-\mathbf{k}'), \tag{3.11}$$

and substitute it in 3.10

$$\begin{aligned}\langle\Delta v_i(T)\rangle = &\, i\iint\sum_{j=1}^{3}(\mathbf{k}\cdot\hat{\mathbf{e}}'_j)d\mathbf{k}\,d\omega\iint\frac{d\mathbf{k}'\,d\omega}{(2\pi)^4}\,\mathbf{k}\cdot\mathbf{k}'\,(\hat{\mathbf{e}}_i\cdot\hat{\mathbf{e}}'_j)\widehat{C}_\Phi(\mathbf{k},\omega)\,\delta(\mathbf{k}-\mathbf{k}')\\ &\times\delta(\omega-\omega')\,e^{i(\mathbf{k}-\mathbf{k}')\cdot\mathbf{r}_0}\int_0^T ds\,e^{i(\mathbf{k}\cdot\mathbf{v}_0-\omega)s}\int_0^T ds'\,(s-s')\,e^{-i(\mathbf{k}'\cdot\mathbf{v}_0-\omega')s'}\\ = &\,\frac{1}{(2\pi)^4}\iint\sum_{j=1}^{3}\frac{\partial}{\partial v_j}d\mathbf{k}\,d\omega\,(\hat{\mathbf{e}}_i\cdot\hat{\mathbf{e}}_j)(\mathbf{k}^2)\,\widehat{C}_\Phi(\mathbf{k},\omega)\int_0^T\int_0^T dsds'e^{i\omega(s-s')}(s-s')\end{aligned} \tag{3.12}$$

In the first integral, we expressed $(i\mathbf{k}\cdot\hat{\mathbf{e}}_j)$ as its Fourier transform $\partial/\partial v_j$. In addition, $(\hat{\mathbf{e}}_i\cdot\hat{\mathbf{e}}_j)(\mathbf{k}^2)$ can be replaced with $(k_i\cdot k_j)$. To avoid the appearance of a factor 2 when

[4] Note that the results calculated in appendix A are independent of whether the subject star is massive or not. Therefore, the final equations are applicable here.

taking the derivative of $\mathbf{k}^2$ we add a $1/2$ factor in the expression as well. Consequently, the first diffusion coefficient will be the following

$$D[\Delta v_i] = \frac{1}{2(2\pi)^4 T} \iint \sum_{j=1}^{3} \frac{\partial}{\partial v_j} d\mathbf{k}\, d\omega\, k_i \cdot k_j\, \widehat{C}_\Phi(\mathbf{k},\omega) \int_0^T \int_0^T ds ds' e^{i\omega(s-s')}(s-s') \tag{3.13}$$

Next, we will proceed to derive the second diffusion coefficient

$$\begin{aligned}\langle \Delta v_i(T) \Delta v_j(T) \rangle = i \iint \frac{d\mathbf{k}\, d\omega}{(2\pi)^4} \sum_{k,l=1}^{3} (\mathbf{k}\cdot\hat{\mathbf{e}}'_k)(\mathbf{k}\cdot\hat{\mathbf{e}}'_l)(\hat{\mathbf{e}}_i\cdot\hat{\mathbf{e}}'_k)(\hat{\mathbf{e}}_j\cdot\hat{\mathbf{e}}'_l) \iint \frac{d\mathbf{k}'\, d\omega'}{(2\pi)^4} (\mathbf{k}) \cdot (\mathbf{k}') \\ \times \langle \widehat{\Phi}(\mathbf{k},\omega)\, \widehat{\Phi}^*(\mathbf{k}',\omega') \rangle\, e^{i(\mathbf{k}-\mathbf{k}')\cdot\mathbf{r}_0} \int_0^T ds\, e^{i(\mathbf{k}\cdot\mathbf{v}_0-\omega)s} \int_0^T ds'\, (s-s')\, e^{-i(\mathbf{k}'\cdot\mathbf{v}_0-\omega')s'}\end{aligned} \tag{3.14}$$

We use the previous results to simplify the above expression

$$\begin{aligned}\langle \Delta v_i(T) \Delta v_j(T) \rangle = i \iint \frac{d\mathbf{k}\, d\omega}{(2\pi)^4} \sum_{k,l=1}^{3} [(\mathbf{k}\cdot\hat{\mathbf{e}}_k)(\mathbf{k}\cdot\hat{\mathbf{e}}_l)(\hat{\mathbf{e}}_i\cdot\hat{\mathbf{e}}_k)(\hat{\mathbf{e}}_j\cdot\hat{\mathbf{e}}_l)]\;\; \widehat{C}_\Phi(\mathbf{k},\omega) \\ \times\; (\mathbf{k}\cdot\mathbf{k}) \int_0^T \int_0^T ds ds' e^{i\omega(s-s')}(s-s')\end{aligned} \tag{3.15}$$

The term inside the integral $(\hat{\mathbf{e}}_i\cdot\hat{\mathbf{e}}_k)(\hat{\mathbf{e}}_j\cdot\hat{\mathbf{e}}_l)$ is equal to $\delta_{ik}\,\delta_{jl}$ so

$$\sum_{k,l=1}^{3} (\mathbf{k}\cdot\hat{\mathbf{e}}_k)(\mathbf{k}\cdot\hat{\mathbf{e}}_l)(\hat{\mathbf{e}}_i\cdot\hat{\mathbf{e}}_k)(\hat{\mathbf{e}}_j\cdot\hat{\mathbf{e}}_l) \;=\; \sum_{k,l=1}^{3} (\mathbf{k}\cdot\hat{\mathbf{e}}_k)(\mathbf{k}\cdot\hat{\mathbf{e}}_l)\,(\delta_{ik}\,\delta_{jl}) \;=\; k_i\, k_j \tag{3.16}$$

Incorporating these simplifications in 3.15 we reach at the following

$$\begin{aligned}D[\Delta v_i \Delta v_j] &= \frac{1}{(2\pi)^4 T} \iint d\mathbf{k}\, d\omega\, k_i k_j\, \widehat{C}_\Phi(\mathbf{k},\omega) \\ &\times \int_0^T \int_0^T ds ds' e^{i\omega(s-s')}(s-s')\end{aligned} \tag{3.17}$$

The relations for 3.13 and 3.17 are then

$$D[\Delta v_i] = \frac{1}{2} \sum_{j=1}^{3} \frac{\partial}{\partial v_j} \iint \frac{\mathrm{d}k\, \mathrm{d}\omega}{(2\pi)^3}\, k_i k_j\, \widehat{C}_\Phi(\mathbf{k},\omega)\, K_T(\omega - \mathbf{k}\cdot\mathbf{v}), \tag{3.18}$$

and

$$D[\Delta v_i \Delta v_j] = \iint \frac{\mathrm{d}k\, \mathrm{d}\omega}{(2\pi)^3}\, k_i k_j\, \widehat{C}_\Phi(\mathbf{k},\omega)\, K_T(\omega - \mathbf{k}\cdot\mathbf{v}), \tag{3.19}$$

where the finite-time kernel $K_T(\omega)$ is defined as

$$K_T(\omega) \equiv \frac{1}{2\pi T}\int_0^T\int_0^T \mathrm{d}s\,\mathrm{d}s'\,e^{i\omega(s-s')} = \frac{1-\cos(\omega T)}{\pi\omega^2 T}, \tag{3.20}$$

and is normalized so that its total area equals 1. Note that equation (3.18) and (3.19) satisfy the fluctuation-dissipation relation for a particle with zero mass.

$$D[\Delta v_i] = \frac{1}{2}\sum_j \frac{\partial}{\partial v_j} D[\Delta v_i \Delta v_j]. \tag{3.21}$$

The timescales determine the kind of process:

- Short-time limit $K_T \sim T/(2\pi)$:, making the process *ballistic* and the diffusion coefficient $D[\Delta v_i \Delta v_j] \simeq \langle \dot{v}_i \dot{v}_j T\rangle$ is the instantaneous coherent (in time) force acting on the test particle.
- Long-time limit $T \to \infty$: $K_T(\omega)$ becomes a delta function $\delta(\omega)$, and the process becomes *diffusive* which is the case of our interest (Bar-Or et al., 2019).

Assuming a finite correlation time T_c, where the correlation function $C_\Phi(\mathbf{r}, t)$ quickly drops to zero for $|t| \gg T_c$, we can simplify the analysis: The correlation time T_c is much shorter than other relevant timescales. This allows us to take the limit $T \to \infty$ and approximate the kernel $K_T(\omega)$ as a *delta function.*

With these considerations, equation (3.18) and (3.19) can then be further simplified.

$$D_i = D[\Delta v_i] = \frac{1}{2}\sum_j \frac{\partial}{\partial v_j}\int \frac{d\mathbf{k}}{(2\pi)^3} k_i k_j \widehat{C}_\Phi(\mathbf{k}, \mathbf{k}\cdot\mathbf{v}), \tag{3.22}$$

$$D_{ij} = D[\Delta v_i \Delta v_j] = \int \frac{d\mathbf{k}}{(2\pi)^3} k_i k_j \widehat{C}_\Phi(\mathbf{k}, \mathbf{k}\cdot\mathbf{v}). \tag{3.23}$$

Clearly, the probability distribution of the velocity of a test particle, $P(v, t)$, is governed by the Fokker-Planck equation derived earlier (2.37).

$$\frac{\partial P(\mathbf{v}, t)}{\partial t} = -\frac{\partial}{\partial v_i}\left(D_i(\mathbf{v})P(\mathbf{v}, t)\right) + \frac{\partial^2}{\partial v_i \partial v_j}\left(D_{ij}(\mathbf{v})P(\mathbf{v}, t)\right). \tag{3.24}$$

Due to equation (3.21), the r.h.s of the above equation could also be written as

$$-\frac{\partial}{\partial v_i}\left(D_i(\mathbf{v})P(\mathbf{v}, t)\right) + \frac{\partial^2}{\partial v_i \partial v_j}\left(D_{ij}(\mathbf{v})P(\mathbf{v}, t)\right) = \frac{1}{2}\frac{\partial}{\partial v_i}\left[D_{ij}\frac{\partial P(\mathbf{v}, t)}{\partial v_j}\right] \tag{3.25}$$

3.1.1 Potential Fluctuations from a Stationary Homogeneous Density Field

We now focus on the particular case in which the potential fluctuations originate from a stationary homogeneous random field of density fluctuations ($\rho(\mathbf{r}, t)$) with a mean field density (ρ_P). Under these assumptions, ($\langle \rho(\mathbf{r}, t)\rangle = 0$) and the correlation function of the density fluctuations can be expressed as follows

$$\langle \rho(\mathbf{r}, t)\rho(\mathbf{r}', t')\rangle = C_\rho(\mathbf{r} - \mathbf{r}', t - t'). \tag{3.26}$$

The potential fluctuations associated with the density fluctuations $\rho(\mathbf{r}, t)$ are given by the Fourier transform of Poisson's equation

$$\widehat{\Phi}(\mathbf{k}, \omega) = -4\pi G \frac{\hat{\rho}(\mathbf{k}, \omega)}{k^2},\; k = |\mathbf{k}| \tag{3.27}$$

Thus the Fourier transforms of the correlation functions are related by

$$\widehat{C}_\Phi(\mathbf{k}, \omega) = \frac{16\pi^2 G^2}{k^4} \widehat{C}_\rho(\mathbf{k}, \omega). \tag{3.28}$$

We now simply substitute this relation in the diffusion coefficients

$$D_i = D[\Delta v_i] = \frac{1}{2} \frac{1}{(2\pi)^3} 16\pi^2 G^2 \sum_j \frac{\partial}{\partial v_j} \int d\mathbf{k} \frac{k_i k_j}{k^4} \widehat{C}_\rho(\mathbf{k}, \omega), \tag{3.29}$$

$$D_{ij} = D[\Delta v_i \Delta v_j] = \frac{16\pi^2 G^2}{(2\pi)^3} \int d\mathbf{k} \frac{k_i k_j}{k^4} \widehat{C}_\rho(\mathbf{k}, \omega) \tag{3.30}$$

The diffusion coefficients equations then become

$$D_i = \frac{G^2}{\pi} \sum_j \frac{\partial}{\partial v_j} \int \frac{k_i k_j}{k^4} \widehat{C}_\rho(\mathbf{k}, \mathbf{k} \cdot \mathbf{v})\, d\mathbf{k}, \tag{3.31}$$

$$D_{ij} = \frac{2G^2}{\pi} \int \frac{k_i k_j}{k^4} \widehat{C}_\rho(\mathbf{k}, \mathbf{k} \cdot \mathbf{v})\, d\mathbf{k}. \tag{3.32}$$

3.2 Classical Two-Body Relaxation

The goal of this section is to retrieve the FP equation for the case where the zero-mass test particle is interacting with an infinite, homogeneous system of classical field particles. This assumption means that the *n-th* field particle travels on a straight line at constant velocity v_n. Moreover, let us consider the individual mass of m_p for each of the field particles, and a distribution function $F_P(\mathbf{v})$ such that $\int d\mathbf{v}\, F_P(\mathbf{v}) = \rho_P$. Another important assumption is that we ignore the self-gravity of the particles, considering only the gravitational forces that they exert on the test particle. The density fluctuations around the mean density ρ_P are given by

$$\rho(\mathbf{r}, t) = m_\mathrm{p} \sum_n \delta(\mathbf{r} - \mathbf{r}_n - \mathbf{v}_n t) - \rho_\mathrm{p}, \tag{3.33}$$

where $(\mathbf{r}_n, \mathbf{v}_n)$ stands for the position and velocity of the field particle n at time $t = 0$. The associated density correlation function is

$$C_\rho(\mathbf{r} - \mathbf{r}', t - t') = \langle \rho(\mathbf{r}, t)\, \rho(\mathbf{r}', t') \rangle = m_\mathrm{p} \int \mathrm{d}\mathbf{v}\, \delta[\mathbf{r} - \mathbf{r}' - \mathbf{v}(t - t')] F_\mathrm{p}(\mathbf{v}), \tag{3.34}$$

and its temporal and spatial Fourier transform is

$$\widehat{C}_\rho(\mathbf{k}, \omega) = 2\pi m_\mathrm{p} \int \mathrm{d}\mathbf{v}'\, \delta(\mathbf{k} \cdot \mathbf{v}' - \omega) F_\mathrm{p}(\mathbf{v}'), \tag{3.35}$$

and substituting it in the diffusion coefficients derived earlier (3.31 and 3.32), we have

$$\begin{aligned} D_i &= \frac{G^2}{\pi}\int\sum_j \frac{\partial}{\partial v_j} d\mathbf{k}\,\frac{k_i k_j}{k^4}\left(2\pi m_\mathrm{p}\int d\mathbf{v}'\,\delta(\mathbf{k}\cdot\mathbf{v}'-\mathbf{k}\cdot\mathbf{v})F_p(\mathbf{v}')\right)\\ &= 2G^2 m_\mathrm{p}\sum_j\int\frac{\partial}{\partial v_j}d\hat{\mathbf{k}}\,\hat{k}_i\hat{k}_j\int d\mathbf{v}'\,\delta(\mathbf{k}\cdot(\mathbf{v}'-\mathbf{v}))F_p(\mathbf{v}')\\ &= 2G^2 m_\mathrm{p}\int d\hat{\mathbf{k}}\,\hat{k}_i\int d\mathbf{v}'\hat{\mathbf{k}}\cdot\frac{\partial}{\partial\mathbf{v}}\,\delta(\hat{\mathbf{k}}\cdot(\mathbf{v}'-\mathbf{v}))F_p(\mathbf{v}') \end{aligned} \tag{3.36}$$

Note that $\hat{\mathbf{k}} = \mathbf{k}/|k|$. In the third line of the above computations, we treated $\sum_j \frac{\partial}{\partial v_j} k_j$ as the dot product between the gradient in v-space and the vector $\mathbf{k}$ in k-space. Letting the gradient in v-space be $\nabla_v f = \left(\frac{\partial}{\partial v_1}, \frac{\partial}{\partial v_2}, \frac{\partial}{\partial v_3}\right)$, and $\mathbf{k} = (k_1, k_2, k_3)$, we can rewrite the expression as $\sum_j \frac{\partial}{\partial v_j} k_j = \mathbf{k}\cdot\nabla_v$.

The second diffusion coefficient is obtained as below

$$\begin{aligned} D_{ij} &= \frac{2G^2}{\pi}\int d\mathbf{k}\,\frac{k_i k_j}{k^4}\left(2\pi m_\mathrm{p}\int d\mathbf{v}'\,\delta(\mathbf{k}\cdot\mathbf{v}'-\mathbf{k}\cdot\mathbf{v})F_p(\mathbf{v}')\right)\\ &= 4G^2 m_\mathrm{p}\int d\mathbf{k}\,\frac{k_i k_j}{k^4}\int d\mathbf{v}'\,\delta(\mathbf{k}\cdot(\mathbf{v}'-\mathbf{v}))F_p(\mathbf{v}')\\ &= 4G^2 m_\mathrm{p}\int d\hat{\mathbf{k}}\,\hat{k}_i\hat{k}_j\int d\mathbf{v}'\,\delta(\mathbf{k}\cdot(\mathbf{v}'-\mathbf{v}))F_p(\mathbf{v}')\\ &= 4G^2 m_\mathrm{p}\frac{\partial^2}{\partial v_i\partial v_j}\int d\mathbf{v}'\,\delta(\mathbf{k}\cdot(\mathbf{v}'-\mathbf{v}))F_p(\mathbf{v}'). \end{aligned} \tag{3.37}$$

To obtain equation (3.36) and (3.37), we used the relation

$$\frac{\partial}{\partial x_{j_1}}\cdots\frac{\partial}{\partial x_{j_\ell}}\int \mathrm{d}\hat{\mathbf{k}}\,\hat{k}_{i_1}\cdots\hat{k}_{i_n}\,\delta(\hat{\mathbf{k}}\cdot\mathbf{x}) = \frac{\partial}{\partial x_{i_1}}\cdots\frac{\partial}{\partial x_{i_n}}\int \mathrm{d}\hat{\mathbf{k}}\,\hat{k}_{j_1}\cdots\hat{k}_{j_\ell}\,\Delta_{n-\ell}(\hat{\mathbf{k}}\cdot\mathbf{x}), \tag{3.38}$$

where

$$\Delta_n(x) = \begin{cases} \frac{1}{2(n-1)!}\frac{x^n}{|x|}, & n>0,\\ \delta^{(n)}(x), & n\le 0, \end{cases} \tag{3.39}$$

The Coloumb logarithm term $\log\Lambda$ is added to the above calculations in order to adjust the strength of the diffusion processes based on the effective range of gravitational interactions. Consequently, these integrals are regulated and divergence is avoided.

$$\begin{aligned} D_i &= 2G^2 m_\mathrm{p}\log\Lambda\int \mathrm{d}\hat{k}\,\hat{k}_i\int \mathrm{d}v'\,\hat{k}\cdot\frac{\partial}{\partial\mathbf{v}}\delta[\hat{k}\cdot(\mathbf{v}'-\mathbf{v})]F_p(\mathbf{v}')\\ &= 2G^2 m_\mathrm{p}\log\Lambda\,\frac{\partial}{\partial v_i}\int \mathrm{d}\hat{k}\int \mathrm{d}v'\,\delta[\hat{k}\cdot(\mathbf{v}'-\mathbf{v})]F_p(\mathbf{v}')\\ &= 4\pi G^2 m_\mathrm{p}\log\Lambda\,\frac{\partial}{\partial v_i}\int \mathrm{d}v'\,\frac{F_p(\mathbf{v}')}{|\mathbf{v}-\mathbf{v}'|}, \end{aligned} \tag{3.40}$$

and

$$\begin{aligned}D_{ij} &= 4G^2 m_{\mathrm{p}} \log\Lambda \int \mathrm{d}\hat{k}\, \hat{k}_i \hat{k}_j \int \mathrm{d}v'\, \delta[\hat{k}\cdot(\mathbf{v}'-\mathbf{v})] F_p(\mathbf{v}') \\ &= 2G^2 m_{\mathrm{p}} \log\Lambda \frac{\partial^2}{\partial v_i \partial v_j} \int \mathrm{d}\hat{k} \int \mathrm{d}v'\, |\hat{k}\cdot(\mathbf{v}'-\mathbf{v})| F_p(\mathbf{v}') \\ &= 4\pi G^2 m_{\mathrm{p}} \log\Lambda \frac{\partial^2}{\partial v_i \partial v_j} \int \mathrm{d}v'\, |\mathbf{v}-\mathbf{v}'| F_p(\mathbf{v}'),\end{aligned} \tag{3.41}$$

Finally, we can replace these results in the FP equation which leads to

$$\frac{\partial P(\mathbf{v},t)}{\partial t} = 2G^2 m_{\mathrm{p}} \sum_{ij} \frac{\partial}{\partial v_i} \int \mathrm{d}\mathbf{k} \int \mathrm{d}\mathbf{v}' \frac{k_i k_j}{k^4} \delta[\mathbf{k}\cdot(\mathbf{v}-\mathbf{v}')] F_{\mathrm{p}}(\mathbf{v}') \frac{\partial}{\partial v_j} P(\mathbf{v},t). \tag{3.42}$$

This relation is the homogeneous Landau equation for a zero-mass test particle (Landau, 1936) describing the evolution of the probability distribution of the velocity in time. We will retrieve a more precise form of this equation later in this thesis.

3.2.1 Maxwellian Velocity Distribution

Let us take a Maxwellian velocity distribution function,

$$f_p(v_p) = \frac{n}{(2\pi\sigma^2)^{3/2}} e^{-v_p^2/(2\sigma^2)}, \tag{3.43}$$

where n is the number density and σ is the one-dimensional velocity dispersion. Next, we proceed to calculate the diffusion coefficients for this scenario. We will start by the diffusion coefficients in terms of Rosenbluth potentials for a zero-mass test particle in an infinite homogeneous medium (Rosenbluth et al., 1957) given below

$$D[\Delta v_i] = 4\pi G^2 m_{\mathrm{p}} (m + m_{\mathrm{p}}) \ln\Lambda \frac{\partial}{\partial v_i} h(\mathbf{x},\mathbf{v}), \tag{3.44}$$

$$D[\Delta v_i \Delta v_j] = 4\pi G^2 m_{\mathrm{p}}^2 \ln\Lambda \frac{\partial^2}{\partial v_i \partial v_j} g(\mathbf{x},\mathbf{v}), \tag{3.45}$$

The functions $h(\mathbf{x},\mathbf{v})$ and $g(\mathbf{x},\mathbf{v})$ are the Rosenbluth potential given by integrals over the distribution function $f_p(\mathbf{x}_p, \mathbf{v}_p)$ of the field stars

$$h(\mathbf{x},\mathbf{v}) = \int d^3 v_p \frac{f_p(\mathbf{x}_p,\mathbf{v}_p)}{|\mathbf{v}-\mathbf{v}_p|}, \tag{3.46}$$

$$g(\mathbf{x},\mathbf{v}) = \int d^3 v_p\, f_p(\mathbf{x}_p,\mathbf{v}_p) |\mathbf{v}-\mathbf{v}_p|. \tag{3.47}$$

The diffusion coefficients can be simplified in a coordinate system aligned with the velocity vector $\mathbf{v}$ (Binney and Tremaine, 2008).

$$D[\Delta v_\parallel] = -\frac{16\pi^2 G^2 m_{\mathrm{p}}(m+m_{\mathrm{p}})\ln\Lambda}{v^2} \int_0^v dv_p\, v_p^2 f_p(x, v_p), \tag{3.48}$$

$$D[(\Delta v_\parallel)^2] = \frac{32\pi^2 G^2 m_{\mathrm{p}}^2 \ln\Lambda}{3} \left(\int_0^v dv_p \frac{v_p^4}{v^3} f_p(x,v_p) + \int_v^\infty dv_p\, v_p f_p(x,v_p) \right), \tag{3.49}$$

$$D[(\Delta v_\perp)^2] = \frac{32\pi^2 G^2 m_{\mathrm{p}}^2 \ln\Lambda}{3} \left(\int_0^v dv_p \left(\frac{3v_p^2}{v} - \frac{v_p^4}{v^3} \right) f_p(x,v_p) + 2\int_v^\infty dv_p\, v_p f_p(x,v_p) \right). \tag{3.50}$$

Then the velocity distribution mentioned in equation (3.43) is inserted above which after a lengthy process of calculation (found in Appendix A.4) gives the following expressions

$$D[\Delta v_\parallel] = -\frac{4\pi G^2 \rho (m+m_\mathrm{p}) \ln\Lambda}{\sigma^2} G(X), \tag{3.51}$$

$$D[(\Delta v_\parallel)^2] = \frac{4\pi G^2 \rho m_\mathrm{p} \ln\Lambda}{\sigma} \frac{G(X)}{X}, \tag{3.52}$$

$$D[(\Delta v_\perp)^2] = \frac{4\pi G^2 \rho m_\mathrm{p} \ln\Lambda}{\sigma} \left[\frac{\mathrm{erf}(X) - G(X)}{X}\right], \tag{3.53}$$

with $\rho = m_\mathrm{p} n$ and $G(X)$ defined as

$$G(X) = \frac{1}{2X^2}\left(\mathrm{erf}(X) - 2\frac{X}{\sqrt{\pi}} e^{-X^2}\right). \tag{3.54}$$

The Cartesian diffusion coefficients can in general be written as

$$D[\Delta v_i] = \frac{v_i}{v} D[\Delta v_\parallel], \tag{3.55}$$

$$D[\Delta v_i \Delta v_j] = \frac{v_i v_j}{v^2}\left(D[(\Delta v_\parallel)^2] - \frac{1}{2} D[(\Delta v_\perp)^2]\right) + \frac{1}{2}\delta_{ij} D[(\Delta v_\perp)^2] \tag{3.56}$$

where

$$D[\Delta v_\parallel] = 4\pi G^2 m_\mathrm{p} (m+m_\mathrm{p}) \ln\Lambda\, h'(v), \tag{3.57}$$

$$D[(\Delta v_\parallel)^2] = 4\pi G^2 m_\mathrm{p}^2 \ln\Lambda\, g''(v), \tag{3.58}$$

$$D[(\Delta v_\perp)^2] = \frac{8\pi G^2 m_\mathrm{p}^2 \ln\Lambda}{v} g'(v). \tag{3.59}$$

To obtain equation (3.55) and (3.56), we started from equationsA.40 and A.41 and used the fact that the Rosenbluth potentials depend only on v, therefore $\partial v_i/\partial v = v_i/v$. $D[(\Delta v_\parallel)^2]$ is the total diffusion rate parallel to the subject star velocity vector $\mathbf{v}$, while $D[(\Delta v_\perp)^2]$ is the total diffusion rate perpendicular to it.This notation implies that $D[(\Delta v_1)^2] = D[(\Delta v_\parallel)^2]$ for the direction parallel to $\mathbf{v}$ and $D[(\Delta v_2)^2] = D[(\Delta v_3)^2] = D[(\Delta v_\perp)^2]$ for the two-dimensional plane perpendicular to $\mathbf{v}$.

3.3 Density Fluctuation from Field Particles

Until now, the system has been modeled using point-like particles, which are idealized objects with simplifying the analysis. However, the analysis is now being expanded to include a system of extended field particles, a more complex and realistic model. In this model, each particle has a density profile $\rho_n(r) = m_\mathrm{p} W_\varepsilon(r)$ with a scale length ε and $\int \mathrm{d}\mathbf{r}\, W_\varepsilon(|\mathbf{r}|) = 1$. The density fluctuations are now given by

$$\rho(\mathbf{r}, t) = m_\mathrm{p} \sum_n W_\varepsilon(|\mathbf{r} - \mathbf{r}_n - \mathbf{v}_n t|) - \rho_\mathrm{p} \tag{3.60}$$

and their correlation function is

$$C_\rho(\mathbf{r}, t) = m_\mathrm{p} \int \mathrm{d}\mathbf{v} \int \mathrm{d}\mathbf{r}'\, W_\varepsilon(\mathbf{r} - \mathbf{r}' - \mathbf{v}t) W_\varepsilon(\mathbf{r}') F_\mathrm{p}(\mathbf{v}). \tag{3.61}$$

As a result of generalizing the system to extended particles, the density distribution is no longer singular. Instead, a *softened*version of Poisson's equation introduces a modification to account for the finite size of the particles. This can involve regularizing the source term (e.g., using a smooth function instead of a delta function) to avoid the singularities at the particle positions, making the equation more physically realistic and mathematically manageable. In this case, we have

$$\Phi_\varepsilon(\mathbf{r},t) = -G\int \mathrm{d}\mathbf{r}' \int \mathrm{d}\mathbf{r}'' \frac{\rho(\mathbf{r}'',t)}{|\mathbf{r}-\mathbf{r}'|} W_\varepsilon(|\mathbf{r}'-\mathbf{r}''|), \tag{3.62}$$

where $W_\varepsilon(r)$ is the softening kernel. As discussed previously in section 2.3.4, this softening cures the divergence in the Coulomb logarithm at small scales (large wavenumbers). The Fourier transform of the softened potential is

$$\widehat{\Phi}_\varepsilon(\mathbf{k},\omega) = -4\pi G\,\widehat{\rho}(\mathbf{k},\omega)\widehat{W}_\varepsilon(k)\,/k^2. \tag{3.63}$$

The diffusion coefficient is the same as in equation (3.41), while the Coulomb logarithm is

$$\log\Lambda_{\mathrm{soft}} = \int_{k_{\min}}^{k_{\max}} \frac{\mathrm{d}k}{k} |\widehat{W}_\varepsilon(k)|^2. \tag{3.64}$$

If we take the density kernel to be Gaussian,

$$W_\varepsilon(r) = \frac{1}{(2\pi\varepsilon^2)^{3/2}} \mathrm{e}^{-\frac{1}{2}r^2/\varepsilon^2}, \quad \widehat{W}_\varepsilon(\mathbf{k}) = \mathrm{e}^{-\frac{1}{2}k^2\varepsilon^2}, \tag{3.65}$$

then we can let $k_{\max} \to \infty$ and obtain

$$\log\Lambda_{\mathrm{soft}} = \tfrac{1}{2}\Gamma(0, k_{\min}^2\varepsilon^2), \tag{3.66}$$

where $\Gamma(n,x) = \int_x^\infty t^{n-1}\mathrm{e}^{-t}\mathrm{d}t$ is the "upper" incomplete Gamma function. In the limit $k_{\min}\varepsilon \to 0$, this expression is equivalent to $\log\Lambda_{\mathrm{soft}} = -\log(k_{\min}\varepsilon) - \frac{1}{2}\gamma_E + \mathrm{O}(k_{\min}\varepsilon)^2 = \log(b_{\max}/\varepsilon) + \mathrm{O}(1)$ with γ_E the Euler constant. This result is consistent with equation (2.27). The objective is to compute the density correlation function for a Maxwellian velocity distribution.

$$F_{\mathrm{p}}(\mathbf{v}) = \frac{\rho_{\mathrm{p}}}{(2\pi\sigma^2)^{3/2}}\, e^{-\frac{v^2}{2\sigma^2}}, \tag{3.67}$$

In the density correlation function in equation (3.61), we should plug in the density kernel as the following

$$C_\rho(\mathbf{r},t) = m_{\mathrm{p}} \int \mathrm{d}v \int \mathrm{d}r'\, W_\varepsilon(r - r' - vt) W_\varepsilon(r') F_p(v). \tag{3.68}$$

$$\begin{aligned} &= m_{\mathrm{p}} \int d\mathbf{v} \int d\mathbf{r}' \frac{1}{(2\pi\varepsilon^2)^{3/2}} e^{-\frac{1}{2\varepsilon^2}(r-r'-vt)^2} \frac{1}{(2\pi\varepsilon^2)^{3/2}} e^{\frac{-1}{2\varepsilon^2}r'^2} \frac{\rho}{(2\pi\sigma^2)^{3/2}} e^{-\frac{v^2}{2\sigma^2}} \\ &= \frac{m_{\mathrm{p}}\rho}{(2\pi\varepsilon^2)^3\,(2\pi\sigma^2)^{3/2}} \int d\mathbf{v} \int d\mathbf{r}' \exp\left[\frac{-1}{2\varepsilon^2}\left(r^2 + r'^2 + v^2t^2 - 2rr' - 2rvt + 2r'vt\right)\right] \\ &\times \exp\left[\frac{-1}{2\varepsilon^2}\left(r'^2\right)\right] \exp\left(\frac{-v^2}{2\sigma^2}\right) \end{aligned} \tag{3.69}$$

For simplification, let us call the constant outside the integral A and rewrite the above relation

$$C_p = A\int dve^{-\frac{v^2}{2\sigma^2}} \exp\left[\frac{-1}{2\varepsilon^2}\left(r^2+v^2t^2-2rvt\right)\right] \underbrace{\int dr' \exp\left[\frac{-1}{2\varepsilon^2}\left(2r'^2+r'(-2r+2vt)\right]\right.}_{I} \tag{3.70}$$

where I is clearly a Gaussian integral

$$\int_{-\infty}^{\infty} e^{-(ax^2+bx)} = e^{\frac{b^2}{4a}}\sqrt{\frac{\pi}{a}} \tag{3.71}$$

Thus

$$\left\{\begin{array}{l} a = \frac{1}{\varepsilon^2} \\ \\ b = \frac{r-vt}{\varepsilon^2} \end{array}\right. \rightarrow \left\{\begin{array}{l} \left(\frac{\pi}{a}\right)^{3/2} = \varepsilon^3\pi^{3/2} \\ \\ \frac{b^2}{4a} = \frac{r^2+v^2t^2-2vtr}{4\varepsilon^2}. \end{array}\right. \tag{3.72}$$

Putting this result together with the whole integral we will obtain the following

$$\begin{aligned} C_\rho &= A\varepsilon^3\pi^{3/2}\int dd\mathbf{v} \exp\left[\frac{-1}{2\varepsilon^2}\left(r^2+v^2t^2-2rvt\right)\right] \\ &\times \exp\left[\frac{1}{4\varepsilon^2}\left(r^2+v^2t^2-2rvt\right)\right]\exp\left(\frac{-v^2}{2\sigma^2}\right) \\ &= A\varepsilon^3\pi^{3/2}\int d\mathbf{v} \exp\left(\frac{-r^2}{4\varepsilon^2}-\frac{v^2t^2}{4\varepsilon^2}+\frac{rvt}{2\varepsilon^2}-\frac{v^2}{2\sigma^2}\right) \\ &= A\varepsilon^3\pi^{3/2}\exp\left(\frac{-r^2}{4\varepsilon^2}\right)\int d\mathbf{v} \exp\left[-v^2\underbrace{\left(\frac{t^2}{4\varepsilon^2}+\frac{1}{2\sigma^2}\right)}_{P}+v\underbrace{\left(\frac{rt}{2\varepsilon^2}\right)}_{b}\right] \end{aligned} \tag{3.73}$$

Another Gaussian integral arises in the calculations above for which we have

$$\left\{\begin{array}{l} \left(\frac{\pi}{a}\right)^{3/2} = \left(\frac{8\pi\varepsilon^2\sigma^2}{2t^2\sigma^2+4\varepsilon^2}\right)^{3/2} = \left(\frac{2\pi\sigma^2}{\left[1+\left(\frac{\sigma t}{\sqrt{2}\varepsilon}\right)\right]^2}\right)^{3/2} \\ \\ \frac{b^2}{4a} = \frac{r^2t^2}{4\varepsilon^4}\frac{2\sigma^2}{4\left(1+\left(\frac{\sigma t}{\sqrt{2}\varepsilon}\right)^2\right)} = \frac{\sigma^2t^2r^2}{8\varepsilon^4\left(1+\left(\frac{\sigma t}{\sqrt{2}\varepsilon}\right)^2\right)} \end{array}\right. \tag{3.74}$$

Note that the integral is over $\mathbf{v}$. So it is a 3-D integral and that is the reason for the power 3/2. Consequently, we will arrive at

$$C_\rho = A\varepsilon^3\pi^{3/2}\left(\frac{2\pi\sigma^2}{1+\left(\frac{\sigma t}{\sqrt{2}\varepsilon}\right)^2}\right)^{3/2}\exp\left(-\frac{r^2}{4\varepsilon^2}\right)\exp\left(\frac{\sigma^2t^4r^2}{8\varepsilon^4\left(1+\left(\frac{\sigma t}{\sqrt{2}\varepsilon}\right)^2\right)}\right) \tag{3.75}$$

First of all, we will workout the exponential part of the above result

$$\exp\left[-\frac{r^2}{4\varepsilon^2}\left(1-\frac{\sigma^2t^2}{2\varepsilon^2\left(1+\left(\frac{\sigma t}{\sqrt{2}\varepsilon}\right)^2\right)}\right)\right], \tag{3.76}$$

and for the constant of our calculations we have

$$
\begin{aligned}
const &= \frac{m_{\mathrm{p}}\rho_p}{(2\pi\varepsilon^2)^3(2\pi\sigma^2)^{3/2}}\varepsilon^3\pi^{3/2}\left(\frac{2\pi\sigma^2}{\left[1+\left(\frac{\sigma t}{\sqrt{2}\varepsilon}\right)^2\right]}\right)^{3/2} \\
&= \frac{m_{\mathrm{p}}\rho_p}{8\pi^{3/2}\varepsilon^3}\frac{1}{\left[1+\left(\frac{\sigma t}{\sqrt{2}\varepsilon}\right)^2\right]^{3/2}}
\end{aligned}
\tag{3.77}
$$

Finally the density correlation function will be

$$
C_\rho(\mathbf{r},t) = \frac{m_{\mathrm{p}}\rho_b}{8\pi^{3/2}\varepsilon^3\left[1+\left(\frac{\sigma t}{\sqrt{2}\varepsilon}\right)^2\right]^{3/2}}\exp\left[-\frac{\left(\frac{r}{2\varepsilon}\right)^2}{1+\left(\frac{\sigma t}{\sqrt{2}\varepsilon}\right)^2}\right]. \tag{3.78}
$$

The expression for the force correlation function $\langle \mathbf{F}(\mathbf{r},t)\cdot\mathbf{F}(\mathbf{r}',t')\rangle = C_F(\mathbf{r}-\mathbf{r}',t-t')$ is

$$
C_F(r,t) = 4\pi G^2\int \mathrm{d}r'\,\frac{C_\rho(r',t)}{|r-r'|} \tag{3.79}
$$

Now we can substitute the density correlation function in the integral

$$
C_F(\mathbf{r},t) = 4\pi G^2\int \mathrm{d}\mathbf{r}'\,\frac{1}{|\mathbf{r}-\mathbf{r}'|}\frac{m_{\mathrm{p}}\rho_b}{8\pi^{3/2}\varepsilon^3\left[1+\left(\frac{\sigma t}{\sqrt{2}\varepsilon}\right)^2\right]^{3/2}}\exp\left[-\frac{(r'/2\varepsilon)^2}{1+\left(\frac{\sigma t}{\sqrt{2}\varepsilon}\right)^2}\right]. \tag{3.80}
$$

Next step is to factor out the constants that do not depend on r' from the integral

$$
\begin{aligned}
C_F(r,t) &= \frac{4\pi G^2 m_{\mathrm{p}}\rho_b}{8\pi^{3/2}\varepsilon^3\left[1+\left(\frac{\sigma t}{\sqrt{2}\varepsilon}\right)^2\right]^{3/2}}\int\frac{\mathrm{d}r'}{|r-r'|}\exp\left[-\frac{(r'/2\varepsilon)^2}{1+\left(\frac{\sigma t}{\sqrt{2}\varepsilon}\right)^2}\right] \\
&= \frac{4\pi G^2 m_{\mathrm{p}}\rho_b}{r}\,\mathrm{erf}\left[\frac{r/2\varepsilon}{\sqrt{1+(\sigma t/\sqrt{2}\varepsilon)^2}}\right].
\end{aligned}
\tag{3.81}
$$

From this result, we can obtain the force correlation function. In general, it is given by

$$
\langle \mathbf{F}(\mathbf{r},t)\cdot\mathbf{F}(\mathbf{r}',t')\rangle = C_F(\mathbf{r}-\mathbf{r}',t-t') \tag{3.82}
$$

Once we substitute equation (3.81), it yields

$$
C_F(\mathbf{r},t) = 4\pi G^2\int \mathrm{d}\mathbf{r}'\frac{C_\rho(\mathbf{r}',t)}{|\mathbf{r}-\mathbf{r}'|} = \frac{4\pi G^2 m_{\mathrm{p}}\rho_{\mathrm{b}}}{r}\mathrm{erf}\left[\frac{r/2\varepsilon}{\sqrt{1+(\sigma t/\sqrt{2}\varepsilon)^2}}\right], \tag{3.83}
$$

which in the limit $\varepsilon \to 0$ asymptotes to (Cohen, 1975)

$$C_F(\mathbf{r}, t) \sim \frac{4\pi G^2 m_{\mathrm{p}} \rho_{\mathrm{b}}}{r} \mathrm{erf}\left(\frac{r}{\sqrt{2}\sigma t}\right). \tag{3.84}$$

This shows that the force correlation has a long-range nature, with the correlation function decaying as $1/r$ which is a typical behavior in gravitational systems. Moreover, it is apparent that as time increases, the system reaches a state of relaxed equilibrium, with the forces between particles becoming less correlated over time, especially for larger distances.

4 Landau Equation and Relaxation in FDM Halos

In this chapter, we extend the derivation from the previous chapter to the case where a zero-mass test particle is diffused by an FDM halo. This modification involves considering the wave-like properties of FDM and how they influence the diffusion and dynamics of test particles. We then further extend the relaxation process by incorporating the effect of dynamical friction, providing a more comprehensive model that includes both the gravitational and quantum contributions to the particle's evolution.

To emphasize the relationship between classical and quantum scenarios, we will approach the problem in a systematic manner. First, we examine the relaxation of classical particles under the influence of a classical halo, where the dynamics are governed solely by gravitational forces. Next, we consider the relaxation of classical particles in the presence of an FDM halo, where quantum effects from the FDM are introduced and the test particle experiences additional diffusive forces due to the quantum pressure of the halo. Finally, we explore the self-relaxation of an FDM halo, where the halo's own quantum properties lead to a dynamical evolution influenced by both self-gravity and the quantum potential, creating a feedback loop in the system.

Throughout these cases, we will draw connections between the classical and quantum descriptions, highlighting how the introduction of FDM modifies the relaxation processes and comparing these to the classical case. By doing so, we aim to deepen our understanding of the role of quantum effects in the evolution of dark matter halos and their impact on the dynamics of test particles within them.

4.1 Relaxation by FDM

In this section, we specifically focus on how stochastic density fluctuations from an FDM halo lead to the diffusion of a zero-mass test particle. These fluctuations arise primarily due to the quantum mechanical nature of FDM, namely the interference patterns of the quantum waves resulting in spatial and temporal density variations within the halo (Hu et al., 2000). According to Ruffini and Bonazzola (1969), the dynamics of the scalar field ψ which describes the wave function of FDM, is governed by the Schrödinger-Poisson coupled system

$$\mathrm{i}\hbar\frac{\partial}{\partial t}\psi(\mathbf{r},t) = -\frac{\hbar^2}{2m_\mathrm{b}}\nabla^2\psi(\mathbf{r},t) + m_\mathrm{b}\Phi(\mathbf{r},t)\psi(\mathbf{r},t), \tag{4.1}$$

$$\nabla^2\Phi(\mathbf{r},t) = 4\pi G|\psi(\mathbf{r},t)|^2. \tag{4.2}$$

Here, m_b is the mass of the FDM particle, $\Phi(\mathbf{r},t)$ is the gravitational potential, and we have assumed that the wavefunction is normalized such that $|\psi(\mathbf{r},t)|^2 = \rho$. The Schrödinger equation describes the evolution of the scalar field $\psi(\mathbf{r},t)$ under its own self-gravity and the Poisson equation describes how the gravitational potential evolves in response to the matter density. The FDM wavefunction can be expanded as a collection of plane waves,

$$\psi(\mathbf{r},t) = \int \mathrm{d}\mathbf{k}\,\varphi(\mathbf{k})\,\mathrm{e}^{\mathrm{i}\mathbf{k}\cdot\mathbf{r}-\mathrm{i}\omega(k)t}, \tag{4.3}$$

where the dispersion relation describes

$$\omega(k) = \frac{\hbar k^2}{2m_\mathrm{b}}. \tag{4.4}$$

Note that we are neglecting gravitational interactions between FDM particles in order to keep the consistency with the classical cases studies earlier. This assumption is similar to the Jeans swindle and is valid when the typical de Broglie wavelength is much smaller than the scale of the system. In addition, assuming each plane wave to have a random phase, as is expected if they arrive in the vicinity of the test particle from large distances and different directions, we can write

$$\langle\varphi(\mathbf{k})\rangle = 0, \quad \langle\varphi(\mathbf{k})\,\varphi(\mathbf{k}')\rangle = 0 \quad \text{for} \quad \mathbf{k} \neq \mathbf{k}'. \tag{4.5}$$

We also assume that

$$\langle\varphi(\mathbf{k})\,\varphi^*(\mathbf{k}')\rangle = f_k(\mathbf{k})\,\delta(\mathbf{k}-\mathbf{k}'). \tag{4.6}$$

where $f_k(\mathbf{k})$ is a distribution function defined such that the mean or ensemble-average mass density in the volume $\mathrm{d}\mathbf{k}$ around $\mathbf{k}$ is $f_k(\mathbf{k})\mathrm{d}\mathbf{k}$.

It is crucial to determine exactly in which limit we are studying FDM to assure whether it should be treated with quantum mechanics or classical physics. The aformentioned assumptions are only valid when the typical de Broglie angular wavelength λ_σ is much larger than the typical distance between FDM particles, $d = (m_\mathrm{b}/\rho_\mathrm{b})^{1/3}$. Thus, we can not generalize the results of this section just by moving to the classical limit $\hbar \to 0$. When the mass of the FDM particle is sufficiently large, specifically $m_\mathrm{s} \approx (\rho_\mathrm{b}\hbar^3/\sigma^3)^{1/4}$, the system's behavior approaches the classical limit. However, classical behavior requires a mass $m_\mathrm{c} \approx \left(\frac{\hbar T_\mathrm{d}}{2}\right)^{3/5}\rho_\mathrm{b}^{2/5}$, so that the position uncertainty is small enough compared to the particle separation (See Appendix A.5). Furthermore, when the particle mass exceeds m_s, the diffusion coefficients approach their classical values, but the system itself may not yet be classical. The classical contribution to the relaxation process becomes negligible at reasonable dark matter particle masses, which are typically far smaller than $m_\mathrm{c} \approx 10^{16}\,\mathrm{eV}$.

Although the system involves quantum mechanics through the wave function and dispersion relation (equations 4.3 and 4.4), the derivations are framed within a classical field theory perspective, with quantum behavior manifesting in the quadratic dispersion relation. The density fluctuations of the FDM field are described as

$$\rho(\mathbf{r},t) = |\psi(\mathbf{r},t)|^2 - \rho_\mathrm{b}, \tag{4.7}$$

where ρ_b is the mean density of the FDM field, $\rho_\mathrm{b} = \langle|\psi(\mathbf{r},t)|^2\rangle = \int \mathrm{d}\mathbf{k}\, f_k(\mathbf{k})$, and the fluctuation is the difference between the square of the field amplitude and this mean density. According to equation (4.3) the density fluctuation can be written as

$$\rho(\mathbf{r},t) = \int \mathrm{d}\mathbf{k} \int \mathrm{d}\mathbf{k}'\varphi(\mathbf{k})\,\varphi^*(\mathbf{k}')\,\mathrm{e}^{\mathrm{i}(\mathbf{k}-\mathbf{k}')\cdot\mathbf{r} - \mathrm{i}[\omega(k)-\omega(k')]t} - \rho_\mathrm{b}. \tag{4.8}$$

Based on equations equation (4.5) and equation (4.6) we conclude that

$$\begin{aligned}\langle\varphi(\mathbf{k}_1)\varphi^*(\mathbf{k}_2)\varphi^*(\mathbf{k}_3)\varphi(\mathbf{k}_4)\rangle &= f_k(\mathbf{k}_1)f_k(\mathbf{k}_3)\delta(\mathbf{k}_1-\mathbf{k}_2)\delta(\mathbf{k}_3-\mathbf{k}_4) \\ &\quad + f_k(\mathbf{k}_1)f_k(\mathbf{k}_2)\delta(\mathbf{k}_1-\mathbf{k}_3)\delta(\mathbf{k}_2-\mathbf{k}_4).\end{aligned} \tag{4.9}$$

Therefore, the density correlation function and its Fourier transform are

$$C_\rho(\mathbf{r},t) = \int \mathrm{d}\mathbf{k} \int \mathrm{d}\mathbf{k}' f_k(\mathbf{k}) f_k(\mathbf{k}')\,\mathrm{e}^{\mathrm{i}(\mathbf{k}-\mathbf{k}')\cdot\mathbf{r} - \mathrm{i}[\omega(k)-\omega(k')]t}, \tag{4.10}$$

$$\widehat{C}_\rho(\mathbf{k},\omega) = (2\pi)^4 \int \mathrm{d}\mathbf{k}' \int \mathrm{d}\mathbf{k}'' f_k(\mathbf{k}') f_k(\mathbf{k}'')\delta(\mathbf{k}-\mathbf{k}'+\mathbf{k}'')\,\delta[\omega-\omega(k')+\omega(k'')], \tag{4.11}$$

or alternatively, considering that each plane wave travels with velocity $\mathbf{v} = \hbar\mathbf{k}/m_\mathrm{b}$, and its velocity distribution function is given by $F_\mathrm{b}(\mathbf{v})\mathrm{d}\mathbf{v} = f_k(\mathbf{k})\mathrm{d}\mathbf{k}$, we can write

$$\widehat{C}_\rho(\mathbf{k},\omega) = (2\pi)^4 \int \mathrm{d}\mathbf{v}_1 \int \mathrm{d}\mathbf{v}_2\, F_\mathrm{b}(\mathbf{v}_1) F_\mathrm{b}(\mathbf{v}_2) \delta\left(\mathbf{k} - \frac{2m_\mathrm{b}}{\hbar}\mathbf{v}_\mathrm{d}\right) \delta\left(\omega - \frac{2m_\mathrm{b}}{\hbar}\mathbf{v}_\mathrm{c}\cdot\mathbf{v}_\mathrm{d}\right). \quad (4.12)$$

where $\mathbf{v}_\mathrm{c} = (\mathbf{v}_1 + \mathbf{v}_2)/2$ and $\mathbf{v}_\mathrm{d} = (\mathbf{v}_1 - \mathbf{v}_2)/2$. In this case, the spatial correlation is directly tied to the velocity difference between particles. This is distinct from the classical scenario where spatial correlation is associated with the distance traveled by a particle over a given time t (see equation (3.35)). Therefore, truncating the integrals at large and small scales reflects a focus on a specific range of velocity differences, which can make the problem more tractable while capturing the most relevant dynamics (Bar-Or et al., 2019).

In the following, we will retrieve the diffusion coefficients for this case. Starting from the simple form of the second diffusion coefficient derived earlier (equation (3.32))

$$D_{ij} = \frac{2G^2}{\pi} \int \frac{k_i k_j}{k^4} \hat{C}_\rho(\mathbf{k}, \mathbf{k}\cdot\mathbf{v})\, d\mathbf{k}. \quad (4.13)$$

Then by substituting the density correlation function, D_{ij} becomes

$$\begin{aligned} D_{ij} &= \frac{2(2\pi)^4 G^2}{\pi} \int d\mathbf{k} \frac{k_i k_j}{k^4} \int d\mathbf{v}_1 \int d\mathbf{v}_2\, F_b(\mathbf{v}_1) F_b(\mathbf{v}_2)\, \delta\left(\mathbf{k} - \frac{2m_b}{\hbar}\mathbf{v}_d\right) \delta\left(\omega - \frac{2m_b}{\hbar}\mathbf{v}_c\cdot\mathbf{v}_d\right) \\ &= 32\pi^3 G^2 \left(\frac{2m_b}{\hbar}\right)^{-2} \int \frac{v_d^i v_d^j}{v_d^4} \int d\mathbf{v}_c \int d\mathbf{v}_d\, F_b(\mathbf{v}_c + \mathbf{v}_d) F_b(\mathbf{v}_c - \mathbf{v}_d) \\ &\times \delta\left(\frac{2m_b}{\hbar}\mathbf{v}_d\cdot\mathbf{v} - \frac{2m_b}{\hbar}\mathbf{v}_d\cdot\mathbf{v}_c\right) \\ &= \frac{32\pi^3 G^2 \hbar^3}{m_b^3} \int \frac{v_d^i v_d^j}{v_d^5} \int d\mathbf{v}_c \int d\mathbf{v}_d\, F_b(\mathbf{v}_c + \mathbf{v}_d) F_b(\mathbf{v}_c - \mathbf{v}_d)\, \delta\left(\hat{\mathbf{v}}_d\cdot\mathbf{v} - \hat{\mathbf{v}}_d\cdot\mathbf{v}_c\right), \end{aligned} \quad (4.14)$$

with $\widehat{\mathbf{v}}_\mathrm{d} \equiv v_d\widehat{\mathbf{k}}$ being the unit vector in the direction of $\mathbf{v}_\mathrm{d}$. We used $d\mathbf{v}_1\, d\mathbf{v}_2 = d\mathbf{v}_c\, d\mathbf{v}_d$. In the second line, we replaced $\mathbf{k}$ with $\frac{2m_b}{\hbar}v_d$ because of the first delta function which in this case, gives us $\int d\mathbf{k}\delta\left(\mathbf{k} - \frac{2m_b}{\hbar}\mathbf{v}_d\right) = 1$. Also note that we utilized the following relation to yield the final result

$$\delta\left(\frac{2m_b}{\hbar}\mathbf{v}_d\cdot\mathbf{v} - \frac{2m_b}{\hbar}\mathbf{v}_d\cdot\mathbf{v}_c\right) = \frac{\hbar}{2m_b v_d}\delta\left(\hat{\mathbf{v}}_d\cdot\mathbf{v} - \hat{\mathbf{v}}_d\cdot\mathbf{v}_c\right). \quad (4.15)$$

To elaborate more on the result in equation (4.14), it is worth mentioning that $F_\mathrm{b}(\mathbf{v}_\mathrm{c} \pm \mathbf{v}_\mathrm{d}) \approx F_\mathrm{b}(\mathbf{v}_\mathrm{c})$. This approximation is justified based on the wave nature of FDM through the following reasoning: The interval on which the integral is being computed is $(k_\mathrm{min}, k_\mathrm{max})$. Since the velocity is related to the wavenumber by $\hbar k/m_b$, we ignore wavenumbers smaller than $k_\mathrm{min} = \frac{1}{b_\mathrm{max}}$, which translates to ignoring velocities smaller than $v_\mathrm{min} = \frac{\hbar}{2m_b b_\mathrm{max}}$. This velocity is also expressed as $v_\mathrm{min} = \frac{\sigma\bar{\sigma}}{2b_\mathrm{max}}$, where $\bar{\sigma} = \frac{\hbar}{m_b\sigma}$ is the typical de Broglie wavelength. So the integration must cut off for $|\mathbf{v}_\mathrm{d}| < v_{d,\mathrm{min}}$, since the integrals over $\mathbf{v}_\mathrm{d}$ diverge logarithmically as $|\mathbf{v}_\mathrm{d}| \to 0$. On the other hand, note that we may also cut off the integration when $|\mathbf{v}_\mathrm{d}| > v_{d,\mathrm{max}}$, where $v_{d,\mathrm{max}} \lesssim \sigma$ so that we stay in the right limit. This is because the integral is dominated by the region $|\mathbf{v}_\mathrm{d}| \ll |\mathbf{v}_\mathrm{c}|$

(Bar-Or et al., 2019). Now we are able to simplify equation (4.14) in the following way

$$
\begin{aligned}
D_{ij} &= \frac{32\pi^3 G^2 \hbar^3}{m_\mathrm{b}^3} \log \Lambda_\mathrm{FDM} \int \mathrm{d}\widehat{\mathbf{k}}\, \widehat{k}_i \widehat{k}_j \int \mathrm{d}\mathbf{v}' F_\mathrm{b}^2(\mathbf{v}') \delta[\widehat{\mathbf{k}}\cdot(\mathbf{v}-\mathbf{v}')] \\
&= 4G^2 m_\mathrm{eff} \log \Lambda_\mathrm{FDM} \int \mathrm{d}\widehat{\mathbf{k}}\, \widehat{k}_i \widehat{k}_j \int \mathrm{d}\mathbf{v}' \delta[\widehat{\mathbf{k}}\cdot(\mathbf{v}-\mathbf{v}')] F_\mathrm{eff}(\mathbf{v}'),
\end{aligned} \tag{4.16}
$$

and

$$
D_i = 4\pi G^2 m_\mathrm{eff} \log \Lambda_\mathrm{FDM} v_i \int \mathrm{d}\mathbf{v}' \frac{F_\mathrm{eff}(\mathbf{v}')}{|\mathbf{v}-\mathbf{v}'|}. \tag{4.17}
$$

where the effective mass is

$$
m_\mathrm{eff} = \frac{(2\pi\hbar)^3 \int \mathrm{d}\mathbf{v}\, F_\mathrm{b}^2(\mathbf{v})}{m_\mathrm{b}^3 \int \mathrm{d}\mathbf{v}\, F_\mathrm{b}(\mathbf{v})}. \tag{4.18}
$$

and the effective distribution function is

$$
F_\mathrm{eff}(\mathbf{v}) = \frac{\int \mathrm{d}\mathbf{v}\, F_\mathrm{b}(\mathbf{v})}{\int \mathrm{d}\mathbf{v}\, F_\mathrm{b}^2(\mathbf{v})} F_\mathrm{b}^2(\mathbf{v}), \tag{4.19}
$$

and is normalized such that $\int \mathrm{d}\mathbf{v}\, F_\mathrm{eff}(\mathbf{v}) = \rho_\mathrm{b}$. Also note that the Coulomb factor is $\log \Lambda_\mathrm{FDM} = \log(v_{d,\max}/v_{d,\min}) = \log(2b_\mathrm{max}/_\sigma) + \mathrm{O}(1)$ (see equation (2.29)). As Bar-Or et al. (2019) argues, examining these diffusion coefficients closely, we find that they align with equation (3.40) and (3.41), originally derived for classical particles. However, several key modifications apply: the particle mass m_p is replaced by the effective mass m_eff, the velocity distribution function $F_\mathrm{b}(\mathbf{v})$ is substituted with the effective distribution function $F_\mathrm{eff}(\mathbf{v})$, and the Coulomb logarithm $\log \Lambda$ is adjusted to $\log \Lambda_\mathrm{FDM}$. Essentially, the halo behaves as though it consists of quasiparticles with an effective mass m_eff, which varies depending on the local density and velocity distribution within the halo. Thus, we demonstrated that the analogy proposed by Hui et al. (2017) that the diffusion coefficients in an FDM halo are the same as a N-body system composed of halo of classical particles with an effective mass $m_\mathrm{eff} \sim \rho\lambda^3$ holds.

These findings offer a straightforward framework for determining the diffusion coefficients for a zero-mass test particle in an FDM halo. Now we can take the effective distribution function to be Maxwellian with the same density and a velocity dispersion $\sigma_\mathrm{eff} = \sigma/\sqrt{2}$. In this case, we the Coulomb logarithm is estimated better. We find

$$
\begin{aligned}
\log \Lambda_\mathrm{FDM} &= \int_{v_{d,\min}}^{\infty} \frac{\mathrm{d}v}{v} \mathrm{e}^{-v^2/\sigma^2} = \tfrac{1}{2}\Gamma(0, v_{d,\min}^2/\sigma^2) \\
&= \log(\sigma/v_{d,\min}) - \tfrac{1}{2}\gamma_E + \mathrm{O}(v_{d,\min}/\sigma)^2.
\end{aligned} \tag{4.20}
$$

Then substituting $v_{d,\min} \simeq \sigma_\sigma/(2b_\mathrm{max})$ leads to

$$
\log \Lambda_\mathrm{FDM} = \tfrac{1}{2}\Gamma(0, \tfrac{1}{4}\lambda_\sigma^2/b_\mathrm{max}^2) = \log(2b_\mathrm{max}/\lambda_\sigma) - \tfrac{1}{2}\gamma_E + \mathrm{O}(\lambda_\sigma/b_\mathrm{max})^2, \tag{4.21}
$$

which is equivalent to the classical case with a softening scale $\varepsilon = \lambda_\sigma/2$ (3.66). Furthermore, the effective mass in terms of the typical de Broglie wavelength $\lambda_\sigma = h/(m_\mathrm{b}\sigma)$ is

$$
m_\mathrm{eff} = \frac{\pi^{3/2}\hbar^3\rho_\mathrm{b}}{m_\mathrm{b}^3\sigma^3} = \rho_\mathrm{b}\left(f\lambda_\sigma\right)^3, \tag{4.22}
$$

where $f = 1/(2\sqrt{\pi}) = 0.282$.

Since the diffusion coefficients are derived from the density correlation function, we can also proceed with deriving the density correlation function for our particular case and compare it with a classical system having a Maxwellian velocity distribution. Starting with the definition of the density correlation function

$$C_\rho(\mathbf{r},t) = \int \mathrm{d}\mathbf{k} \int \mathrm{d}\mathbf{k}' f_k(\mathbf{k}) f_k(\mathbf{k}')\, \mathrm{e}^{\mathrm{i}(\mathbf{k}-\mathbf{k}')\cdot\mathbf{r} - \mathbf{i}[\omega(k)-\omega(k')]t}, \tag{4.23}$$

we compute it for a Maxwellian velocity distribution.

$$F_\mathrm{p}(\mathbf{v}) = \frac{\rho_\mathrm{p}}{(2\pi\sigma^2)^{3/2}} \mathrm{e}^{-v^2/\left(2\sigma^2\right)} \tag{4.24}$$

Knowing that $F_\mathrm{p}(\mathbf{v})\mathrm{d}\mathbf{v} = \mathrm{d}\mathbf{k} f_k(\mathbf{k})$ and $\mathbf{v} = \frac{\hbar\mathbf{k}}{m_b}$ we will arrive at the following

$$f_k(\mathbf{k}) = F_\mathrm{p}(\mathbf{v}) \left(\frac{m_b}{\hbar}\right)^3 \tag{4.25}$$

Inserting these into 4.23 we find

$$C_\rho(\mathbf{r},t) = \left(\frac{m_b}{\hbar}\right)^6 \int \mathrm{d}\mathbf{k} \int \mathrm{d}\mathbf{k}' \frac{\rho_\mathrm{b}}{(2\pi\sigma^2)^{3/2}} \mathrm{e}^{-\frac{(\hbar k)^2}{2m_b^2\sigma^2}} \frac{\rho_\mathrm{b}}{(2\pi\sigma^2)^{3/2}} \mathrm{e}^{-\frac{(\hbar k')^2}{2m_b^2\sigma^2}} \mathrm{e}^{\mathrm{i}(\mathbf{k}-\mathbf{k}')\cdot\mathbf{r} - \mathbf{i}[\omega(k)-\omega(k')]t} \tag{4.26}$$

Since $\omega(k) = \frac{\hbar k^2}{2m}$ we can rewrite 4.26 as below

$$C_\rho(\mathbf{r},t) = \left(\frac{m_b}{\hbar}\right)^6 \frac{\rho_\mathrm{b}^2}{(2\pi\sigma^2)^3} \int \mathrm{d}\mathbf{k} \int \mathrm{d}\mathbf{k}' \mathrm{e}^{-\frac{\hbar^2 k^2}{2m_b^2\sigma^2}} \mathrm{e}^{-\frac{\hbar^2 k'^2}{2m_b^2\sigma^2}} \mathrm{e}^{\mathrm{i}(\mathbf{k}-\mathbf{k}')\cdot\mathbf{r} - \mathbf{i}\left(\frac{\hbar k^2}{2m_b} - \frac{\hbar k'^2}{2m_b}\right)t} \tag{4.27}$$

or more simply

$$C_\rho(\mathbf{r},t) = \left(\frac{m_b}{\hbar}\right)^6 \frac{\rho_\mathrm{b}^2}{(2\pi\sigma^2)^3} \int \mathrm{d}\mathbf{k} \mathrm{e}^{-\left(\frac{\hbar^2}{2m_b^2\sigma^2} + i\frac{\hbar t}{2m_b}\right)k^2 + ir\cdot\mathbf{k}} \times \int \mathrm{d}\mathbf{k}' \mathrm{e}^{-\left(\frac{\hbar^2}{2m_b^2\sigma^2} - i\frac{\hbar t}{2m_b}\right)k'^2 - ir\cdot\mathbf{k}'} \tag{4.28}$$

which is the multiplication of two Gaussian integrals. We use the relation below

$$\int_{-\infty}^{\infty} e^{ax^2+bx} = e^{\frac{b^2}{4a}} \sqrt{\frac{\pi}{a}} \tag{4.29}$$

In our case

$$\begin{cases} a = \frac{\hbar}{2m}\left(\frac{\hbar}{m\sigma^2} + it\right) = \frac{\lambda\sigma}{2}\left(\frac{\lambda}{\sigma} + it\right) = \frac{\lambda^2}{2}\left(1 + \frac{it\sigma}{\lambda}\right), b = ir \\ a' = \frac{\hbar}{2m}\left(\frac{\hbar}{m\sigma^2} - it\right) \frac{\lambda\sigma}{2}\left(\frac{\lambda}{\sigma} - it\right) = \frac{\lambda^2}{2}\left(1 - \frac{it\sigma}{\lambda}\right), b' = -ir \end{cases} \tag{4.30}$$

Therefore, for the exponential term of 4.29 we will have the following

$$
\begin{aligned}
&\exp\left[\frac{1}{4}\left(\frac{b^2}{a}+\frac{b'^2}{a'}\right)\right] \\
&=\exp\left[\frac{1}{4}\left(\frac{-2m_b r^2}{\hbar\left(\frac{\hbar}{m_b\sigma^2}+it\right)}+\frac{2m_b r^2}{\hbar\left(\frac{\hbar}{m_b\sigma^2}-it\right)}\right)\right] \\
&=\exp\left[\frac{m_b r^2}{2\hbar}\left(\frac{-m_b\sigma^2}{\hbar+itm_b\sigma^2}+\frac{m_b\sigma^2}{\hbar-itm_b\sigma^2}\right)\right] \\
&=\exp\left[\frac{r^2m_b^2\sigma^2}{2\hbar^2}\left(\frac{-2\hbar}{\hbar^2+t^2m_b^2\sigma^4}\right)\right] \\
&=\exp\left[\frac{-r^2}{2\lambda_b^2}\left(\frac{2\hbar}{\hbar\left(1+\left(\frac{\sigma t}{\lambda_b}\right)^2\right)^{1/2}}\right)\right] \\
&=\exp\left[-\frac{\left(r/\lambda_\sigma\right)^2}{1+\left(\sigma t/\lambda_\sigma\right)^2}\right]
\end{aligned}
\tag{4.31}
$$

In the above calculation, we used $\lambda_b=\frac{\hbar}{\sigma m_b}$. Then the constant in 4.28 will be

$$
\begin{aligned}
const. &= \left(\frac{m_b}{\hbar}\right)^6\frac{\rho_{\mathrm{b}}^2}{\left(2\pi\sigma^2\right)^3}\left(\frac{\pi}{a}\right)^{3/2}\left(\frac{\pi}{a'}\right)^{3/2} \\
&= \left(\frac{m_b}{\hbar}\right)^6\frac{\pi^3\rho_{\mathrm{b}}^2}{\left(2\pi\sigma^2\right)^3}\left(\frac{2}{\lambda^2}\right)^3\left(\frac{1}{1+\left(\frac{\sigma t}{\lambda}\right)^2}\right)^{3/2} \\
&= \frac{\rho_b^2\sigma^6\lambda^6}{\sigma^6\lambda^6}\frac{1}{\left(1+\left(\frac{\sigma t}{\lambda}\right)^2\right)^{3/2}}
\end{aligned}
\tag{4.32}
$$

since $m_b/\hbar=\lambda\sigma$. Ultimately, this yields

$$
C_\rho(\mathbf{r},t)=\frac{\rho_b^2}{\left(1+\left(\frac{\sigma t}{\lambda}\right)^2\right)^{3/2}}\exp\left[-\frac{\left(r/\lambda_\sigma\right)^2}{1+\left(\sigma t/\lambda_\sigma\right)^2}\right]
\tag{4.33}
$$

By comparing this result with 3.81, it becomes evident that the density correlation function mirrors that of a classical system with a Maxwellian distribution function characterized by a velocity dispersion $\sigma_{\mathrm{p}}=\sigma_{\mathrm{eff}}$ verifying the claim by Hui et al. (2017). This system features a Gaussian density kernel with a softening parameter $\varepsilon=\lambda_\sigma/2$ and quasiparticles of mass $m_{\mathrm{p}}=m_{\mathrm{eff}}$. It should be noted that equation (4.33) eliminates any ambiguity related to the Coulomb logarithm.

To approximate m_{eff}, we assume a relationship between the density ρ, the radius r, and either the one-dimensional velocity dispersion σ or the circular speed v_{c}, similar to a singular isothermal sphere (Bar-Or et al., 2019)

$$
\rho_{\mathrm{b}}(r)=\frac{\sigma^2}{2\pi Gr^2}=\frac{v_{\mathrm{c}}^2}{4\pi Gr^2}.
\tag{4.34}
$$

This yields the following expression for $m_{\rm eff}$

$$m_{\rm eff} = \frac{\pi^{1/2}\hbar^3}{2^{1/2}Gm_{\rm b}^3 v_{\rm c} r^2} = 1.03\times 10^7 M_\odot \left(\frac{r}{1\,{\rm kpc}}\right)^{-2}\left(\frac{m_{\rm b}}{10^{-22}\,{\rm eV}}\right)^{-3}\left(\frac{v_{\rm c}}{200\,{\rm km\ s^{-1}}}\right)^{-1}. \tag{4.35}$$

The corresponding de Broglie wavelength is given by

$$\lambda_\sigma = \frac{h}{m_{\rm b}\sigma} = 0.85\,{\rm kpc}\left(\frac{m_{\rm b}}{10^{-22}\,{\rm eV}}\right)^{-1}\left(\frac{v_{\rm c}}{200\,{\rm km\ s^{-1}}}\right)^{-1}. \tag{4.36}$$

4.2 Dynamical Friction

Chandrasekhar's theory of dynamical friction describes the deceleration experienced by a massive test particle as it moves through a background medium of lighter particles due to gravitational interactions. This is a fundamental concept in astrophysics, explaining phenomena like the sinking of massive objects (e.g., stars, black holes, or satellite galaxies) into the centers of clusters or halos (Chandrasekhar, 1943).

In this section, we study the influence from an FDM field on a massive particle. The movement of such a particle creates a gravitational wake behind it through the FDM field, which induces a dynamical friction force or drag. Consequently, this force results in an additional contribution to the velocity change for a massive particle (Bar-Or et al., 2019). FDM is expected to suppress the overdensity, reducing the drag.

The objective is to compute the diffusion coefficients with the described assumptions. To begin our calculations, let us work out a relation for the friction force exerted on the test particle, of mass m_t and velocity v_t, and the FDM field with velocity $\mathbf{v} = \hbar\mathbf{k}/m_b$. The FDM field interacts with the test particle gravitationally, but its self-gravity is ignored. As Hui et al. (2017) argues, this is the classic Coulomb scattering problem. To write the frictional force, FDM is taken as a superfluid and we can write the frictional force as a surface integral of the fluid's momentum flux density tensor. After applying the divergence theorem, we arrive at

$$\mathbf{F}_{\rm f} = \int d\mathbf{r}\rho\frac{\partial\Phi}{\partial z}, \tag{4.37}$$

with Φ as the gravitational potential. Here, we assume that the drag is being exerted in z direction. Further, by taking the above integral for a spherical surface, the frictional force on the test particle becomes

$$\mathbf{F}_{\rm f} = -4\pi G^2 m_{\rm t}^2\rho_{\rm b}\frac{\mathbf{v}_{\rm t}-\mathbf{v}}{|\mathbf{v}_{\rm t}-\mathbf{v}|^3}C\left(\beta,\gamma\right), \tag{4.38}$$

where

$$
\begin{aligned}
C =& \frac{e^{\pi\beta}[\Gamma(1-i\beta)]^2}{2\beta}\int_0^{2kr}\mathrm{d}q\Bigg[\left(\frac{kr}{\beta}+1\right)\left(\frac{q}{kr-1}\right)|M(i\beta,1,iq)|^2 \\
&+ q\,\mathrm{Im}\big[M(i\beta,1,iq)^{*}M(i\beta,2,iq)\big] + \beta q|M(i\beta+1,2,iq)|^2\Bigg] \\
=& \frac{e^{\pi\beta}[\Gamma(1-i\beta)]^2}{2\beta}\int_0^{2kr}\mathrm{d}q\,|M(i\beta,1,iq)|^2\left(\frac{q}{kr-2}-\log\frac{q}{2kr}\right), \\
\beta =& \frac{Gm_b m_{\mathrm{t}}}{\hbar|\mathbf{v}_{\mathrm{t}}-\mathbf{v}|}, \\
\gamma =& \frac{m_b b_{\mathrm{max}}}{\hbar}|\mathbf{v}_{\mathrm{t}}-\mathbf{v}|.
\end{aligned}
\tag{4.39}
$$

Here, b_{max} is some large radius around m_{t}, beyond which we assume that the gravitational force from the medium can be ignored. Integrating equation (4.38) over $F_{\mathrm{b}}(\mathbf{v})$, we obtain the rate of velocity drift due to dynamical friction,

$$
D_{\mathrm{f}}[\Delta v_i] = -4\pi G^2 m_{\mathrm{t}}\int\mathrm{d}\mathbf{v}'\,\frac{v_{\mathrm{t},i}-v_i'}{|\mathbf{v}_{\mathrm{t}}-\mathbf{v}'|^3}\,F_{\mathrm{b}}(\mathbf{v}')\,C\left(\frac{Gm_{\mathrm{b}}m_{\mathrm{t}}}{\hbar|\mathbf{v}_{\mathrm{t}}-\mathbf{v}'|},\frac{m_{\mathrm{b}}b_{\mathrm{max}}}{\hbar}|\mathbf{v}_{\mathrm{t}}-\mathbf{v}'|\right). \tag{4.40}
$$

The first diffusion coefficient defined as the rate of change in the particle's velocity due to the frictional force (or the rate of velocity drift) is derived by integrating the frictional force over the distribution function. Therefore, the drift coefficient for a system with smaller de Broglie wavelength compared to the system size is

$$
\begin{aligned}
D_{\mathrm{f}}[\Delta v_i] \simeq& -4\pi G^2 m_{\mathrm{t}}\log\Lambda_{\mathrm{FDM}}\int\mathrm{d}\mathbf{v}'\,\frac{v_i-v_i'}{|\mathbf{v}-\mathbf{v}'|^3}F_{\mathrm{b}}(\mathbf{v}') \\
=& 4\pi G^2 m_{\mathrm{t}}\log\Lambda_{\mathrm{FDM}}v_i\int\mathrm{d}\mathbf{v}'\,\frac{1}{|\mathbf{v}-\mathbf{v}'|}F_{\mathrm{b}}(\mathbf{v}').
\end{aligned}
\tag{4.41}
$$

Comparing this result is with the classical case, it is evident that they are identical. However in this scenario, the Coulomb logarithm is defined by the ratio of the size of the system to the de Broglie wavelength (see equation (2.26) and (2.29)). In addition, $D_{\mathrm{f}}[\Delta v_i]$ is identical to the drift coefficient for a test particle $D_i = D[\Delta v_i]$ derived in equation (3.40), except that the particle mass m_{p} is replaced by the massive body's mass m_{t}. For the Maxwellian velocity distribution, $D_{\mathrm{f}}[\Delta v_i] = (v_i/v)D_{\mathrm{f}}[\Delta v_\parallel]$, where

$$
D_{\mathrm{f}}[\Delta v_\parallel] = -\frac{4\pi G^2\rho_{\mathrm{b}}m_{\mathrm{t}}\log\Lambda_{\mathrm{FDM}}}{\sigma^2}\,\mathbb{G}(X), \tag{4.42}
$$

with $\mathbb{G}(X)$ defined in equation (3.54) (Bar-Or et al., 2019).

4.2.1 Survival of Globular Clusters in the Fornax Dwarf Galaxy

The Fornax dwarf spheroidal galaxy presents a long-standing puzzle in the context of cold dark matter CDM dynamics: its five globular clusters (GCs) have not yet spiraled into the center due to dynamical friction. In a CDM halo, dynamical friction leads to the gradual inspiral of massive objects through interactions with the surrounding dark matter particles, as described by Chandrasekhar's dynamical friction formula

$$\mathbf{F}_f \sim -\frac{4\pi G^2 m^2 \rho}{v^2} \ln \Lambda, \tag{4.43}$$

where $\mathbf{F}_f$ is the dynamical friction force, m is the mass of the globular cluster, ρ is the ambient dark matter density, v is the velocity of the cluster, and $\ln \Lambda$ is the Coulomb logarithm. According to CDM predictions, this force should lead to a rapid inward migration of the globular clusters, yet observations show that they remain at large radii, contradicting theoretical expectations.

In the FDM scenario, quantum pressure and wave-like interference significantly alter the nature of dynamical friction. Unlike CDM, where a persistent gravitational wake enhances drag, FDM exhibits wave interference effects that suppress the coherence of these wakes. Consequently, the effective dynamical friction force is reduced, leading to an extended inspiral timescale for the globular clusters. Moreover, FDM suppresses small-scale structure formation, reducing the local density enhancements responsible for gravitational drag.

For an FDM particle, the timescale for dynamical friction increases substantially, naturally explaining the survival of Fornax's globular clusters over cosmic time. This suggests that FDM provides a viable resolution to this longstanding problem in galactic dynamics.

We expect similar globular cluster longevity in other dwarf spheroidal galaxies. Precision proper motion studies of Fornax's globular clusters could further constrain the impact of dynamical friction in different dark matter models, providing a powerful test of the FDM hypothesis.

4.3 Landau Equations

Now we aim to study the kinetic equation, specifically the Landau equation, in different scenarios to explore the behavior of test particles interacting with a halo. In order to observe the connections between the classical and quantum cases, we will consider several relaxation processes.

We consider an infinite halo that is homogeneous in a time-averaged sense, characterized by a mean density ρ_0. Additionally, we adopt the Jeans swindle, which entails neglecting any acceleration resulting from ρ_0, and focus exclusively on the contributions from the density perturbations.

We introduce the halo's distribution function $F_\mathrm{b}(\mathbf{v})$, such that $F_\mathrm{b}(\mathbf{v})\mathrm{d}\mathbf{r}\mathrm{d}\mathbf{v}$ represents the time-averaged mass of halo particles within the phase-space volume element $\mathrm{d}\mathbf{r}\mathrm{d}\mathbf{v}$. Consequently, the mean density and the one-dimensional velocity dispersion are expressed as

$$\rho_0 = \int \mathrm{d}\mathbf{v}\, F_\mathrm{b}(\mathbf{v}); \quad 3\rho_0\sigma^2 = \int \mathrm{d}\mathbf{v}\, v^2 F_\mathrm{b}(\mathbf{v}). \tag{4.44}$$

4.3.1 Relaxation of Particles by Particles

The original standard FP equation of Chandrasekhar (1943), derived in section 2, describes the evolution of the distribution function of velocity (or its probability) due to interactions between the test objects and the background halo particles. An equivalent way to show such a time evolution and model relaxation is through the classical Landau equation (Landau, 1936; Chavanis, 2013). We obtained the homogeneous Landau equation for the case of a zero-mass test particle without considering a frictional force. For a more general case of a halo composed of classical particles of mass m and a population of point-like classical test objects of mass m_t with distribution function $F(\mathbf{v})$ the classical Landau equation reads

$$\frac{\partial F(\mathbf{v})}{\partial t} = 2G^2 \ln\Lambda \frac{\partial}{\partial v_i} \int \mathrm{d}\mathbf{v}'\, u_{ij}(\mathbf{v}-\mathbf{v}') \left[m F_{\mathrm{b}}(\mathbf{v}') \frac{\partial F(\mathbf{v})}{\partial v_j} - m_{\mathrm{t}} \frac{\partial F_{\mathrm{b}}(\mathbf{v}')}{\partial v'_j} F(\mathbf{v}) \right], \tag{4.45}$$

where

$$u_{ij}(\mathbf{v}) = \int \mathrm{d}\widehat{\mathbf{k}}\, \widehat{k}_i \widehat{k}_j\, \delta_{\mathrm{D}}(\widehat{\mathbf{k}}\cdot\mathbf{v}) = \pi \frac{\partial^2 v}{\partial v_i \partial v_j} = \pi \frac{v^2 \delta_{ij} - v_i v_j}{v^3}, \tag{4.46}$$

is the collision kernel. It merits attention that the first term in 4.45 represents the diffusion and the second term stems from dynamical friction and as mentioned earlier in this section, depends only on the test mass. For the Coulomb factor, we can take $k_{\max} \simeq \sigma^2/[G(m_{\mathrm{t}}+m)]$ corresponding to the scale associated with strong deflections in two-body encounters (Bar-Or et al., 2021).

4.3.2 Relaxation of Particles by Waves

Consider the scenario where the diffusion of classical test particles is driven by a background fuzzy halo consisting of ultra-light particles fundamentally conforming to a wave-like nature, each with an individual mass m_{b}. The evolution of the distribution function for the classical test particles is described by a modified Landau equation

$$\frac{\partial F(\mathbf{v})}{\partial t} = 2G^2 \ln\Lambda \frac{\partial}{\partial v_i} \int \mathrm{d}\mathbf{v}'\, u_{ij}(\mathbf{v}-\mathbf{v}') \left\{ \left[m_{\mathrm{b}} + \frac{h^3}{m_{\mathrm{b}}^3} F_{\mathrm{b}}(\mathbf{v}') \right] F_{\mathrm{b}}(\mathbf{v}') \frac{\partial F(\mathbf{v})}{\partial v_j} - m_{\mathrm{t}} \frac{\partial F_{\mathrm{b}}(\mathbf{v}')}{\partial v'_j} F(\mathbf{v}) \right\}, \tag{4.47}$$

Notably, the Coulomb logarithm's maximum wave number, $k_{\max}$, is redefined to

$$k_{\max} \simeq \min\left\{ \frac{m_{\mathrm{b}}\sigma}{\hbar}, \frac{\sigma^2}{G(m_{\mathrm{t}}+m_{\mathrm{b}})} \right\}. \tag{4.48}$$

This formulation closely resembles the original Landau equation, with the key distinction lying in the diffusion term. Here, the background classical particle mass m is instead replaced by the expression below

$$m_{\mathrm{b}} + \left(\frac{h}{m_{\mathrm{b}}}\right)^3 F_{\mathrm{b}}(\mathbf{v}'). \tag{4.49}$$

This adjustment highlights the interplay between the wave nature of the fuzzy halo particles and the classical dynamics of the test particles (Bar-Or et al., 2021).

4.3.3 Relaxation of Waves by Waves

The Landau equation can be extended to model the self-consistent evolution of a halo distribution function composed of ultra-light fuzzy particles. In this context, equation (4.47) is modified to

$$\begin{aligned} \frac{\partial F_{\mathrm{b}}(\mathbf{v})}{\partial t} = 2G^2 \ln\Lambda \frac{\partial}{\partial v_i} \int \mathrm{d}\mathbf{v}'\, u_{ij}(\mathbf{v}-\mathbf{v}') \Bigg\{ & \left[m_{\mathrm{b}} + \frac{h^3}{m_{\mathrm{b}}^3} F_{\mathrm{b}}(\mathbf{v}') \right] F_{\mathrm{b}}(\mathbf{v}') \frac{\partial F_{\mathrm{b}}(\mathbf{v})}{\partial v_j} \\ & - \left[m_{\mathrm{b}} + \frac{h^3}{m_{\mathrm{b}}^3} F_{\mathrm{b}}(\mathbf{v}) \right] \frac{\partial F_{\mathrm{b}}(\mathbf{v}')}{\partial v'_j} F_{\mathrm{b}}(\mathbf{v}) \Bigg\}. \end{aligned} \tag{4.50}$$

describing the relaxation of FDM halo induced by iteself. This equation closely resembles equation (4.47). However, a significant distinction arises in the friction term, where the test particle mass $m_{\rm t}$ is replaced by

$$m_{\rm b} + \left(\frac{h}{m_{\rm b}}\right)^3 F_{\rm b}(\mathbf{v}). \tag{4.51}$$

In the subsequent sections, we aim to derive equation (4.50) using the BNUU equation, followed by a more rigorous approach based on the quasi-linear expansion of the SP system.

It is significant to point out the argument of Bar-Or et al. (2021) that 4.50 is a flux-conservative equation. In other words, it has the form $\partial F_{\rm b}/\partial t = -\partial F_i/\partial v_i$ where

$$F_i = -D_i(\mathbf{v})F_{\rm b}(\mathbf{v}) + \frac{1}{2}\frac{\partial}{\partial v_j}\left[D_{ij}(\mathbf{v})F_{\rm b}(\mathbf{v})\right]. \tag{4.52}$$

which is a reminder of the FP equation

$$\frac{\partial F_{\rm b}(\mathbf{v})}{\partial t} = -\frac{\partial}{\partial v_i}\left[D_i(\mathbf{v})F_{\rm b}(\mathbf{v})\right] + \frac{1}{2}\frac{\partial^2}{\partial v_i \partial v_j}\left[D_{ij}(\mathbf{v})F_{\rm b}(\mathbf{v})\right], \tag{4.53}$$

Thus, we can conclude the equivalence of the FP and Landau equations and use them interchangeably to describe the evolution of the distribution function as a function of velocity. It means that

$$\begin{aligned}
&2G^2 \ln\Lambda \frac{\partial}{\partial v_i}\int \mathrm{d}\mathbf{v}'\, u_{ij}(\mathbf{v}-\mathbf{v}')\left\{\left[m_{\rm b} + \frac{h^3}{m_{\rm b}^3}F_{\rm b}(\mathbf{v}')\right]F_{\rm b}(\mathbf{v}')\frac{\partial F_{\rm b}(\mathbf{v})}{\partial v_j}\right. \\
&\left. - \left[m_{\rm b} + \frac{h^3}{m_{\rm b}^3}F_{\rm b}(\mathbf{v})\right]\frac{\partial F_{\rm b}(\mathbf{v}')}{\partial v'_j}\, F_{\rm b}(\mathbf{v})\right\} = -\frac{\partial}{\partial v_i}\left[D_i(\mathbf{v})F_{\rm b}(\mathbf{v})\right] + \frac{1}{2}\frac{\partial^2}{\partial v_i \partial v_j}\left[D_{ij}(\mathbf{v})F_{\rm b}(\mathbf{v})\right]
\end{aligned} \tag{4.54}$$

From this equality, the first-order or drift coefficients read

$$\begin{aligned}
D_i^{\rm c}(\mathbf{v}) &= 4G^2 m_{\rm b} \ln\Lambda \int \mathrm{d}\mathbf{v}'\, u_{ij}(\mathbf{v}-\mathbf{v}')\,\frac{\partial F_{\rm b}(\mathbf{v}')}{\partial v'_j}, \\
D_i^{\rm b}(\mathbf{v}) &= 2G^2 \frac{h^3}{m_{\rm b}^3} \ln\Lambda \int \mathrm{d}\mathbf{v}'\, u_{ij}(\mathbf{v}-\mathbf{v}')\left[F_{\rm b}(\mathbf{v})\,\frac{\partial F_{\rm b}(\mathbf{v}')}{\partial v'_j} + \frac{\partial F_{\rm b}^2(\mathbf{v}')}{\partial v'_j}\right],
\end{aligned} \tag{4.55}$$

and the second-order or diffusion coefficients are given by

$$\begin{aligned}
D_{ij}^{\rm c}(\mathbf{v}) &= 4G^2 m_{\rm b} \ln\Lambda \int \mathrm{d}\mathbf{v}'\, u_{ij}(\mathbf{v}-\mathbf{v}')\, F_{\rm b}(\mathbf{v}'), \\
D_{ij}^{\rm b}(\mathbf{v}) &= 4G^2\, \frac{h^3}{m_{\rm b}^3}\, \ln\Lambda \int \mathrm{d}\mathbf{v}'\, u_{ij}(\mathbf{v}-\mathbf{v}')\, F_{\rm b}^2(\mathbf{v}'),
\end{aligned} \tag{4.56}$$

with this in mind that $D_i(\mathbf{v}) = D_i^c(\mathbf{v}) + D_i^b(\mathbf{v})$ and $D_{ij}(\mathbf{v}) = D_{ij}^c(\mathbf{v}) + D_{ij}^b(\mathbf{v})$, where the first contributions are from the classical diffusion coefficients and the second ones are related to bosons or wave interference. Moreover, based on equation (**??**) we can rewrite the $D_i^{\rm c}(\mathbf{v})$ as below

$$\begin{aligned}
D_i^{\rm c}(\mathbf{v}) =&\ 4\pi G^2 m_{\rm b} \ln\Lambda \int \mathrm{d}\mathbf{v}'\, \frac{\partial^2}{\partial v_i \partial v_j}|\mathbf{v}-\mathbf{v}'|\,\frac{\partial F_{\rm b}(\mathbf{v}')}{\partial v'_j} \\
=&\ 8\pi G^2 m_{\rm b} \ln\Lambda\, \frac{\partial}{\partial v_i}\int \mathrm{d}\mathbf{v}'\, \frac{F_{\rm b}(\mathbf{v}')}{|\mathbf{v}-\mathbf{v}'|},
\end{aligned} \tag{4.57}$$

We will now show how to derive to this form of the coefficient starting from substituting the kernel in the integral in equation (4.55).

$$D_i^c(\mathbf{v}) = 4\pi G^2 m_b \ln\Lambda \int d\mathbf{v}' \left(\frac{\delta_{ij}}{|\mathbf{v}-\mathbf{v}'|} - \frac{(v_i - v_i')(v_j - v_j')}{|\mathbf{v}-\mathbf{v}'|^3} \right) \frac{\partial F_b(\mathbf{v}')}{\partial v_j'}. \tag{4.58}$$

The next step involves differentiating the integrand. The derivative $\frac{\partial}{\partial v_i}$ acts on both the kernel $|\mathbf{v}-\mathbf{v}'|$ and the velocity distribution $F_b(\mathbf{v}')$. We will now handle each term individually.

For the first term $\frac{\delta_{ij}}{|\mathbf{v}-\mathbf{v}'|}$, when we apply the derivative $\frac{\partial}{\partial v_i}$ to the first term, it acts on $\frac{\delta_{ij}}{|\mathbf{v}-\mathbf{v}'|}$. This results in

$$\frac{\partial}{\partial v_i}\left(\frac{\delta_{ij}}{|\mathbf{v}-\mathbf{v}'|}\right) = -\frac{(v_i - v_i')}{|\mathbf{v}-\mathbf{v}'|^3}. \tag{4.59}$$

For the second term $\frac{(v_i-v_i')(v_j-v_j')}{|\mathbf{v}-\mathbf{v}'|^3}$, we apply $\frac{\partial}{\partial v_i}$ to $\frac{(v_i-v_i')(v_j-v_j')}{|\mathbf{v}-\mathbf{v}'|^3}$. Using the chain rule and the fact that v_i appears explicitly in the numerator, the result will be

$$\frac{\partial}{\partial v_i}\left(\frac{(v_i - v_i')(v_j - v_j')}{|\mathbf{v}-\mathbf{v}'|^3}\right) = \frac{(v_j - v_j')}{|\mathbf{v}-\mathbf{v}'|^3}. \tag{4.60}$$

After applying the derivative to both terms, we obtain the following expression for $D_i^c(\mathbf{v})$:

$$D_i^c(\mathbf{v}) = 4\pi G^2 m_b \ln\Lambda \int d\mathbf{v}' \left(-\frac{(v_i - v_i')}{|\mathbf{v}-\mathbf{v}'|^3}\frac{\partial F_b(\mathbf{v}')}{\partial v_j'} + \frac{(v_j - v_j')}{|\mathbf{v}-\mathbf{v}'|^3}\frac{\partial F_b(\mathbf{v}')}{\partial v_j'} \right). \tag{4.61}$$

To simplify the integral, we now use integration by parts. Specifically, we use the fact that

$$\int d\mathbf{v}' \frac{\partial}{\partial v_j'}\left(\frac{F_b(\mathbf{v}')}{|\mathbf{v}-\mathbf{v}'|}\right) = 0, \tag{4.62}$$

which holds under the assumption that $F_b(\mathbf{v}')$ vanishes at infinity (or that the boundary terms do not contribute). This allows us to move the derivative $\frac{\partial}{\partial v_j'}$ from the kernel $|\mathbf{v}-\mathbf{v}'|$ to the distribution function $F_b(\mathbf{v}')$, and reduce the integral to

$$D_i^c(\mathbf{v}) = -\frac{\partial}{\partial v_i}\int d\mathbf{v}' \frac{F_b(\mathbf{v}')}{|\mathbf{v}-\mathbf{v}'|}. \tag{4.63}$$

Thus, after integration by parts and pulling out the derivative $\frac{\partial}{\partial v_i}$, we obtain the final result

$$D_i^c(\mathbf{v}) = 8\pi G^2 m_b \ln\Lambda \frac{\partial}{\partial v_i}\int d\mathbf{v}' \frac{F_b(\mathbf{v}')}{|\mathbf{v}-\mathbf{v}'|}. \tag{4.64}$$

We can also retrieve a similar form for the bosonic first order coefficient

$$\begin{aligned} D_i^{\mathrm{b}}(\mathbf{v}) &= 2G^2\frac{h^3}{m_{\mathrm{b}}^3}\ln\Lambda\int \mathrm{d}\mathbf{v}' \frac{\partial^2}{\partial v_i \partial v_j}|\mathbf{v}-\mathbf{v}'| \left[F_{\mathrm{b}}(\mathbf{v})\frac{\partial F_{\mathrm{b}}(\mathbf{v}')}{\partial v_j'} + \frac{\partial F_{\mathrm{b}}^2(\mathbf{v}')}{\partial v_j'}\right] \\ &= 4\pi G^2\frac{h^3}{m_{\mathrm{b}}^3}\ln\Lambda\left[\frac{\partial}{\partial v_i}\int \mathrm{d}\mathbf{v}' \frac{F_{\mathrm{b}}^2(\mathbf{v}')}{|\mathbf{v}-\mathbf{v}'|} + F_{\mathrm{b}}(\mathbf{v})\frac{\partial}{\partial v_i}\int \mathrm{d}\mathbf{v}' \frac{F_{\mathrm{b}}(\mathbf{v}')}{|\mathbf{v}-\mathbf{v}'|}\right] \\ &= 4\pi G^2 m_{\mathrm{eff}}\ln\Lambda\left[\frac{\partial}{\partial v_i}\left[\int \mathrm{d}\mathbf{v}' \frac{F_{\mathrm{eff}}(\mathbf{v}')}{|\mathbf{v}-\mathbf{v}'|}\right] + \frac{F_{\mathrm{eff}}(\mathbf{v})}{F_{\mathrm{b}}(\mathbf{v})}\frac{\partial}{\partial v_i}\left[\int \mathrm{d}\mathbf{v}' \frac{F_{\mathrm{b}}(\mathbf{v}')}{|\mathbf{v}-\mathbf{v}'|}\right]\right]. \end{aligned} \tag{4.65}$$

while equation (4.56) reduces to the following by simply replacing $u_{ij}(\mathbf{v}-\mathbf{v}')$ with $\frac{\partial^2}{\partial v_i \partial v_j}|\mathbf{v}-\mathbf{v}'|$

$$
\begin{aligned}
D^{\mathrm{c}}_{ij}(\mathbf{v}) &= 4\pi G^2 m_{\mathrm{b}} \ln\Lambda \, \frac{\partial^2}{\partial v_i \partial v_j} \int \mathrm{d}\mathbf{v}' \, |\mathbf{v}-\mathbf{v}'| \, F_{\mathrm{b}}(\mathbf{v}'), \\
D^{\mathrm{b}}_{ij}(\mathbf{v}) &= 4\pi G^2 \frac{h^3}{m_{\mathrm{b}}^3} \ln\Lambda \, \frac{\partial^2}{\partial v_i \partial v_j} \int \mathrm{d}\mathbf{v}' \, |\mathbf{v}-\mathbf{v}'| \, F^2_{\mathrm{b}}(\mathbf{v}') \\
&= 4\pi G^2 m_{\mathrm{eff}} \ln\Lambda \, \frac{\partial^2}{\partial v_i \partial v_j} \int \mathrm{d}\mathbf{v}' \, |\mathbf{v}-\mathbf{v}'| \, F_{\mathrm{eff}}(\mathbf{v}'),
\end{aligned}
\tag{4.66}
$$

where $F_{\mathrm{eff}}(\mathbf{v})$ and m_{eff} are defined as

$$
F_{\mathrm{eff}}(\mathbf{v}) = \frac{\int \mathrm{d}\mathbf{v}' \, F_{\mathrm{b}}(\mathbf{v}')}{\int \mathrm{d}\mathbf{v}' \, F^2_{\mathrm{b}}(\mathbf{v}')} F^2_{\mathrm{b}}(\mathbf{v}); \quad m_{\mathrm{eff}} = \frac{h^3}{m_{\mathrm{b}}^3} \frac{\int \mathrm{d}\mathbf{v} \, F^2_{\mathrm{b}}(\mathbf{v})}{\int \mathrm{d}\mathbf{v} \, F_{\mathrm{b}}(\mathbf{v})}. \tag{4.67}
$$

Hence, once again, this time through the Landau equation, we demonstrated that $D^{\mathrm{b}}_{ij}(\mathbf{v})$ for FDM and the classical case are identical. The mass of the particle and the DF are replaced by their effective counterparts, m_{eff} and F_{eff}, respectively. Specifically, for a Maxwellian distribution function, these diffusion coefficients match those of a halo composed of classical particles with an effective mass given by

$$
m_{\mathrm{eff}} = \rho_0 \left(\frac{\lambda_\sigma}{\sqrt{4\pi}} \right)^3 \tag{4.68}
$$

and an effective velocity dispersion

$$
\sigma_{\mathrm{eff}} = \frac{\sigma}{\sqrt{2}}. \tag{4.69}
$$

4.4 The FDM Landau Equation

We now proceed to manipulate equation (4.50) in order to explore its form in the specific case of an isotropic distribution function, where $F_{\mathrm{b}}(\mathbf{v})$ depends solely on $v = |\mathbf{v}|$. For the sake of brevity in equation (4.50), let us call the terms in square brackets $C(v')$ and $C(v)$ respectively. Now we will rewrite the equation with these considerations

$$
\begin{aligned}
\frac{\partial F_{\mathrm{b}}(\mathbf{v})}{\partial t} = 2G^2 \ln\Lambda \frac{\partial}{\partial v_i} \int \mathrm{d}\mathbf{v}' \, u_{ij}(\mathbf{v}-\mathbf{v}') \Big\{ & C(v') F_{\mathrm{b}}(v') \frac{\partial F_{\mathrm{b}}(v)}{\partial v_j} \\
& - C(v) \, \frac{\partial F_{\mathrm{b}}(v')}{\partial v'_j} \, F_{\mathrm{b}}(\check{}) \Big\}
\end{aligned}
\tag{4.70}
$$

The first integral is

$$
\begin{aligned}
& \frac{\partial F_{\mathrm{b}}(v)}{\partial v_j} \int \mathrm{d}\mathbf{v}' \;\; u_{ij}(\mathbf{v}-\mathbf{v}') \, F_b(v') \, C(v') \\
= & \frac{v_j}{v} \frac{dF_{\mathrm{b}}(v)}{dv} \int d\hat{\mathbf{v}} \, u_{ij}(\mathbf{v}-\mathbf{v}') \int dv' v'^2 F_b(v') \, C(v'),
\end{aligned}
\tag{4.71}
$$

since $\mathrm{d}\mathbf{v}'$ can be written as $d\hat{\mathbf{v}} \, dv' \, v'^2$ and $\frac{\partial}{\partial v_j}$ as $\frac{v_j}{v}\frac{d}{dv}$. Then according to the properties of the Rosenbluth potentials (Binney and Tremaine, 2008)

$$
\int \mathrm{d} \, u_{ij}(\mathbf{v}-\mathbf{v}') = \begin{cases} 4\pi^2 \left(\dfrac{\delta_{ij}}{v} - \dfrac{v_i v_j}{v^3} - \dfrac{v'^2 \delta_{ij}}{3v^3} + \dfrac{v'^2 v_i v_j}{v^5} \right) & \text{for} \quad v' < v, \\[2ex] \dfrac{8\pi^2}{3} \dfrac{\delta_{ij}}{v'} & \text{for} \quad v < v', \end{cases} \tag{4.72}
$$

we can solve the first integral as the following

$$\begin{aligned}
&\frac{v_j}{v}\frac{dF_{\rm b}(v)}{dv}\left\{\int_0^v dv'v'^2F_b(v')\,C(v')\,4\pi^2\left(\frac{\delta_{ij}}{v}-\frac{v_iv_j}{v^3}-\frac{v'^2\delta_{ij}}{3v^3}+\frac{v'^2v_iv_j}{v^5}\right)\right.\\
&\qquad\left.+\int_v^\infty dv'v'^2F_b(v')\,C(v')\,\frac{8\pi^2}{3}\frac{\delta_{ij}}{v'}\right\}\\
=&\frac{v_j}{v}\frac{dF_{\rm b}(v)}{dv}\frac{4\pi^2}{3}\left\{3\int_0^v dv'v'^2F_b(v')\,C(v')\,\left(\frac{\delta_{ij}}{v}-\frac{v_iv_j}{v^3}-\frac{v'^2\delta_{ij}}{3v^3}+\frac{v'^2v_iv_j}{v^5}\right)\right.\\
&\qquad\left.+2\int_v^\infty dv'v'F_b(v')\,C(v')\,\delta_{ij}\right\}
\end{aligned} \tag{4.73}$$

For the case where $i=j$ the above expression will be equal to

$$\begin{aligned}
&\frac{v_i}{v}\frac{dF_{\rm b}(v)}{dv}\frac{4\pi^2}{3}\left\{3\int_0^v dv'v'^2F_b(v')\,C(v')\,\left(\frac{1}{v}-\frac{v_i^2}{v^3}-\frac{v'^2}{3v^3}+\frac{v'^2v_i^2}{v^5}\right)\right.\\
&\qquad\left.+2\int_v^\infty dv'v'F_b(v')\,C(v')\right\}
\end{aligned} \tag{4.74}$$

Now we can apply the derivative with respect to v_i to this result

$$\begin{aligned}
&\frac{4\pi^2}{3}\frac{\partial}{\partial v_i}\left\{3\frac{v_i}{v}\frac{dF_{\rm b}(v)}{dv}\int_0^v dv'v'^2F_b(v')\,C(v')\,\left(\frac{1}{v}-\frac{v_i^2}{v^3}-\frac{v'^2}{3v^3}+\frac{v'^2v_i^2}{v^5}\right)\right.\\
&\qquad\left.+2\frac{v_i}{v}\frac{dF_{\rm b}(v)}{dv}\int_v^\infty dv'v'F_b(v')\,C(v')\right\}
\end{aligned} \tag{4.75}$$

Let us calculate each term individually. The first term neglecting the constants is

$$\begin{aligned}
&\frac{\partial}{\partial v_i}\left\{\frac{v_i}{v}\frac{dF_{\rm b}(v)}{dv}\int_0^v dv'v'^2F_b(v')\,C(v')\,\left(\frac{1}{v}-\frac{v_i^2}{v^3}-\frac{v'^2}{3v^3}+\frac{v'^2v_i^2}{v^5}\right)\right\}\\
=&\frac{v^2-v_i^2}{v^3}\frac{dF_{\rm b}(v)}{dv}\int_0^v dv'v'^2F_b(v')\,C(v')\,\left(\frac{1}{v}-\frac{v_i^2}{v^3}-\frac{v'^2}{3v^3}+\frac{v'^2v_i^2}{v^5}\right)\\
+&\frac{v_i^2}{v^2}\frac{d^2F_{\rm b}(v)}{dv^2}\int_0^v dv'v'^2F_b(v')\,C(v')\,\left(\frac{1}{v}-\frac{v_i^2}{v^3}-\frac{v'^2}{3v^3}+\frac{v'^2v_i^2}{v^5}\right)\\
+&\frac{v_i}{v}\frac{dF_{\rm b}(v)}{dv}\int_0^v dv'v'^2F_b(v')\,C(v')\,\frac{\partial}{\partial v_i}\left(\frac{1}{v}-\frac{v_i^2}{v^3}-\frac{v'^2}{3v^3}+\frac{v'^2v_i^2}{v^5}\right)
\end{aligned} \tag{4.76}$$

After some rearrangement, we will reach

$$\begin{aligned}
&\frac{dF_{\rm b}(v)}{dv}\int_0^v dv'v'^2F_b(v')\,C(v')\,\left(\frac{1}{v^2}-\frac{v_i^2}{v^4}-\frac{v'^2}{3v^4}+\frac{v'^2v_i^2}{v^6}-\frac{v_i^2}{v^4}+\frac{v_i^4}{v^6}+\frac{v'^2v_i^2}{3v^6}-\frac{v'^2v_i^4}{v^8}\right)\\
+&\frac{d^2F_{\rm b}(v)}{dv^2}\int_0^v dv'v'^2F_b(v')\,C(v')\,\left(\frac{v_i^2}{v^3}-\frac{v_i^4}{v^5}-\frac{v'^2v_i^2}{3v^5}+\frac{v'^2v_i^4}{v^7}\right)\\
+&\frac{dF_{\rm b}(v)}{dv}\int_0^v dv'v'^2F_b(v')\,C(v')\,\left(-\frac{v_i^2}{v^4}+\frac{3v_i^4}{v^6}-\frac{2v_i^2}{v^4}+\frac{v'^2v_i^2}{v^6}+\frac{2v'^2v_i^2}{v^6}-\frac{5v_i^4v'^2}{v^8}\right)
\end{aligned} \tag{4.77}$$

We should now perform a summation over i on the above expression which taking into account that $\sum_i v_i^2 = v^2$. This leads to

$$\begin{aligned}
&\frac{dF_\mathrm{b}(v)}{dv}\int_0^v dv' v'^2 F_b(v')\,C(v')\left(\frac{2}{v^2}\right)\\
&+\frac{d^2F_\mathrm{b}(v)}{dv^2}\int_0^v dv' v'^2 F_b(v')\,C(v')\left(\frac{2v'^2}{v^3}\right)\\
&+\frac{dF_\mathrm{b}(v)}{dv}\int_0^v dv' v'^2 F_b(v')\,C(v')\left(-2\frac{v'^2}{v^4}\right)\\
&=\frac{2}{v^2}\left\{\frac{dF_\mathrm{b}(v)}{dv}\int_0^v dv' v'^2 F_b(v')\,C(v')\left(1-\frac{v'^2}{v^2}\right)+\frac{d^2F_\mathrm{b}(v)}{dv^2}\int_0^v dv' v'^2 F_b(v')\,C(v')\left(\frac{v'^2}{v}\right)\right\}\\
&=\frac{2}{v^2}\frac{d}{dv}\left(\frac{dF_\mathrm{b}(v)}{dv}\int_0^v dv' v'^2 F_b(v')\,C(v')\,\frac{v'^2}{v}\right)
\end{aligned} \tag{4.78}$$

To get the other term in equation (4.75), we only need to simplify the expression below since the integral part is not dependent on v,

$$\begin{aligned}
\frac{\partial}{\partial v_i}\left\{\frac{v_i}{v}\frac{dF_\mathrm{b}(v)}{dv}\right\} &= \frac{dF_\mathrm{b}(v)}{dv}\frac{\partial}{\partial v_i}\left(\frac{v_i}{v}\right)+\frac{v_i}{v}\frac{\partial}{\partial v_i}\left(\frac{dF_\mathrm{b}(v)}{dv}\right)\\
&=\frac{v^2-v_i^2}{v^3}\frac{dF_\mathrm{b}(v)}{dv}+\left(\frac{v_i}{v}\right)^2\frac{d^2F_\mathrm{b}(v)}{dv^2}.
\end{aligned} \tag{4.79}$$

Applying a summation over i gives

$$\sum_i \frac{\partial}{\partial v_i}\left\{\frac{v_i}{v}\frac{dF_\mathrm{b}(v)}{dv}\right\} = \frac{3}{v}\frac{dF_\mathrm{b}(v)}{dv}-\frac{1}{v}\frac{dF_\mathrm{b}(v)}{dv}+\frac{d^2F_\mathrm{b}(v)}{dv^2}=\frac{2}{v}\frac{dF_\mathrm{b}(v)}{dv}+\frac{d^2F_\mathrm{b}(v)}{dv^2}. \tag{4.80}$$

since $\sum_i v_i^2 = v^2$. We can also rewrite this result in the form below

$$\frac{1}{v^2}\frac{d}{dv}\left\{v^2\frac{dF_b(v)}{dv}\right\} \tag{4.81}$$

Now that both terms of 4.75 are simplified, the first term of equation (4.70) could be written as

$$\frac{16\pi^2G^2\ln\Lambda}{3}\frac{1}{v^2}\frac{d}{dv}\left(\frac{3}{v}\frac{dF_\mathrm{b}(v)}{dv}\int_0^v dv' v'^4 F_b(v')\,C(v')+\frac{dF_\mathrm{b}(v)}{dv}\int_v^\infty dv' v' F_b(v')\,C(v')\right) \tag{4.82}$$

Then for the second term in the original equation (4.70) we can write

$$\begin{aligned}
&\iint dv'\,d\hat{\mathbf{v}}'\,u_{ij}(\mathbf{v}-\mathbf{v}')\,v'^2\,C(v)\,\frac{dF_\mathrm{b}(v')}{dv'_j}\,F_\mathrm{b}(v)\\
&=C(v)F_\mathrm{b}(v)\iint dv'\,d\hat{\mathbf{v}}'\,u_{ij}(\mathbf{v}-\mathbf{v}')\,v'^2\,\frac{v'_j}{v'}\frac{dF_\mathrm{b}(v')}{dv'}\\
&=C(v)F_\mathrm{b}(v)\iint dv'\,d\hat{\mathbf{v}}'\,u_{ij}(\mathbf{v}-\mathbf{v}')v'_jv'\,\frac{dF_\mathrm{b}(v')}{dv'}
\end{aligned} \tag{4.83}$$

We can use the properties of the Rosenbluth potentials as stated in Binney and Tremaine (2008),

$$\int \mathrm{d}\,u_{ij}(\mathbf{v}-\mathbf{v}')\,v'_j = \begin{cases}\dfrac{8\pi^2}{3}\dfrac{v'^2v_i}{v^3} & \text{for}\quad v'<v,\\[2ex] \dfrac{8\pi^2}{3}\dfrac{v_i}{v'} & \text{for}\quad v<v',\end{cases} \tag{4.84}$$

to obtain the following result for the second term in 4.70

$$
\begin{aligned}
&-2G^2 \ln\Lambda \frac{\partial}{\partial v_i}\left(C(v)F_{\mathrm{b}}(v) \left\{ \int_0^v dv' \, \frac{8\pi^2}{3}\frac{v'^2 v_i}{v^3} v' \, \frac{dF_{\mathrm{b}}(v')}{dv'} + \int_v^\infty dv' \frac{8\pi^2}{3}\frac{v_i}{v'} v' \frac{dF_{\mathrm{b}}(v')}{dv'} \right\}\right) \\
&= -2G^2 \frac{8\pi^2}{3} \ln\Lambda \frac{\partial}{\partial v_i}\left\{ \frac{v_i}{v^3} C(v)F_{\mathrm{b}}(v) \int_0^v dv' \, v'^3 \, \frac{dF_{\mathrm{b}}(v')}{dv'} \right\},
\end{aligned}
\tag{4.85}
$$

where the second integral simply disappears as it has no v dependence. Now we are going to solve the integral by parts. The above expression will be

$$
-\frac{16\pi^2 G^2}{3} \ln\Lambda \frac{\partial}{\partial v_i}\left\{ \frac{v_i}{v^3} C(v)F_{\mathrm{b}}(v) \left(-3 \int_0^v dv' v'^2 F_{\mathrm{b}}(v') \right) \right\}. \tag{4.86}
$$

Note that we neglected the boundary term of the integral since it is equal to zero. To proceed to the next step shorten the expression in curly brackets by writing it as $\frac{v_i}{v^3} f(v)\, g(v')$ and calculate its derivative with respect to v_i.

$$
\frac{\partial}{\partial v_i}\left(\frac{v_i}{v^3} f(v)\, g(v') \right) = \frac{\partial}{\partial v_i}\left(\frac{v_i}{v^3} \right) f(v)\, g(v') + \frac{v_i}{v^3} \frac{\partial \left(f(v)\, g(v') \right)}{\partial v_i}. \tag{4.87}
$$

Using the quotient rule

$$
\frac{\partial}{\partial v_i}\left(\frac{v_i}{v^3} \right) = \frac{\frac{\partial v_i}{\partial v_i} v^3 - v_i \frac{\partial v^3}{\partial v_i}}{v^6}, \tag{4.88}
$$

where

$$
\frac{\partial v_i}{\partial v_i} = 1, \qquad \frac{\partial v^3}{\partial v_i} = 3v^2 \frac{\partial v}{\partial v_i}, \quad \text{and} \quad \frac{\partial v}{\partial v_i} = \frac{v_i}{v}. \tag{4.89}
$$

Substituting the derivatives yields

$$
\frac{\partial v^3}{\partial v_i} = 3v^2 \frac{v_i}{v}. \tag{4.90}
$$

Thus

$$
\frac{\partial}{\partial v_i}\left(\frac{v_i}{v^3} \right) = \frac{v^3 - 3v_i^2}{v^6} = \frac{v^2 - 3v_i^2}{v^5}. \tag{4.91}
$$

For $\frac{\partial (f(v)\, g(v'))}{\partial v_i}$ we use the following relation

$$
\frac{\partial \left(f(v)\, g(v') \right)}{\partial v_i} = \frac{v_i}{v} \frac{d \left(f(v)\, g(v') \right)}{dv}. \tag{4.92}
$$

Then we substitute this into the second term

$$
\frac{v_i}{v^3} \frac{\partial \left(f(v)\, g(v') \right)}{\partial v_i} = \frac{v_i}{v^3} \cdot \frac{v_i}{v} \frac{d \left(f(v)\, g(v') \right)}{dv} = \frac{v_i^2}{v^4} \frac{d \left(f(v)\, g(v') \right)}{dv}. \tag{4.93}
$$

Now we are going to sum the two terms over i

$$
\sum_i \frac{\partial}{\partial v_i}\left(\frac{v_i}{v^3} \right) = \sum_i \frac{v^2 - 3v_i^2}{v^5}. \tag{4.94}
$$

Using the fact that $\sum_i v_i^2 = v^2$, we find

$$
\sum_i \frac{v^2 - 3v_i^2}{v^5} = \frac{3v^2}{v^5} - \frac{3\sum_i v_i^2}{v^5} = \frac{3v^2}{v^5} - \frac{3v^2}{v^5} = 0. \tag{4.95}
$$

And for the other term we have

$$\begin{aligned}\sum_i \frac{v_i^2}{v^4}\frac{d\left(f(v)\,g(v')\right)}{dv} &= \frac{\sum_i v_i^2}{v^4}\frac{d\left(f(v)\,g(v')\right)}{dv} = \sum_i \frac{v_i^2}{v^4}\frac{d\left(f(v)\,g(v')\right)}{dv} \\ &= \frac{v^2}{v^4}\frac{d\left(f(v)\,g(v')\right)}{dv} = \frac{1}{v^2}\frac{d\left(f(v)\,g(v')\right)}{dv}.\end{aligned} \tag{4.96}$$

Combining the two terms, we obtain

$$\sum_i \frac{\partial}{\partial v_i}\left(\frac{v_i}{v^3}f(v)g(v')\right) = \frac{1}{v^2}\frac{d\left(f(v)g(v')\right)}{dv}. \tag{4.97}$$

With all these considerations, we can now rewrite equation (4.86) as

$$\begin{aligned}&16\pi^2G^2\ln\Lambda\frac{\partial}{\partial v_i}\left\{\frac{v_i}{v^3}C(v)F_{\rm b}(v)\left(\int_0^v dv'v'^2F_{\rm b}(v')\right)\right\}\\ =&16\pi^2G^2\ln\Lambda\frac{1}{v^2}\frac{d}{dv}\left\{C(v)F_{\rm b}(v)\left(\int_0^v dv'v'^2F_{\rm b}(v')\right)\right\}\end{aligned} \tag{4.98}$$

Finally, we need to put the results obtained in equation (4.82) and (4.98) together in 4.70 which gives

$$\begin{aligned}\frac{\partial F_{\rm b}(v)}{\partial t} = \frac{16\pi^2G^2\ln\Lambda}{3}\frac{1}{v^2}\frac{\mathrm{d}}{\mathrm{d}v}\Bigg\{&\frac{1}{v}\frac{\mathrm{d}F_{\rm b}(v)}{\mathrm{d}v}\int_0^v \mathrm{d}v'\,v'^4F_{\rm b}(v')\left[m_{\rm b}+\frac{h^3}{m_{\rm b}^3}F_{\rm b}(v')\right]\\ &+v^2\frac{\mathrm{d}F_{\rm b}(v)}{\mathrm{d}v}\int_v^\infty \mathrm{d}v'\;v'F_{\rm b}(v')\left[m_{\rm b}+\frac{h^3}{m_{\rm b}^3}F_{\rm b}(v')\right]\\ &+3F_{\rm b}(v)\left[m_{\rm b}+\frac{h^3}{m_{\rm b}^3}F_{\rm b}(v)\right]\int_0^v \mathrm{d}v'\,v'^2F_{\rm b}(v')\Bigg\}.\end{aligned} \tag{4.99}$$

This relation describes the self-consistent evolution of a halo's isotropic distribution function composed of ultra-light fuzzy particles.

Let us analyze this result in the limit where there are many particles per unit phase-space cell of volume h^3. Mathematically, this corresponds to the limit

$$\frac{h^3}{m_{\rm b}^4}F_{\rm b} \gg 1, \quad \text{or equivalently,} \quad m_{\rm eff} \simeq \rho_0\left(\frac{h}{m_{\rm b}\sigma}\right)^3 \gg m_{\rm b}. \tag{4.100}$$

Then equation (4.99) reduces to

$$\frac{\partial F_{\rm b}(\mathbf{v})}{\partial t} = 2G^2\ln\Lambda\frac{h^3}{m_{\rm b}^3}\frac{\partial}{\partial v_i}\int \mathrm{d}\mathbf{v}'\,u_{ij}(\mathbf{v}-\mathbf{v}')\left[F_{\rm b}^2(\mathbf{v}')\frac{\partial F_{\rm b}(\mathbf{v})}{\partial v_j} - F_{\rm b}^2(\mathbf{v})\frac{\partial F_{\rm b}(\mathbf{v}')}{\partial v_j'}\right] \tag{4.101}$$

$$\begin{aligned}= \frac{16\pi^2G^2\ln\Lambda}{3}\frac{h^3}{m_{\rm b}^3}\frac{1}{v^2}\frac{\mathrm{d}}{\mathrm{d}v}\Bigg[&\frac{1}{v}\frac{\mathrm{d}F_{\rm b}(v)}{\mathrm{d}v}\int_0^v \mathrm{d}v'\,v'^4F_{\rm b}^2(v')\\ &+v^2\frac{\mathrm{d}F_{\rm b}(v)}{\mathrm{d}v}\int_v^{+\infty}\mathrm{d}v'\,v'F_{\rm b}^2(v') + 3F_{\rm b}^2(v)\int_0^v \mathrm{d}v'\,v'^2F_{\rm b}(v')\Bigg].\end{aligned} \tag{4.102}$$

It should be emphasized that the distribution function is dependent on $\mathbf{v}$ meaning that this equation holds for the evolution of non-isotropic $F_{\rm b}(\mathbf{v})$ as well under the condition that we are studying it in the limit of high phase-space density i.e. equation (4.100) (Bar-Or et al., 2021).

In general, when the distribution function conforms to Bose-Einstein statistics

$$F_{\rm b}(v) = \frac{m_{\rm b}^4}{h^3}\frac{1}{{\rm e}^{\frac{1}{2}\beta v^2}/z - 1}, \tag{4.103}$$

the l.h.s of the Landau equation is zero, therefore it is considered as the generic steady state solution where the inverse temperature β and the fugacity z are determined from the conservation of mass and kinetic energy per unit volume from equation (4.44)(Bar-Or et al., 2021). In practice, one has

$$\rho_0 = \int d\mathbf{v} F_b(\mathbf{v}) = \frac{m_b^4}{h^3}\int \frac{4\pi v^2 dv}{{\rm e}^{\frac{1}{2}\beta v^2}/z - 1} \tag{4.104}$$

for the background density. To solve the above integral we use the definition $x = \frac{\beta v^2}{2}$. Therefore, we can rewrite it in terms of x as the following

$$\rho_0 = \frac{m_b^4}{h^3}\frac{4\pi}{\beta}\left(\frac{2}{\beta}\right)^{1/2}\int \frac{x^{1/2}dx}{\frac{e^x}{z} - 1} = \frac{m_b^4}{h^3}\frac{4\pi}{\beta}\left(\frac{2}{\beta}\right)^{1/2}\frac{\sqrt{\pi}}{2}\,{\rm Li}_{3/2}(z) = \frac{m_b^4(2\pi)^{3/2}}{h^3\beta^{3/2}}\,{\rm Li}_{3/2}(z), \tag{4.105}$$

where we used the definition of polylogarithm

$${\rm Li}_n(z) = \frac{1}{\Gamma(n)}\int_0^\infty \frac{x^{n-1}dx}{e^x/z - 1} \simeq \sum_{k=1}^{\infty}\frac{z^k}{k^n}, \tag{4.106}$$

and

$$\int_0^\infty \frac{x^{n-1}dx}{e^x/z - 1} = \Gamma(n)\,{\rm Li}_n(z). \tag{4.107}$$

It must be acknowledged that ${\rm Li}_n(z)$ reduces to $\zeta(n)$ for $z = 1$ which is the Riemann zeta function. In our case, $n = 3/2$ and $\Gamma(3/2) = \frac{\sqrt{\pi}}{2}$. Also from

$$3\rho_o\sigma^2 = \int d\mathbf{v} v^2 F(\mathbf{v}), \tag{4.108}$$

we can write

$$\rho_0\sigma^2 = \frac{1}{3}\int {\rm d}\mathbf{v}\, v^2 F_{\rm b}(\mathbf{v}) = \frac{m_b^4}{h^3}\int \frac{4\pi v^4 dv}{{\rm e}^{\frac{1}{2}\beta v^2}/z - 1} \tag{4.109}$$

which in terms of x is

$$\rho_0\sigma^2 = \frac{1}{3}\frac{m_b^4}{h^3}\left(\frac{2}{\beta}\right)^2\left(\frac{1}{2\beta}\right)^{1/2}\int \frac{4\pi x^{3/2}dx}{{\rm e}^x/z - 1} = \frac{1}{3}\frac{4\pi m_b^4}{h^3}\frac{2^{3/2}}{\beta}\frac{3\sqrt{\pi}}{4}\,{\rm Li}_{5/2}(z) = \frac{m_b^4(2\pi)^{3/2}}{h^3\beta^{5/2}}\,{\rm Li}_{5/2}(z) \tag{4.110}$$

since $\Gamma(5/2) = \frac{3\sqrt{\pi}}{4}$. Combining equation (4.105) and (4.110) gives

$$\frac{\rho_0^{5/2}}{(\rho_0\sigma^2)^{3/2}} = \left(\frac{m_b^4(2\pi)^{3/2}}{h^3\beta^{3/2}}\,{\rm Li}_{3/2}(z)\right)^{5/2}\left(\frac{h^3\beta^{5/2}}{m^4(2\pi)^{3/2}}\frac{1}{{\rm Li}_{5/2}(z)^{3/2}}\right)^{3/2} \tag{4.111}$$

$$\longrightarrow \frac{\rho_o}{\sigma^3} = \frac{(2\pi)^{3/2}m_b^4}{h^3}\frac{{\rm Li}_{3/2}(z)^{5/2}}{{\rm Li}_{5/2}(z)^{3/2}} \longrightarrow \sigma^3 = \frac{h^3\rho_0}{m_{\rm b}^4(2\pi)^{3/2}}\frac{{\rm Li}_{5/2}^{3/2}(z)}{{\rm Li}_{3/2}^{5/2}(z)}$$

It is worthwhile to calculate the minimum value of σ^3 reached at $z = 1$,

$$\sigma_c^3 = \frac{\zeta^{3/2}(5/2)}{\zeta^{5/2}(3/2)} \frac{h^3 \rho_0}{m_\mathrm{b}^4 (2\pi)^{3/2}} \\ \simeq 1.09 \left(100\,\mathrm{km\ s^{-1}}\right)^3 \frac{\rho_0}{0.01\,\mathrm{pc}^{-3}} \left(\frac{m_\mathrm{b}}{20\,\mathrm{eV}}\right)^{-4}. \tag{4.112}$$

At this point, value of β is given by

$$\beta_c = \frac{\zeta(5/2)}{\zeta(3/2)} \frac{1}{2} = \left[\frac{m_\mathrm{b}\zeta(3/2)}{\rho_0}\right]^{2/3} \frac{m_\mathrm{b}^2}{2\pi\hbar^2}. \tag{4.113}$$

However, in the case of FDM with the typical proposed boson masses $m_\mathrm{b} = 10^{-21}$–$10^{-22}\,\mathrm{eV}$, the value of σ_c is much larger compared to galaxy velocity dispersions. In this situation, the distribution function of the steady state is no longer described by equation (4.104). Instead, a Bose-Einstein condensate or soliton term is added in the distribution function relateion which is given by

$$F_\mathrm{b}(v) = \frac{m_\mathrm{b}^4}{h^3} \frac{1}{\mathrm{e}^{\frac{1}{2}\beta v^2} - 1} + \rho_\mathrm{s}\, \delta_\mathrm{D}(\mathbf{v}), \tag{4.114}$$

where

$$\beta^{5/2} = \frac{m_\mathrm{b}^4 (2\pi)^{3/2}}{h^3 \rho_0 \sigma^2} \zeta(5/2). \tag{4.115}$$

Finally, the density in the soliton is obtained from the mass and energy conservation as the following

$$\rho_\mathrm{s} = \left(1 - \frac{3/2}{\beta^{3/2}}\right)\rho_0 = \left(1 - \frac{\sigma^{6/5}}{6/5}\right)\rho_0, \tag{4.116}$$

5 Kinetic Theory from BNUU and SP Frameworks

In this section, we provide a rigorous step-by-step derivation of the kinetic equation from the Boltzmann-Nordheim-Uehling-Uhlenbeck (BNUU) equation which describes the rate of change in the distribution function as a result of collisions. To begin with, we will conduct a general study of the BNUU equation, analyzing its broad framework and underlying principles. Following this, we will focus on the specific case of weak deflections, carefully examining the implications in this limit. Finally, we will attempt to derive the kinetic equation from the BNUU framework, seeking to establish a direct connection between the two.

Further in this chapter, we will represent a wave-mechanical approach to the kinetic equation, i.e. the Schrödinger-Poisson system of equations from which we show a derivation of the kinetic equation describing the self-consistent relaxation in a homogeneous halo.

5.1 BNUU equation

The Boltzmann equation is a fundamental tool in statistical mechanics that describes the evolution of the distribution function $f(\mathbf{x}, \mathbf{v}, t)$ in phase space. It governs the time-dependent behavior of f, accounting for free-streaming dynamics and collisional interactions. The equation is expressed as

$$\frac{\partial f}{\partial t} + \mathbf{v} \cdot \nabla_{\mathbf{x}} f + \mathbf{F} \cdot \nabla_{\mathbf{v}} f = \left(\frac{\partial f}{\partial t} \right)_{\text{coll}}, \tag{5.1}$$

where $\mathbf{F}$ represents the force acting on the particles, and the collisional term on the right-hand side accounts for the effects of particle interactions[5](Binney and Tremaine, 2008).

In gravitational systems, the Boltzmann equation provides the basis for understanding dynamical processes such as phase-space mixing and energy redistribution, which are keys to relaxation and equilibrium states. When applied to long-range interactions like gravity, the collisional term is often adapted to include mechanisms such as Landau damping or violent relaxation, making the equation suitable for studying self-gravitating systems (Binney and Tremaine, 2008; Kolb and Turner, 1990).

For a classical two-particle scattering process with four different particles participating that can be written as $1 + 2 \leftrightarrow 3 + 4$, the evolution of the distribution function of the particle with momentum $\mathbf{p}_1$ is described as

$$\frac{\partial f(\mathbf{p}_1)}{\partial t} = \int \mathrm{d}\mathbf{p}_2 \mathrm{d}\mathbf{p}_3 \mathrm{d}\mathbf{p}_4 S^{(4)}(\mathbf{p}_1, \mathbf{p}_2, \mathbf{p}_3, \mathbf{p}_4) \left[f(\mathbf{p}_3) f(\mathbf{p}_4) - f(\mathbf{p}_1) f(\mathbf{p}_2) \right] \tag{5.2}$$

where $\mathbf{p}$ is the momentum and $f(\mathbf{p})\mathrm{d}\mathbf{r}\mathrm{d}\mathbf{p}$ represents the number of particles in a phase-space volume element $\mathrm{d}\mathbf{r}\mathrm{d}\mathbf{p}$. This equation quantifies how particle collisions redistribute particles in velocity space. The scattering kernel $S^{(4)}$ encodes the probability of a collision between particles. More precisely, it describes the rate at which particles with momenta $\mathbf{p}_1$ and $\mathbf{p}_2$ are scattered into momenta $\mathbf{p}_3$ and $\mathbf{p}_4$. The gain term $f(\mathbf{p}_3)f(\mathbf{p}_4)$ accounts for particles being scattered into the state with momentum $\mathbf{p}_1$ while the loss term $f(\mathbf{p}_1)f(\mathbf{p}_2)$

[5] In chapter 2, we studied the collisionless Boltzmann equation (2.1); however note that we are using a different notation here.

represents particles being scattered out of the state with momentum $\mathbf{p}_1$. Particularly, the term

$$S^{(4)}(\mathbf{p}_1,\mathbf{p}_2,\mathbf{p}_3,\mathbf{p}_4)f(\mathbf{p}_1)f(\mathbf{p}_2)\,\mathrm{d}\mathbf{p}_1\,\mathrm{d}\mathbf{p}_2\,\mathrm{d}\mathbf{p}_3\,\mathrm{d}\mathbf{p}_4 \tag{5.3}$$

represents the scattering rate per unit volume at which particles are scattered from the momentum-space volumes $\mathrm{d}\mathbf{p}_1$ and $\mathrm{d}\mathbf{p}_2$ into the volumes $\mathrm{d}\mathbf{p}_3$ and $\mathrm{d}\mathbf{p}_4$ (Bar-Or et al., 2021).

equation (5.3) could be generalized to quantum systems as the following

$$\begin{aligned}\frac{\partial f(\mathbf{p}_1)}{\partial t} =&\int \mathrm{d}\mathbf{p}_2\mathrm{d}\mathbf{p}_3\mathrm{d}\mathbf{p}_4\, S^{(4)}(\mathbf{p}_1,\mathbf{p}_2,\mathbf{p}_3,\mathbf{p}_4)\big\{f(\mathbf{p}_3)f(\mathbf{p}_4)[1+\epsilon h^3 f(\mathbf{p}_1)][1+\epsilon h^3 f(\mathbf{p}_2)]\\ &- f(\mathbf{p}_1)f(\mathbf{p}_2)[1+\epsilon h^3 f(\mathbf{p}_3)][1+\epsilon h^3 f(\mathbf{p}_4)]\big\},\end{aligned} \tag{5.4}$$

known as the Boltzmann–Nordheim–Uehling–Uhlenbeck BNUU equation (Nordheim, 1928; Uehling and Uhlenbeck, 1933; Erdős et al., 2004), where $+1$ for bosons, and -1 for fermions so that a factor such as $1 - h^3 f(\mathbf{p}_i)$ prevents particles from being scattered into states that are completely occupied, in accordance with the Pauli exclusion principle and a factor of the form $1 + h^3 f(\mathbf{p}_i)$ is the Bose enhancement factor describing the tendency of the production of species i to be favored if it is a boson or to be *slowed down* if it is a fermion. Naively, we can think of the former effect as a consequence of the Pauli exclusion principle. Since we cannot have two fermions with the same quantum numbers in a system, as long as they are produced, they must gain higher and higher energies, making their production more and more difficult. This is no more valid in the case of bosons and, indeed, there is an enhancement instead of a suppression. Furthermore, for $\epsilon = 0$ equation (5.4) reduces to the Boltzmann equation for a classical system (equation (5.3))

For the purpose of brevity, we substitute $\mathbf{p}_3$ with the momentum transfer $\mathbf{q} = \mathbf{p}_3 - \mathbf{p}_1$. Moreover, since momentum is conserved during collisions, the function $S^{(4)}$ must include a delta factor such as $\delta_{\mathrm{D}}(\mathbf{p}_3+\mathbf{p}_4-\mathbf{p}_1-\mathbf{p}_2)$. Then $S^{(4)}$ is re-expressed as a function of three variables, $S(\mathbf{p}_1 + \frac{1}{2}\mathbf{q}, \mathbf{p}_2 - \frac{1}{2}\mathbf{q}; \mathbf{q}) \equiv S^{(4)}(\mathbf{p}_1, \mathbf{p}_2, \mathbf{p}_1 + \mathbf{q}, \mathbf{p}_4)\,\delta_{\mathrm{D}}(\mathbf{p}_4 + \mathbf{q} - \mathbf{p}_2)$. Performing the integral over $\mathbf{p}_4$ leads to

$$\begin{aligned}\frac{\partial f(\mathbf{p}_1)}{\partial t} =& \int \mathrm{d}\mathbf{p}_2\,\mathrm{d}\mathbf{q}\, S(\mathbf{p}_1 + \frac{1}{2}\mathbf{q}, \mathbf{p}_2 - \frac{1}{2}\mathbf{q}; \mathbf{q})\big\{f(\mathbf{p}_1+\mathbf{q})f(\mathbf{p}_2-\mathbf{q})[1+\epsilon h^3 f(\mathbf{p}_1)][1+\epsilon h^3 f(\mathbf{p}_2)]\\ &- f(\mathbf{p}_1)f(\mathbf{p}_2)[1+\epsilon h^3 f(\mathbf{p}_1+\mathbf{q})][1+\epsilon h^3 f(\mathbf{p}_2-\mathbf{q})]\big\}.\end{aligned} \tag{5.5}$$

5.1.1 Weak Deflection Approximation

We will now study equation (5.4) in a weak deflection approximation i.e. a situation where the scattering angle or the deviation of a particle's trajectory from its original path is small. This typically occurs when the forces involved in the interaction are weak, resulting in minimal energy transfer and only slight changes in the momentum of the particles (Landau and Lifshitz, 1980).

In this limit, we assume that $\mathbf{q}$ is small and that S varies slowly with $\mathbf{q}$ in its first two arguments. This allows us to expand equation (5.5) to the second order in $\mathbf{q}$. We can expand each term separately

$$S\left(\mathbf{p}_1 + \mathbf{q}/2, \mathbf{p}_2 - \mathbf{q}/2; \mathbf{q}\right) \simeq S\left(\mathbf{p}_1, \mathbf{p}_2; \mathbf{q}\right) + \frac{1}{2}q_i\frac{\partial S}{\partial p_{1,i}} - \frac{1}{2}q_i\frac{\partial S}{\partial p_{2,i}} = S + \frac{1}{2}q_i\partial_{1,2}S - \frac{1}{2}q_i\partial_{2,i}S \tag{5.6}$$

where S stands for $S(\mathbf{p}_1, \mathbf{p}_2; \mathbf{q})$. Notable is that the above expansion is only done up to the first order in $\mathbf{q}$, because the remaining terms vanish at zero order in $\mathbf{q}$.

$$
\begin{aligned}
f(\mathbf{p}_1 + \mathbf{q})\, f(\mathbf{p}_2 - \mathbf{q}) \simeq & \left(f(p_1) + q_i \frac{\partial f(p_1)}{\partial p_{1,i}} + \frac{1}{2} q_i q_2 \frac{\partial^2 f(p_1)}{\partial p_1 \partial p_{2j}} \right) \\
& \times \left(f(p_2) - q_k \frac{\partial f(p_i)}{\partial p_{2,i}} - \frac{1}{2} q_k q_m \frac{\partial^2 f(p_i)}{\partial p_{2,k} \partial p_{2,m}} \right)
\end{aligned}
\tag{5.7}
$$

The notation is abbreviated as $f_1 = f(\mathbf{p}_1)$, $\partial_t f = \partial f/\partial t$, $\partial_{1,i} f = \partial f/\partial p_{1i}$, $\partial_{1,ij} f = \partial^2 f/\partial p_{1i} \partial p_{1j}$, etc. Then we can approximate equation (5.5) as

$$
\begin{aligned}
\partial_t f(\mathbf{p}_1) = & \int \mathrm{d}\mathbf{p}_2 \mathrm{d}\mathbf{q} \left(S + q_i \partial_{1,i} S - q_i \partial_{2,i} S \right) \\
& \times \Big[(f_1 + q_i \partial_{1,i} f_1 + q_i q_j \partial_{1,ij} f_2)(f_2 - q_k \partial_{2,k} f_2 + q_k q_m \partial_{2,km} f_2) \\
& \times (1 + \epsilon h^3 f_1)(1 + \epsilon h^3 f_2) - f_1 f_2 (1 + \epsilon h^3 f_1 + \epsilon h^3 q_i \partial_{1,i} f_1 + \epsilon h^3 q_i q_j \partial_{1,ij} f_1) \\
& \times (1 + \epsilon h^3 f_2 - \epsilon h^3 q_k \partial_{2,k} f_2 + \epsilon h^3 q_k q_m \partial_{2,km} f_2) \Big].
\end{aligned}
$$

It must be noted that S is even in $\mathbf{q}$ by equation (5.14) due to the principle of detailed balance, which ensures that the scattering process and its reverse are in equilibrium, maintaining symmetry between the forward and backward directions of scattering. It means that if the direction of the momentum transfer $\mathbf{q}$ is reversed, the value of the scattering cross-section remains the same. This is a consequence of fundamental conservation laws. This results in vanishing the terms that are first order in $\mathbf{q}$ vanish when integrated. Thus, equation (5.8) simplifies to

$$
\begin{aligned}
\partial_t f(\mathbf{p}_1) = & \int \mathrm{d}\mathbf{p}_2 \mathrm{d}\mathbf{q}\, q_i q_j \big\{ S[\partial_{1,ij} f_1 f_2 (1 + \epsilon h^3 f_2) + \partial_{2,ij} f_2 f_1 (1 + \epsilon h^3 f_1) \\
& - 2 \partial_{1,i} f_1\, \partial_{2,j} f_2 (1 + \epsilon h^3 f_1 + \epsilon h^3 f_2)] + (\partial_{1,i} S - \partial_{2,i} S)[\partial_{1,j} f_1 f_2 (1 + \epsilon h^3 f_2) \\
& - \partial_{2,j} f_2 f_1 (1 + \epsilon h^3 f_1)] \big\}.
\end{aligned}
\tag{5.8}
$$

We can integrate the term below by parts

$$
\begin{aligned}
& - \frac{1}{2} \int \mathrm{d}\mathbf{p}_2 \mathrm{d}\mathbf{q}\ q_i q_j\ \partial_{2,i} S[\partial_{1,j} f_1 f_2 (1 + \epsilon h^3 f_2) - \partial_{2,j} f_2 f_1 (1 + \epsilon h^3 f_1)] \\
= & - \frac{1}{2} \int \mathrm{d}\mathbf{p}_2 \mathrm{d}\mathbf{q}\ q_i q_j\ \Big\{ S \left[\partial_{1,j} f_1 f_2 \left(1 + \epsilon h^3 f_2\right) - \partial_{3,j} f_2 f_1 \left(1 + \epsilon h^3 f_1\right) \right] \\
& S \left[\partial_{1,j} f_1 f_2 \left(1 + \epsilon h^3 f_2\right) + \partial_{1,j} f_1 f_2 \epsilon h^3 \partial_{2,j} f_2 + \partial_{ij,2} f_2 f_1 \left(1 + \epsilon h^3 f_1\right] \right. \Big\} \\
= & - \frac{1}{2} \int \mathrm{d}\mathbf{p}_2 \mathrm{d}\mathbf{q}\ q_i q_j\ \Big\{ S \left[\partial_{1,j} f_1 f_2 \left(1 + \epsilon h^3 f_2\right) - \partial_{2,j} f_2 f_1 \left(1 + \epsilon h^3 f_1\right) \right] \\
& - \partial_{1,j} h_1 \partial_{2,1} f_2 \left(1 + 2\epsilon h^3 f_2\right) + \partial_{ij,2} f_2 f_1 \left(1 + \epsilon h^3 f_1\right) \Big\}
\end{aligned}
\tag{5.9}
$$

The last term in above relation cancels the second term of equation (5.8) and we obtain

$$\begin{aligned}
\partial_t f(\mathbf{p}_1) =& \int \mathrm{d}\mathbf{p}_2 \mathrm{d}\mathbf{q}\, q_i q_j \big\{ S[\partial_{1,ij} f_1 f_2 (1+\epsilon h^3 f_2) - 2\partial_{1,i} f_1\, \partial_{2,j} f_2 (1+\epsilon h^3 f_1 + \epsilon h^3 f_2) \\
&+ \partial_{1,j} f_1 f_2 \left(1+\epsilon h^3 f_2\right) - \partial_{2,j} f_2 f_1 \left(1+\epsilon h^3 f_1\right) - \partial_{1,j} h_1 \partial_{2,1} f_2 \left(1+2\epsilon h^3 f_2\right)] \\
&+ \partial_{1,i} S[\partial_{1,j} f_1 f_2 (1+\epsilon h^3 f_2) - \partial_{2,j} f_2 f_1 (1+\epsilon h^3 f_1)] \big\} \\
=& \int \mathrm{d}\mathbf{p}_2 \mathrm{d}\mathbf{q}\, q_i q_j \big\{ S[\partial_{1,ij} f_1 f_2 (1+\epsilon h^3 f_2) - \partial_{1,i} f_1\, \partial_{2,j} f_2 (1+2\epsilon h^3 f_2 - 2 - 2\epsilon h^3 f_1 - 2\epsilon h^3 f_2) \\
&+ \partial_{1,j} f_1 f_2 \left(1+\epsilon h^3 f_2\right) - \partial_{2,j} f_2 f_1 \left(1+\epsilon h^3 f_1\right) + \partial_{1,i} S[\partial_{1,j} f_1 f_2 (1+\epsilon h^3 f_2) \qquad (5.10) \\
&- \partial_{2,j} f_2 f_1 (1+\epsilon h^3 f_1)] \big\} \qquad (5.11)
\end{aligned}$$

Remember that terms containing first order in q vanish at integration.

$$\int \mathrm{d}\ \mathbf{p}_2 \mathrm{d}\mathbf{q}\, q_i q_j\ \partial_{1,j} f_1 f_2 \left(1+\epsilon h^3 f_2\right) - \partial_{2,j} f_2 f_1 \left(1+\epsilon h^3 f_1\right) = 0 \qquad (5.12)$$

Finally, we will arrive at

$$\begin{aligned}
\partial_t f(\mathbf{p}_1) =& \int \mathrm{d}\mathbf{p}_2 \mathrm{d}\mathbf{q}\, q_i q_j \big\{ S[\partial_{1,ij} f_1 f_2 (1+\epsilon h^3 f_2) - \partial_{1,i} f_1\, \partial_{2,j} f_2 (1+2\epsilon h^3 f_1)] \\
&+ \partial_{1,i} S[\partial_{1,j} f_1 f_2 (1+\epsilon h^3 f_2) - \partial_{2,j} f_2 f_1 (1+\epsilon h^3 f_1)] \big\} \\
=& \,\partial_{1,i} \int \mathrm{d}\mathbf{p}_2 \mathrm{d}\mathbf{q}\, q_i q_j S[\partial_{1,j} f_1 f_2 (1+\epsilon h^3 f_2) - \partial_{2,j} f_2 f_1 (1+\epsilon h^3 f_1)] \qquad (5.13)
\end{aligned}$$

Specifically, for gravitational scattering between particles of mass m_b, the expression for function S is given by

$$S(\mathbf{a}, \mathbf{b}; \mathbf{q}) = \frac{4G^2 m_\mathrm{b}^5}{q^4}\, \delta_\mathrm{D}[(\mathbf{b}-\mathbf{a})\cdot \mathbf{q}]. \qquad (5.14)$$

In this relation, the delta function enforces the conservation of relative momentum in the collision. Consequently, the magnitudes of momentum differences $|\mathbf{p}_4 - \mathbf{p}_3|$ and $|\mathbf{p}_2 - \mathbf{p}_1|$ are equal. The factor q^{-4} reflects the angular dependence of the Coulomb differential scattering cross-section, which behaves as $|\sin^2(\theta/2)|^{-4}$, where θ is the scattering angle (Goodman, 1983; Bar-Or et al., 2021).

Substituting S and carrying out the integral over $\mathbf{q}$ yields

$$\int \mathrm{d}\mathbf{q}\, q_i q_j S(\mathbf{p}_1, \mathbf{p}_2; \mathbf{q}) = \int \mathrm{d}\mathbf{q}\, q_i q_j \frac{4G^2 m_b^5}{q^4} \delta_D[(b-a)\cdot q] = 4G^2 m_\mathrm{b}^5 \ln\Lambda\, u_{ij}(\mathbf{p}_1 - \mathbf{p}_2), \qquad (5.15)$$

where u_{ij} is the collision kernel, and $\Lambda = q_\mathrm{max}/q_\mathrm{min}$ with q_max and q_min the maximum and minimum impact parameters included in the integral.

Now we change the variables from momentum $\mathbf{p}$ to velocity $\mathbf{v} = \mathbf{p}/m_\mathrm{b}$, from $\mathbf{v}_1$ and $\mathbf{v}_2$ to $\mathbf{v}$ and $\mathbf{v}'$, and from the number density in position-momentum phase space $f(\mathbf{p})$ to the mass density in position-velocity space $F_\mathrm{b}(\mathbf{v}) = m_\mathrm{b}^4 f(m_\mathrm{b}\mathbf{v})$. Then we reach at the kinetic equation as the following

$$\begin{aligned}
\frac{\partial F_\mathrm{b}(\mathbf{v})}{\partial t} = 2G^2 \ln\Lambda \frac{\partial}{\partial v_i} \int \mathrm{d}\mathbf{v}'\, u_{ij}(\mathbf{v}-\mathbf{v}') \Big\{ &\left[m_\mathrm{b} + \epsilon \frac{h^3}{m_\mathrm{b}^3} F_\mathrm{b}(\mathbf{v}') \right] F_\mathrm{b}(\mathbf{v}') \frac{\partial F_\mathrm{b}(\mathbf{v})}{\partial v_j} \\
&- \left[1 + \epsilon \frac{h^3}{m_\mathrm{b}^3} F_\mathrm{b}(\mathbf{v}) \right] \frac{\partial F_\mathrm{b}(\mathbf{v}')}{\partial v_j'} F_\mathrm{b}(\mathbf{v}) \Big\}.
\end{aligned} \qquad (5.16)$$

5.2 Schrödinger-Poisson System of Equations

The aim of this section is to obtain the kinetic equation from a different perspective: the gravitational interactions among waves. This approach is particularly suited to the case of FDM due to its intrinsic wave-like nature. The evolution of such waves, which interact gravitationally, is governed by the Schrödinger-Poisson system of equations as described below

$$\mathrm{i}\hbar \frac{\partial \psi(\mathbf{r},t)}{\partial t} = -\frac{\hbar^2}{2m_\mathrm{b}}\nabla^2\psi(\mathbf{r},t) + m_\mathrm{b}\Phi(\mathbf{r},t)\psi(\mathbf{r},t), \tag{5.17}$$

$$\nabla^2\Phi(\mathbf{r},t) = 4\pi G(|\psi(\mathbf{r},t)|^2 - \rho_0). \tag{5.18}$$

where $\psi(\mathbf{r},t)$ is the complex wavefunction representing the FDM field. $\Phi(\mathbf{r},t)$ is the gravitational potential. In the Poisson equation, the term ρ_0 is the background density and appears because of the Jeans swindle. The Schrödinger equation accounts for the evolution of the wavefunction and the Poisson equation determines the gravitational potential.

5.2.1 Wigner Function Evolution

Let us begin the calculations by introducing the Wigner function (Wigner, 1932), given by

$$W(\mathbf{r},\mathbf{v},t) = \int \frac{\mathrm{d}\mathbf{s}}{(2\pi)^3}\,\mathrm{e}^{-\mathrm{i}\mathbf{v}\cdot\mathbf{s}}\,\psi\big(\mathbf{r}+\hbar\mathbf{s}/m_\mathrm{b},t\big)\,\psi^*\big(\mathbf{r}-\hbar\mathbf{s}/m_\mathrm{b},t\big) \tag{5.19}$$

The Wigner distribution function serves as a bridge between quantum mechanics and classical mechanics. It is defined in phase space and represents a quasi-probability distribution of a system. Unlike classical probability distributions, the Wigner function can assume negative values, which is a distinctive feature of quantum behavior and highlights the non-classical nature of the system

This function is particularly valuable in the study of fuzzy dark matter (FDM), as it enables the wave properties of the system to be expressed in a form that closely resembles classical distributions, thus facilitating a connection between the quantum wave dynamics and the classical kinetic framework. The Wigner distribution can be seen as the quantum analog to the discrete classical phase-space distribution function $F_d(\mathbf{x},\mathbf{v},t)$, which is given by

$$F_d(\mathbf{r},\mathbf{v},t) = m_b \sum_{i=1}^{N} \delta_D\left[\mathbf{r}-\mathbf{r}_i(t)\right]\,\delta_D\left[\mathbf{v}-\mathbf{v}_i(t)\right], \tag{5.20}$$

where δ_D denotes the Dirac delta function, and the sum runs over all N particles.

In this context, $W(\mathbf{r},\mathbf{v},t)$ can be interpreted classically as the density of bosons in the infinitesimal volume $\mathrm{d}\mathbf{r}\,\mathrm{d}\mathbf{v}$ of phase space. When averaged over realizations, $\overline{W} = \langle W\rangle$ represents the quantum analog of the mean phase-space distribution function, $F_b = \langle F_d\rangle$, which is the distribution function whose corresponding kinetic equation we aim to derive. This connection allows for a seamless transition from quantum to classical descriptions, essential for modeling systems such as FDM, where both wave-like and particle-like behaviors are at play (Bar-Or et al., 2021).

It should also be noted that W and $\overline{W}$ satisfy the respective normalization relations as given below

$$\int \mathrm{d}\mathbf{v}\,W(\mathbf{r},\mathbf{v},t) = |\psi(\mathbf{r},t)|^2; \quad \int \mathrm{d}\mathbf{v}\,\overline{W}(\mathbf{v}) = \rho_0, \tag{5.21}$$

where we used $\int \mathrm{d}\mathbf{v}/(2\pi)^3 \mathrm{e}^{-\mathrm{i}\mathbf{v}\cdot\mathbf{s}} = \delta_{\mathrm{D}}(\mathbf{s})$.

The evolution of $W(\mathbf{r}, \mathbf{v}, t)$ follows from the Schrödinger equation (5.17). To use this feature, we take the time derivative of the Wigner function

$$\frac{\partial W}{\partial t} = \int \frac{d\mathbf{s}}{(2\pi)^3} e^{-i\mathbf{v}\cdot\mathbf{s}} \left[\frac{\partial}{\partial t}\psi\left(\mathbf{r}_+\right)\psi^*\left(\mathbf{r}_-\right) + \psi\left(\mathbf{r}_+\right)\frac{\partial}{\partial t}\psi\left(\mathbf{r}_-\right)\right] \tag{5.22}$$

For simplicity we used $\mathbf{r}_+$ and $\mathbf{r}_-$ instead of $\mathbf{r} + \hbar\mathbf{s}/m_{\mathrm{b}}$ and $\mathbf{r} + \hbar\mathbf{s}/m_{\mathrm{b}}$ respectively. Next we will substitute the Schrodinger equation for ψ and $\psi*$ in the above result

$$\begin{aligned}\frac{\partial W}{\partial t} = \int \frac{ds}{(2\pi)^3} e^{-i\mathbf{v}\cdot\mathbf{s}} &\left[\left(\frac{i\hbar}{2m_b}\nabla^2\psi(\mathbf{r}_+) + \frac{i}{\hbar}m_b\Phi\psi(\mathbf{r}_+)\right)\psi^*(\mathbf{r}_-)\right. \\ &\left. + \psi(\mathbf{r}_+)\left(\frac{-i\hbar}{2mb}\nabla^2\psi^*(\mathbf{r}_-) - \frac{i}{\hbar}m_b\Phi\psi^*(\mathbf{r}_-)\right)\right.,\end{aligned} \tag{5.23}$$

and the spatial derivative is (Bar-Or et al., 2021)

$$\nabla^2\psi\left(r_\pm\right) = \pm\frac{2m_b}{\hbar}\frac{\partial}{\partial s}\cdot\left[\nabla\psi\left(r_\pm\right)\right] \tag{5.24}$$

Therefore, the kinetic terms on the right hand side involving the Laplacian $\nabla^2\psi$ can written in the form

$$\begin{aligned}&\frac{i\hbar}{2m_b}\int \frac{d\mathbf{s}}{(2\pi)^3} e^{-i\mathbf{v}\cdot\mathbf{s}} \left(\psi^*(\mathbf{r}_-)\nabla^2\psi(\mathbf{r}_+) - \psi(\mathbf{r}_+)\nabla^2\psi^*(\mathbf{r}_-)\right) \\ &= i\int \frac{d\mathbf{s}}{(2\pi)^3} e^{-i\mathbf{v}\cdot\mathbf{s}} \left(\psi^*(\mathbf{r}_-)\frac{\partial}{\partial s}\cdot\left[\nabla\psi(\mathbf{r}_+)\right] + \psi(\mathbf{r}_+)\frac{\partial}{\partial s}\cdot\left[\nabla\psi^*(\mathbf{r}_-)\right]\right).\end{aligned} \tag{5.25}$$

The integral is computed in Appendix A.6. From there, equation (5.25) is simplified to $-\mathbf{v}\cdot\nabla W$. Finally equation (5.23) will simplify into

$$\frac{\partial W}{\partial t} + \mathbf{v}\cdot\nabla W = i\frac{m_b}{\hbar}\int \frac{d\mathbf{s}}{(2\pi)^3} e^{-i\mathbf{v}\cdot\mathbf{s}}\left[\Phi(\mathbf{r}_+) - \Phi(\mathbf{r}_-)\right]\psi(\mathbf{r}_+)\psi^*(\mathbf{r}_-) \tag{5.26}$$

We can also express this result in a more compact form

$$\frac{\partial W(\mathbf{r}, \mathbf{v}, t)}{\partial t} + \mathbf{v}\cdot W(\mathbf{r}, \mathbf{v}, t) = \mathfrak{D}\left[\Phi(\mathbf{r}, t), W(\mathbf{r}, \mathbf{v}, t)\right]. \tag{5.27}$$

In this expression, the non-linear term on the right-hand side is

$$\mathfrak{D}\left[\Phi(\mathbf{r}, t), W(\mathbf{r}, \mathbf{v}, t)\right] \equiv \mathrm{i}\int \mathrm{d}\mathbf{k}\int_{\mathcal{B}} \frac{\mathrm{d}\omega}{2\pi}\, \mathrm{e}^{\mathrm{i}(\mathbf{k}\cdot\mathbf{r} - \omega t)}\, \widehat{\Phi}(\mathbf{k}, \omega)\, \widehat{\mathfrak{D}}_{\mathbf{k}}\left[W(\mathbf{r}, \mathbf{v}, t)\right]. \tag{5.28}$$

Here, the Fourier-Laplace transformed potential $\widehat{\Phi}(\mathbf{k}, \omega)$ is introduced via the following

$$\widehat{\Phi}(\mathbf{k}, \omega) = \int \frac{\mathrm{d}\mathbf{r}}{(2\pi)^3}\int_0^\infty \mathrm{d}t\, \mathrm{e}^{-\mathrm{i}(\mathbf{k}\cdot\mathbf{r} - \omega t)}\, \Phi(\mathbf{r}, t); \quad \Phi(\mathbf{r}, t) = \int \mathrm{d}\mathbf{k}\int_{\mathcal{B}} \frac{\mathrm{d}\omega}{2\pi}\, \mathrm{e}^{\mathrm{i}(\mathbf{k}\cdot\mathbf{r} - \omega t)}\, \widehat{\Phi}(\mathbf{k}, \omega), \tag{5.29}$$

where $\mathcal{B}$ is chosen such that $\mathrm{Im}(\omega)$ is large enough to avoid any issues with convergence or the improper handling of poles. This means that the Bromwich contour[6] should pass

[6] The Bromwich contour is a vertical path in the complex plane, selected to lie to the right of all singularities (poles) of the integrand, ensuring the convergence of the inverse Laplace transform.

above all poles of the integrand, which ensures that the inverse Fourier-Laplace transform correctly recovers the potential $\Phi(\mathbf{r}, t)$ from its transform $\hat{\Phi}(\mathbf{k}, \omega)$.

Additionally, the finite-difference operator is defined as

$$\widehat{\mathfrak{D}}_{\mathbf{k}}\big[W(\mathbf{v})\big] = \frac{m_{\mathrm{b}}}{\hbar}\left[W\left(\mathbf{v} + \frac{\hbar}{2m_{\mathrm{b}}}\mathbf{k}\right) - W\left(\mathbf{v} - \frac{\hbar}{2m_{\mathrm{b}}}\mathbf{k}\right)\right]. \tag{5.30}$$

In the classical limit where $\hbar \to 0$, this finite-difference operator simplifies to

$$\widehat{\mathfrak{D}}_{\mathbf{k}}\big[W(\mathbf{r}, \mathbf{v}, t)\big] \to \mathbf{k}\cdot\frac{\partial W(\mathbf{r}, \mathbf{v}, t)}{\partial \mathbf{v}}; \quad \mathfrak{D}\big[\Phi(\mathbf{r}, t), W(\mathbf{r}, \mathbf{v}, t)\big] \to \Phi(\mathbf{r}, t)\cdot\frac{\partial W(\mathbf{r}, \mathbf{v}, t)}{\partial \mathbf{v}}; \tag{5.31}$$

Thus, equation (5.27) reduces to the classical collisionless Boltzmann equation i.e. equation (5.1) but with the collision term on the r.h.s. equal to zero.

$$\frac{\partial W}{\partial t} + \mathbf{v}\cdot W - \Phi\cdot\frac{\partial W}{\partial \mathbf{v}} = 0. \tag{5.32}$$

5.2.2 Impact of Quantum Fluctuations on the Halo

Now to see how quantum fluctuations influence the halo distribution function, we study the evolution of the perturbed Wigner function which is in fact an extension of equation (5.27). We add a perturbation term to the Wigner function around its ensemble average

$$W = \overline{W} + f. \tag{5.33}$$

Clearly both terms satisfy equation (5.27). Therefore, in the linear regime the evolutions read

$$\frac{\partial f(\mathbf{r}, \mathbf{v}, t)}{\partial t} + \mathbf{v}\cdot f(\mathbf{r}, \mathbf{v}, t) = \mathfrak{D}\big[\Phi(\mathbf{r}, t), \overline{W}(\mathbf{r}, \mathbf{v}, t)\big], \tag{5.34}$$

$$\frac{\partial \overline{W}(\mathbf{r}, \mathbf{v}, t)}{\partial t} + \mathbf{v}\cdot\overline{W}(\mathbf{r}, \mathbf{v}, t) = \big\langle \mathfrak{D}\big[\Phi(\mathbf{r}, t), f(\mathbf{r}, \mathbf{v}, t)\big]\big\rangle. \tag{5.35}$$

$\overline{W}$ is a quasi-stationary solution of the l.h.s. of equation (5.35), meaning that $\overline{W} = \overline{W}(\mathbf{v}, t)$ is homogeneous and changes only slowly in time. This means that the distribution function $\overline{W}$ depends only on the velocity $\mathbf{v}$ and time t, and not directly on position $\mathbf{r}$. Consequently, the system is approximated as evolving slowly, and we treat it as nearly steady-state at any given time. It is essential to note that this approximation holds only in the weak-coupling limit, where interactions between particles or system components are relatively weak.

We can claim that l.h.s. of equation (5.35) represents the ensemble-averaged collisionless Boltzmann equation, which describes the evolution of the system in the absence of interactions or external forces, effectively capturing the free streaming of components. This part of the equation governs how the distribution functions evolve in phase space when no perturbations are present. On the other hand, the r.h.s includes the collision term, which accounts for the interactions and perturbations affecting the system. As Bar-Or et al. (2021) states, since both the potential $\Phi(\mathbf{r}, t)$ and the perturbed distribution function $f(\mathbf{r}, \mathbf{v}, t)$ are quadratic in the wavefunction, the collision term involves the product of four factors of the wavefunction $\psi(\mathbf{r}, t)$, evaluated at different locations.

This reflects the nonlinear nature of the interactions, where the perturbations can influence multiple particles or system components simultaneously, leading to more complex behavior in the evolution of the distribution function.

We take the Laplace-Fourier transform of the evolution of perturbations which reads

$$\mathcal{L}\left(\frac{\partial f(\mathbf{r},\mathbf{v},t)}{\partial t}+\mathbf{v}\cdot f(\mathbf{r},\mathbf{v},t)\right)=\mathcal{L}\left(\mathfrak{D}\left[\Phi(\mathbf{r},t),\overline{W}(\mathbf{v})\right]\right), \tag{5.36}$$

Starting with the Fourier transform of f we will have

$$\hat{f}(\mathbf{k},\mathbf{v},t)=\int\frac{d\mathbf{r}}{(2\pi)^3}e^{-i\mathbf{k}\cdot\mathbf{r}}f(\mathbf{r},\mathbf{v},t) \tag{5.37}$$

Now, we apply the Laplace transform to the equation and replace time t with the frequency ω

$$\mathcal{L}\left(\frac{\partial f(\mathbf{r},\mathbf{v},t)}{\partial t}\right)=i\omega\hat{f}(\mathbf{k},\mathbf{v},\omega)-\hat{f}_0(\mathbf{k},\mathbf{v}) \tag{5.38}$$

with $\hat{f}_0(\mathbf{k},\mathbf{v})$ being $\hat{f}_0(\mathbf{k},\mathbf{v})=\hat{f}_0(\mathbf{k},\mathbf{v},t=0)$, then the transform of the second term of the l.h.s becomes

$$\mathcal{L}\left(\mathbf{v}\cdot f(\mathbf{r},\mathbf{v},t)\right)=-i\mathbf{k}\cdot\mathbf{v}\hat{f}(\mathbf{r},\mathbf{v},\omega), \tag{5.39}$$

then for the r.h.s we can use the definition given earlier in equation (5.28). In this case, the r.h.s transforms as

$$\mathcal{L}\left(\mathfrak{D}\left[\Phi(\mathbf{r},t),\overline{W}(\mathbf{v})\right]\right)=i\widehat{\Phi}(\mathbf{k},\omega)\,\widehat{\mathfrak{D}}_{\mathbf{k}}\left[\overline{W}(\mathbf{v})\right] \tag{5.40}$$

Putting these relations together and substituting them in the original equation (equation (5.36)), we achieve

$$i\omega\hat{f}(\mathbf{k},\mathbf{v},\omega)-\hat{f}_0(\mathbf{k},\mathbf{v})-i\mathbf{k}\cdot\mathbf{v}\hat{f}(\mathbf{k},\mathbf{v},\omega)=i\widehat{\Phi}(\mathbf{k},\omega)\,\widehat{\mathfrak{D}}_{\mathbf{k}}\left[W(\mathbf{v})\right] \tag{5.41}$$

After some rearrangement, we arrive at equation 56 in the paper

$$\hat{f}(\mathbf{k},\mathbf{v},\omega)=-\frac{\widehat{\mathfrak{D}}_{\mathbf{k}}\left[\overline{W}(\mathbf{v})\right]}{\omega-\mathbf{k}\cdot\mathbf{v}}\,\widehat{\Phi}(\mathbf{k},\omega)+\mathrm{i}\frac{\hat{f}_0(\mathbf{k},\mathbf{v})}{\omega-\mathbf{k}\cdot\mathbf{v}}. \tag{5.42}$$

5.2.3 Balescu–Lenard kinetic equation

Now consider the normalization equations below

$$\int\mathrm{d}\mathbf{v}\,W(\mathbf{r},\mathbf{v},t)=|\psi(\mathbf{r},t)|^2;\quad\int\mathrm{d}\mathbf{v}\,\overline{W}(\mathbf{v})=\rho_0. \tag{5.43}$$

Using the above relations and the fact that $W=\overline{W}+f$ will help us rewrite the Poisson equation in a different form

$$\begin{aligned}\nabla^2\Phi(\mathbf{r},t)&=4\pi G(|\psi(\mathbf{r},t)|^2-\rho_0)=4\pi G\int d\mathbf{v}\left(W(\mathbf{r},\mathbf{v},t)-\overline{W}(\mathbf{v})\right)\\&=4\pi G\int d\mathbf{v}f(\mathbf{r},\mathbf{v},t)\end{aligned} \tag{5.44}$$

Taking the Laplace-Fourier transform of the last result leads to

$$(ik^2)\widehat{\Phi}(\mathbf{k},\omega) = 4\pi G \int d\mathbf{v} \hat{f}(\mathbf{k},\mathbf{v},\omega) \;\rightarrow \widehat{\Phi}(\mathbf{k},\omega) = -\frac{4\pi G}{k^2}\int d\mathbf{v} \hat{f}(\mathbf{k},\mathbf{v},\omega) \tag{5.45}$$

To proceed further, we can also act the same operator on the r.h.s of the above expression on both sides of equation (5.42) which results in

$$\begin{aligned} -\frac{4\pi G}{k^2}\int d\mathbf{v} \hat{f}(\mathbf{k},\mathbf{v},\omega) = & \frac{4\pi G}{k^2}\widehat{\Phi}(\mathbf{k},\omega)\int d\mathbf{v}\frac{\widehat{\mathfrak{D}}_{\mathbf{k}}\left[\overline{W}(\mathbf{v})\right]}{\omega - \mathbf{k}\cdot\mathbf{v}} \\ & - \frac{4\pi G i}{k^2}\int d\mathbf{v}\frac{1}{\omega - \mathbf{k}\cdot\mathbf{v}}\hat{f}_0(\mathbf{k},\omega) \end{aligned} \tag{5.46}$$

Based on what we derived in 5.45, the l.h.s can simply be replaced with $\widehat{\Phi}(\mathbf{k},\omega)$. There, we can rewrite the above equation

$$\widehat{\Phi}(\mathbf{k},\omega)\left(1 - \frac{4\pi G}{k^2}\int d\mathbf{v}\frac{\widehat{\mathfrak{D}}_{\mathbf{k}}\left[\overline{W}(\mathbf{v})\right]}{\omega - \mathbf{k}\cdot\mathbf{v}}\right) = -\frac{4\pi G i}{k^2}\int d\mathbf{v}\frac{1}{\omega - \mathbf{k}\cdot\mathbf{v}}\hat{f}_0(\mathbf{k},\omega) \tag{5.47}$$

Thus, we can obtain $\widehat{\Phi}(\mathbf{k},\omega)$ in the following form

$$\widehat{\Phi}(\mathbf{k},\omega) = \frac{1}{\epsilon(\mathbf{k},\omega)}\,\frac{4\pi G}{\mathrm{i}k^2}\int \mathrm{d}\mathbf{v}\,\frac{\widehat{f_0}(\mathbf{k},\mathbf{v})}{\omega - \mathbf{k}\cdot\mathbf{v}}, \tag{5.48}$$

where the dielectric function is

$$\epsilon(\mathbf{k},\omega) = 1 - \frac{4\pi G}{k^2}\int \mathrm{d}\mathbf{v}\,\frac{\widehat{\mathfrak{D}}_{\mathbf{k}}\left[\overline{W}(\mathbf{v})\right]}{\omega - \mathbf{k}\cdot\mathbf{v}}. \tag{5.49}$$

In accordance with the convention established in equation (5.29), this corresponds to substituting $\omega_{\mathrm{R}} \rightarrow \omega_{\mathrm{R}} + \mathrm{i}0^+$ and using the Plemelj formula

$$\frac{1}{\omega_{\mathrm{R}} + \mathrm{i}0^+} = \mathcal{P}\left(\frac{1}{\omega_{\mathrm{R}}}\right) - \mathrm{i}\pi\delta_{\mathrm{D}}(\omega_{\mathrm{R}}), \tag{5.50}$$

for $\omega_{\mathrm{R}} \in \mathbb{R}$ and with $\mathcal{P}$ being Cauchy's principal value [7].

To connect the long-term evolution of the mean distribution function, $\partial\overline{W}(\mathbf{v},t)/\partial t$, with the correlations of the initial distribution function fluctuations $\widehat{f_0}(\mathbf{k},\mathbf{v})$, we now refer to equation (5.35)

$$\frac{\partial\overline{W}(\mathbf{r},\mathbf{v},t)}{\partial t} + \mathbf{v}\cdot\overline{W}(\mathbf{r},\mathbf{v},t) = \left\langle \mathfrak{D}\left[\Phi(\mathbf{r},t), f(\mathbf{r},\mathbf{v},t)\right]\right\rangle. \tag{5.51}$$

[7] Cauchy's principal value is a method to assign a finite value to improper integrals that diverge at singularities. For an integral $\int_a^b f(x)\,dx$ with a singularity at $x = c$, the principal value is defined as

$$\mathcal{P}\int_a^b f(x)\,dx = \lim_{\epsilon\to 0}\left(\int_a^{c-\epsilon} f(x)\,dx + \int_{c+\epsilon}^b f(x)\,dx\right).$$

By excluding an infinitesimal symmetric region around the singularity and taking the limit as this region shrinks to zero, $\mathcal{P}$ balances the contributions on either side of the singularity to produce a finite result.

Since we are considering a homogeneous $\overline{W}$, the second term vanishes. Furthermore, we use equation (5.28) to replace the term on the r.h.s which gives

$$\frac{\partial \overline{W}(\mathbf{v},t)}{\partial t} = \mathrm{i}\int \mathrm{d}\mathbf{k}\mathrm{d}\mathbf{k}'\, \mathrm{e}^{\mathrm{i}(\mathbf{k}+\mathbf{k}')\cdot\mathbf{r}}\, \widehat{\mathfrak{D}}_{\mathbf{k}'}\left[\int \frac{\mathrm{d}\omega}{2\pi}\frac{\mathrm{d}\omega'}{2\pi}\, \mathrm{e}^{-\mathrm{i}(\omega+\omega')t}\left\langle \widehat{f}(\mathbf{k},\mathbf{v},\omega)\, \widehat{\Phi}(\mathbf{k}',\omega')\right\rangle\right]. \tag{5.52}$$

Equation (5.42) has two terms and consequently, we get two contributions from substituting the expression for $\hat{f}(\mathbf{k},\mathbf{v},\omega)$ in the above equation resulting in

$$\frac{\partial \overline{W}(\mathbf{v},t)}{\partial t} = F_1(\mathbf{v}) + F_2(\mathbf{v}), \tag{5.53}$$

where

$$\begin{aligned} F_1(\mathbf{v}) &= -\int \mathrm{d}\mathbf{k}\mathrm{d}\mathbf{k}'\, \mathrm{e}^{\mathrm{i}(\mathbf{k}+\mathbf{k}')\cdot\mathbf{r}}\, \widehat{\mathfrak{D}}_{\mathbf{k}'}\left[\int \frac{\mathrm{d}\omega}{2\pi}\frac{\mathrm{d}\omega'}{2\pi}\frac{\mathrm{e}^{-\mathrm{i}(\omega+\omega')t}}{\omega-\mathbf{k}\cdot\mathbf{v}}\left\langle \widehat{f}_0(\mathbf{k},\mathbf{v})\, \widehat{\Phi}(\mathbf{k}',\omega')\right\rangle\right] \\ F_2(\mathbf{v}) &= -\mathrm{i}\int \mathrm{d}\mathbf{k}\mathrm{d}\mathbf{k}'\, \mathrm{e}^{\mathrm{i}(\mathbf{k}+\mathbf{k}')\cdot\mathbf{r}}\, \widehat{\mathfrak{D}}_{\mathbf{k}'}\left[\widehat{\mathfrak{D}}_{\mathbf{k}}\left[\overline{W}(\mathbf{v})\right]\int \frac{\mathrm{d}\omega}{2\pi}\frac{\mathrm{d}\omega'}{2\pi}\frac{\mathrm{e}^{-\mathrm{i}(\omega+\omega')t}}{\omega-\mathbf{k}\cdot\mathbf{v}}\left\langle \widehat{\Phi}(\mathbf{k},\omega)\, \widehat{\Phi}(\mathbf{k}',\omega')\right\rangle\right]. \end{aligned} \tag{5.54}$$

To progress further, we use equation (5.48) to substitute $\widehat{\Phi}(\mathbf{k},\omega)$. This yields

$$\begin{aligned} F_1(\mathbf{v}) = \mathrm{i}\int \mathrm{d}\mathbf{k}\mathrm{d}\mathbf{k}'\, \mathrm{e}^{\mathrm{i}(\mathbf{k}+\mathbf{k}')\cdot\mathbf{r}}\, \widehat{\mathfrak{D}}_{\mathbf{k}'}\Bigg[\frac{4\pi G}{k'^2}\int \mathrm{d}\mathbf{v}'\int \frac{\mathrm{d}\omega}{2\pi}\frac{\mathrm{d}\omega'}{2\pi}\frac{1}{\epsilon(\mathbf{k}',\omega')}\frac{\mathrm{e}^{-\mathrm{i}(\omega+\omega')t}}{(\omega-\mathbf{k}\cdot\mathbf{v})(\omega'-\mathbf{k}'\cdot\mathbf{v}')} \\ \times\left\langle \widehat{f}_0(\mathbf{k},\mathbf{v})\, \widehat{f}_0(\mathbf{k}',\mathbf{v}')\right\rangle\Bigg], \end{aligned} \tag{5.55}$$

$$\begin{aligned} F_2(\mathbf{v}) = \mathrm{i}\int \mathrm{d}\mathbf{k}\mathrm{d}\mathbf{k}'\, \mathrm{e}^{\mathrm{i}(\mathbf{k}+\mathbf{k}')\cdot\mathbf{r}}\, \widehat{\mathfrak{D}}_{\mathbf{k}'}\Bigg[\frac{(4\pi G)^2}{k^2k'^2}\widehat{\mathfrak{D}}_{\mathbf{k}}\left[\overline{W}(\mathbf{v})\right]\int \mathrm{d}\mathbf{v}'\mathrm{d}\int \frac{\mathrm{d}\omega}{2\pi}\frac{\mathrm{d}\omega'}{2\pi}\frac{1}{\epsilon(\mathbf{k},\omega)\,\epsilon(\mathbf{k}',\omega')} \\ \times\frac{\mathrm{e}^{-\mathrm{i}(\omega+\omega')t}}{(\omega-\mathbf{k}\cdot\mathbf{v})(\omega-\mathbf{k}\cdot\mathbf{v}')(\omega'-\mathbf{k}')}\times\left\langle \widehat{f}_0(\mathbf{k},\mathbf{v}')\, \widehat{f}_0(\mathbf{k}',)\right\rangle\Bigg]. \end{aligned} \tag{5.56}$$

Now we need to describe the initial fluctuations' correlations within the system. For a homogeneous system, these correlations depend only on the relative separation $\mathbf{r}-\mathbf{r}'$ of the points, as opposed to their absolute positions. Assuming that particle velocities are chosen independently from the time-averaged distribution function $F_b(\mathbf{v})$, the correlation function vanishes when $\mathbf{v}\neq\mathbf{v}'$ (Bar-Or et al., 2021). Thus, we can express the correlations as follows

$$\begin{aligned} \langle f_0(\mathbf{r},\mathbf{v})f_0(\mathbf{r}',\mathbf{v}')\rangle &= \delta_D(\mathbf{v}-\mathbf{v}')C(\mathbf{r}-\mathbf{r}',\mathbf{v}), \\ \langle \hat{f}_0(\mathbf{k},\mathbf{v})\hat{f}_0(\mathbf{k}',\mathbf{v}')\rangle &= \delta_D(\mathbf{k}+\mathbf{k}')\delta_D(\mathbf{v}'-\mathbf{v})\hat{C}(\mathbf{k},\mathbf{v}), \end{aligned} \tag{5.57}$$

where $\hat{C}(\mathbf{k},\mathbf{v})$ represents the Fourier transform of the correlation function $C(\mathbf{r}-\mathbf{r}',\mathbf{v})$ (See Appendix A.7). Since the distribution function $W(\mathbf{r},\mathbf{v},t)$ is real, $f_0(\mathbf{r},\mathbf{v})$ is also real. Consequently, $C(\mathbf{r},\mathbf{v})$ is also real and an even function of r. As a result, $\hat{C}(\mathbf{k},\mathbf{v})$ is both real and an even function of $\mathbf{k}$. Considering that $\widehat{\mathfrak{D}}_{-\mathbf{k}}[\overline{W}(\mathbf{v})] = -\widehat{\mathfrak{D}}_{\mathbf{k}}[\overline{W}(\mathbf{v})]$ and substituting 5.57 into 5.55 and 5.56, the following expressions are obtained

$$
\begin{aligned}
F_1(\mathbf{v}) &= -\mathrm{i}\!\int\! \mathrm{d}\mathbf{k}\, \widehat{\mathfrak{D}}_{\mathbf{k}} \left[\frac{4\pi G}{k^2}\, \widehat{C}(\mathbf{k},\mathbf{v}) \!\int\! \frac{\mathrm{d}\omega}{2\pi}\frac{\mathrm{d}\omega'}{2\pi}\, \frac{1}{\epsilon(-\mathbf{k},\omega')}\, \frac{\mathrm{e}^{-\mathrm{i}(\omega+\omega')t}}{(\omega-\mathbf{k}\cdot\mathbf{v})(\omega'+\mathbf{k}\cdot\mathbf{v})} \right], \\
F_2(\mathbf{v}) &= -\mathrm{i}\!\int\! \mathrm{d}\mathbf{k}\, \widehat{\mathfrak{D}}_{\mathbf{k}} \left[\frac{(4\pi G)^2}{k^4} \widehat{\mathfrak{D}}_{\mathbf{k}}\big[\overline{W}(\mathbf{v})\big] \!\int\! \mathrm{d}\mathbf{v}'\, \widehat{C}(\mathbf{k},\mathbf{v}') \right. \\
&\qquad \left. \times \int \frac{\mathrm{d}\omega}{2\pi}\frac{\mathrm{d}\omega'}{2\pi}\, \frac{1}{\epsilon(\mathbf{k},\omega)\,\epsilon(-\mathbf{k},\omega')}\, \frac{\mathrm{e}^{-\mathrm{i}(\omega+\omega')t}}{(\omega-\mathbf{k}\cdot\mathbf{v})(\omega-\mathbf{k}\cdot\mathbf{v}')(\omega'+\mathbf{k}\cdot\mathbf{v}')} \right],
\end{aligned}
\tag{5.58}
$$

For the case of an initially stable system, we can compute all the inverse Lapalace transforms in the above results

$$
\begin{aligned}
F_1(\mathbf{v}) &= \mathrm{i}\!\int\! \mathrm{d}\mathbf{k}\, \widehat{\mathfrak{D}}_{\mathbf{k}} \left[\frac{4\pi G}{k^2} \frac{\widehat{C}(\mathbf{k},\mathbf{v})}{|\epsilon(\mathbf{k},\mathbf{k}\cdot\mathbf{v})|^2}\, \epsilon(\mathbf{k},\mathbf{k}\cdot\mathbf{v}) \right], \\
F_2(\mathbf{v}) &= -\mathrm{i}\!\int\! \mathrm{d}\mathbf{k}\, \widehat{\mathfrak{D}}_{\mathbf{k}} \left(\frac{(4\pi G)^2}{k^4} \widehat{\mathfrak{D}}_{\mathbf{k}}\big[\overline{W}(\mathbf{v})\big] \!\int\! \mathrm{d}\mathbf{v}'\, \frac{\widehat{C}(\mathbf{k},\mathbf{v}')}{|\epsilon(\mathbf{k},\mathbf{k}\cdot\mathbf{v}')|^2} \left\{ \mathcal{P}\left[\frac{1}{\mathbf{k}\cdot(\mathbf{v}-\mathbf{v}')} \right] + \mathrm{i}\pi\delta_{\mathrm{D}}[\mathbf{k}\cdot(\mathbf{v}-\mathbf{v}')] \right\} \right).
\end{aligned}
\tag{5.59}
$$

In the above calculations, the dielectric function $\epsilon(\mathbf{k},\mathbf{k}\cdot\mathbf{v})$ is introduced which is given by equation (5.49) and the Plemelj formula in equation (5.50) as,

$$
\epsilon(\mathbf{k},\mathbf{k}\cdot\mathbf{v}) = 1 - \frac{4\pi G}{k^2}\mathcal{P}\!\int\! \mathrm{d}\mathbf{v}' \frac{\widehat{\mathfrak{D}}_{\mathbf{k}}[\overline{W}(\mathbf{v}')]}{\mathbf{k}\cdot(\mathbf{v}-\mathbf{v}')} + \frac{4\pi^2 G}{k^2}\,\mathrm{i}\!\int\! \mathrm{d}\mathbf{v}'\, \delta_{\mathrm{D}}[\mathbf{k}\cdot(\mathbf{v}-\mathbf{v}')]\, \widehat{\mathfrak{D}}_{\mathbf{k}}\big[\overline{W}(\mathbf{v}')\big]. \tag{5.60}
$$

The first integral in this result must be zero since $\widehat{\mathfrak{D}}_{\mathbf{k}}[\overline{W}(\mathbf{v})]$ is an odd function of $\mathbf{k}$. Therefore, the imaginary part is what remains. Another way to justify this is to argue that $F_1(\mathbf{v})$ and $F_2(\mathbf{v})$ must be real. So 5.59 simplifis into

$$
\begin{aligned}
F_1(\mathbf{v}) &= -\pi\!\int\! \mathrm{d}\mathbf{k}\, \widehat{\mathfrak{D}}_{\mathbf{k}} \left[\frac{(4\pi G)^2}{k^4} \!\int\! \mathrm{d}\mathbf{v}'\, \delta_{\mathrm{D}}[\mathbf{k}\cdot(\mathbf{v}-\mathbf{v}')]\, \widehat{\mathfrak{D}}_{\mathbf{k}}\big[\overline{W}(\mathbf{v}')\big]\, \frac{\widehat{C}(\mathbf{k},\mathbf{v})}{|\epsilon(\mathbf{k},\mathbf{k}\cdot\mathbf{v})|^2} \right], \\
F_2(\mathbf{v}) &= \pi\!\int\! \mathrm{d}\mathbf{k}\, \widehat{\mathfrak{D}}_{\mathbf{k}} \left[\frac{(4\pi G)^2}{k^4} \!\int\! \mathrm{d}\mathbf{v}'\, \delta_{\mathrm{D}}[\mathbf{k}\cdot(\mathbf{v}-\mathbf{v}')]\, \widehat{\mathfrak{D}}_{\mathbf{k}}\big[\overline{W}(\mathbf{v})\big]\, \frac{\widehat{C}(\mathbf{k},\mathbf{v}')}{|\epsilon(\mathbf{k},\mathbf{k}\cdot\mathbf{v})|^2} \right].
\end{aligned}
\tag{5.61}
$$

Now this result should be replaced in 5.53 to finally obtain the kinetic equation

$$
\frac{\partial \overline{W}}{\partial t} = \pi\!\int\! \mathrm{d}\mathbf{k}\, \widehat{\mathfrak{D}}_{\mathbf{k}} \left[\frac{(4\pi G)^2}{k^4} \!\int\! \mathrm{d}\mathbf{v}'\, \frac{\delta_{\mathrm{D}}[\mathbf{k}\cdot(\mathbf{v}-\mathbf{v}')]}{|\epsilon(\mathbf{k},\mathbf{k}\cdot\mathbf{v})|^2} \left(\widehat{\mathfrak{D}}_{\mathbf{k}}\big[\overline{W}(\mathbf{v})\big]\, \widehat{C}(\mathbf{k},\mathbf{v}') - \widehat{\mathfrak{D}}_{\mathbf{k}}\big[\overline{W}(\mathbf{v}')\big]\, \widehat{C}(\mathbf{k},\mathbf{v}) \right) \right]. \tag{5.62}
$$

Now it remains to calculate explicitly the autocorrelation function $\widehat{C}(\mathbf{k},\mathbf{v}')$.

First let us start by considering the classical case. In that regime, the system's discrete distribution function is given by

$$
F_{\mathrm{d}}(\mathbf{r},\mathbf{v},t) = m_{\mathrm{b}} \sum_{i=1}^{N} \delta_{\mathrm{D}}\left[\mathbf{r}-\mathbf{r}_i(t)\right] \delta_{\mathrm{D}}\left[\mathbf{v}-\mathbf{v}_i(t)\right], \tag{5.63}
$$

where at the initial time, the phase-space positions and velocities of the particles are drawn independently from another, uniformly in space, and according to the DFF_{b}(v) for their velocities. Similarly to Eq. (52), the instantaneous fluctuations in the system's DF are given by $f = F_\mathrm{d} - F_\mathrm{b}$. At the initial time, we can then write

$$\langle f_0(\mathbf{r},\mathbf{v}) f_0(\mathbf{r}',\mathbf{v}')\rangle = m_\mathrm{b}^2 \sum_{i,j} \langle \delta_\mathrm{D}(\mathbf{r}-\mathbf{r}_i)\,\delta_\mathrm{D}(\mathbf{v}-\mathbf{v}_i)\,\delta_\mathrm{D}(\mathbf{r}'-\mathbf{r}_j)\,\delta_\mathrm{D}(\mathbf{v}'-\mathbf{v}_j)\rangle - F_\mathrm{b}(\mathbf{v}) F_\mathrm{b}(\mathbf{v}'), \tag{5.64}$$

where we dropped the time dependence ($t = 0$) to shorten the notation. As the particles are chosen independently, there are two types of terms in the double sum, depending on whether $i = j$ or $i \neq j$. We then get

$$\begin{aligned}\langle f_0(\mathbf{r},\mathbf{v}) f_0(\mathbf{r}',\mathbf{v}')\rangle =& m_\mathrm{b}^2 \delta_\mathrm{D}(\mathbf{r}-\mathbf{r}')\,\delta_\mathrm{D}(\mathbf{v}-\mathbf{v}') \sum_i \langle \delta_\mathrm{D}(\mathbf{r}-\mathbf{r}_i)\,\delta_\mathrm{D}(\mathbf{v}-\mathbf{v}_i)\rangle \\ &+ m_\mathrm{b}^2 \sum_{i\neq j} \langle \delta_\mathrm{D}(\mathbf{r}-\mathbf{r}_i)\,\delta_\mathrm{D}(\mathbf{v}-\mathbf{v}_i)\rangle \langle \delta_\mathrm{D}(\mathbf{r}'-\mathbf{r}_j)\,\delta_\mathrm{D}(\mathbf{v}'-\mathbf{v}_j)\rangle \\ &- F_\mathrm{b}(\mathbf{v}) F_\mathrm{b}(\mathbf{v}')\end{aligned} \tag{5.65}$$

Since F_b obeys the normalization convention $\int \mathrm{d}\mathbf{v} F_\mathrm{b}(\mathbf{v}) = \rho_0$, we have

$$\langle \delta_\mathrm{D}(\mathbf{r}-\mathbf{r}_i)\,\delta_\mathrm{D}(\mathbf{v}-\mathbf{v}_i)\rangle = \frac{1}{N m_\mathrm{b}} F_\mathrm{b}(\mathbf{v}). \tag{5.66}$$

As a consequence, in the limit $N \gg 1$, the last two terms in Eq. 5.65 cancel and we have

$$\langle f_0(\mathbf{r},\mathbf{v}) f_0(\mathbf{r}',\mathbf{v}')\rangle = m_\mathrm{b} F_\mathrm{b}(\mathbf{v}) \delta_\mathrm{D}(\mathbf{r}-\mathbf{r}')\,\delta_\mathrm{D}(\mathbf{v}-\mathbf{v}') \tag{5.67}$$

Following the convention from 5.31, this can be rewritten in Fourier space as

$$\left\langle \widehat{f_0}(\mathbf{k},\mathbf{v}) \widehat{f_0}(\mathbf{k}',\mathbf{v}')\right\rangle = \frac{1}{(2\pi)^3} m_\mathrm{b} F_\mathrm{b}(\mathbf{v}) \delta_\mathrm{D}(\mathbf{k}+\mathbf{k}')\,\delta_\mathrm{D}(\mathbf{v}-\mathbf{v}'), \tag{5.68}$$

and the needed correlation function from 5.57 is then

$$\widehat{C}(\mathbf{k},\mathbf{v}) = \frac{1}{(2\pi)^3} m_\mathrm{b} F_\mathrm{b}(\mathbf{v}) \tag{5.69}$$

We note that this correlation function is independent of $\mathbf{k}$, a consequence of our assumption that the initial positions of the particles are chosen independently from a homogeneous distribution.

Let us now adapt this calculation to the FDM case and compute the statistics of the persistent fluctuations present in the Wigner distribution function of the halo. We consider the following wavefunction

$$\psi(\mathbf{r},t) = \int \mathrm{d}\mathbf{k} \varphi(\mathbf{k}) \mathrm{e}^{\mathrm{i}[\mathbf{k}\cdot\mathbf{r} - \omega(k)t]} \tag{5.70}$$

In the limit where the potential fluctuations $\Phi(\mathbf{r},t)$ vanish, this wavefunction is a solution of the free Schrödinger equation provided that it satisfies the dispersion relation

$$\omega(k) = \frac{\hbar k^2}{2 m_\mathrm{b}}. \tag{5.71}$$

Let us now assume that the wavefunction in $\mathbf{k}$-space, $\varphi(\mathbf{k})$, is the sum of Gaussian wavepackets of the form

$$\varphi(\mathbf{k}) = A \sum_{i=1}^{N} \mathrm{e}^{\mathrm{i}\phi_i} \mathrm{e}^{-\mathrm{i}\mathbf{k}\cdot\mathbf{r}_i} \mathrm{e}^{-|\mathbf{k} - m_\mathrm{b}\mathbf{v}_i/\hbar|^2 \epsilon^2} \tag{5.72}$$

In that expression, $\{\mathbf{r}_i, \mathbf{v}_i\}$ are random positions and velocities drawn independently from the DF$F_{\mathrm{b}}(\mathbf{v})$, and $\{\phi_i\}$ are independent random phases. In addition, ϵ is an ad hoc parameter, so that ϵ and $\hbar/(2m_{\mathrm{b}}\epsilon)$ are respectively the initial uncertainties in the positions and velocities. This parameter will prove to be useful in managing our asymptotic developments. In the above, we also introduced the prefactor A that is tuned to satisfy the normalization condition stemming from normalizations, namely that $\left\langle|\psi(\mathbf{r},t)|^2\right\rangle = \rho_0$. Let us now determine the value of A. Starting from 5.70, we write

$$\left\langle|\psi(\mathbf{r},t)|^2\right\rangle = \int \mathrm{d}\mathbf{k}\ \mathrm{d}\mathbf{k}' \left\langle\varphi(\mathbf{k})\varphi^*(\mathbf{k}')\right\rangle \mathrm{e}^{\mathrm{i}(\mathbf{k}-\mathbf{k}')\cdot\mathbf{r}}\mathrm{e}^{-\mathrm{i}t[\omega(k)-\omega(k')]} \tag{5.73}$$

The two-point correlation function of $\varphi(\mathbf{k})$ is

$$\begin{aligned}\left\langle\varphi(\mathbf{k})\varphi^*(\mathbf{k}')\right\rangle &= A^2\sum_{i,j}\left\langle \mathrm{e}^{\mathrm{i}(\phi_i-\phi_j)}\mathrm{e}^{-\mathrm{i}\mathbf{k}\cdot\mathbf{r}_i}\mathrm{e}^{\mathrm{i}\mathbf{k}'\cdot\mathbf{r}_j}\mathrm{e}^{-|\mathbf{k}-m_{\mathrm{b}}\mathbf{v}_i/\hbar|^2\epsilon^2}\mathrm{e}^{-|\mathbf{k}'-m_{\mathrm{b}}\mathbf{v}_j/\hbar|^2\epsilon^2}\right\rangle \\ &= A^2\sum_{i}\left\langle \mathrm{e}^{-\mathrm{i}(\mathbf{k}-\mathbf{k}')\cdot\mathbf{r}_i}\mathrm{e}^{-|\mathbf{k}-m_{\mathrm{b}}\mathbf{v}_i/\hbar|^2\epsilon^2}\mathrm{e}^{-|\mathbf{k}'-m_{\mathrm{b}}\mathbf{v}_i/\hbar|^2\epsilon^2}\right\rangle \\ &= A^2\sum_{i}\int \mathrm{d}\mathbf{r}\mathrm{d}\mathbf{v}\left\langle\delta_{\mathrm{D}}(\mathbf{r}-\mathbf{r}_i)\,\delta_{\mathrm{D}}(\mathbf{v}-\mathbf{v}_i)\right\rangle \\ &\quad\times \mathrm{e}^{-\mathrm{i}(\mathbf{k}-\mathbf{k}')\cdot\mathbf{r}}\mathrm{e}^{-|\mathbf{k}-m_{\mathrm{b}}\mathbf{v}/\hbar|^2\epsilon^2}\mathrm{e}^{-|\mathbf{k}'-m_{\mathrm{b}}\mathbf{v}/\hbar|^2\epsilon^2}\end{aligned} \tag{5.74}$$

To get the second line we noted that $\left\langle \mathrm{e}^{\mathrm{i}(\phi_i-\phi_j)}\right\rangle$ is non-zero only for $i=j$. Using 5.66, one can write

$$\begin{aligned}\left\langle\varphi(\mathbf{k})\varphi^*(\mathbf{k}')\right\rangle &= \frac{A^2}{m_{\mathrm{b}}}\int \mathrm{d}\mathbf{d}\ \mathrm{d}\mathbf{v}F_{\mathrm{b}}(\mathbf{v})\mathrm{e}^{-\mathrm{i}(\mathbf{k}-\mathbf{k}')\cdot\mathbf{r}}\mathrm{e}^{-|\mathbf{k}-m_{\mathrm{b}}\mathbf{v}/\hbar|^2\epsilon^2}\mathrm{e}^{-|\mathbf{k}'-m_{\mathrm{b}}\mathbf{v}/\hbar|^2\epsilon^2} \\ &= \frac{(2\pi)^3A^2}{m_{\mathrm{b}}}\delta_{\mathrm{D}}(\mathbf{k}-\mathbf{k}')\int \mathrm{d}\mathbf{v}F_{\mathrm{b}}(\mathbf{v})\mathrm{e}^{-2|\mathbf{k}-m_{\mathrm{b}}\mathbf{v}/\hbar|^2\epsilon^2}\end{aligned} \tag{5.75}$$

We can now use this result to pursue the simplification of 5.73. We have

$$\left\langle|\psi(\mathbf{r},t)|^2\right\rangle = \frac{(2\pi)^3A^2}{m_{\mathrm{b}}}\int \mathrm{d}\mathbf{k}\ \mathrm{d}\mathbf{v}F_{\mathrm{b}}(\mathbf{v})\mathrm{e}^{-2|\mathbf{k}-m_{\mathrm{b}}\mathbf{v}/\hbar|^2\epsilon^2} = \frac{2^{3/2}\pi^{9/2}A^2}{\epsilon^3 m_{\mathrm{b}}}\int \mathrm{d}\mathbf{v}F_{\mathrm{b}}(\mathbf{v}). \tag{5.76}$$

Recalling the normalization relations that $\int \mathrm{d}\mathbf{v}F_{\mathrm{b}}(\mathbf{v}) = \rho_0$, we obtain the value of A as

$$A = \frac{\epsilon^{3/2}m_{\mathrm{b}}^{1/2}}{2^{3/4}\pi^{9/4}} \tag{5.77}$$

Relying on the definition of the Wigner function, we can now compute $W(\mathbf{r},\mathbf{v},t)$

associated with 5.70. Following some cumbersome calculations, it takes the form

$$
\begin{aligned}
W(\mathbf{r}, \mathbf{v}, t) &= \int \frac{\mathrm{d}\mathbf{s}}{(2\pi)^3} \mathrm{e}^{-\mathrm{i}\mathbf{v}\cdot\mathbf{s}} \psi\left(\mathbf{r} + \frac{1}{2}\hbar\mathbf{s}/m_{\mathrm{b}}, t\right) \psi^*\left(\mathbf{r} - \frac{1}{2}\hbar\mathbf{s}/m_{\mathrm{b}}, t\right) \\
&= \left(\frac{2m_{\mathrm{b}}}{\hbar}\right)^3 \int \ \mathrm{d}\mathbf{k}_1 \ \mathrm{d}\mathbf{k}_2 \varphi\left(\mathbf{k}_1\right) \varphi^*\left(\mathbf{k}_2\right) \delta_{\mathrm{D}}\left(\mathbf{k}_1 + \mathbf{k}_2 - \frac{2m_{\mathrm{b}}}{\hbar}\mathbf{v}\right) \mathrm{e}^{\mathrm{i}(\mathbf{k}_1 - \mathbf{k}_2)\cdot(\mathbf{r} - \mathbf{v}t)} \\
&= m_{\mathrm{b}} \left(\frac{m_{\mathrm{b}}}{\pi\hbar}\right)^3 \sum_{i,j} \mathrm{e}^{\mathrm{i}(\phi_i - \phi_j)} \exp\left[-\frac{2\epsilon^2 m_{\mathrm{b}}^2}{\hbar^2}\left|\frac{1}{2}\left(\mathbf{v}_i + \mathbf{v}_j\right) - \mathbf{v}\right|^2\right] \\
&\quad \times \exp\left[-\frac{1}{2\epsilon^2}\left|\frac{1}{2}\left(\mathbf{r}_i + \mathbf{r}_j\right) - \mathbf{r} + \mathbf{v}t\right|^2\right] \\
&\quad \times \exp\left\{-\mathrm{i}\frac{m_{\mathrm{b}}}{\hbar}\left[\left(\mathbf{r}_i - \mathbf{r}_j\right)\cdot\mathbf{v} + \left[\frac{1}{2}\left(\mathbf{r}_i + \mathbf{r}_j\right) - \mathbf{r} + \mathbf{v}t\right]\cdot\left(\mathbf{v}_i - \mathbf{v}_j\right)\right]\right\}
\end{aligned}
\tag{5.78}
$$

In the second line we have used the relation $\omega\left(k_2\right) - \omega\left(k_1\right) = \frac{1}{2}\left(\hbar/m_{\mathrm{b}}\right)\left(k_2^2 - k_1^2\right) = \frac{1}{2}\left(\hbar/m_{\mathrm{b}}\right)\left(\mathbf{k}_2 + \mathbf{k}_1\right)\cdot\left(\mathbf{k}_2 - \mathbf{k}_1\right)$; when multiplied by the delta function in that equation this reduces to $\mathbf{v}\cdot\left(\mathbf{k}_2 - \mathbf{k}_1\right)$.

To verify these calculations, we will now apply the same method as in 5.74 to compute the ensemble-averaged Wigner function. Due to the presence of the factor $\mathrm{e}^{\mathrm{i}(\phi_i - \phi_j)}$ in 5.78, only contributions with $i = j$ remain. All in all, we obtain

$$
\begin{aligned}
\overline{W}(\mathbf{r}, \mathbf{v}, t) &= \left(\frac{m_{\mathrm{b}}}{\pi\hbar}\right)^3 \int \ \mathrm{d}\mathbf{r}'\mathrm{d}\mathbf{v}' F_{\mathrm{b}}\left(\mathbf{v}'\right) \exp\left[-\frac{2\epsilon^2 m_{\mathrm{b}}^2}{\hbar^2}\left|\mathbf{v}' - \mathbf{v}\right|^2\right] \exp\left[-\frac{1}{2\epsilon^2}\left|\mathbf{r}' - \mathbf{r} + \mathbf{v}t\right|^2\right] \\
&\simeq F_{\mathrm{b}}(\mathbf{v})
\end{aligned}
\tag{5.79}
$$

To get the last line, we assumed that $\epsilon \gg \lambda_\sigma = \hbar/\left(m_{\mathrm{b}}\sigma\right)$, with σ the system's typical velocity; physically, this means that the size of the wavepacket is much larger than the typical de Broglie wavelength. In that limit, we can then use the replacement

$$
\mathrm{e}^{-\alpha|\mathbf{v}|^2/\sigma^2} \underset{\alpha\gg 1}{\longrightarrow} \frac{\pi^{3/2}}{\alpha^{3/2}} \delta_{\mathrm{D}}(\mathbf{v}/\sigma),
\tag{5.80}
$$

with $\alpha^{-1} = \hbar^2/\left(2\epsilon^2 m_{\mathrm{b}}^2 \sigma^2\right)$ our small parameter. Thus we have recovered in 5.79 the known result that the ensemble-averaged Wigner function is the same as the DF.

Having computed the Wigner distribution in 5.78, we can now find the correlation of its fluctuations at the initial time, as required by 5.57. Following $W = \overline{W} + f$, we write

$$
\left\langle f_0(\mathbf{r}, \mathbf{v}) f_0\left(\mathbf{r}', \mathbf{v}'\right)\right\rangle = \left\langle W(\mathbf{r}, \mathbf{v}) W\left(\mathbf{r}', \mathbf{v}'\right)\right\rangle - \overline{W}(\mathbf{r}, \mathbf{v}) \overline{W}\left(\mathbf{r}', \mathbf{v}'\right),
\tag{5.81}
$$

where all the functions are evaluated at the initial time. Glancing back at 5.78, we note that the Wigner function can be rewritten in the shorter form

$$
W(\mathbf{r}, \mathbf{v}) = \sum_{i,j} \mathrm{e}^{\mathrm{i}(\phi_i - \phi_j)} g_{ij}(\mathbf{r}, \mathbf{v}),
\tag{5.82}
$$

where the expression for the function $g_{ij}(\mathbf{r}, \mathbf{v})$ naturally follows from 5.78. As a result, the ensemble average in the r.h.s. of 5.81 takes the form

$$
\left\langle W(\mathbf{r}, \mathbf{v}) W\left(\mathbf{r}', \mathbf{v}'\right)\right\rangle = \sum_{\substack{i,j \\ k,l}} \left\langle \mathrm{e}^{\mathrm{i}(\phi_i - \phi_j + \phi_k - \phi_l)} g_{ij}(\mathbf{r}, \mathbf{v}) g_{kl}\left(\mathbf{r}', \mathbf{v}'\right)\right\rangle
\tag{5.83}
$$

Because the wavepackets are drawn independently, the phase term $\left\langle e^{i(\phi_i-\phi_j+\phi_k-\phi_l)}\right\rangle$ is non-zero only in three cases, namely (i) $i=j=k=l$; (ii) $i=j$ and $k=l$ with $i\neq k$; (iii) $i=l$ and $j=k$ with $i\neq k$. In the limit $N\gg 1$, we can then rewrite 5.83 as

$$\langle W(\mathbf{r},\mathbf{v})W(\mathbf{r}',\mathbf{v}')\rangle = N\left\langle g_{ii}(\mathbf{r},\mathbf{v})g_{ii}(\mathbf{r}',\mathbf{v}')\right\rangle + N^2\left\langle g_{ii}(\mathbf{r},\mathbf{v})g_{kk}(\mathbf{r}',\mathbf{v}')\right\rangle + N^2\left\langle g_{ik}(\mathbf{r},\mathbf{v})g_{ki}(\mathbf{r}',\mathbf{v}')\right\rangle, \tag{5.84}$$

where, in the last two terms, it is understood that $\{\mathbf{r}_i,\mathbf{v}_i\}$ and $\{\mathbf{r}_k,\mathbf{v}_k\}$ are two independent sets of random variables. Let us now compute in turn each of the terms appearing in 5.84. We can first write

$$\begin{aligned}
N\left\langle g_{ii}(\mathbf{r},\mathbf{v})g_{ii}(\mathbf{r}',\mathbf{v}')\right\rangle =& m_\mathrm{b}\left(\frac{m_\mathrm{b}}{\pi\hbar}\right)^6\int \mathrm{d}\mathbf{v}_i F_\mathrm{b}(\mathbf{v}_i)\exp\left[-\frac{2\epsilon^2 m_\mathrm{b}^2}{\hbar^2}\left(|\mathbf{v}_i-\mathbf{v}|^2+|\mathbf{v}_i-\mathbf{v}'|^2\right)\right]\\
&\times\int \mathrm{d}\mathbf{r}_i\exp\left[-\frac{1}{2\epsilon^2}\left(|\mathbf{r}_i-\mathbf{r}|^2+|\mathbf{r}_i-\mathbf{r}'|^2\right)\right]\\
=& m_\mathrm{b}\left(\frac{m_\mathrm{b}}{\pi\hbar}\right)^6\exp\left[-\frac{\epsilon^2 m_\mathrm{b}^2}{\hbar^2}|\mathbf{v}-\mathbf{v}'|^2\right]\\
&\times\int \mathrm{d}\mathbf{v}_i F_\mathrm{b}(\mathbf{v}_i)\exp\left[-\frac{4\epsilon^2 m_\mathrm{b}^2}{\hbar^2}\left|\mathbf{v}_i-\frac{1}{2}(\mathbf{v}+\mathbf{v}')\right|^2\right]\\
&\times\exp\left[-\frac{1}{4\epsilon^2}|\mathbf{r}-\mathbf{r}'|^2\right]\int \mathrm{d}\mathbf{r}_i\exp\left[-\frac{1}{\epsilon^2}\left|\mathbf{r}_i-\frac{1}{2}(\mathbf{r}+\mathbf{r}')\right|^2\right]\\
\simeq& m_\mathrm{b}\delta_\mathrm{D}(\mathbf{r}-\mathbf{r}')\,\delta_\mathrm{D}(\mathbf{v}-\mathbf{v}')\,\overline{W}(\mathbf{v}),
\end{aligned}\tag{5.85}$$

where to get the last line, we assumed once again that $\epsilon\gg\lambda_\sigma$, and used the asymptotic replacement from 5.80. The second term from 5.84 reads

$$\begin{aligned}
N^2\left\langle g_{ii}(\mathbf{r},\mathbf{v})g_{kk}(\mathbf{r}',\mathbf{v}')\right\rangle =& \left(\frac{m_\mathrm{b}}{\pi\hbar}\right)^3\int \mathrm{d}\mathbf{r}_i\,\mathrm{d}\mathbf{v}_i F_\mathrm{b}(\mathbf{v}_i)\exp\left[-\frac{2\epsilon^2 m_\mathrm{b}^2}{\hbar^2}|\mathbf{v}_i-\mathbf{v}|^2\right]\exp\left[-\frac{1}{2\epsilon^2}|\mathbf{r}_i-\mathbf{r}|^2\right]\\
&\times\left(\frac{m_\mathrm{b}}{\pi\hbar}\right)^3\int \mathrm{d}\mathbf{r}_k\,\mathrm{d}\mathbf{v}_k F_\mathrm{b}(\mathbf{v}_k)\exp\left[-\frac{2\epsilon^2 m_\mathrm{b}^2}{\hbar^2}|\mathbf{v}_k-\mathbf{v}'|^2\right]\\
&\times\exp\left[-\frac{1}{2\epsilon^2}|\mathbf{r}_k-\mathbf{r}'|^2\right]\\
=&\overline{W}(\mathbf{r},\mathbf{v})\overline{W}(\mathbf{r}',\mathbf{v}')
\end{aligned}\tag{5.86}$$

where we used the result from 5.79. The last term from 5.84 then reads

$$
\begin{aligned}
N^2 \left\langle g_{ik}(\mathbf{r},\mathbf{v}) g_{ki}\left(\mathbf{r}',\mathbf{v}'\right)\right\rangle &= \left(\frac{m_{\mathrm{b}}}{\pi\hbar}\right)^6 \int \mathrm{d}\mathbf{r}_i\ \mathrm{d}\mathbf{v}_i\ \mathrm{d}\mathbf{r}_k\ \mathrm{d}\mathbf{v}_k F_{\mathrm{b}}\left(\mathbf{v}_i\right) F_{\mathrm{b}}\left(\mathbf{v}_k\right) \\
&\quad \times \exp\left[-\frac{2\epsilon^2 m_{\mathrm{b}}^2}{\hbar^2}\left(\left|\frac{1}{2}\left(\mathbf{v}_i+\mathbf{v}_k\right)-\mathbf{v}\right|^2+\left|\frac{1}{2}\left(\mathbf{v}_i+\mathbf{v}_k\right)-\mathbf{v}'\right|^2\right)\right] \\
&\quad \times \exp\left[-\frac{1}{2\epsilon^2}\left(\left|\frac{1}{2}\left(\mathbf{r}_i+\mathbf{r}_k\right)-\mathbf{r}\right|^2+\left|\frac{1}{2}\left(\mathbf{r}_i+\mathbf{r}_k\right)-\mathbf{r}'\right|^2\right)\right] \\
&\quad \times \exp\left\{-\mathrm{i}\frac{m_{\mathrm{b}}}{\hbar}\left[\left(\mathbf{r}_i-\mathbf{r}_k\right)\cdot\left(\mathbf{v}-\mathbf{v}'\right)-\left(\mathbf{r}-\mathbf{r}'\right)\cdot\left(\mathbf{v}_i-\mathbf{v}_k\right)\right]\right\} \\
&= \left(\frac{m_{\mathrm{b}}}{\pi\hbar}\right)^6 \exp\left[-\frac{\epsilon^2 m_{\mathrm{b}}^2}{\hbar^2}\left|\mathbf{v}-\mathbf{v}'\right|^2\right] \exp\left[-\frac{1}{4\epsilon^2}\left|\mathbf{r}-\mathbf{r}'\right|^2\right] \\
&\quad \times \int \mathrm{d}\mathbf{r}_i\ \mathrm{d}\mathbf{v}_i\ \mathrm{d}\mathbf{r}_k\ \mathrm{d}\mathbf{v}_k F_{\mathrm{b}}\left(\mathbf{v}_i\right) F_{\mathrm{b}}\left(\mathbf{v}_k\right) \\
&\quad \times \exp\left[-\frac{4\epsilon^2 m_{\mathrm{b}}^2}{\hbar^2}\left|\frac{1}{2}\left(\mathbf{v}_i+\mathbf{v}_k\right)-\frac{1}{2}\left(\mathbf{v}+\mathbf{v}'\right)\right|^2\right] \\
&\quad \times \exp\left[-\frac{1}{\epsilon^2}\left|\frac{1}{2}\left(\mathbf{r}_i+\mathbf{r}_k\right)-\frac{1}{2}\left(\mathbf{r}+\mathbf{r}'\right)\right|^2\right] \\
&\quad \times \exp\left\{-\mathrm{i}\frac{m_{\mathrm{b}}}{\hbar}\left[\left(\mathbf{r}_i-\mathbf{r}_k\right)\cdot\left(\mathbf{v}-\mathbf{v}'\right)-\left(\mathbf{r}-\mathbf{r}'\right)\cdot\left(\mathbf{v}_i-\mathbf{v}_k\right)\right]\right\}
\end{aligned} \tag{5.87}
$$

At this stage, the asymptotic formula from 5.80 has to be used carefully, because the complex exponential from 5.87 is rapidly fluctuating. To clarify this calculation, let us perform the change of variables

$$
\left\{\begin{array}{l} \sigma_{\mathbf{r}}=\frac{1}{2}\left(\mathbf{r}_i+\mathbf{r}_k\right), \\ \delta_{\mathbf{r}}=\mathbf{r}_i-\mathbf{r}_k, \end{array}\right. ; \quad \left\{\begin{array}{l} \sigma_{\mathbf{v}}=\frac{1}{2}\left(\mathbf{v}_i+\mathbf{v}_k\right), \\ \delta_{\mathbf{v}}=\mathbf{v}_i-\mathbf{v}_k \end{array}\right. \tag{5.88}
$$

equation (5.87) becomes

$$
\begin{aligned}
N^2 \left\langle g_{ik}(\mathbf{r},\mathbf{v}) g_{ki}\left(\mathbf{r}',\mathbf{v}'\right)\right\rangle &= \left(\frac{m_{\mathrm{b}}}{\pi\hbar}\right)^6 \exp\left[-\frac{\epsilon^2 m_{\mathrm{b}}^2}{\hbar}\left|\mathbf{v}-\mathbf{v}'\right|^2\right] \exp\left[-\frac{1}{4\epsilon^2}\left|\mathbf{r}-\mathbf{r}'\right|^2\right] \\
&\times \int \mathrm{d}\boldsymbol{\sigma}_{\mathbf{v}} \mathrm{d}\boldsymbol{\delta}_{\mathbf{v}} F_{\mathrm{b}}\left(\boldsymbol{\sigma}_{\mathbf{v}}+\frac{1}{2}\boldsymbol{\delta}_{\mathbf{v}}\right) F_{\mathrm{b}}\left(\boldsymbol{\sigma}_{\mathbf{v}}-\frac{1}{2}\boldsymbol{\delta}_{\mathbf{v}}\right) \\
&\times \exp\left[-\frac{4\epsilon^2 m_{\mathrm{b}}^2}{\hbar^2}\left|\boldsymbol{\sigma}_{\mathbf{v}}-\frac{1}{2}\left(\mathbf{v}+\mathbf{v}'\right)\right|^2\right] \exp\left[-\mathrm{i}\frac{m_{\mathrm{b}}}{\hbar}\left(\mathbf{r}-\mathbf{r}'\right)\cdot\boldsymbol{\delta}_{\mathbf{v}}\right] \\
&\times \int \mathrm{d}\boldsymbol{\sigma}_{\mathbf{r}} \mathrm{d}\boldsymbol{\delta}_{\mathbf{r}} \exp\left[-\frac{1}{\epsilon^2}\left|\boldsymbol{\sigma}_{\mathbf{r}}-\frac{1}{2}\left(\mathbf{r}+\mathbf{r}'\right)\right|^2\right] \exp\left[-\mathrm{i}\frac{m_{\mathrm{b}}}{\hbar}\boldsymbol{\delta}_{\mathbf{r}}\cdot\left(\mathbf{v}-\mathbf{v}'\right)\right].
\end{aligned} \tag{5.89}
$$

In this expression, we note that the exponential factor $\exp\left[-\frac{1}{4\epsilon^2}\left|\mathbf{r}-\mathbf{r}'\right|^2\right]$ is nearly zero unless $\left|\mathbf{r}-\mathbf{r}'\right| \lesssim \epsilon$. In that regime, the complex exponential $\exp\left[-\mathrm{i}\frac{m_{\mathrm{b}}}{\hbar}\left(\mathbf{r}-\mathbf{r}'\right)\cdot\boldsymbol{\delta}_{\mathbf{v}}\right]$ will average to nearly zero unless $\left|\boldsymbol{\delta}_{\mathbf{v}}\right| \lesssim \hbar/\left(\epsilon m_{\mathrm{b}}\right)=\sigma\lambda_\sigma/\epsilon$. Given our assumption that $\epsilon \gg \lambda_\sigma$, we conclude that the dominant contribution to the integral comes from $\left|\delta_{\mathrm{v}}\right| \ll \sigma$. We recall that the typical variance of $F_{\mathrm{b}}(\mathbf{v})$ is σ, so in 5.89 we may perform the replacement $F_{\mathrm{b}}\left(\boldsymbol{\sigma}_{\mathbf{v}}+\frac{1}{2}\delta_{\mathbf{v}}\right) F_{\mathrm{b}}\left(\sigma_{\mathrm{v}}-\frac{1}{2}\delta_{\mathbf{v}}\right) \rightarrow F_{\mathrm{b}}^2\left(\sigma_{\mathrm{v}}\right)$. We get

$$
\begin{aligned}
N^2 \left\langle g_{ik}(\mathbf{r},\mathbf{v}) g_{ki}\left(\mathbf{r}',\mathbf{v}'\right)\right\rangle \simeq\; & 2^6 \delta_{\mathrm{D}}\left(\mathbf{r}-\mathbf{r}'\right)\delta_{\mathrm{D}}\left(\mathbf{v}-\mathbf{v}'\right) \\
& \int \mathrm{d}\boldsymbol{\sigma}_{\mathbf{r}} \mathrm{d}\boldsymbol{\sigma}_{\mathbf{v}} \exp\left[-\frac{1}{\epsilon^2}\left|\boldsymbol{\sigma}_{\mathbf{r}}-\mathbf{r}\right|^2\right] F_{\mathrm{b}}^2\left(\boldsymbol{\sigma}_{\mathbf{v}}\right) \exp\left[-\frac{4\epsilon^2 m_{\mathrm{b}}^2}{\hbar^2}\left|\boldsymbol{\sigma}_{\mathbf{v}}-\mathbf{v}\right|^2\right] \\
\simeq\; & \frac{h^3}{m_{\mathrm{b}}^3}\delta_{\mathrm{D}}\left(\mathbf{r}-\mathbf{r}'\right)\delta_{\mathrm{D}}\left(\mathbf{v}-\mathbf{v}'\right)\overline{W}^2(\mathbf{v})
\end{aligned} \tag{5.90}
$$

Gathering together equation (5.85), (5.86), and 5.89, we can now rewrite the correlation from 5.81 to obtain

$$
\left\langle f_0(\mathbf{r},\mathbf{v}) f_0\left(\mathbf{r}',\mathbf{v}'\right)\right\rangle = \left[m_{\mathrm{b}} + \frac{h^3}{m_{\mathrm{b}}^3}\overline{W}(\mathbf{v})\right]\overline{W}(\mathbf{v})\delta_{\mathrm{D}}\left(\mathbf{r}-\mathbf{r}'\right)\delta_{\mathrm{D}}\left(\mathbf{v}-\mathbf{v}'\right) \tag{5.91}
$$

Following 5.57 and 5.29, we finally obtain the needed correlation function as

$$
\widehat{C}(\mathbf{k},\mathbf{v}) = \frac{1}{(2\pi)^3}\left[m_{\mathrm{b}} + \frac{h^3}{m_{\mathrm{b}}^3}\overline{W}(\mathbf{v})\right]\overline{W}(\mathbf{v}), \tag{5.92}
$$

which reduces to the classical correlation function 5.69 as $h \to 0$.

The next step would be to insert 5.92 into 5.62 leading to

$$
\begin{aligned}
\frac{\partial \overline{W}(\mathbf{v})}{\partial t} = 2G^2 \int \mathrm{d}\mathbf{k} \int \mathrm{d}\mathbf{v}'\, \widehat{\mathfrak{D}}_{\mathbf{k}} \Bigg\{ & \frac{\delta_{\mathrm{D}}[\mathbf{k}\cdot(\mathbf{v}-\mathbf{v}')]}{k^4|\epsilon(\mathbf{k},\mathbf{k}\cdot\mathbf{v})|^2}\widehat{\mathfrak{D}}_{\mathbf{k}}\left[\overline{W}(\mathbf{v})\right]\overline{W}(\mathbf{v}')\left[m_{\mathrm{b}} + \frac{h^3}{m_{\mathrm{b}}^3}\overline{W}(\mathbf{v}')\right] \\
& - \frac{\delta_{\mathrm{D}}[\mathbf{k}\cdot(\mathbf{v}-\mathbf{v}')]}{k^4|\epsilon(\mathbf{k},\mathbf{k}\cdot\mathbf{v})|^2}\widehat{\mathfrak{D}}_{\mathbf{k}}\left[\overline{W}(\mathbf{v}')\right]\overline{W}(\mathbf{v})\left[m_{\mathrm{b}} + \frac{h^3}{m_{\mathrm{b}}^3}\overline{W}(\mathbf{v})\right]\Bigg\}.
\end{aligned} \tag{5.93}
$$

equation (5.93) is a Balescu–Lenard (BL) type kinetic equation describing the self-consistent relaxation of a homogeneous FDM halo. In particular, we note that this kinetic equation involves the dielectric function which describes how the fluctuations are dressed by collective effects (Bar-Or et al., 2019).

We assume that $\mathbf{k}$ is small compared to the characteristic scale of changes in $\overline{W}(\mathbf{v})$. In this case we can replace the discrete derivatives in $\widehat{\mathfrak{D}}_{\mathbf{k}}[\overline{W}(\mathbf{v})]$ with their continuous analogs (equation (5.31)). Equation (5.93) then becomes

$$
\begin{aligned}
\frac{\partial \overline{W}(\mathbf{v})}{\partial t} = & 2G^2 \int \mathrm{d}\mathbf{k}\, \mathbf{k}\cdot\frac{\partial}{\partial \mathbf{v}} \int \mathrm{d}\mathbf{v}'\, \frac{\delta_{\mathrm{D}}[\mathbf{k}\cdot(\mathbf{v}-\mathbf{v}')]}{k^4|\epsilon(\mathbf{k},\mathbf{k}\cdot\mathbf{v})|^2} \\
& \times \left\{\mathbf{k}\cdot\frac{\partial \overline{W}(\mathbf{v})}{\partial \mathbf{v}}\overline{W}(\mathbf{v}')\left[m_{\mathrm{b}} + \frac{h^3}{m_{\mathrm{b}}^3}\overline{W}(\mathbf{v}')\right] - \mathbf{k}\cdot\frac{\partial \overline{W}(\mathbf{v}')}{\partial \mathbf{v}'}\overline{W}(\mathbf{v})\left[m_{\mathrm{b}} + \frac{h^3}{m_{\mathrm{b}}^3}\overline{W}(\mathbf{v})\right]\right\}.
\end{aligned} \tag{5.94}
$$

Assuming that the system is much smaller than the effective Jeans allows us to neglect collective effects and set $1/|\epsilon|^2 \to 1$. Equation (5.94) finally becomes

$$
\begin{aligned}
\frac{\partial \overline{W}(\mathbf{v})}{\partial t} = & 2G^2 \ln\Lambda \frac{\partial}{\partial v_i} \int \mathrm{d}\mathbf{v}'\, u_{ij}(\mathbf{v}-\mathbf{v}') \\
& \times \left\{\frac{\partial \overline{W}(\mathbf{v})}{\partial v_j}\overline{W}(\mathbf{v}')\left[m_{\mathrm{b}} + \frac{h^3}{m_{\mathrm{b}}^3}\overline{W}(\mathbf{v}')\right] - \frac{\partial \overline{W}(\mathbf{v}')}{\partial v_j'}\overline{W}(\mathbf{v})\left[m_{\mathrm{b}} + \frac{h^3}{m_{\mathrm{b}}^3}\overline{W}(\mathbf{v})\right]\right\}
\end{aligned} \tag{5.95}
$$

where $u_{ij}(\mathbf{v})$ is defined as

$$u_{ij}(\mathbf{v}) = \int \mathrm{d}\widehat{\mathbf{k}}\, \widehat{k}_i \widehat{k}_j \, \delta_{\mathrm{D}}(\widehat{\mathbf{k}} \cdot \mathbf{v}) = \pi \frac{\partial^2 v}{\partial v_i \partial v_j} = \pi \frac{v^2 \delta_{ij} - v_i v_j}{v^3}, \tag{5.96}$$

We have therefore reached our final result, as we have recovered the kinetic equation (4.50) describing the self-consistent relaxation of a homogeneous halo.

6 Linear Stability

Stability is a fundamental concept in understanding the long-term behavior of dynamical systems, including FDM halos. It refers to the system's ability to return to equilibrium or maintain its structure when subjected to small perturbations. In the context of FDM halos, stability analysis reveals whether density fluctuations will grow or decay over time, which is crucial for predicting the halo's evolution. An unstable halo may undergo significant changes, potentially leading to fragmentation or collapse, while a stable one will maintain its configuration, allowing for smoother relaxation and evolution. Understanding these stability properties provides critical insights into the behavior of FDM halos and their role in cosmic structure formation.

6.1 Quantum Jeans Scale

An infinite homogeneous system is susceptible to an instability characterized by the classical Jeans wavenumber k_J in the classical or particle limit (Binney and Tremaine, 2008). For a Maxwellian distribution function,

$$F_\mathrm{b}(\mathbf{v}) = \frac{\rho_0}{(2\pi\sigma^2)^{3/2}}\,\mathrm{e}^{-|\mathbf{v}|^2/(2\sigma^2)}, \tag{6.1}$$

the Jeans wave number is

$$k_\mathrm{J} = \frac{(4\pi G\rho_0)^{1/2}}{\sigma}. \tag{6.2}$$

The Jeans wavenumber, k_J, defines the boundary between scales where gravitational forces dominate causing instability and scales where opposing forces maintain stability. Perturbations with wavenumbers smaller than or equal to the Jeans wavenumber (k_J) correspond to larger-scale disturbances. At these scales, gravitational forces dominate over opposing pressure or dispersion forces, leading to gravitational collapse. In the opposite limit, perturbations with wavenumbers larger than k_J correspond to smaller-scale disturbances. These scales are stabilized because pressure or velocity dispersion forces counteract self-gravity, preventing collapse. Thus, the system becomes unstable to large-scale perturbations (low k) but remains stable against small-scale ones (high k).

Below, we attempt to derive the quantum Jeans wavenumber, which sets the scale at which the halo becomes unstable to perturbations with wavenumber $k < \tilde{k}_J$, for a halo composed of waves with zero velocity dispersion (i.e., an unperturbed wavefunction $\psi(\mathbf{r}, t) = \text{const.}$) rather than particles.

To obtain the modified Jeans wave number for an FDM halo, we replace the classical kinetic pressure of particles with an effective quantum pressure arising from the uncertainty principle. This quantum pressure, derived in Appendix A.2, introduces a scale-dependent stabilization mechanism that suppresses structure formation below a critical wavelength. Understanding this characteristic scale is essential for predicting density fluctuations and the large-scale structure formation in the presence of FDM.

We can show that an FDM halo, can be described using modified hydrodynamic equations (Chavanis, 2011)

$$\frac{\partial\rho}{\partial t} + \nabla\cdot(\rho\mathbf{u}) = 0, \tag{6.3}$$

$$\frac{\partial\mathbf{u}}{\partial t} + (\mathbf{u}\cdot\nabla)\mathbf{u} = -\frac{1}{\rho}\nabla p - \nabla\Phi - \frac{\hbar^2}{2m^2}\nabla\Big(\frac{\Delta\sqrt{\rho}}{\sqrt{\rho}}\Big) \tag{6.4}$$

$$\Delta\Phi = 4\pi G(\rho - \rho_0), \tag{6.5}$$

where $\mathbf{u}$ is the velocity field and ρ_0 corresponds to the background density. Moreover, the third term on the right-hand side of equation (6.4) is the quantum potential (equivalent to quantum pressure). This term counteract gravitational collapse and is defined as follows

$$Q = -\frac{\hbar^2}{2m}\frac{\Delta\sqrt{\rho}}{\sqrt{\rho}} = -\frac{\hbar^2}{4m}\left[\frac{\Delta\rho}{\rho} - \frac{1}{2}\frac{(\nabla\rho)^2}{\rho^2}\right] \tag{6.6}$$

Equation (6.3), (6.4) and (6.5) are referred to as the quantum barotropic Euler-Poisson equations (Chavanis, 2011). In the classical limit $\hbar \to 0$, the quantum potential disappears and we recover the ordinary barotropic Euler equations Now we can perturb equation (6.3), (6.4) and (6.5) to a linear level. In this case $\rho = \rho_0, \mathbf{u} = 0, \Phi = 0$ and the perturbed equations are

$$\frac{\partial\delta\rho}{\partial t} + \rho\nabla\cdot\delta\mathbf{u} = 0, \tag{6.7}$$

$$\rho_0\frac{\partial\delta\mathbf{u}}{\partial t} = -c_s^2\nabla\delta\rho - \rho_0\nabla\delta\Phi + \frac{h^2}{4m^2}\nabla(\Delta\delta\rho) \tag{6.8}$$

$$\Delta\delta\Phi = 4\pi G\delta\rho \tag{6.9}$$

It it worth mnetionening that the first term on the r.h.s of equation (6.8) was originally $\rho(-\frac{1}{\rho}\Delta p)$ in the unperturbed equation. We use

$$p = \frac{2\pi a\hbar^2}{m_b^3}\rho^2 \tag{6.10}$$

Thus, we can use the definition of the speed of sound

$$c_s^2 = \frac{\partial p}{\partial\rho} = \frac{4\pi a\hbar^2}{m_b^3}\rho \tag{6.11}$$

Therefore

$$\Delta p = \frac{\partial p}{\partial r} = \frac{\partial p}{\partial\rho}\frac{\partial\rho}{\partial r} = c_s^2\Delta\rho. \tag{6.12}$$

Taking the time derivative of equation (6.7) gives

$$\frac{\partial}{\partial t}(\frac{\partial\delta\rho}{\partial t}) = -\frac{\partial}{\partial t}(\rho_0\nabla\cdot\delta\mathbf{u}) = \nabla\cdot\delta\mathbf{u}\frac{\partial\rho_0}{\partial t} + \rho_0\frac{\partial\nabla\delta u}{\partial t} = \rho_0\frac{\partial\nabla\delta u}{\partial t}, \tag{6.13}$$

since $\frac{\partial\rho_0}{\partial t} = 0$. Then taking a spatial derivative from equation (6.8) yields

$$\nabla(\rho_0\frac{\partial\delta\mathbf{u}}{\partial t}) = -c_s^2\Delta\rho - \rho_0\Delta\Phi + \frac{h^2}{4m_b^2}(\Delta^2\delta\rho) \tag{6.14}$$

The l.h.s is $\rho_0\frac{\partial\Delta u}{\partial t}$ which from equation (6.13) is $\frac{\partial^2\delta\rho}{\partial t^2}$. Also the second term in the r.h.s is $4\pi G\delta\rho$ from the perturbed Poisson equation. As a result, we arrive at the following

$$\frac{\partial^2\delta\rho}{\partial t^2} = -\frac{\hbar^2}{4m_b^2}\Delta^2\delta\rho + c_s^2\Delta\delta\rho + 4\pi G\rho_0\delta\rho. \tag{6.15}$$

Expanding the perturbation in plane waves of the form $\delta\rho(\mathbf{r},t) \propto \exp[i(\mathbf{k}\cdot\mathbf{r} - \omega t)]$, we obtain the dispersion relation

$$\omega^2 = \frac{\hbar^2 k^4}{4m_b^2} + c_s^2 k^2 - 4\pi G \rho_0. \tag{6.16}$$

The pressure is zero ($p = 0$) when the particles interact only via gravity. Hence, the dispersion relation reduces to

$$\omega^2 = \frac{\hbar^2 k^4}{4m_b^2} - 4\pi G \rho_0. \tag{6.17}$$

The above result demonstrates the scale at which gravitational forces and quantum mechanics due to the Heisenberg's uncertainty principle are in competition.

$$\tilde{k}_{\rm J} = \left(\frac{16\pi G m_b^2 \rho_0}{\hbar^2}\right)^{1/4}. \tag{6.18}$$

6.2 Dielectric Function in FDM

In plasma physics and gravitational instability theory, the dielectric function $\epsilon(k,\omega)$ describes how a medium responds to perturbations. In FDM, the linear response theory gives a dielectric function that modifies the gravitational potential due to the quantum corrections and stability properties of the halo are determined from it. The Jeans scale in FDM is directly linked to the dielectric function through its role in modifying the stability of density perturbations, analogous to the way plasma oscillations modify electrostatic potentials in plasma physics. In an FDM halo with non-zero velocity dispersion, the effective Jeans wavenumber can be determined from the dielectric function equation (5.49) that can be written as

$$\epsilon(k,\omega) = 1 - \frac{4\pi G m_{\rm b}}{k^2 \hbar} \int \frac{\mathrm{d}u}{\omega - ku} \left[F_\parallel\left(u + \frac{\hbar k}{2m_{\rm b}}\right) - F_\parallel\left(u - \frac{\hbar k}{2m_{\rm b}}\right)\right], \tag{6.19}$$

with $F_\parallel(u) = \int \mathrm{d}v_1 \mathrm{d}v_2\, F_{\rm b}[(v_1^2 + v_2^2 + u^2)^{1/2}]$ and v_1 and v_2 are the velocities along the two axes perpendicular to $\mathbf{k}$.

In the context of perturbation theory, the stability of a system can be analyzed by examining the dielectric function $\epsilon(k,\omega)$. The system is said to be linearly unstable if there exists a frequency ω with a positive imaginary component and a real wavenumber k such that

$$\epsilon(k,\omega) = 0. \tag{6.20}$$

A perturbation with such a frequency exhibits an exponential growth in time, leading to instability. To understand the transition between stability and instability, we consider the *marginal stability limit*, where the imaginary part of ω approaches zero

$$\Im(\omega) \to 0. \tag{6.21}$$

This assumption allows us to determine the boundary at which perturbations cease to decay and begin to grow, marking the onset of instability. In this regime, the frequency ω is approximately real, and the dispersion relation derived from $\epsilon(k,\omega) = 0$ provides insight into the system's behavior at the stability threshold.

If the dielectric function permits solutions where $\Im(\omega) > 0$, the perturbations grow exponentially as

$$e^{\Im(\omega)t}, \tag{6.22}$$

indicating an unstable system. Conversely, if $\Im(\omega) < 0$, perturbations decay, leading to stability. The marginal stability criterion ($\Im(\omega) \to 0$) identifies the transition point where stability is lost and exponential growth begins.

Therefore, the system is linearly unstable if there exists a positive complex frequency ω and a real wavenumber k such that $\epsilon(k,\omega) = 0$. Placing ourselves at the limit of marginal stability, we can use the Plemelj formula from equation (5.50) to rewrite equation (6.19) as

$$\begin{aligned}\epsilon(k,\omega) = 1 - \frac{4\pi G m_\mathrm{b}}{k^2\hbar}\mathcal{P}\!\int \frac{\mathrm{d}u}{\omega - ku}\left[F_\parallel\left(u + \frac{\hbar k}{2m_\mathrm{b}}\right) - F_\parallel\left(u - \frac{\hbar k}{2m_\mathrm{b}}\right)\right] \\ + \mathrm{i}\frac{4\pi^2 G m_\mathrm{b}}{k^3\hbar}\left[F_\parallel\left(\frac{\omega}{k} + \frac{\hbar k}{2m_\mathrm{b}}\right) - F_\parallel\left(\frac{\omega}{k} - \frac{\hbar k}{2m_\mathrm{b}}\right)\right].\end{aligned} \tag{6.23}$$

In order to have $\epsilon(k,\omega) = 0$, both the real part and the imaginary part of equation (6.23) must vanish. This ensures that we have a physically meaningful solution where both the conservative (real part) and dissipative (imaginary part) effects balance out. To simplify our analysis, we assume that the distribution function $F_\mathrm{b}(v)$ is a monotonically decreasing function of $v = |\mathbf{v}|$, meaning that higher velocity states are less populated. This assumption effectively excludes the presence of two-stream instabilities [8], which typically arise when multiple velocity components contribute significantly to the dynamics.

Given this assumption, it follows directly that the parallel velocity distribution function $F_\parallel(u)$ exhibits the following properties: it is an even function of u, meaning that $F_\parallel(-u) = F_\parallel(u)$, and it is monotonically decreasing for $u > 0$ and monotonically increasing for $u < 0$, which aligns with the physical intuition that the probability density of particles decreases as the magnitude of the velocity increases (Bar-Or et al., 2021).

As a consequence of these properties, the second term in equation (6.23) vanishes if and only if either $k = 0$ or $\omega = 0$. The first case, $k = 0$, corresponds to spatially homogeneous perturbations, which do not lead to collective oscillations or instabilities and are therefore not of primary physical interest. We thus disregard this case and instead focus on the second possibility, $\omega = 0$, which corresponds to marginal stability.

This assumption is crucial when analyzing the stability properties of the system, as it simplifies the dispersion relation and allows us to determine conditions under which the system transitions between stable and unstable regimes.

For simplicity, let us further assume that the system's unperturbed distribution function is Maxwellian (see equation (6.1)). In that case, we can rewrite the dielectric function from equation (6.19) as

$$\epsilon(k,\omega) = 1 - \frac{4\pi G m_\mathrm{b}\rho_0}{\sqrt{2\pi}\,k^2\sigma\hbar}\int \frac{\mathrm{d}v}{\omega - kv}\left[\mathrm{e}^{-[v+\hbar k/(2m_\mathrm{b})]^2/(2\sigma^2)} - \mathrm{e}^{-[v-\hbar k/(2m_\mathrm{b})]^2/(2\sigma^2)}\right] \tag{6.24}$$

The constant before the integral can be rewritten as

$$\frac{4\pi G m_\mathrm{b}\rho_0}{\sqrt{2\pi}\,k^2\sigma\hbar} = (\frac{k_J}{k})^2\frac{m_b}{\hbar\sqrt{2\pi}} \tag{6.25}$$

[8] Two-stream instabilities typically occur when there are two separate velocity groups that are moving in opposite directions or have different characteristics, and their interaction can lead to instability under certain conditions, resulting in growth of perturbations or oscillations.

For even more simplification we introduce the following definitions

$$\varpi \equiv \frac{\omega}{\sqrt{2}k\sigma} \tag{6.26}$$

$$\eta \equiv \sqrt{2}\left(\frac{k_{\mathrm{J}}}{\tilde{k}_{\mathrm{J}}}\right)^2 = \frac{\sqrt{2\pi G\rho_0}\hbar}{\sigma^2 m_{\mathrm{b}}} \tag{6.27}$$

$$\simeq 0.0315\left(\frac{m_{\mathrm{b}}}{10^{-22}\,\mathrm{eV}}\right)^{-1}\left(\frac{\rho_0}{0.01\,\mathrm{pc}^{-3}}\right)^{1/2}\left(\frac{\sigma}{100\,\mathrm{km\ s}^{-1}}\right)^{-2}$$

$$\longrightarrow \frac{\hbar}{m} = \frac{\sqrt{2}\eta\sigma}{k_J} \tag{6.28}$$

$$x\frac{v}{\sqrt{2}\sigma} \longrightarrow dv = \sqrt{2}\sigma dx \tag{6.29}$$

Note that $\eta \ll 1$ corresponds to the classical limit, while $\eta \gg 1$ is associated with the quantum limit. Now equation (6.24) becomes

$$\begin{aligned}\epsilon(k,\omega) &= 1 - \left(\frac{k_{\mathrm{J}}}{k}\right)^3 \frac{1}{2\sqrt{\pi}\eta}\int \frac{\mathrm{d}x}{\varpi - x}\left[\mathrm{e}^{-[x+k\eta/(2k_{\mathrm{J}})]^2} - \mathrm{e}^{-[x-k\eta/(2k_{\mathrm{J}})]^2}\right] \\ &= 1 - \left(\frac{k_{\mathrm{J}}}{k}\right)^3 \frac{1}{2\eta}\left[Z\left(\varpi - \frac{k\eta}{2k_{\mathrm{J}}}\right) - Z\left(\varpi + \frac{k\eta}{2k_{\mathrm{J}}}\right)\right]\end{aligned} \tag{6.30}$$

where we introduced the plasma dispersion function, defined as

$$Z(\varpi) = \frac{1}{\sqrt{\pi}}\int_{-\infty}^{\infty}\mathrm{d}s\,\frac{\mathrm{e}^{-s^2}}{s-\varpi} = \begin{cases}\displaystyle\int_{-\infty}^{\infty}\mathrm{d}s\,\frac{\mathrm{e}^{-s^2}}{s-\varpi} & \text{if} \quad \mathrm{Im}(\varpi) > 0, \\ \displaystyle\mathcal{P}\int_{-\infty}^{\infty}\mathrm{d}s\,\frac{\mathrm{e}^{-s^2}}{s-\varpi} + \pi\mathrm{i}\mathrm{e}^{-\varpi^2} & \text{if} \quad \mathrm{Im}(\varpi) = 0, \\ \displaystyle\int_{-\infty}^{\infty}\mathrm{d}s\,\frac{\mathrm{e}^{-s^2}}{s-\varpi} + 2\pi\mathrm{i}\mathrm{e}^{-\varpi^2} & \text{if} \quad \mathrm{Im}(\varpi) < 0.\end{cases} \tag{6.31}$$

Based on equation (6.30), the requirement of marginal stability at $\varpi = 0$ means that

$$k_{\mathrm{c}}^3 = \frac{k_{\mathrm{J}}^3}{2\eta}\left[Z\left(-\frac{k_{\mathrm{c}}\eta}{2k_{\mathrm{J}}}\right) - Z\left(\frac{k_{\mathrm{c}}\eta}{2k_{\mathrm{J}}}\right)\right], \tag{6.32}$$

with k_{c} the critical wavenumber at marginal stability. For $x \in \mathbb{R}$, we can use the two expansions from Fried and Conte (1961)

$$Z(x) \simeq \begin{cases}\mathrm{i}\sqrt{\pi}\mathrm{e}^{-x^2} - 2x & \text{for} \quad |x| \ll 1, \\ \mathrm{i}\sqrt{\pi}\mathrm{e}^{-x^2} - \dfrac{1}{x} & \text{for} \quad |x| \gg 1.\end{cases} \tag{6.33}$$

Then we can approximate the r.h.s. of equation (6.32) as

$$k_{\mathrm{c}} \simeq \begin{cases}k_{\mathrm{J}} & \text{for} \quad \eta \ll 1, \\ \tilde{k}_{\mathrm{J}} & \text{for} \quad \eta \gg 1.\end{cases} \tag{6.34}$$

We therefore recover the known result that in the limit $\eta \ll 1$ ($k_{\mathrm{J}} \ll \tilde{k}_{\mathrm{J}}$), the system's stability is determined by classical physics and the critical wavenumber is k_{J}, while in

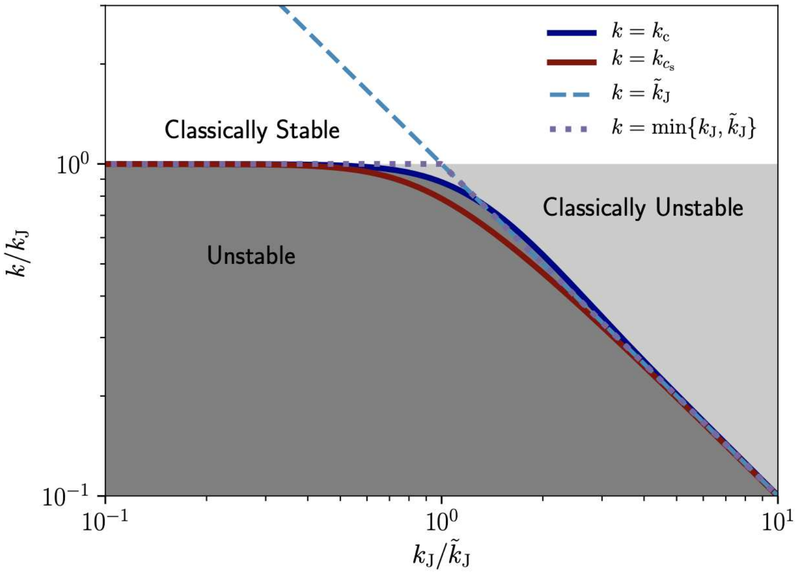

Figure 6.1: Figure adapted from Bar-Or et al. (2021); Linear stability of a Maxwellian DF. The critical wavenumber k_c that separates stable and unstable perturbations is shown as a function of the ratio between the classical Jeans wavenumber k_J and the quantum Jeans wavenumber $\tilde{k}_J$ (blue line). Perturbations with wavenumber $k > k_c$ are stable and perturbations with wavenumber $k < k_c$ are unstable. This critical wavenumber k_c can be approximated by $\min\{k_J, \tilde{k}_J\}$ (dotted line). The critical wavenumber k_{c_s} for a fluid system is also shown (see equation (6.35))

the limit $\eta \gg 1$ ($k_J \gg \tilde{k}_J$), stability is dominated by quantum effects and the critical wavenumber is $\tilde{k}_J$. This behavior is illustrated in Fig. 6.2, where we show the critical wavenumber for a Maxwellian DF as determined from equation (6.32), as a function of the ratio $k_J/\tilde{k}_J$.

Chavanis (2011) derived a simplified dispersion relation by treating the fuzzy halo as a fluid with a sound speed, c_s. This sound speed is assumed to represent the halo's velocity dispersion, i.e., $c_s = \sigma$. Based on this assumption, the dispersion relation is given by

$$k_{c_s}^2 = \frac{k_J^2}{\eta^2}\left[\sqrt{1+2\eta^2} - 1\right]. \tag{6.35}$$

In this framework, perturbations with wavenumbers $k > k_{c_s}$ remain stable, while those with $k < k_{c_s}$ are unstable. The prediction made by equation (6.35) is illustrated in Fig. 6.2, where it accurately captures the transition from the classical to the quantum regime as the ratio $k_J/\tilde{k}_J$ is varied.

In Fig. 6.2, we highlight the significance of collective effects in modifying relaxation, as captured by the factor $1/|\epsilon(k,\omega)|^2$ in equation 5.94. The dielectric function $\epsilon(k,\omega)$ is defined by equation 6.30.

We observe that the influence of collective effects diminishes (i.e., $\epsilon(k,\omega) \to 1$) as the system stabilizes (i.e., $k \gg k_c$). Furthermore, for a fixed ratio k/k_c, the increasing significance of quantum effects (i.e., $\eta \gg 1$) leads to a suppression of collective effects, with $\epsilon(k,\omega) \sim \eta^{-3}$.

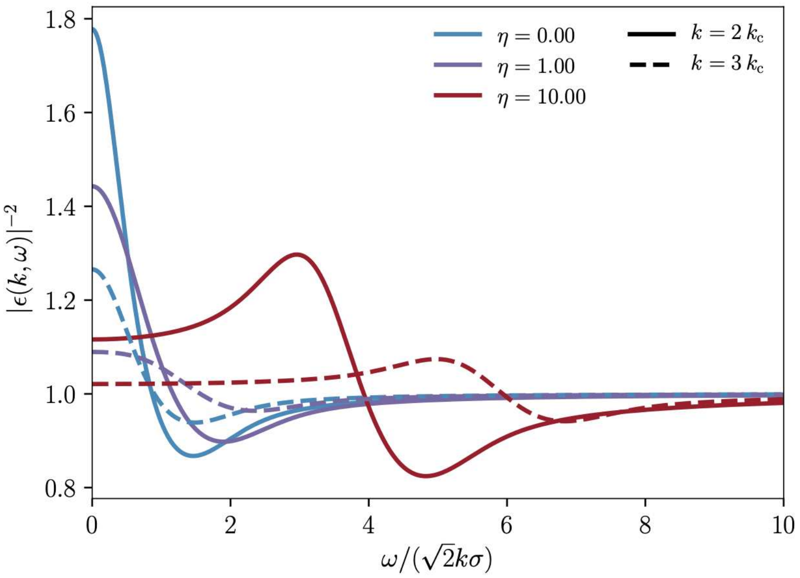

Figure 6.2: Figure adapted from Bar-Or et al. (2021); Illustration of the self-gravitating dressing of perturbations by collective effects, as measured by the dielectric function $1/|\epsilon(k,\omega)|^2$, for different values of the stability parameter $k/k_{\rm c}$, and the quantum parameter η.

7 FDM Halo and Baryonic Matter Interactions

As mentioned in the first chapter, the interactions of the FDM particles with each other results in the formation of the soliton. In this chapter however, we introduce the effects of the interaction of an FDM halo with baryonic objects.

7.1 Mass segregation

In CDM models, dark matter is composed of elementary particles that are very light compared to astrophysical objects like black holes or globular clusters. Therefore, when a massive object (such as a black hole or star cluster) moves through a CDM halo, it loses energy through dynamical friction. This friction causes the object to spiral inward toward the center of the halo, as the dark matter particles drag on the object, slowing it down. The same thing could still happen even if the CDM particles are macroscopic objects, say of 1–30 $M_\odot$, they are much less massive than objects such as supermassive black holes or globular clusters.(Tremaine and Weinberg, 1975; Begelman and Rees, 1980).

In FDM, the situation changes significantly. Fuzzy dark matter consists of quasiparticles with a non-zero mass, which contrasts with the negligible mass of CDM particles. Due to the quantum nature of FDM, the interaction between the massive object and the dark matter halo is different. When a massive object (e.g., a black hole or a stellar object) moves through an FDM halo, it still experiences dynamical friction, which tends to make it lose orbital energy and move inward. However, unlike in CDM, the object can also gain energy through gravitational interactions with the FDM quasiparticles. This is because FDM particles have a quantum pressure that creates a more structured, less homogeneous background than CDM, allowing for energy exchange between the object and the dark matter.

As the massive object interacts with the FDM halo, it will lose energy due to dynamical friction, but it will also gain energy from the interactions with FDM quasiparticles. This leads to a process where the object and the dark matter particles tend to reach energy equipartition, a state where the energy between the object and the FDM particles becomes balanced. When this energy equipartition occurs, the inspiral of the massive object may stall, as it cannot lose enough energy to continue its inward motion. This contrasts with the CDM scenario, where the object can continue to spiral inward without significant energy gain from the halo.

The same effect applies to individual stars within a stellar system embedded in an FDM halo. Instead of the stars being subject to the usual dynamical friction that causes them to lose energy and spiral inward (as in the case with CDM), the stars in an FDM halo will gain energy from interactions with the FDM quasiparticles. This can lead to the expansion of the stellar system, as stars gain kinetic energy from the dark matter field.

For massive objects like black holes or clusters of stars, the fact that their inspiral is stalled due to energy equipartition with the FDM could have significant implications for the formation of supermassive black holes at the centers of galaxies. In CDM models, black holes continue to grow by accreting dark matter and gas, but in FDM, the interaction with the dark matter may prevent further inward movement once equipartition is reached.

For stellar systems, the expansion of stellar systems due to interactions with FDM quasiparticles could lead to observable effects in galaxy dynamics. Stars could move to higher velocities, and the system could become more diffuse, affecting the overall galactic morphology.

This process highlights a key difference between CDM and FDM in the behavior of dark matter halos. While CDM halos allow for continued inspiral and contraction of objects due to dynamical friction, FDM halos, with their quantum pressure and energy exchange, can lead to a different dynamical behavior, including stalling of massive objects' inward movement and expansion of stellar systems.

In summary, the relaxation effects in FDM halos due to energy exchange between massive objects and quasiparticles can significantly alter the dynamics of systems embedded in such halos, leading to stalled inspirals and stellar system expansion, which contrasts with the behavior observed in CDM halos.

Having established the qualitative framework, we now proceed to a mathematical description of these processes in a galaxy composed entirely of FDM. We consider a background density ρ_b and assume a Maxwellian velocity distribution with dispersion σ. Our calculations build upon the results derived in 4.1, namely equation (4.16) and (4.17)

$$\begin{aligned} D_{ij} &= \frac{32\pi^3 G^2 \hbar^3}{m_\mathrm{b}^3} \log \Lambda_\mathrm{FDM} \int \mathrm{d}\widehat{\mathbf{k}}\, \widehat{k}_i \widehat{k}_j \int \mathrm{d}\mathbf{v}' F_\mathrm{b}^2(\mathbf{v}') \delta[\widehat{\mathbf{k}} \cdot (\mathbf{v} - \mathbf{v}')] \\ &= 4G^2 m_\mathrm{eff} \log \Lambda_\mathrm{FDM} \int \mathrm{d}\widehat{\mathbf{k}}\, \widehat{k}_i \widehat{k}_j \int \mathrm{d}\mathbf{v}' \delta[\widehat{\mathbf{k}} \cdot (\mathbf{v} - \mathbf{v}')] F_\mathrm{eff}(\mathbf{v}'), \end{aligned} \tag{7.1}$$

and

$$D_i = 4\pi G^2 m_\mathrm{eff} \log \Lambda_\mathrm{FDM} v_i \int \mathrm{d}\mathbf{v}' \frac{F_\mathrm{eff}(\mathbf{v}')}{|\mathbf{v} - \mathbf{v}'|}. \tag{7.2}$$

where the following definitions for the effective mass and effective distribution

$$m_\mathrm{eff} = \frac{(2\pi\hbar)^3 \int \mathrm{d}\mathbf{v}\, F_\mathrm{b}^2(\mathbf{v})}{m_\mathrm{b}^3 \int \mathrm{d}\mathbf{v}\, F_\mathrm{b}(\mathbf{v})} \tag{7.3}$$

$$F_\mathrm{eff}(\mathbf{v}) = \frac{\int \mathrm{d}\mathbf{v}\, F_\mathrm{b}(\mathbf{v})}{\int \mathrm{d}\mathbf{v}\, F_\mathrm{b}^2(\mathbf{v})} F_\mathrm{b}^2(\mathbf{v}), \tag{7.4}$$

which is normalized such that $\int \mathrm{d}\mathbf{v}\, F_\mathrm{eff}(\mathbf{v}) = \rho_\mathrm{b}$. For the Maxwellian velocity distribution, $D_\mathrm{f}[\Delta v_i] = (v_i/v) D_\mathrm{f}[\Delta v_\parallel]$, where

$$D_\mathrm{f}[\Delta v_\parallel] = -\frac{4\pi G^2 \rho_\mathrm{b} m_\mathrm{t} \log \Lambda_\mathrm{FDM}}{\sigma^2} \mathbb{G}(X), \tag{7.5}$$

with $\mathbb{G}(X)$ defined as (see equation (3.54))

$$\mathbb{G}(X) \equiv \frac{1}{2X^2} \left[\mathrm{erf}(X) - \frac{2X}{\sqrt{\pi}} \mathrm{e}^{-X^2} \right]. \tag{7.6}$$

. Then, following the procedure in Appendix A.4 gives

$$D\left[\Delta v_\parallel\right] = -\frac{4\pi G^2 \rho_\mathrm{b} m_\mathrm{eff} \log \Lambda_\mathrm{FDM}}{\sigma_\mathrm{eff}^2} \left[\mathbb{G}\left(X_\mathrm{eff}\right) + \mu_\mathrm{eff} \mathbb{G}(X)\right] \tag{7.7}$$

$$D\left[\left(\Delta v_\parallel\right)^2\right] = \frac{4\sqrt{2}\pi G^2 \rho_\mathrm{b} m_\mathrm{eff} \log \Lambda_\mathrm{FDM}}{\sigma_\mathrm{eff}} \frac{\mathbb{G}\left(X_\mathrm{eff}\right)}{X_\mathrm{eff}} \tag{7.8}$$

$$D\left[\left(\Delta \mathbf{v}_\perp\right)^2\right] = \frac{4\sqrt{2}\pi G^2 \rho_\mathrm{b} m_\mathrm{eff} \log \Lambda_\mathrm{FDM}}{\sigma_\mathrm{eff}} \frac{\mathrm{erf}\left(X_\mathrm{eff}\right) - \mathbb{G}\left(X_\mathrm{eff}\right)}{X_\mathrm{eff}} \tag{7.9}$$

where $\sigma_{\text{eff}}^2/\sigma^2 = 1/2$, $X = v/\sqrt{2}\sigma$, $X_{\text{eff}} = v/\sqrt{2}\sigma_{\text{eff}} = v/\sigma$, and

$$\mu_{\text{eff}} \equiv \frac{m_{\text{t}}}{m_{\text{eff}}}\frac{\sigma_{\text{eff}}^2}{\sigma^2} = \frac{m_{\text{t}}}{2m_{\text{eff}}} \tag{7.10}$$

is the effective mass ratio. The factor of 2 in the definition of μ_{eff}, and the classical diffusion coefficient analogous to equation (7.7) for a halo composed of particles of mass m_{p} is

$$D[\Delta v_{\|}] = -\frac{4\pi G^2 \rho_{\text{p}} m_{\text{p}} \log \Lambda_{\text{cl}}}{\sigma^2}(1+\mu_{\text{cl}})\mathbb{G}(X), \tag{7.11}$$

where $\mu_{\text{cl}} = m_{\text{t}}/m_{\text{p}}$ (without a factor of 2) (Bar-Or et al., 2019).

Now we calculate the specific energy diffusion coefficients. The rate of change of the kinetic energy of the subject star is

$$\begin{aligned} D[\Delta E] &= m\sum_{i=1}^{3}\left(v_i D[\Delta v_i] + \frac{1}{2}D[\Delta v_i \Delta v_i]\right) \\ &= m\left(vD[\Delta v_{\|}] + \frac{1}{2}D[(\Delta v_{\|})^2] + \frac{1}{2}D[(\Delta \vec{v}_{\perp})^2]\right) \end{aligned} \tag{7.12}$$

The specific energy diffusion coefficients are the following

$$\begin{aligned} D\left[\Delta E\right] &= vD\left[\Delta v_{\|}\right] + \frac{1}{2}D\left[\left(\Delta v_{\|}\right)^2\right] + \frac{1}{2}D\left[\left(\Delta \mathbf{v}_{\perp}\right)^2\right] \\ &= \frac{4\sqrt{2}\pi G^2 \rho_b m_{\text{eff}} \log \Lambda_{FDM}}{\sigma_{\text{eff}}} \\ &\times \left[-\frac{v}{\sqrt{2}\sigma_{\text{eff}}}(G(X_{\text{eff}}) + \mu_{\text{eff}}G(X)) + \frac{G(X_{\text{eff}})}{2X_{\text{eff}}} + \frac{\text{erf}(X_{\text{eff}})}{2X_{\text{eff}}} - \frac{G(X_{\text{eff}})}{2X_{\text{eff}}}\right] \end{aligned} \tag{7.13}$$

From the definition of $\mathbb{G}(X)$ we can write

$$\frac{\text{erf}\left(X_{\text{eff}}\right)}{2X_{\text{eff}}} = X_{\text{eff}}G\left(X_{\text{eff}}\right) + \frac{e^{-X_{\text{eff}}^2}}{\sqrt{\pi}} \tag{7.14}$$

We can write the term in the square brackets using the above relation and replacing $v/\sqrt{2}\sigma_{\text{eff}}$ with X_{eff} in the following form

$$-X_{\text{eff}}(G(X_{\text{eff}}) + \mu_{\text{eff}}G(X)) + \frac{G(X_{\text{eff}})}{2X_{\text{eff}}} + X_{\text{eff}}G\left(X_{\text{eff}}\right) + \frac{e^{-X_{\text{eff}}^2}}{\sqrt{\pi}} - \frac{G(X_{\text{eff}})}{2X_{\text{eff}}} \tag{7.15}$$

and finally after some simplifications we will arrive at the mean energy change per unit time

$$\begin{aligned} D\left[\Delta E\right] &= \frac{4\sqrt{2\pi}G^2\rho_b m_{\text{eff}} \log \Lambda_{FDM}}{\sigma_{\text{eff}}} e^{-X_{\text{eff}}^2}\left[1 - \frac{\mu_{\text{eff}}\sqrt{\pi}X_{\text{eff}}G(X)}{e^{-X_{\text{eff}}^2}}\right] \\ &= \frac{8\sqrt{\pi}G^2\rho_{\text{b}} m_{\text{eff}} \log \Lambda_{\text{FDM}}}{\sigma} \exp\left(-v^2/\sigma^2\right)\left[1 - \mu_{\text{eff}}K(v/\sigma)\right] \end{aligned} \tag{7.16}$$

where

$$K(x) \equiv \frac{\sqrt{\pi}}{x}\mathrm{e}^{x^2}\,\text{erf}(x/\sqrt{2}) - \sqrt{2}\mathrm{e}^{x^2/2}.$$

(7.17)

This result demonstrates the energy evolution of a massive body moving in an FDM halo governed by the interplay between stochastic diffusion (heating) and dynamical friction (cooling). These two competing processes determine whether the body gains or loses energy over time, affecting its orbital evolution and the overall structure of stellar systems embedded in FDM halos.

The first term inside the brackets, $\exp(-X_{\rm eff}^2)$, corresponds to stochastic diffusion (heating). This effect arises from the potential fluctuations of the FDM field, which act as a random force that injects energy into the massive body's orbit. The strength of this effect depends on the effective mass of the FDM perturbations, $m_{\rm eff}$, and the velocity of the body relative to the velocity dispersion of the FDM background. Since this term is always positive, it continuously pumps energy into the orbit, leading to potential halo expansion and suppressing inspiral effects. This diffusion mechanism is unique to FDM and is absent in CDM models, where density fluctuations are far weaker at small scales (Hui et al., 2017; Bar-Or et al., 2019).

In contrast, the second term, $-\mu_{\rm eff}\sqrt{\pi}X_{\rm eff}\mathbb{G}(X)$, represents dynamical friction (cooling). This term describes the back-reaction of the massive body on the surrounding FDM field. As the body moves, it perturbs the local FDM density, creating an overdense wake that exerts a drag force. This process extracts energy from the massive body's orbit, leading to a gradual inspiral over time (Binney and Tremaine, 2008; Chandrasekhar, 1943). Since this effect is proportional to $\mu_{\rm eff}$, which depends on the mass of the moving body, more massive objects experience stronger cooling. This term is identical to the classical Chandrasekhar dynamical friction formula used in CDM, meaning that dynamical friction behaves the same way in both CDM and FDM.

The competition between these two processes is captured by the ratio $\mu_{\rm eff}K(v/\sigma)$, which determines whether the body gains or loses energy. If diffusion dominates, the body gains energy and moves to a higher orbit, leading to halo expansion and suppressed mass segregation. Conversely, if dynamical friction dominates, the body loses energy and spirals inward, leading to mass segregation.

The key distinction between FDM and CDM arises from the presence of diffusion. In CDM halos, only dynamical friction is present, leading to efficient orbital decay of massive objects such as globular clusters and black holes. However, in FDM halos, the additional diffusion term can counteract dynamical friction, potentially stalling inspirals or even causing outward migration under certain conditions (Lancaster and Challinor, 2020). This fundamental difference alters the long-term evolution of satellite galaxies, black holes, and star clusters embedded in FDM halos, setting FDM apart from standard CDM predictions.

For the second order energy diffusion coefficient we have

$$\begin{aligned} D\left[(\Delta E)^2\right] &= v^2 D\left[\left(\Delta v_\parallel\right)^2\right] \\ &= \frac{4\sqrt{2}\pi G^2\rho_{\rm b}m_{\rm eff}\log\Lambda_{\rm FDM}}{\sigma_{\rm eff}}\frac{\mathbb{G}\left(X_{\rm eff}\right)v^2}{X_{\rm eff}} \\ &= 8\sqrt{2}\pi G^2\rho_{\rm b}m_{\rm eff}\log\Lambda_{\rm FDM}\frac{\mathbb{G}\left(X_{\rm eff}\right)\left(v^2/2\sigma_{\rm eff}\right)}{X_{\rm eff}} \\ &= 8\sqrt{2}\pi G^2\rho_{\rm b}m_{\rm eff}\sigma_{\rm eff}\log\Lambda_{\rm FDM}X_{\rm eff}\mathbb{G}\left(X_{\rm eff}\right), \end{aligned} \tag{7.18}$$

To examine this process in greater depth, we consider a system composed of an ensemble of massive bodies, each with mass m_t moving through a uniform background of FDM. The velocity distribution of these bodies follows a Maxwellian distribution function $F_t(\mathbf{v}_t)$ with density ρ_t and velocity dispersion σ_t. specific to the massive bodies.

Flow of specific energy into the orbits of the massive objects due to the combined effects of stochastic fluctuations in the gravitational potential and dynamical friction is

$$\begin{aligned}\langle\dot{E}\rangle &= \frac{1}{\rho_{\mathrm{t}}}\int \mathrm{d}\mathbf{v}_{\mathrm{t}} F_{\mathrm{t}}\left(\mathbf{v}_{\mathrm{t}}\right) D[\Delta E] \\ &= \frac{1}{\rho_t}\frac{\rho_t}{\left(2\pi\sigma_t^2\right)^{3/2}}\frac{8\sqrt{\pi}G^2\rho_b m_{\mathrm{eff}}\log\Lambda_{FDM}}{\sigma}\int d\mathbf{v}_t e^{-\frac{v_t^2}{2\sigma_t^2}} e^{-\frac{v_t^2}{\sigma^2}}\left[1-\mu_{\mathrm{eff}}K(v_t/\sigma)\right]\end{aligned} \tag{7.19}$$

After computing each term in the integral (see Appendix A.8), we obtain

$$\langle\dot{E}\rangle = \frac{8\sqrt{\pi}G^2\rho_b m_{\mathrm{eff}}\log\Lambda_{\mathrm{FDM}}}{\sigma\left(1+2\sigma_t^2/\sigma^2\right)^{3/2}}\left(1-\mu_{\mathrm{eff}}\sqrt{2}\left(\frac{1+(2\sigma_t^2/\sigma^2)}{1+(\sigma_t^2/\sigma^2)}\right)^{3/2}\right) \tag{7.20}$$

When $m_{\mathrm{t}} \ll m_{\mathrm{eff}}$ or $\mu_{\mathrm{eff}} \ll 1$, the heating process dominates, and the energy change can be simplified using the form provided in equation (7.20). The energy exchange becomes predominantly positive, leading to an increase in the velocity dispersion of the massive object. In CDM however, dynamical friction usually dominates, and the velocity dispersion typically decreases over time.

7.2 Heating and Cooling Timescales

We can now express the rate of change of the velocity dispersion σ_{t}^2 in terms of the heating timescale T_{heat}. For systems where heating dominates, we write the equation for σ_{t}^2 as follows

$$\sigma_{\mathrm{t}}^2 t = \tfrac{2}{3}\langle\dot{E}\rangle = \frac{\sigma^2}{T_{\mathrm{heat}}}\left(1+\frac{2\sigma_{\mathrm{t}}^2}{\sigma^2}\right)^{-3/2}. \tag{7.21}$$

The heating timescale T_{heat} is defined as

$$T_{\mathrm{heat}} = \frac{3\sigma^3}{16\sqrt{\pi}G^2\rho_{\mathrm{b}} m_{\mathrm{eff}}\log\Lambda_{\mathrm{FDM}}}, \tag{7.22}$$

where ρ_{b} is the background density of the FDM. This timescale characterizes the rate at which energy is transferred to the massive body from the FDM field.

We now consider the solution to the equation for the evolution of σ_{t}^2. By integrating equation (7.21), we find

$$\frac{\sigma_{\mathrm{t}}^2(t)}{\sigma^2} = \frac{1}{2}\left\{5t/T_{\mathrm{heat}} + \left[1+\frac{2\sigma_{\mathrm{t}}^2(0)}{\sigma^2}\right]^{5/2}\right\}^{2/5} - \frac{1}{2}. \tag{7.23}$$

This solution suggests that the velocity dispersion σ_{t}^2 increases over time due to heating, and it asymptotically approaches a value related to the timescale T_{heat}. In particular, the velocity dispersion will exceed σ after a time $t \sim 3T_{\mathrm{heat}}$. The time evolution of σ_{t}^2 reflects the unique dynamical behavior of systems in FDM halos, where heating leads to an expansion of the system, unlike the contraction observed in CDM halos due to dynamical friction.

On the other hand, when $\mu_{\mathrm{eff}} \gg 1$, cooling dominates the energy exchange process. In this regime, the rate of change of the velocity dispersion σ_{t}^2 can be expressed as

$$\sigma_{\mathrm{t}}^2 t = -\frac{\sigma_{\mathrm{t}}^2}{T_{\mathrm{cool}}}\left(1+\sigma_{\mathrm{t}}^2/\sigma^2\right)^{-3/2}, \tag{7.24}$$

where the cooling timescale T_{cool} is defined as

$$T_{\mathrm{cool}} = \frac{3\sigma^3}{8\sqrt{2\pi}G^2 m_{\mathrm{t}}\,\rho_{\mathrm{b}}\log\Lambda_{\mathrm{FDM}}}. \tag{7.25}$$

This expression reflects the cooling process driven by the dynamical friction between the massive body and the FDM field, where the body transfers energy into the FDM field as it moves through the halo. As in the classical case of CDM, the cooling timescale is independent of the effective mass of the FDM particles m_{eff}, but it is modified by the Coulomb logarithm term $\log\Lambda_{\mathrm{FDM}}$, which accounts for the specifics of the FDM halo and the particle's interactions within it.

The classical cooling timescale in the context of CDM halos is derived from the standard dynamical friction theory, where the drag force acting on the massive body is proportional to its velocity, resulting in a loss of energy from the body and a corresponding reduction in its velocity dispersion. In the case of FDM, however, the cooling term is affected by the wave-like properties of the dark matter, which alter the nature of the interactions and modify the Coulomb logarithm $\log\Lambda_{\mathrm{FDM}}$.

Thus, the cooling term in FDM halos behaves similarly to the classical dynamical friction result, but with the distinction that it involves quantum effects that influence the timescale over which the velocity dispersion evolves.

When the heating timescale T_{heat} and the cooling timescale T_{cool} are both smaller than the system's lifetime, the velocity distribution of the ensemble of massive objects will relax towards a steady state. This steady-state distribution function $F_{\mathrm{t}}(\mathbf{v})$ is determined by the zero-flux condition in energy space. Specifically, the distribution function must satisfy the following equation (Bar-Or et al., 2019)

$$\frac{d}{dv}\left\{D[(\Delta E)^2]\,v\,F_t(v)\right\} = 2v^2 D[(\Delta E)]F_t(v) \tag{7.26}$$

or alternatively,

$$\frac{d\,(vF_t(v))}{vF_t(v)} = \left[2v\frac{D[(\Delta E)]}{D[(\Delta E)^2]}\right]dv. \tag{7.27}$$

By solving this equation, we obtain the steady-state distribution function for the massive objects

$$F_t(v) \propto \frac{1}{v}\exp\left(\int_0^v 2v'\frac{D[(\Delta E)]}{D[(\Delta E)^2]}\right). \tag{7.28}$$

This solution provides the velocity distribution of the massive objects at equilibrium, where the energy flux between the objects and the FDM halo is balanced.

The diffusion coefficients that govern the energy exchanges between the massive bodies and the FDM field depend linearly on the halo mass density ρ_b. As a result, the steady-state velocity distribution $F_{\mathrm{t}}(v)$ of the massive bodies is influenced by ρ_b only indirectly, through the effective mass m_{eff}, which is a function of ρ_b (as shown in equation (4.22)). Specifically, m_{eff} determines the coupling strength between the bodies and the FDM field, thereby affecting the dynamics of the system and the resulting velocity distribution.

In a classical N-body system composed of particles of mass m, the velocity distribution $F_{\text{t}}(v)$ is Maxwellian, with a mean-square velocity proportional to $3(m_{\text{eff}}/m_{\text{t}})\sigma^2$. This classical Maxwellian distribution assumes that the particles are interacting via Newtonian gravity and undergo isotropic random motion.

However as it is stated in Bar-Or et al. (2019), the velocity distribution for an ensemble of massive bodies interacting gravitationally with an FDM halo is only approximately Maxwellian, as shown in Figure 7.1. While the shape of the distribution is not a perfect Maxwellian, it is close to one, with the mean-square velocity following the relation $3\sigma_{\text{eff}}^2/\mu_{\text{eff}}$, which is similar to the classical result, $3(m_{\text{eff}}/m_{\text{t}})\sigma^2$, but with the effective mass m_{eff} replacing the particle mass m (Figure 7.2). This approximation shows that while the system's behavior retains some classical characteristics, the presence of the FDM field modifies the velocity distribution in a way that depends on the effective mass and the halo properties.

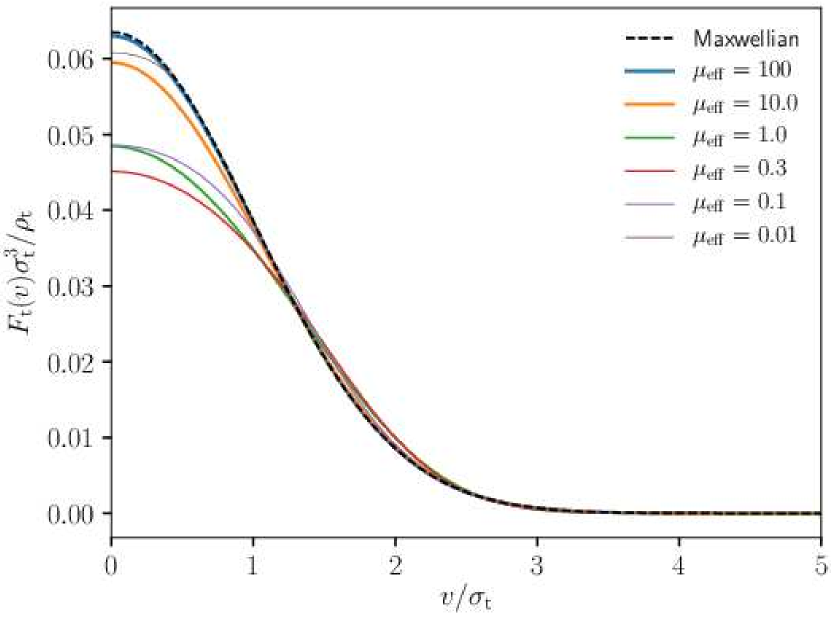

Figure 7.1: The steady-state velocity distribution for an ensemble of massive bodies interacting with an FDM field, as obtained from equation (7.28) for several values of the effective mass ratio $\mu_{\text{eff}} \equiv m_{\text{t}}/(2m_{\text{eff}})$ (solid lines). The velocity is plotted in units of the velocity dispersion, σ_{t}, where $\sigma_{\text{t}}^2 = \langle v^2 \rangle/3$. The steady-state velocity distribution approaches a Maxwellian (dashed line) in the limits $\mu_{\text{eff}} \to 0$ and $\mu_{\text{eff}} \to \infty$. Figure adapted from Bar-Or et al. (2019)

7.3 Structure of the FDM halo

To further study some specific examples of dynamical interaction between an FDM halo the and baryonic objects orbiting within it, we introduce a simplified model for the FDM halo which is useful for understanding the structure and dynamics of FDM halos without requiring a full numerical wave simulation. This model consists of two main

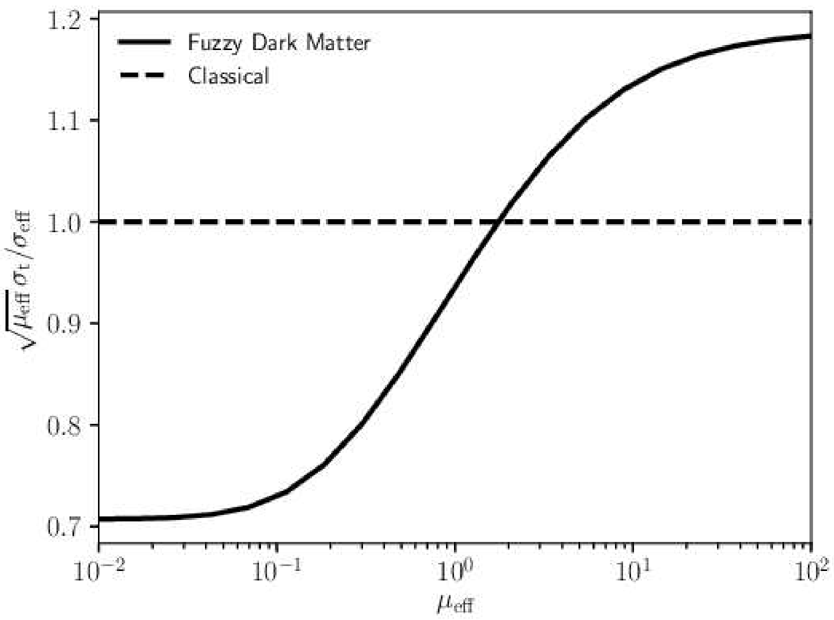

Figure 7.2: In thermal equilibrium, the velocity dispersion $\sigma_{\rm t}$ of an ensemble of baryons is related to the effective velocity dispersion $\sigma_{\rm eff} = \sigma/\sqrt{2}$ of theFDM halo. The ratio of dispersions depends on the effective mass ratio $\mu_{\rm eff} \equiv m_{\rm t}/(2m_{\rm eff})$ (solid line) and is close to (within 30%) but not equal to the standard relation $\sqrt{m_{\rm t}/m_{\rm p}}\,\sigma_{\rm t}/\sigma = 1$ (dashed line) that corresponds to the thermal equilibrium in a background of classical particles of mass $m_{\rm p}$ and velocity dispersion σ. Figure adapted from Bar-Or et al. (2019)

components: The solitonic core and the surrounding halo. Below, we discuss the details of each component.

7.3.1 The Soliton Core

Near the center of an FDM halo, the wave-like nature of the ultralight bosonic dark matter field results in the formation of a soliton core. This soliton represents a stable, self-gravitating ground-state solution to the Schrödinger–Poisson equations, arising from the balance between quantum pressure—due to the uncertainty principle—and gravitational attraction (Schive et al., 2014b). The density profile of the soliton can be approximated by

$$\rho_{\rm s}(r) \approx \frac{0.019 M_\odot\,{\rm pc}^{-3}}{[1+0.091(r/r_{\rm s})^2]^8}\left(\frac{m_{\rm b}}{10^{-22}\,{\rm eV}}\right)^{-2}\left(\frac{r_{\rm s}}{\rm kpc}\right)^{-4}, \tag{7.29}$$

where $r_{\rm s}$ is the characteristic soliton core radius, and $m_{\rm b}$ is the mass of the FDM particle. The total mass of the soliton is given by integrating the density profile

$$M_{\rm s} = 4\pi\int_0^\infty r^2 {\rm d}r\,\rho_{\rm s}(r) = 2.2\times 10^8 M_\odot\left(\frac{r_{\rm s}}{\rm kpc}\right)^{-1}\left(\frac{m_{\rm b}}{10^{-22}\,{\rm eV}}\right)^{-2}. \tag{7.30}$$

Numerical simulations of FDM halo evolution in a cosmological context indicate that the soliton core radius is related to the total virial mass of the halo $M_{\rm h}$ through the empirical scaling relation (Schive et al., 2014b)

$$r_{\rm s} \simeq 0.16\,{\rm kpc}\left(\frac{m_{\rm b}}{10^{-22}\,{\rm eV}}\right)^{-1}\left(\frac{M_{\rm h}}{10^{12}M_\odot}\right)^{-1/3}. \tag{7.31}$$

Interestingly, outside the soliton, the relation between the halo mass and the peak circular velocity $v_{\rm max}$ remains consistent with the expectations from CDM models (Klypin et al., 2011):

$$v_{\rm max} = 155\,{\rm km\ s^{-1}}\left(\frac{M_{\rm h}}{10^{12}M_\odot}\right)^{0.316}. \tag{7.32}$$

Combining these relations, the soliton core radius can be expressed in terms of the peak circular velocity as

$$r_{\rm s} \simeq 0.12\,{\rm kpc}\left(\frac{m_{\rm b}}{10^{-22}\,{\rm eV}}\right)^{-1}\left(\frac{v_{\rm max}}{200\,{\rm km\ s^{-1}}}\right)^{-1.05}. \tag{7.33}$$

A key feature of FDM models is that the de Broglie wavelength associated with the dark matter particles is comparable to the size of the soliton, a direct consequence of wave interference effects. This can be verified in two ways

1. The de Broglie wavelength for a particle moving at circular velocity at radius r outside the soliton is

$$\lambda = \frac{h}{m_{\rm b}}\left(\frac{r}{GM_{\rm s}}\right)^{1/2} = 3.91\,r_{\rm s}\left(\frac{r}{r_{\rm s}}\right)^{1/2}. \tag{7.34}$$

   This implies that the de Broglie wavelength near the soliton boundary is of the same order as $r_{\rm s}$.

2. The de Broglie wavelength for a particle moving at the peak circular velocity $v_{\rm max}$ is

$$\lambda = \frac{h}{m_{\rm b}v_{\rm max}} = 0.60\,{\rm kpc}\left(\frac{m_{\rm b}}{10^{-22}\,{\rm eV}}\right)^{-1}\left(\frac{v_{\rm max}}{200\,{\rm km\ s^{-1}}}\right)^{-1}. \tag{7.35}$$

   Again, this result is within a factor of a few of $r_{\rm s}$ (see equation (7.33)).

These two independent estimates suggest a fundamental link between the soliton size and the de Broglie scale of the system. Furthermore, an intriguing numerical finding is that the peak circular velocity within the soliton is consistently about 25% smaller than the peak circular velocity of the halo, regardless of the halo mass or FDM particle mass. This relation remains unexplained and appears to be an emergent property of the structure formation process in FDM scenarios (Bar-Or et al., 2019).

In contrast to FDM, where the soliton core is a smooth, well-defined feature resulting from quantum mechanical effects, CDM halos are characterized by sharp central density cusps. The classical view of CDM halos involves hierarchical mergers and rapid relaxation, leading to a high concentration of mass in the center of halos. The density profile typically follows a power law such as the Navarro-Frenk-White (NFW) profile (Navarro et al., 1997a)

$$\rho_{\rm CDM}(r) = \frac{\rho_0}{(r/r_s)(1+r/r_s)^2}. \tag{7.36}$$

In the NFW profile, ρ_0 is a characteristic density, and r_s is the scale radius, marking the transition between the steep inner profile and the flatter outer profile. The NFW profile predicts a steep central cusp, leading to the well-known *core-cusp* problem in simulations of CDM halos, where the central densities are too high compared to observations of galaxy dynamics, particularly in low-mass systems (Moore et al., 1999).

For comparison, FDM halos, with their soliton cores, avoid the cusp problem due to the smoothness of the core, which results from the quantum pressure. The soliton's density profile follows a shallower curve near the center, which is more consistent with the observed flatness of central galaxy rotation curves. In fact, the soliton core represents a viable solution to the over-concentration of dark matter in the center of galaxies that CDM models often fail to reproduce (Schive et al., 2014a,b).

Moreover, the size of the soliton core scales with the mass of the FDM particle $m_{\rm b}$, with larger mass FDM particles leading to smaller soliton cores (equation (7.31)) (Schive et al., 2014a). In contrast, the size of the central cusp in CDM halos is more strongly linked to halo mass, with the central density and size of the cusp being much more sensitive to cosmological parameters and halo formation histories (Navarro et al., 1997a; Mo et al., 2010).

The impact of these differences is most notable in the small-scale structure of the universe. While CDM halos tend to form dense, compact substructures (e.g., dwarf galaxies) with steep central profiles (Klypin et al., 2011), FDM halos predict a smoother, less clustered distribution of dark matter at small scales, potentially leading to fewer or different dark matter-dominated dwarf galaxies (Schive et al., 2014b; Hui et al., 2017).

The soliton cores in FDM models could also have implications for the central dynamics of galaxies. For example, the smaller central densities in FDM halos could lead to differences in the way baryons interact with dark matter. This may affect galaxy formation and evolution, particularly in terms of star formation rates and galaxy rotation curves (Hui et al., 2017; Schneider et al., 2020).

In summary, the soliton core of FDM halos represents a striking departure from the standard CDM scenario, offering a possible solution to the central density problem. The comparison highlights the important role of quantum pressure in shaping the structure of dark matter halos and provides a valuable observational test for distinguishing between FDM and CDM models in the study of galaxy dynamics and formation (Schive et al., 2014b; Klypin et al., 2011).

7.3.2 The Halo

Beyond the soliton core, the FDM density profile is expected to resemble that of CDM halos, although the structure differs in the outer regions due to the wave-like nature of the FDM field. While CDM halos are typically described by the Navarro–Frenk–White (NFW) profile (Navarro et al., 1997a), the FDM halo has a shallower outer profile, which is often modeled using a singular isothermal sphere (SIS) approximation. This model is characterized by the following density distribution

$$\rho_{\rm b}(r) = \frac{\sigma^2}{2\pi G r^2}, \tag{7.37}$$

This approach effectively captures the large-scale behavior of the FDM density, particularly in regions far from the soliton core, where quantum effects become less significant and the system behaves more classically.

To describe the mass enclosed within a radius r in these outer regions, we can define the effective mass as the mass contained within the radius r, given by (see equation (4.22))

$$m_{\text{eff}} = \frac{\pi^{3/2}\hbar^3 \rho_{\text{b}}}{m_{\text{b}}^3 \sigma^3} = \rho_{\text{b}} \left(f \lambda_\sigma \right)^3. \tag{7.38}$$

In theFDM field at radius $r \gg r_{\text{s}}$ is then given by (see equation (7.39))

$$m_{\text{eff}} = \frac{\pi^{1/2}\hbar^3}{2^{1/2} G m_{\text{b}}^3 v_{\text{c}} r^2} = 1.03 \times 10^7 M_\odot \left(\frac{r}{1\,\text{kpc}} \right)^{-2} \left(\frac{m_{\text{b}}}{10^{-22}\,\text{eV}} \right)^{-3} \left(\frac{v_{\text{c}}}{200\,\text{km s}^{-1}} \right)^{-1}, \tag{7.39}$$

Moreover, in the case of FDM, the velocity dispersion σ is typically related to the mass of the bosonic particle m_{b}, which influences the de Broglie wavelength associated with the dark matter. In the outer halo, this mass relationship governs the behavior of the system.

The typical de Broglie wavelength λ of a particle in the halo can be approximated as (see equation (7.40))

$$\lambda = \frac{h}{m_{\text{b}} v_{\text{c}}} = 0.85\,\text{kpc} \left(\frac{m_{\text{b}}}{10^{-22}\,\text{eV}} \right)^{-1} \left(\frac{v_{\text{c}}}{200\,\text{km s}^{-1}} \right)^{-1}. \tag{7.40}$$

This wavelength defines the scale of quantum effects and plays a role in determining the behavior of the FDM halo at small scales.

Compared to CDM halos, FDM halos exhibit a smoother transition from the central soliton core to the outer regions, with the SIS providing a reasonable approximation for the density distribution at larger radii. In figure 7.3, the density profile of a CDM and FDM halo are shown. For the FDM, the halo is considered to have a solitonic density profile for the center and an NFW for the outer regions. You can refer to Appendix A.1 for details of the plot.

This difference in structure has important implications for understanding small-scale structure formation, as the lower central densities and smoother outer profiles of FDM halos could affect galaxy dynamics and the distribution of dark matter on subgalactic scales (Schive et al., 2014a,b).

7.4 Inspiral of a Massive Object

It is crucial to understand the inspiraling behavior of a mass m_{t} initially in a circular orbit with a given radius. When the effective mass ratio μ_{eff} is significantly greater than one, the object will spiral inward toward the central soliton. The timescale for this inward motion, known as the inspiral timescale, depends on factors such as the object's mass, the radius of the orbit, and the central velocity dispersion of the galaxy. If the object's initial radius is sufficiently small, it will complete its spiral motion within the age of the galaxy.

However, as the object moves closer to the center, the effective mass of the central region increases, leading to a stalling effect at a certain radius. This stalling radius arises when the effective mass ratio μ_{eff} falls below unity. The interplay between the inspiral timescale, the stalling radius, and the initial orbital radius is crucial in understanding the behavior of objects within FDM halos. Additionally, correlations between the mass of the central black hole and the velocity dispersion of the galaxy provide further constraints on

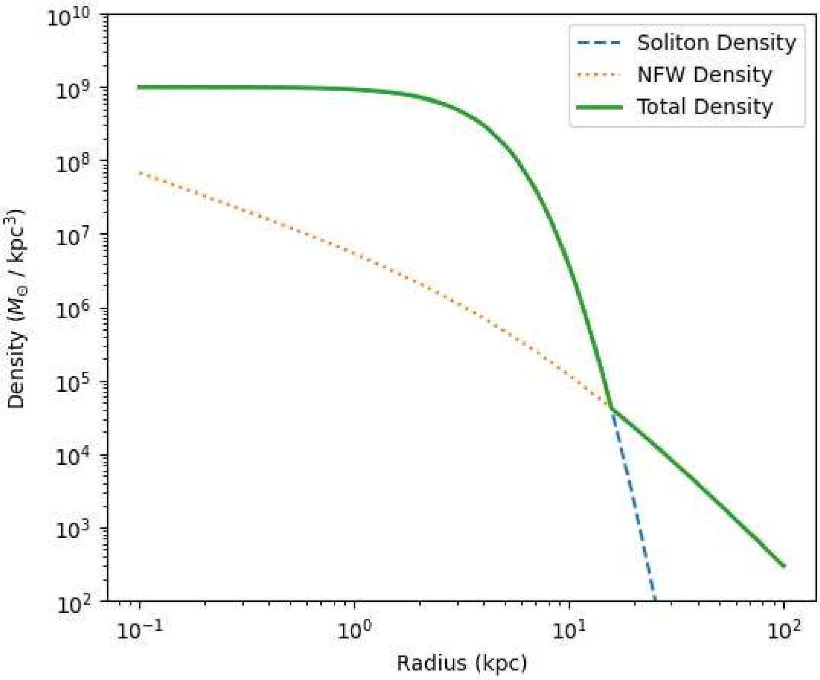

Figure 7.3: The comparison between the CDM (NFW Density) and the FDM (Total density) simulated density profiles corresponding to the following values that correspond to a Milky-Way-like galaxy: $r_s = 10, \rho_0 = 10^6, r_c = 1, \rho_c = 10^9$.

these dynamics, particularly for early-type galaxies, such as ellipticals and spiral bulges. This section delves into the details of these processes, exploring the conditions under which an object will spiral inward, the timescales involved, and the effects of the central mass distribution on its motion. Below, we study in detail this example as mentioned in Bar-Or et al. (2019).

The timescale for the inspiral of an object of mass $m_{\rm t}$ with an effective mass ratio $\mu_{\rm eff} \gg 1$ (equation (7.16)) toward the central soliton, which was originally on a circular orbit with radius $r_{\rm i}$ is given by (Binney and Tremaine, 2008)

$$\begin{aligned} t_{\rm inspiral} &= \frac{1.65\, r_{\rm i}^2 \sigma}{\log \Lambda_{\rm FDM} G m_{\rm t}} \\ &= \frac{84.9\,{\rm Gyr}}{\log \Lambda_{\rm FDM}} \frac{10^7 M_\odot}{m_{\rm t}} \frac{v_{\rm c}}{200\,{\rm km\ s^{-1}}} \left(\frac{r_{\rm i}}{4\,{\rm kpc}}\right)^2 . \end{aligned} \tag{7.41}$$

The object will complete its spiral toward the center within the age of the galaxy, $T_{\rm age}$, if the initial radius satisfies

$$r_{\rm i} < 2.08\,{\rm kpc} \left(\frac{\log \Lambda_{\rm FDM}}{\log 10} \frac{m_{\rm t}}{10^7 M_\odot} \frac{T_{\rm age}}{10\,{\rm Gyr}} \frac{200\,{\rm km\ s^{-1}}}{v_{\rm c}}\right)^{1/2} . \tag{7.42}$$

However, as the orbit shrinks, the effective mass of the central region grows according to the relation r^{-2} (equation 7.39), meaning that $\mu_{\rm eff} \propto r^2$. This results in a stalling radius where $\mu_{\rm eff}$ falls below unity, given by

$$r_{\rm stall} = (2\pi)^{1/4} \left(\frac{\hbar^3}{G m_{\rm t} m_{\rm b}^3 v_{\rm c}}\right)^{1/2} = 1.43\,{\rm kpc} \left(\frac{m_{\rm t}}{10^7 M_\odot}\right)^{-1/2} \left(\frac{m_{\rm b}}{10^{-22}\,{\rm eV}}\right)^{-3/2} \left(\frac{v_{\rm c}}{200\,{\rm km\ s^{-1}}}\right)^{-1/2} . \tag{7.43}$$

For early-type galaxies (ellipticals and spiral bulges), there exists a correlation between the mass of the central black hole $M_\bullet$ and the galaxy's velocity dispersion *sigma* (Kormendy and Bender, 2013), given by

$$\log_{10} \frac{M_\bullet}{10^9 M_\odot} = -0.51 \pm 0.05 + (4.4 \pm 0.3) \log_{10} \frac{\sigma}{200\,\mathrm{km\ s^{-1}}} \tag{7.44}$$

with a scatter of about 0.3 dex. Assuming that the circular speed and velocity dispersion are related by $\sigma = v_c/\sqrt{2}$, as in the isothermal sphere model, and that the inspiraling object's mass is $m_t = f M_\bullet$ with $f < 1$, these relations can be rewritten as

$$r_i < 3.1\,\mathrm{kpc} \left(\frac{f}{0.1} \frac{\log \Lambda_{\mathrm{FDM}}}{\log 10} \frac{T_{\mathrm{age}}}{10\,\mathrm{Gyr}} \right)^{1/2} \left(\frac{\sigma}{200\,\mathrm{km\ s^{-1}}} \right)^{1.7}; \tag{7.45}$$

$$r_{\mathrm{stall}} = 0.70\,\mathrm{kpc} \left(\frac{f}{0.1} \right)^{-1/2} \left(\frac{m_b}{10^{-22}\,\mathrm{eV}} \right)^{-3/2} \left(\frac{\sigma}{200\,\mathrm{km\ s^{-1}}} \right)^{-2.7}. \tag{7.46}$$

As we expected, the results suggest that the inspiral of supermassive black holes within FDM halos could halt at orbital radii on the order of several hundred parsecs, a scenario previously considered by Hui et al. (2017). While the physical mechanism behind this appears to be sound, two limitations arise from these calculations since according to equation (7.34) and (7.35), de Broglie wavelength just outside the soliton is of order the soliton radius (Bar-Or et al., 2019).

1. De Broglie Wavelength and Coulomb Logarithm: For the relevant parameters, the stalling radius r_{stall} may be comparable to or even smaller than the typical de Broglie wavelength λ_σ (equation 7.40). This implies that the maximum scale for which our classical approximations hold is $b_{\max} \simeq r_{\mathrm{stall}}$. In this case, the argument of the Coulomb logarithm becomes $\Lambda_{\mathrm{FDM}} = 2r_{\mathrm{stall}}/_\sigma$ (equation 4.21), which could be small enough to challenge the assumption that $\Lambda_{\mathrm{FDM}} \gg 1$.

   When the stalling radius r_{stall} approaches or is smaller than the de Broglie wavelength λ_σ, the classical treatment of interactions becomes questionable. Specifically, the Coulomb logarithm Λ_{FDM} decreases ($\Lambda_{\mathrm{FDM}} = 2r_{\mathrm{stall}}/_\sigma$) and may no longer be large enough to justify the use of the classical approximation. As a result, the assumption that $\Lambda_{\mathrm{FDM}} \gg 1$ may no longer hold, potentially invalidating some of the approximations employed in these calculations.

2. Soliton Core Radius and Heating Effects: The stalling radius, at which the object stops spiraling inward, is not much larger than the core radius of the central soliton, r_s (equation 7.31). Within the core of the soliton, heating from FDM fluctuations, which could otherwise influence the dynamics of the system, essentially vanishes.

   This occurs because the soliton's central region is in a stable ground-state configuration, where fluctuations in the fuzzy dark matter field are minimal and do not contribute to heating. Despite this, dynamical friction—a different mechanism influencing the object's motion—remains effective even within the soliton core. Additionally, although heating from FDM fluctuations may be absent in the ground state, simulations indicate that density oscillations could still inject energy into nearby objects, potentially affecting their dynamics.

In Figure 7.4, we show how energy diffusion from scattering by FDM quasiparticles disrupts the otherwise deterministic inspiral driven by dynamical friction. The orbit of a massive object ($m_\mathrm{t} = 4 \times 10^5 M_\odot$) in a singular isothermal sphere (equation 7.37) with a circular velocity of $v_\mathrm{c} = 200\,\mathrm{km\ s}^{-1}$ is followed, with random velocity changes applied using the diffusion coefficients (7.7)–(7.9) for $m_\mathrm{b} = 10^{-21}\,\mathrm{eV}$. This process was repeated 1000 times, and Figure 7.4 presents the median and 68% confidence band for the orbital radius over time. For comparison, we also show results based solely on dynamical friction (equation 4.42) for both FDM and CDM halos, differing only in the Coulomb logarithm. These results corroborate our expectation that a massive object undergoing inspiral due to dynamical friction will stall at a radius where $\mu_\mathrm{eff} \approx 1$.

In Figure 7.5, we illustrate the relationship between the maximum inspiral radius r_i (equation 7.42), the stalling radius r_stall (equation 7.43), and the typical de Broglie wavelength λ_σ (equation 7.40) for a galaxy with a circular velocity $v_\mathrm{c} = 200\,\mathrm{km\ s}^{-1}$, across a range of massive objects and FDM particle masses.

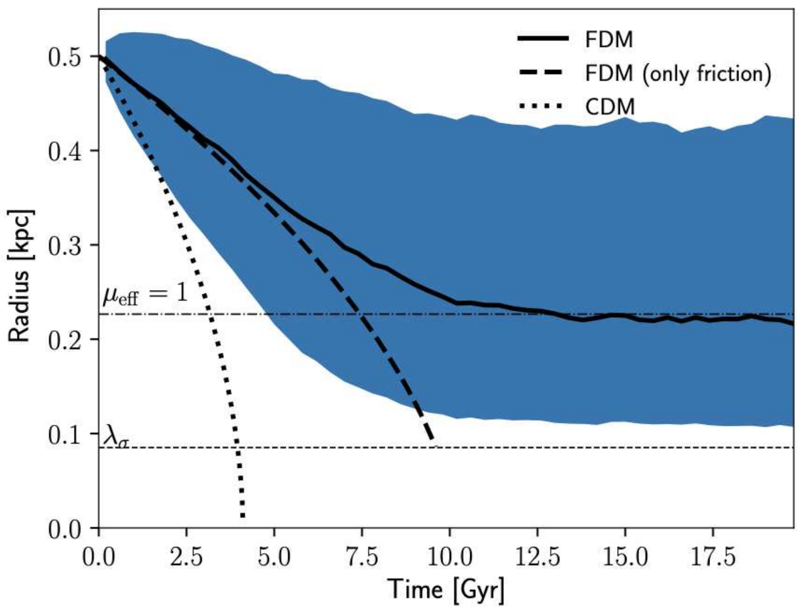

Figure 7.4: Figure adapted from Bar-Or et al. (2019). The inspiral of a massive object ($m_\mathrm{t} = 4 \times 10^5 M_\odot$) on a circular orbit in a spherical galaxy with constant circular speed $v_\mathrm{c} = 200\,\mathrm{km\ s}^{-1}$ (equation (7.37)). The dotted line shows the evolution of the orbital radius due to dynamical friction if the galaxy is composed of CDM (equation (7.11) with $\mu_\mathrm{cl} \gg 1$). The dashed line shows the evolution due to dynamical friction if the galaxy is composed of FDM (equation (4.42)) and diffusion terms are ignored. This differs from the CDM case only through the Coulomb logarithm. The solid line and shaded region show the evolution in an FDM galaxy including both dynamical friction and diffusion, assuming an FDM mass $m_\mathrm{b} = 10^{-21}\,\mathrm{eV}$. We have carried out 1000 realizations of the orbital evolution, and the solid line and shaded region show the median and central 68% region. The median radius saturates close to where $\mu_\mathrm{eff} = 1$ (dashed-dotted horizontal line). This behavior is different from the case where diffusion is ignored (dashed line), for which dynamical friction causes the orbit to decay at least down to the de Broglie wavelength λ_σ (dashed horizontal line).

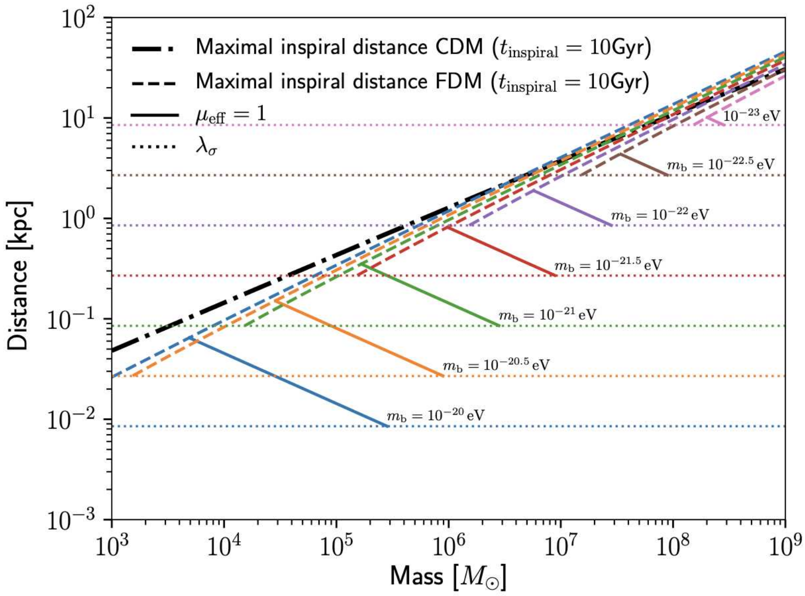

Figure 7.5: Figure adapted from Bar-Or et al. (2019). A massive object initially on a circular orbit will spiral to the center within 10 Gyr if it lies below the dashed lines (equation (7.42)). Different colors represent different assumptions about the mass of the FDM particle, and the heavy dashed-dotted black line shows the same curve for CDM. The solid lines show the radius $r_{\rm stall}$ (equation (7.43)) where stochastic potential fluctuations cause the inspiral to stall. The solid lines terminate when the stalling radius is smaller than the typical de Broglie wavelength λ_σ (dotted lines); at smaller distances, the evolution is dominated by interactions with the soliton, which exerts dynamical friction but has no potential fluctuations. We assume that the density of the FDM is that of a singular isothermal sphere (equation (7.37)) with circular speed $v_{\rm c} = 200\,{\rm km\ s}^{-1}$.

7.5 Heating of a Spherical Stellar Population

We examine the impact of Fuzzy Dark Matter fluctuations on a stellar system with a Maxwellian distribution function and velocity dispersion $\sigma_{\rm t}$. The gravitational potential is assumed to be dominated by FDM, with the typical radius of the stellar system given by $r_\star$. Since the effective mass $m_{\rm eff}$ of FDM is much larger than the mass of any individual star, dynamical friction and cooling are negligible. The heating timescale is described by the following equation

$$T_{\rm heat} = \frac{3 m_{\rm b}^3 v_{\rm c}^2 r_\star^4}{8\hbar^3 \log \Lambda_{\rm FDM}}, \tag{7.47}$$

which can be approximated as

$$T_{\rm heat} \approx \frac{2.08\,{\rm Gyr}}{\log \Lambda_{\rm FDM}} \left(\frac{r_\star}{1\,{\rm kpc}}\right)^4 \left(\frac{m_{\rm b}}{10^{-22}\,{\rm eV}}\right)^3 \left(\frac{v_{\rm c}}{200\,{\rm km\ s}^{-1}}\right)^2. \tag{7.48}$$

Heating is significant when $T_{\rm heat}$ is less than a third of the age of the galaxy, $T_{\rm age}$. This condition is satisfied when the stellar system's radius is smaller than the heating radius $r_{\rm heat}$

$$r_{\rm heat} = 1.13\,{\rm kpc} \left(\log \Lambda_{\rm FDM} \frac{T_{\rm age}}{10\,{\rm Gyr}}\right)^{1/4} \left(\frac{v_{\rm c}}{200\,{\rm km\ s}^{-1}}\right)^{-1/2} \left(\frac{m_{\rm b}}{10^{-22}\,{\rm eV}}\right)^{-3/4}. \tag{7.49}$$

These approximations are valid when the orbital radius is much larger than the de Broglie wavelength. Setting $r_\star = \lambda_\sigma$, the minimum heating time is

$$T_{\rm heat}^{\rm min} = \frac{24\pi^4\hbar}{m_{\rm b} v_{\rm c}^2 \log\Lambda_{\rm FDM}} \approx 0.43\,{\rm Gyr}\left(\frac{m_{\rm b}}{10^{-22}\,{\rm eV}}\right)^{-1}\left(\frac{v_{\rm c}}{200\,{\rm km\ s^{-1}}}\right)^{-2}. \tag{7.50}$$

Here, the Coulomb logarithm $\log\Lambda_{\rm FDM}$ is evaluated at $b_{\rm max} = \lambda_\sigma$, so $\log\Lambda_{\rm FDM} = \log\frac{2b_{\rm max}}{\sigma} = \log(4\pi) \approx 2.5$.

It is important to note that the term heating is somewhat misleading, as the interaction with FDM fluctuations adds energy to the stellar population, causing it to expand. The velocity dispersion of the stars may either increase or decrease, depending on the galaxy's radial gravitational potential. To illustrate this process, we followed the evolution of test particles representing stars in an isothermal density distribution (equation (7.37)), where the potential was modified to $\Phi(r) = \frac{1}{2}v_{\rm c}^2\log(r^2 + r_0^2)$. This modification ensures the integral over the radial distribution remains convergent for $\sigma_{\rm t}^2 \leq 3v_{\rm c}^2$. The value of r_0 is set to $0.2\lambda_\sigma$, and the diffusion coefficients were disabled for $r < \lambda_\sigma$. We used the diffusion coefficients from equations (7.7)–(7.9) (Bar-Or et al., 2019).

In Figure 7.6, we show the evolution of an FDM halo with $v_{\rm c} = 200\,{\rm km\ s^{-1}}$ and $m_{\rm b} = 10^{-21}\,{\rm eV}$. This figure displays the expansion (upper panels) and heating (lower panels) of a system of 5600 test particles with initial velocity dispersions $\sigma_{\rm t} = v_{\rm c}/2$ (left panels) and $\sigma_{\rm t} = v_{\rm c}/\sqrt{2}$ (right panels). In both cases, within a few Gyr, the velocity dispersion of the test particles exceeds that of the FDM (dashed horizontal lines), and the stellar density develops a core in the region outside the de Broglie wavelength and inside the radius where $T_{\rm heat}$ equals the age (shaded regions). Our assumption that fluctuations in the FDM density have no effect inside the de Broglie wavelength λ_σ is an oversimplification, so the sharp changes in density and dispersion at λ_σ are unrealistic (Bar-Or et al., 2019).

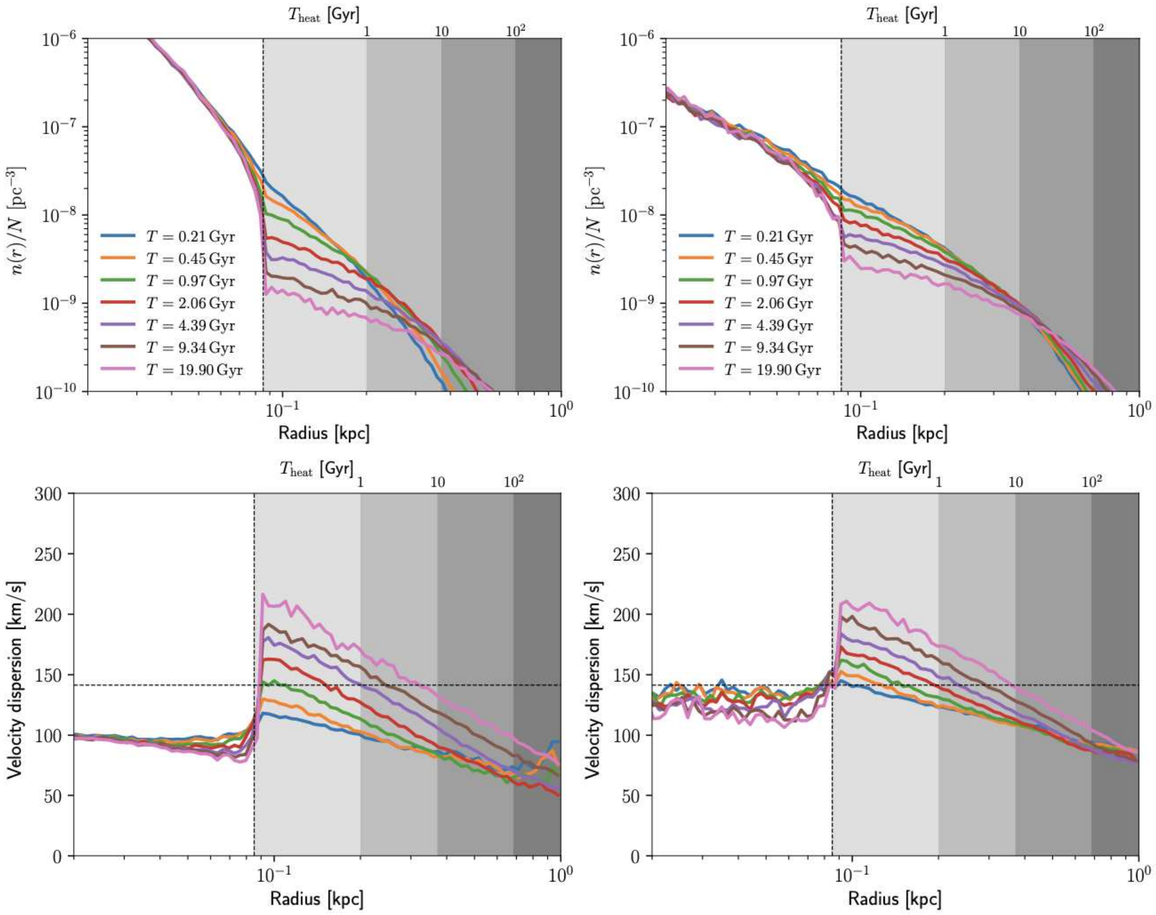

Figure 7.6: The expansion of a system of test particles in an isothermal FDM halo with particle mass $m_{\rm b} = 10^{-21}\,$eV and circular speed $v_{\rm c} = 200\,$km s^{-1}. The velocity dispersion $\sigma = v_{\rm c}/\sqrt{2} \simeq 141\,$km s^{-1} (dashed horizontal lines). The test-particle distribution is initially isothermal with velocity dispersion $\sigma_{\rm t} = v_{\rm c}/2 = 100\,$km s^{-1} (left panels) and $v_{\rm c}/\sqrt{2} \approx 141\,$km s^{-1} (right panels). In the region outside the de Broglie wavelength λ_σ (dashed vertical lines), where the heating time is less than the age (top axis and shaded regions), the number density decreases (upper panels) and the velocity dispersion increases (bottom panels) as a function of time. Figure adapted from Bar-Or et al. (2019)

8 Conclusions

FDM presents a compelling alternative to cold dark matter, offering potential solutions to several discrepancies between CDM predictions and observed galactic structures on scales smaller than approximately 30 kpc. Unlike CDM, which struggles to fully explain certain small-scale features, FDM introduces a unique set of physical phenomena driven by its wave-like nature. One striking distinction lies in the evolution of density fluctuations within an isolated halo. In the case of CDM, density and gravitational potential fluctuations gradually dissipate over time as sub-halos are disrupted and tidal streams undergo phase mixing. In contrast, an isolated FDM halo exhibits persistent and dynamic density fluctuations, a consequence of the finite number of eigenstates that contribute to its structure. These ongoing oscillations introduce a fundamentally different dynamical behavior compared to the more dissipative evolution seen in CDM.

A test particle traversing the fluctuating gravitational potential of an FDM halo undergoes stochastic variations in velocity, leading to diffusive orbital evolution. To characterize this process, we computed the diffusion coefficients that govern its motion. For a Maxwellian velocity distribution with dispersion σ, these coefficients are analogous to those in a classical N-body system, provided that the following modifications are applied,

(i) The classical system is reinterpreted as being composed of quasiparticles with an effective mass m_{eff} that depends on the local density, as defined in equation (4.22).

(ii) The velocity dispersion of these quasiparticles is adjusted to $\sigma/2$, reflecting the inherent differences between particle-based and wave-based descriptions.

(iii) The lower bound of the scale range in the Coulomb logarithm, which in classical systems is typically set by b_{90} (the impact parameter for a 90° deflection), is instead replaced by $\lambda\sigma/2$, where λ is the typical de Broglie wavelength associated with the FDM.

A similar modification applies to the dynamical friction force experienced by a massive particle orbiting within an FDM halo. While the force retains its classical form, the Coulomb logarithm is adjusted according to the last criterion, incorporating the wave-like properties of FDM into the dynamical evolution.

In this thesis, we assumed that the mean gravitational potential is infinite and homogeneous. In the classical case, this assumption implies that unperturbed particles move along straight-line trajectories with constant velocity. In contrast, within an FDM halo, it implies that the unperturbed wave function consists of a superposition of plane waves with constant wavenumber and frequency.

This is a standard simplification that remains reasonably accurate when the Coulomb logarithm is much greater than unity, which typically occurs when the radial scale is significantly larger than the characteristic de Broglie wavelength. However, the impact of FDM-induced scattering on stellar systems is generally most pronounced at radii comparable to the wavelength. In such cases, our current derivation is incomplete, necessitating further numerical and theoretical investigations.

Further in this work, we investigated the self-consistent relaxation of an FDM halo driven by the unavoidable and undamped quantum fluctuations it must sustain including the dynamical friction. The primary result was presented in equation (4.50), which represents the appropriate generalization of the classical Fokker-Planck (FP) equation to the quantum regime. Subsequently, we demonstrated how this kinetic equation can be derived either from the heuristic Boltzmann-Nordheim-Uehling-Uhlenbeck (BNUU) equation or from the quasi-linear perturbation of the Schrödinger-Poisson (SP) system. In particular, we showed that diffusion can be enhanced by collective effects, which modify the perturbations. The strength of these collective effects is encapsulated in the dielectric function equation (5.49), as illustrated in equation (5.94) through a Balescu–Lenard (BL) type kinetic equation.

In Chapter 6, we analyzed the linear stability of a homogeneous FDM halo, clarifying the connection between the classical and quantum limits.

We demonstrated that a massive object undergoing inspiral due to dynamical friction experiences stochastic velocity fluctuations once it reaches a radius where its mass is comparable to the effective mass of the FDM quasiparticles. At this point, energy injection from FDM fluctuations occurs at a rate comparable to the energy dissipation from dynamical friction, leading to a tendency for the inspiral to stall.

Stars, being significantly lighter than the FDM quasiparticles, will, on average, gain energy from FDM-induced fluctuations in regions where the relaxation time is much shorter than the age of the galaxy. As a result, stellar systems on scales ranging from a few hundred parsecs to a few kiloparsecs will tend to expand, with the heating time within the system being comparable to its lifetime. Consequently, one should not expect to observe stellar systems in which the heating time is significantly shorter than the age of the galaxy.

At present, neither of these physical processes provides a robust new constraint on the allowed mass range of FDM particles. Other effects of relaxation due to FDM have been discussed by Hui et al. (2017).

We have focused exclusively on the impact of FDM fluctuations on the orbits of classical objects such as stars and black holes. However, FDM fluctuations also influence the structure and evolution of the FDM halo itself. Analyzing these effects requires different approaches, as explored in previous studies (e.g., (Levkov et al., 2018; Mocz et al., 2018).

Naturally, this work represents only a first step toward a comprehensive description of FDM halo evolution. A crucial next step is to extend the present derivation to inhomogeneous FDM halos. As long as the typical de Broglie wavelength λ_σ remains small compared to the halo size, a reasonable first approximation would be to treat the FDM diffusion coefficients (equation (4.65) and (4.66) as local diffusion coefficients within an inhomogeneous FP equation analogous to equation (4.53). For more precise analyses, recent advances in the study of classical self-gravitating systems-such as the derivation of the inhomogeneous BL equation (Chavanis, 2013)-would be particularly valuable.

FDM halos with sufficiently low velocity dispersion—including all galactic velocity dispersions if the particle mass $m_b \ll 1\,\mathrm{eV}$—inevitably relax into a Bose-Einstein condensate. Understanding the formation and growth of this condensate is essential for determining the long-term fate of FDM halos.

Finally, if FDM is to be considered a viable alternative to classical CDM, the kinetic theory presented here must be further developed in a cosmological context (see, e.g., Amin and Mocz (2019)).

A Appendix

A.1 A Numerical Simulation

Numerical simulations provide a valuable tool for studying the evolution of dark matter halos, allowing us to test theoretical predictions and explore dynamical effects that are difficult to capture analytically.

This chapter describes the numerical methods used to simulate the evolution of CDM and FDM halos. The simulation involves initializing particle distributions, assigning velocities, and computing density grids. The numerical implementation is performed in Python. To observe the behavior of FDM arising from it wave nature, we specifically assumed an additional kind of dark matter with initial conditions similar to FDM but without quantum effect, particularly quantum pressure allowing for a direct comparison between the two scenarios.

A.1.1 Particle Distribution Initialization

In simulating the dynamics of dark matter halos, the initial distribution of particles plays a crucial role in shaping the evolution of the system. For this, the following density profiles are considered: the Navarro-Frenk-White (NFW) and the soliton density profile. Each profile represents a different assumption about the structure and distribution of matter within the halo.

The NFW profile is described as

$$\rho(r) = \frac{\rho_0}{\left(\frac{r}{r_s}\right)\left(1 + \frac{r}{r_s}\right)^2} \tag{A.1}$$

where r is the radial distance from the center of the halo, ρ_0 is the characteristic density, and r_s is the scale radius, which marks the transition between the inner and outer regions of the halo. The NFW profile is characterized by a steep inner cusp and a flatter outer profile, making it well-suited for modeling large dark matter halos in cosmological simulations.

The NFW profile leads to a concentration of dark matter near the center of the halo, with the density falling off as r^{-3} at large radii. This behavior reflects the hierarchical structure formation in the universe, where small halos merge to form larger structures.

For the density profile of the FDM halo, we specifically combine two different functional forms that describe different regions of the halo: the soliton core and the NFW profile. The total density profile is a hybrid of these two profiles, representing the core and outer regions of the halo.

The soliton core density profile is given by

$$\rho_{\text{soliton}}(r) = \frac{\rho_c}{\left(1 + 0.091\left(\frac{r}{r_c}\right)^2\right)^8} \tag{A.2}$$

where ρ_c is the central density of the soliton core and r_c is the core radius, which determines the scale at which the soliton profile begins to flatten.

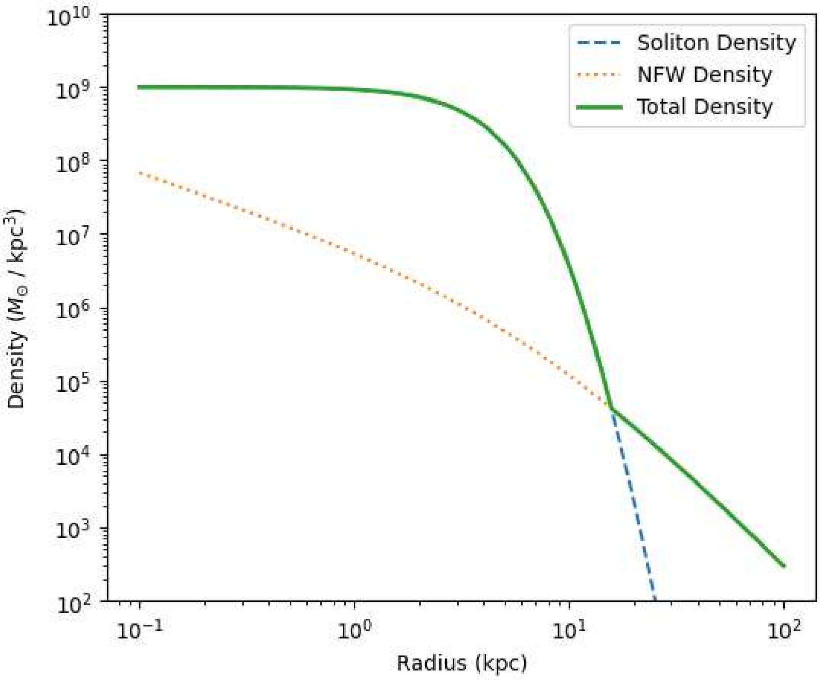

Figure A.1: The comparison between the CDM (NFW Density) and the FDM (Total density) simulated density profiles corresponding to the following values: $r_s = 10, \rho_0 = 10^6, r_c = 1, \rho_c = 10^9$.

This profile represents the smooth, central region of a FDM halo, where the quantum effects of the dark matter cause it to behave like a wave, leading to a smooth density distribution in the inner regions. The soliton profile decreases as r increases, but it flattens out significantly in the core due to the quantum pressure associated with FDM.

The total density profile for FDM is a combination of the soliton and NFW profiles, with the core dominated by the soliton profile and the outer regions dominated by the NFW profile. The total density is given by (Yavetz et al., 2022; Kawai and Meneghetti, 2024)

$$\rho_{\text{total}}(r) = \begin{cases} \rho_{\text{soliton}}(r) & \text{if } r < \frac{r_c}{2} \\ \max(\rho_{\text{soliton}}(r), \rho_{\text{NFW}}(r)) & \text{if } r \geq \frac{r_c}{2} \end{cases} \tag{A.3}$$

The condition $r < \frac{r_c}{2}$ ensures that the soliton profile dominates in the inner core, while for $r \geq \frac{r_c}{2}$, the profile takes the maximum of the soliton and NFW densities, ensuring a smooth transition from the quantum-dominated core to the NFW outer halo.

This hybrid profile represents the structure of a halo that has a soliton core in the center (as expected in FDM models) and an NFW outer region (as expected in CDM models), allowing the model to capture both the quantum and classical aspects of dark matter halos.

In figure A.1, we show the resultant density profiles comparison for CDM and FDM halos

The next step is to generate a spatial distribution of particles following the mentioned density profiles. The particles are transformed into 2D Cartesian coordinates to simulate the density distribution in a halo structure.

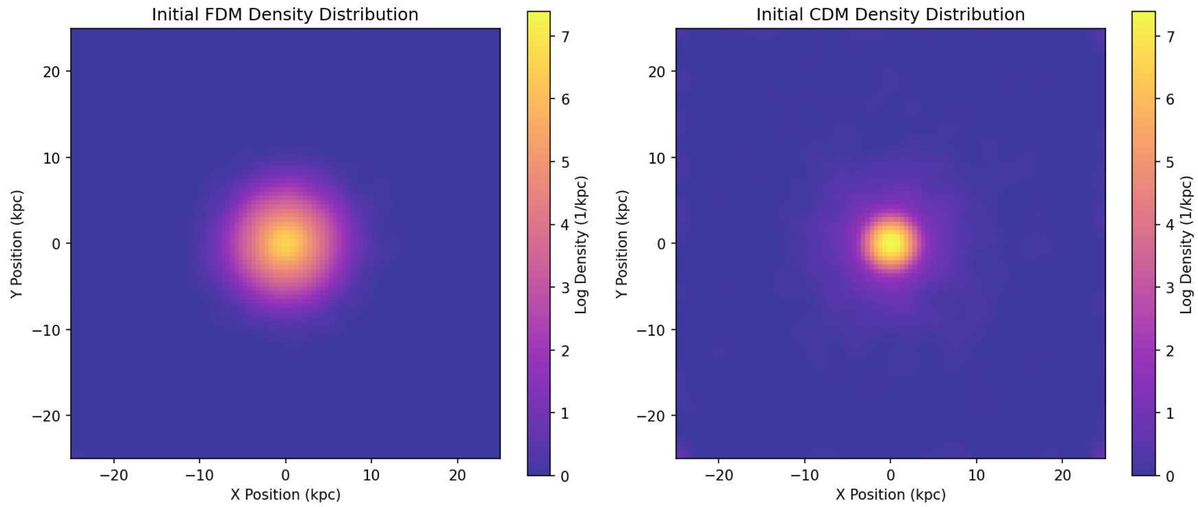

Figure A.2: The initial density grid of FDM and CDM halo

A.1.2 Density Grid Initialization

We use euqations A.1 and A.2 as the distribution functions to generate the position for N samples. Then we create density grids to visulaize both halos. The extracted 2D density slice is displayed using a colormap representation in figure A.2 where the density values are mapped to a color scale. The color intensity in the plot reflects the density amplitude, with a colorbar indicating the density scale. The axes are labeled according to the spatial extent of the simulation domain, ranging from $-L/2$ to $L/2$.

This visualization provides an intuitive representation of the FDM halo structure, allowing for the analysis of wave-like interference patterns and density fluctuations over time.

FDM density distribution is characterized by a larger, smoother core compared to CDM. This is due to the wave-like nature of FDM, which is modeled as an ultra-light boson. The wave-like behavior leads to interference patterns and a smooth central core, known as a soliton, which resists gravitational collapse. The quantum pressure, governed by the Heisenberg uncertainty principle, imposes a minimum length scale on the density distribution, resulting in a larger core. Additionally, outside the core, density decreases gradually, with possible interference fringes.

The core of an FDM halo, which scales with the de Broglie wavelength, is surrounded by a more diffuse envelope resembling the structure of a CDM halo at large radii. The core size depends on the particle mass and velocity, with ultra-light FDM leading to kpc-scale cores.

In contrast, CDM exhibits a denser and more concentrated core due to its collisionless and classical behavior. CDM consists of massive, non-relativistic particles that collapse under gravity into more compact structures, resulting in a sharp, dense central cusp. This is predicted by the NFW profile, where density increases sharply near the center and declines at large radii. Without quantum pressure, CDM particles can collapse into very tight orbits, forming steep central peaks.

The key physical mechanisms in FDM include gravitational relaxation and the absence of quantum support, whereas in CDM, gravitational collapse and hierarchical structure formation lead to a cuspy density profile. These differences arise from the fundamental nature of the two types of dark matter: FDM responds to gravity as a wave, while CDM behaves as a particle.

The observable consequences in astrophysics include the core-cusp problem, where FDM explains the cored profiles observed in dwarf galaxies, while CDM predicts cusps, which contradict some observations. FDM also suppresses structure formation below a characteristic scale, resulting in fewer low-mass halos. The interference patterns in FDM halos may impact weak lensing or stellar streams.

A.2 Quantum Potential Calculation

Coles and Spencer (2002) used Madelung (1926) transformation to obtain the Schrodinger equation from continuity (A.4) and Euler (A.5) equations below for a flow with an irrotational velocity field i.e. $v \equiv \nabla\Phi$.

$$\frac{\partial \rho}{\partial t} + \nabla \cdot (\rho \nabla \cdot \mathbf{v}) = 0 \tag{A.4}$$

$$\frac{\partial \mathbf{v}}{\partial t} + (\mathbf{v} \cdot \nabla)\mathbf{v} + \frac{1}{m}\nabla P + \nabla \Phi = 0 \tag{A.5}$$

where Φ is the gravitational potential that satisfies the Poisson equation (**??**) and P representing the pressure. Furthermore, equation (A.5) for a self-gravitating pressureless fluid in a static Universe can be integrated to obtain the Bernoulli equation

$$\frac{\partial \Phi}{\partial t} + \frac{1}{2}(\nabla \Phi)^2 = -V \tag{A.6}$$

Now we implement the Madelung transformation by moving to the following fields

$$\psi = \sqrt{\rho}\, e^{i\varphi/\hbar} \tag{A.7}$$

$$\rho = |\psi|^2 \tag{A.8}$$

Then taking the time derivative from A.7 we arrive at

$$\frac{\partial \psi}{\partial t} = \left[\frac{\partial \sqrt{\rho}}{\partial t} + \frac{i}{\hbar}\sqrt{\rho}\frac{\partial \varphi}{\partial t}\right] e^{i\varphi/\hbar} \tag{A.9}$$

We now proceed to evaluate the spatial derivatives.

$$\nabla \psi = \left(\nabla\sqrt{\rho} + i\frac{\sqrt{\rho}}{\hbar}\nabla\varphi\right) e^{2\varphi/\hbar}$$

$$\nabla^2 \psi = \left(\nabla^2\sqrt{\rho} - \frac{\sqrt{\rho}}{\hbar^2}(\nabla\varphi)^2 + \frac{i}{\hbar}\left[\sqrt{\rho}\nabla^2\varphi + 2\nabla\sqrt{\rho}\cdot\nabla\varphi\right]\right) e^{i\varphi/\hbar} \tag{A.10}$$

The term inside the square brackets can be obtained from the continuity equation (A.4)

$$\frac{\partial \rho}{\partial t} + \nabla \cdot (\rho \nabla \varphi) = 0$$

$$2\sqrt{\rho}\frac{\partial \sqrt{\rho}}{\partial t} + 2\sqrt{\rho}\nabla\sqrt{\rho}\nabla\varphi + \rho\nabla^2\varphi = 0$$

$$2\sqrt{\rho}\frac{\partial \sqrt{\rho}}{\partial t} = -\left[\sqrt{\rho}\nabla^2\Phi + 2\nabla\sqrt{\rho}\cdot\nabla\Phi\right] \tag{A.11}$$

Substituting A.11 into A.10 we get

$$\nabla^2\psi = \left(\nabla^2\sqrt{\rho} - \frac{\sqrt{\rho}}{\hbar^2}(\nabla\varphi)^2 - \frac{i}{\hbar}2\sqrt{\rho}\frac{\partial\sqrt{\rho}}{\partial t}\right)e^{i\varphi/\hbar} \tag{A.12}$$

By restructuring the equation slightly and simplifying the exponential term from both sides, we arrive at

$$\nabla^2\psi = \left(-\frac{\hbar^2}{\sqrt{\rho}}\nabla^2\psi e^{-i\varphi/\hbar} + \frac{\hbar^2}{\sqrt{\rho}}(\nabla\sqrt{\rho})^2 - \frac{2i\hbar}{\sqrt{\rho}}\frac{\partial\sqrt{\rho}}{\partial t}\right) \tag{A.13}$$

We can now insert the temporal and spatial derivatives, in the LHS of the Bernoulli equation (A.6) and deduce the following

$$-\frac{\hbar^2}{2\sqrt{\rho}}e^{-i\varphi/\hbar}\nabla^2\psi + \frac{\hbar^2}{2\sqrt{\rho}}\nabla^2\sqrt{\rho} - \frac{i\hbar}{\sqrt{\rho}}e^{-i\varphi/\hbar}\frac{\partial\psi}{\partial t} = -\Phi \tag{A.14}$$

By implementing a minor reorganization, we yield

$$i\hbar\frac{\partial\psi}{\partial t} = -\frac{\hbar^2}{2}\nabla^2\psi + \left(\Phi + \frac{\hbar^2}{2}\frac{\nabla^2\sqrt{\rho}}{\sqrt{\rho}}\right)\psi \tag{A.15}$$

This results looks like the Schrodinger equation except for the term $\frac{\nabla^2\sqrt{\rho}}{\sqrt{\rho}}$ called *quantum potential* (Bohm, 1952; Chavanis, 2011) which appears when one attempts to describe a quantum phenomenon with the use of classical fluid physics. This term was approximated to be zero by previous authors (Widrow and Kaiser, 1993). Having started from the original Schrodinger equation (without the quantum pressure) and followed the above steps in a reverse order, This term would resemble pressure gradient in the Bernoulli equation.

A.3 Geometry of an Encounter

Suppose that in a particular encounter the subject and field stars with masses m and m_a have velocities $\mathbf{v}$ and $\mathbf{v_a}$ respectively. The relative velocity is $\mathbf{V} = \mathbf{v} - \mathbf{v_a}$. Its initial value is V_0 and the change in velocity caused by the encounter is $\Delta\mathbf{V}$. The change in velocity of the subject star $\Delta\mathbf{v}$ is given by

$$\Delta\mathbf{v} = \frac{m_a}{m + m_a}\Delta\mathbf{V}. \tag{A.16}$$

We introduce a coordinate system $\hat{\mathbf{e}}'_1, \hat{\mathbf{e}}'_2, \hat{\mathbf{e}}'_3$, such that $\hat{\mathbf{e}}'_1$ is parallel to $\mathbf{V_0}$ (see figureA.3). Thus

$$\mathbf{V_0}\cdot\hat{\mathbf{e}}'_1 = |\mathbf{V_0}| \equiv V_0 \quad ; \quad \mathbf{V_0}\cdot\hat{\mathbf{e}}'_2 = \mathbf{V_0}\cdot\hat{\mathbf{e}}'_3 = 0. \tag{A.17}$$

We denote the angle between the plane of the relative orbit and $\hat{\mathbf{e}}'_2$ by ϕ. The change in $\mathbf{v}$ during the encounter may be written

$$\Delta\mathbf{v} = -\Delta v_\parallel\hat{\mathbf{e}}'_1 + \Delta v_\perp\left(-\hat{\mathbf{e}}'_2\cos\phi + \hat{\mathbf{e}}'_3\sin\phi\right), \tag{A.18}$$

where $\Delta v_\parallel$ and $\Delta v_\perp$ are the magnitudes of the components of $\Delta\mathbf{v}$ that are parallel and perpendicular to $\mathbf{V_0}$. The signs are chosen to ensure that $\Delta v_\parallel$ and $\Delta v_\perp$ are positive if the interaction between the two particles is attractive.

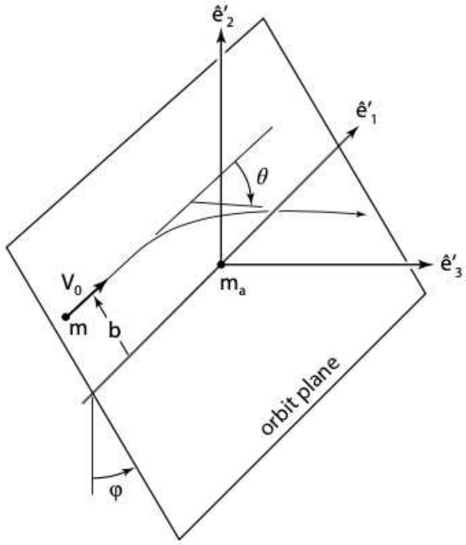

Figure A.3: Geometry of an encounter. The angle θ is the deflection angle

Using the identity $\Delta\mathbf{v} = \sum_{k=1}^{3}(\Delta\mathbf{v}\cdot\hat{\mathbf{e}}'_k)\hat{\mathbf{e}}'_k$ we have

$$\Delta v_i = \sum_{k=1}^{3}(\Delta\mathbf{v}\cdot\hat{\mathbf{e}}'_k)(\hat{\mathbf{e}}_i\cdot\hat{\mathbf{e}}'_k), \tag{A.19}$$

$$\Delta v_i \Delta v_j = \sum_{k,l=1}^{3}(\Delta\mathbf{v}\cdot\hat{\mathbf{e}}'_k)(\Delta\mathbf{v}\cdot\hat{\mathbf{e}}'_l)(\hat{\mathbf{e}}_i\cdot\hat{\mathbf{e}}'_k)(\hat{\mathbf{e}}_j\cdot\hat{\mathbf{e}}'_l). \tag{A.20}$$

A.4 Calculation of the Diffusion Coefficients for a Maxwellian Distribution

the diffusion coefficients $D[\Delta v_i]$ and $D[\Delta v_i \Delta v_j]$ quantify the average changes in velocity components of a subject star due to local encounters with field stars. These encounters are assumed to involve independent, two-body interactions. The gravitational potential of the overall system is neglected, allowing for a local approximation where the relative motion is hyperbolic, dictated by initial velocity V_0 and impact parameter b. First of all, let's begin by averaging equation (A.19) and (A.20).

$$\Delta v_i = \sum_{k=1}^{3}(\Delta\mathbf{v}\cdot\hat{\mathbf{e}}'_k)(\hat{\mathbf{e}}_i\cdot\hat{\mathbf{e}}'_k), \tag{A.21}$$

$$\Delta v_i \Delta v_j = \sum_{k,l=1}^{3}(\Delta\mathbf{v}\cdot\hat{\mathbf{e}}'_k)(\Delta\mathbf{v}\cdot\hat{\mathbf{e}}'_l)(\hat{\mathbf{e}}_i\cdot\hat{\mathbf{e}}'_k)(\hat{\mathbf{e}}_j\cdot\hat{\mathbf{e}}'_l). \tag{A.22}$$

Since all angles $0 \leq \phi \leq 2\pi$ are equally probable, and $\Delta v_{\|}$ and $\Delta v_{\perp}$ do not depend on ϕ, we can take averages of the above equations over ϕ using the fact that$\langle\cos^2\phi\rangle =$

$\langle \sin^2 \phi \rangle = \frac{1}{2}$.

$$\begin{aligned}\langle \Delta v_i \rangle &= -\Delta v_\parallel (\hat{\mathbf{e}}_i \cdot \hat{\mathbf{e}}_1), \\ \langle \Delta v_i \Delta v_j \rangle &= (\Delta v_\parallel)^2 (\hat{\mathbf{e}}_i \cdot \hat{\mathbf{e}}_1)(\hat{\mathbf{e}}_j \cdot \hat{\mathbf{e}}_1) \\ &\quad + \frac{1}{2}(\Delta v_\perp)^2 \left((\hat{\mathbf{e}}_i \cdot \hat{\mathbf{e}}_2)(\hat{\mathbf{e}}_j \cdot \hat{\mathbf{e}}_2) - (\hat{\mathbf{e}}_i \cdot \hat{\mathbf{e}}_3)(\hat{\mathbf{e}}_j \cdot \hat{\mathbf{e}}_3)\right),\end{aligned} \tag{A.23}$$

where

$$\Delta v_\perp = \frac{2 m_a v_0}{m + m_a} \frac{b/b_{90}}{1 + b^2/b_{90}^2}, \tag{A.24}$$

$$\Delta v_\parallel = \frac{2 m_a v_0}{m + m_a} \frac{1}{1 + b^2/b_{90}^2}. \tag{A.25}$$

To derive these, we are going to consider a hyperbolic encounter between m and m_a as the masses of the subject star and field stars, respectively. The deflection angle of the encounter, $\theta_{\rm defl}$ which is given by

$$\theta_{\rm defl} = 2 \tan^{-1}\left(\frac{G(M+m)}{bV_0^2}\right) = 2 \tan^{-1}\left(\frac{b_{90}}{b}\right). \tag{A.26}$$

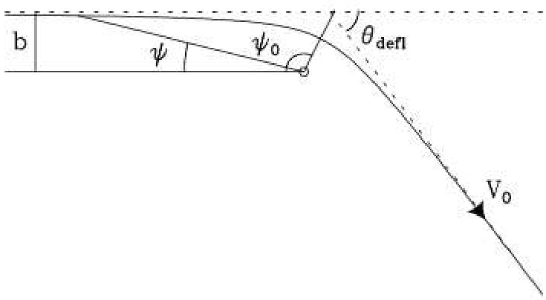

Figure A.4: The motion of the reduced particle during a hyperbolic encounter(Binney and Tremaine, 2008).

By conservation of energy, the relative speed after the encounter equals the initial speed V_0. Hence, the components $\Delta V_\parallel$ and $\Delta V_\perp$ of $\Delta \vec{V}$ parallel and perpendicular to the original relative velocity vector $\vec{V}_0$ are given by

$$|\Delta V_\perp| = V_0 \sin \theta_{\rm defl} = V_0 |\sin 2\psi_0| = \frac{2V_0 |\tan \psi_0|}{1 + \tan^2 \psi_0} = \frac{2V_0 (b/b_{90})}{1 + b^2/b_{90}^2}, \tag{A.27}$$

$$|\Delta V_\parallel| = V_0 (1 - \cos \theta_{\rm defl}) = V_0 (1 + \cos 2\psi_0) = \frac{2V_0}{1 + \tan^2 \psi_0} = \frac{2V_0}{1 + b^2/b_{90}^2}. \tag{A.28}$$

where b is the impact parameter and $b_{90} = G(m + m_a)/v_0^2$ is for the 90 deflection radius. Also ψ_0 is given by $-bV_0^2/G(m + m_a)$ and is achieved by writing the equation for a Keplerian orbit and computing the angular momentum. To obtain A.24 and A.25 we simply multiply the above results by $m_a/(m_a + m)$.

We now sum the effects of all the encounters. The number density of field stars in the velocity-space volume $d^3 v_a$ is $f_a(v_a) d^3 v_a$. The number of encounters in a time Δt with impact parameters between b and $b+db$ is just this density times the volume of an annulus with inner radius b, outer radius $b+db$, and length $v_0\Delta t$, that is $2\pi b db v_0 \Delta t f_a(v_a) d^3 v_a$.

Thus

$$D[\Delta v_i] = \frac{\langle \Delta v_i \rangle}{\Delta t} = 2\pi \int d^3 v_a db b f_a(v_a) v_0 \langle \Delta v_i \rangle_\phi, \tag{A.29}$$

The integrals involved are:

$$\int_0^{b_{\max}} db b \Delta v_\parallel = \frac{2\,(m_a v_0 b_{90}^2)}{m+m_a} \ln(1+\Lambda^2), \tag{A.30}$$

$$\int_0^{b_{\max}} db b (\Delta v_\parallel)^2 = 2\left(\frac{m_a v_0 b_{90}}{m+m_a}\right)^2 \left(1 - \frac{1}{1+\Lambda^2}\right), \tag{A.31}$$

$$\int_0^{b_{\max}} db b (\Delta v_\perp)^2 = 2\left(\frac{m_a v_0 b_{90}}{m+m_a}\right)^2 \left(\ln(1+\Lambda^2) + \frac{1}{1+\Lambda^2} - 1\right), \tag{A.32}$$

where $\Lambda = \frac{b_{\max}}{b_{90}}$. $b_{\max}$ is given approximately by the radius of the subject star's orbit. In most applications, Λ is very large, and therefore without loss of accuracy we can discard terms involving $(1+\Lambda^2)^{-1}$ and replace $\ln(1+\Lambda^2)$ by $\ln\Lambda$. Furthermore, although this is a less accurate approximation, we can discard terms of order unity compared to those of order $\ln\Lambda$. In this manner we arrive at a simplified version of the equations, keeping only terms of order $\ln\Lambda$,

$$\begin{aligned} \int_0^{b_{\max}} db b \Delta v_\parallel &= \frac{2 m_a v_0 b_{90}^2}{m+m_a} \ln\Lambda, \\ \int_0^{b_{\max}} db b (\Delta v_\parallel)^2 &= 0, \\ \int_0^{b_{\max}} db b (\Delta v_\perp)^2 &= 4\left(\frac{m_a v_0 b_{90}}{m+m_a}\right)^2 \ln\Lambda. \end{aligned} \tag{A.33}$$

We can now compute the diffusion coefficients as below

$$D[\Delta v_i] = -4\pi \frac{m_a}{m+m_a} \int d^3 v_a\, V_0^2 b_{90}^2 f_a(v_a) \ln\Lambda (\hat{\mathbf{e}}_i \cdot \hat{\mathbf{e}}_1), \tag{A.34}$$

$$D[\Delta v_i \Delta v_j] = 4\pi \left(\frac{m_a}{m+m_a}\right)^2 \int d^3 v_a\, V_0^3 b_{90}^2 f_a(v_a) \ln\Lambda \left[(\hat{\mathbf{e}}_i \cdot \hat{\mathbf{e}}_2)(\hat{\mathbf{e}}_j \cdot \hat{\mathbf{e}}_2) + (\hat{\mathbf{e}}_i \cdot \hat{\mathbf{e}}_3)(\hat{\mathbf{e}}_j \cdot \hat{\mathbf{e}}_3)\right]. \tag{A.35}$$

Since we assume that $\ln\Lambda$ is large, we do not make any significant additional error by replacing the factor V_0 in Λ by some typical stellar speed $v_{\rm typ}$. Thus

$$\Lambda = \frac{b_{\max} v_{\rm typ}^2}{G(m+m_a)}, \tag{A.36}$$

which is independent of v_a so $\ln\Lambda$ may be taken outside the integral. Also, the expressions involving unit vectors can be simplified, since $\sum_{p=1}^{3} (\hat{\mathbf{e}}_i \cdot \hat{\mathbf{e}}_p)(\hat{\mathbf{e}}_j \cdot \hat{\mathbf{e}}_p) = \hat{\mathbf{e}}_i \cdot \hat{\mathbf{e}}_j = \delta_{ij}$, and $(\hat{\mathbf{e}}_i \cdot \hat{\mathbf{e}}_1) = V_{0i}/V_0$. After eliminating b_{90}, we obtain

$$D[\Delta v_i] = -4\pi G^2 m_a (m+m_a) \ln\Lambda \int d^3 v_a \frac{f_a(v_a)}{V_0^3} V_{0i}, \tag{A.37}$$

$$D[\Delta v_i \Delta v_j] = 4\pi G^2 m_a^2 \ln\Lambda \int d^3 v_a \frac{f_a(v_a)}{V_0}\left(\delta_{ij} - \frac{V_{0i}V_{0j}}{V_0^2}\right). \tag{A.38}$$

These equations can be simplified further by noting that $V_0 = \left[\sum_{i=1}^3 (v_i - v_{ai})^2\right]^{1/2}$, so

$$\frac{\partial}{\partial v_i}\frac{1}{V_0} = -\frac{V_{0i}}{V_0^3}; \quad \frac{\partial^2}{\partial v_i \partial v_j} = \frac{\delta_{ij}}{V_0} - \frac{V_{0i}V_{0j}}{V_0^3}. \tag{A.39}$$

The expressions for the diffusion coefficients will then become

$$D[\Delta v_i] = 4\pi G^2 m_a(m+m_a)\ln\Lambda \frac{\partial}{\partial v_i} h(\mathbf{x},\mathbf{v}), \tag{A.40}$$

$$D[\Delta v_i \Delta v_j] = 4\pi G^2 m_a^2 \ln\Lambda \frac{\partial^2}{\partial v_i \partial v_j} g(\mathbf{x},\mathbf{v}), \tag{A.41}$$

The functions $h(\mathbf{x},\mathbf{v})$ and $g(\mathbf{x},\mathbf{v})$ are the Rosenbluth potential given by integrals over the distribution function $f_a(\mathbf{x}_a,\mathbf{v}_a)$ of the field stars:

$$h(\mathbf{x},\mathbf{v}) = \int d^3 v_a \frac{f_a(\mathbf{x}_a,\mathbf{v}_a)}{|\mathbf{v}-\mathbf{v}_a|}, \tag{A.42}$$

$$g(\mathbf{x},\mathbf{v}) = \int d^3 v_a\, f_a(\mathbf{x}_a,\mathbf{v}_a)|\mathbf{v}-\mathbf{v}_a|. \tag{A.43}$$

The symmetry of the problem implies that if the distribution function f_a is isotropic, then:

$$D[(\Delta v_x)^2] = D[(\Delta v_y)^2] = D[(\Delta v_z)^2], \tag{A.44}$$

$$D[\Delta v_x] = D[\Delta v_y] = D[\Delta v_z] = 0, \tag{A.45}$$

$$D[\Delta v_x \Delta v_y] = D[\Delta v_x \Delta v_z] = D[\Delta v_y \Delta v_z] = 0. \tag{A.46}$$

The diffusion coefficients can thus be simplified in a coordinate system aligned with the velocity vector $\mathbf{v}$. Using integrals over the field-star distribution function, the coefficients become:

$$D[\Delta v_\parallel] = -\frac{16\pi^2 G^2 m_a(m+m_a)\ln\Lambda}{v^2}\int_0^v dv_a\, v_a^2 f_a(x,v_a), \tag{A.47}$$

$$D[(\Delta v_\parallel)^2] = \frac{32\pi^2 G^2 m_a^2 \ln\Lambda}{3}\left(\int_0^v dv_a \frac{v_a^4}{v^3} f_a(x,v_a) + \int_v^\infty dv_a\, v_a f_a(x,v_a)\right), \tag{A.48}$$

$$D[(\Delta v_\perp)^2] = \frac{32\pi^2 G^2 m_a^2 \ln\Lambda}{3}\left(\int_0^v dv_a \left(\frac{3v_a^2}{v} - \frac{v_a^4}{v^3}\right) f_a(x,v_a) + 2\int_v^\infty dv_a\, v_a f_a(x,v_a)\right). \tag{A.49}$$

In the case where the field-star distribution is Maxwellian

$$f_a(v_a) = \frac{n}{(2\pi\sigma^2)^{3/2}} e^{-v_a^2/(2\sigma^2)}, \tag{A.50}$$

where n is the number density and σ is the one-dimensional velocity dispersion. To compute the integrals involved in the coefficients expressions after substituting the number density, we take $X = v/\sqrt{2}\sigma$, $x = v_a/\sqrt{2}\sigma$ and therefore $dx = dv_a/\sqrt{2}\sigma$. Thus they will be calculated as the following

$$\begin{aligned}\int_0^v dv_a v_a^2\, e^{-v_a^2/(2\sigma^2)} &= \int_0^X \sqrt{2}\sigma dx\, (\sqrt{2}\sigma x)^2 e^{-x^2} = 2\sqrt{2}\sigma^3 \int_0^X dx\, x^2 e^{-x^2} \\ = \frac{2\sqrt{2}\sigma^3 e^{-X^2}[\sqrt{\pi}e^{X^2}\,\mathrm{erf}(X) - 2X]}{4} &= \frac{\sqrt{2}}{2}\sigma^3 \left(\sqrt{\pi}\,\mathrm{erf}(X) - 2Xe^{-X^2}\right)\end{aligned} \tag{A.51}$$

$$\begin{aligned}\int_0^v dv_a\, v_a^4 e^{-v_a^2/2\sigma^2} &= \int_0^X \sqrt{2}\sigma dx(\sqrt{2}\sigma x)^4 e^{-x^2} = 4\sqrt{2}\sigma^5 \int_0^X dx\, x^4 e^{-x^2} \\ &= \frac{\sqrt{2}\sigma^5}{2} e^{-X^2}\left(3\sqrt{\pi}\, e^{X^2}\ \mathrm{erf}(X) - 4X^3 - 6X\right)\end{aligned} \tag{A.52}$$

$$\begin{aligned}\int_v^\infty dv_a\, v_a e^{-v_a^2/2\sigma^2} &= \int_X^\infty \sqrt{2}\sigma dx(\sqrt{2}\sigma x) e^{-x^2} = 2\sigma^2 \int_X^\infty dx\, x\, e^{-x^2} \\ &= \sigma^2 e^{-X^2}\end{aligned} \tag{A.53}$$

Therefore

$$\begin{aligned}D[\Delta v_\parallel] &= -\frac{2\pi^{1/2}G^2\rho(m+m_a)\ln\Lambda}{\sigma^2}\left(\frac{\sqrt{\pi}\,\mathrm{erf}(X) - 2Xe^{-X^2}}{X^2}\right) \\ &= -\frac{4\pi G^2\rho(m+m_a)\ln\Lambda}{\sigma^2}\left(\frac{1}{2X^2}\right)\left(\mathrm{erf(X)} - \frac{2\mathrm{X}\,\mathrm{e}^{-\mathrm{X}^2}}{\sqrt{\pi}}\right)\end{aligned} \tag{A.54}$$

$$\begin{aligned}D[(\Delta v_\parallel)^2] &= \frac{32\pi^2 G^2 m_a^2 n\ln\Lambda}{3(2\pi\sigma^2)^{3/2}}\left[\frac{\sqrt{2}\sigma^5}{4\sqrt{2}\sigma^3}\left(\frac{3\sqrt{\pi}\ \mathrm{erf}(X)}{X^3} - 4e^{-X^2} - \frac{6e^{-X^2}}{X^2}\right) + \sigma^2\, e^{-X^2}\right] \\ &= \frac{32\pi^2 G^2 m_a n\ln\Lambda\sigma^2}{(2\pi\sigma^2)^{3/2}}\left(\frac{1}{2X^2}\right)\left[\frac{\sqrt{\pi}\,\mathrm{erf(X)}}{2X} - e^{-X^2}\right] \\ &= \frac{4\sqrt{2}\pi G^2 m_a n\ln\Lambda}{\sigma}\left(\frac{1}{2X^3}\right)\left[\mathrm{erf(X)} - \frac{2Xe^{-X^2}}{\sqrt{\pi}}\right]\end{aligned} \tag{A.55}$$

$$\begin{aligned}D[(\Delta v_\parallel)^2] &= \frac{32\pi^2 G^2 m_a^2 n\ln\Lambda}{3(2\pi\sigma^2)^{3/2}}[\frac{3\sqrt{2}\sigma^3}{2\sqrt{2}\sigma X}\left(\sqrt{\pi}\,\mathrm{erf}(X) - 2Xe^{-X^2}\right) \\ &- \frac{\sqrt{2}\sigma^5}{4\sqrt{2}\sigma^3 X^3}e^{-X^2}\left(3\sqrt{\pi}\, e^{X^2}\ \mathrm{erf}(X) - 4X^3 - 6X\right) + 2\sigma^2\, e^{-X^2}] \\ &= \frac{4\sqrt{2}\pi G^2 m_a n\ln\Lambda}{\sigma}\left(\frac{1}{X}\right)\left[\mathrm{erf(X)} - \left(\frac{1}{2X^2}\right)\left[\mathrm{erf(X)} - \frac{2\mathrm{Xe}^{-\mathrm{X}^2}}{\sqrt{\pi}}\right]\right]\end{aligned} \tag{A.56}$$

The diffusion coefficients will finally reduce to the relations below after simplifications

$$D[\Delta v_\parallel] = -\frac{4\pi G^2\rho(m+m_a)\ln\Lambda}{\sigma^2}G(X), \tag{A.57}$$

$$D[(\Delta v_\parallel)^2] = \frac{4\pi G^2\rho m_a\ln\Lambda}{\sigma}\frac{G(X)}{X}, \tag{A.58}$$

$$D[(\Delta v_\perp)^2] = \frac{4\pi G^2\rho m_a\ln\Lambda}{\sigma}\left[\frac{\mathrm{erf}(X) - G(X)}{X}\right], \tag{A.59}$$

with $\rho = m_a n$ and $G(X)$ defined as

$$G(X) = \frac{1}{2X^2}\left(\mathrm{erf}(X) - 2\frac{X}{\sqrt{\pi}}e^{-X^2}\right). \tag{A.60}$$

A.5 The Classical Limit of Fuzzy Dark Matter

In our derivations in Section 3.3, we assumed that each plane wave has a random phase and is moving with velocity $\mathbf{v} = \hbar\mathbf{k}/m_\mathrm{b}$. These assumptions are valid if the number of particles per wave $N \sim \rho_\mathrm{b}\lambda^3/m_\mathrm{b} \sim \rho_\mathrm{b}\hbar^3/(\sigma^3 m_\mathrm{b}^4)$ is large. Thus, our assumptions are valid when

$$m_\mathrm{b} \ll m_\mathrm{s} \equiv \left(\frac{\rho_\mathrm{b}\hbar^3}{\sigma^3}\right)^{1/4} = \left(\frac{\hbar^3}{2\pi G\sigma r^2}\right)^{1/4} \simeq 35\,\mathrm{eV}\left(\frac{r}{1\,\mathrm{kpc}}\right)^{-1/2}\left(\frac{\sigma}{200\,\mathrm{km\ s^{-1}}}\right)^{-1/4}, \tag{A.61}$$

in which we have used equation (7.37). From equation (4.22), we can see that the condition $m_\mathrm{b} \ll m_\mathrm{s}$ is equivalent to $m_\mathrm{b} \ll m_\mathrm{eff}$, that is, each quasiparticle of mass m_eff must contain many FDM particles of mass m_b.

At even larger masses, the system will behave like a classical system of free particles of mass m_b. Consider a free particle at position $x \pm \Delta x_0$ and velocity $v \pm \Delta v_0$, where Δx_0 and Δv_0 are the initial uncertainties in position and velocity, and $\Delta x_0 \Delta v_0 \geq \hbar/(2m_\mathrm{b})$. After a time T, the uncertainty in position is $\Delta x = \Delta x_0 + \Delta v_0 T \geq \Delta x_0(1 + \hbar T/[2m_\mathrm{b}(\Delta x_0)^2])$. The slowest scattering events have $T \simeq T_\mathrm{d}$ where $T_\mathrm{d} = r/\sigma$ is the dynamical time and r is the orbit radius. If the particles are to behave classically, the position uncertainty cannot grow significantly during the scattering and cannot exceed the typical distance between particles $d = (m_\mathrm{b}/\rho_\mathrm{b})^{1/3}$, demanding that $d \gg \Delta x_0 \gg (\hbar T_\mathrm{d}/2m_\mathrm{b})^{1/2}$. Therefore, we can define a critical particle mass m_c at which $d = (\hbar T_\mathrm{d}/2m_\mathrm{b})^{1/2}$, and the particles behave classically if

$$m_\mathrm{b} \gg m_\mathrm{c} \equiv \rho_\mathrm{b}^{2/5}(\hbar T_\mathrm{d}/2)^{3/5} = \frac{1}{2}\left(\frac{\hbar^3\sigma}{\pi^2 G^2 r}\right)^{1/5} = 1.25\times10^{16}\,\mathrm{eV}\left(\frac{r}{1\,\mathrm{kpc}}\right)^{-1/5}\left(\frac{\sigma}{200\,\mathrm{km\ s^{-1}}}\right)^{1/5}. \tag{A.62}$$

Thus, there is an intermediate range $m_\mathrm{s} \lesssim m_\mathrm{b} \lesssim m_\mathrm{c}$ in which the behavior needs further investigation, which we now undertake.

To make these arguments more quantitative we consider the following wave function:

$$\psi(\mathbf{r}, t) = \int \mathrm{d}\mathbf{k}\,\varphi(\mathbf{k})\mathrm{e}^{\mathrm{i}\mathbf{k}\cdot\mathbf{r} - \mathrm{i}\omega(k)t}, \tag{A.63}$$

where $\omega(k)$ is given by equation (4.4), and the wave function in $\mathbf{k}$–space is a sum of Gaussian wavepackets,

$$\varphi(\mathbf{k}) = \sum_{n=1}^{N} \frac{\varepsilon^{3/2} m_\mathrm{b}^{1/2}}{2^{3/4}\pi^{9/4}} \mathrm{e}^{-|\mathbf{k} - m_\mathrm{b}\mathbf{v}_n/\hbar|^2\varepsilon^2} \mathrm{e}^{\mathrm{i}\phi_n - \mathrm{i}\mathbf{k}\cdot\mathbf{r}_n}. \tag{A.64}$$

Here $\{\mathbf{r}_n\}$, $\{\mathbf{v}_n\}$ are random positions and velocities drawn from the DF $F_\mathrm{b}(\mathbf{v})$, $\{\phi_n\}$ are independent random phases, and ε is the initial uncertainty in position. The normalization is such that $\langle|\psi|^2\rangle = \rho_\mathrm{b}$.

The correlation function of $\varphi(\mathbf{k})$ is given by $\langle\varphi(\mathbf{k})\varphi^*(\mathbf{k}')\rangle = f_k(\mathbf{k})\delta(\mathbf{k}-\mathbf{k}')$, where

$$f_k(\mathbf{k}) = \frac{8\varepsilon^3}{(2\pi)^{3/2}}\int \mathrm{d}\mathbf{v} F_\mathrm{b}(\mathbf{v})\mathrm{e}^{-2\varepsilon^2|\mathbf{k}-m_\mathrm{b}\mathbf{v}/\hbar|^2}, \tag{A.65}$$

and as expected the mean density is stationary, $\rho_\mathrm{b} = \langle|\psi(\mathbf{r},t)|^2\rangle = \int\mathrm{d}\mathbf{k}\, f_k(\mathbf{k}) = \int\mathrm{d}\mathbf{v}\, F_\mathrm{b}(\mathbf{v})$.

Assuming $F_\mathrm{b}(\mathbf{v})$ is a Maxwellian DF with velocity dispersion σ, the correlation function for the density fluctuations $\rho(\mathbf{r},t) = |\psi(\mathbf{r},t)|^2 - \rho_\mathrm{b}$ is

$$\begin{aligned}\langle\rho(\mathbf{r},t)\rho(\mathbf{r}',t')\rangle = {} & \frac{\rho_\mathrm{b}^2}{\left[1+(1+\alpha_1^2)^2(\sigma\Delta t/_\sigma)^2\right]^{3/2}}\exp\left[-\frac{(|\Delta\mathbf{r}|/_\sigma)^2(1+\alpha_1^2)}{1+(1+\alpha_1^2)^2(\sigma\Delta t/_\sigma)^2}\right] \\ & + \frac{m_\mathrm{b}\rho_\mathrm{b}}{8\pi^{3/2}\varepsilon^3\left[1+(\sigma\Delta t/\sqrt{2}\varepsilon)^2+\alpha_2^2/2\right]^{3/2}}\exp\left[-\frac{(|\Delta\mathbf{r}|/2\varepsilon)^2}{1+(\sigma\Delta t/\sqrt{2}\varepsilon)^2+\alpha_2^2/2}\right].\end{aligned} \tag{A.66}$$

Here we have defined $\Delta\mathbf{r} = \mathbf{r}-\mathbf{r}'$, $\Delta t = t-t'$, $T = \sqrt{t^2+t'^2}$, and two dimensionless parameters $\alpha_1 =_\sigma /(2\varepsilon)$ and $\alpha_2 = \hbar T/(2m_\mathrm{b}\varepsilon^2)$.

Since we require the correlations to be stationary over a dynamical time $T_\mathrm{d} \sim r/\sigma$, we can set $\varepsilon^2 \gg_\sigma r \gg_\sigma^2$ so $\alpha_1 \ll 1$. Moreover, when $T \lesssim T_\mathrm{d}$, we have $\alpha_2 < \hbar T_\mathrm{d}/(2m_\mathrm{b}\varepsilon^2) \sim_\sigma r/\varepsilon^2 \ll 1$. Then, equation (A.66) becomes

$$C(\mathbf{r},t) = \frac{\rho_\mathrm{b}^2}{\left[1+(\sigma t/_\sigma)^2\right]^{3/2}}\exp\left[-\frac{(r/_\sigma)^2}{1+(\sigma t/_\sigma)^2}\right] + \frac{m_\mathrm{b}\rho_\mathrm{b}}{8\pi^{3/2}\varepsilon^3\left[1+(\sigma t/\sqrt{2}\varepsilon)^2\right]^{3/2}}\exp\left[-\frac{(r/2\varepsilon)^2}{1+(\sigma t/\sqrt{2}\varepsilon)^2}\right]. \tag{A.67}$$

By comparing this result to the correlation function we obtained for FDM (equation (4.33)) and for classical particles (equation (3.78)), we can see that it is the sum of the FDM (first term) and the classical (second term) limits. The diffusion coefficients for a zero-mass test particle are now (see equation (7.7)–7.9 and 3.51–3.53)

$$D[\Delta v_\parallel] = -4\pi G^2\rho_\mathrm{b}\left[\frac{m_\mathrm{eff}\log\Lambda_\mathrm{FDM}}{\sigma_\mathrm{eff}^2}\mathbb{G}(X_\mathrm{eff}) + \frac{m_\mathrm{b}\log\Lambda_\mathrm{soft}}{\sigma^2}\mathbb{G}(X)\right], \tag{A.68}$$

$$D[(\Delta v_\parallel^2)] = 4\sqrt{2}\pi G^2\rho_\mathrm{b}\left[\frac{m_\mathrm{eff}\log\Lambda_\mathrm{FDM}}{\sigma_\mathrm{eff}}\frac{\mathbb{G}(X_\mathrm{eff})}{X_\mathrm{eff}} + \frac{m_\mathrm{b}\log\Lambda_\mathrm{soft}}{\sigma}\frac{\mathbb{G}(X)}{X}\right], \tag{A.69}$$

$$D[(\Delta\mathbf{v}_\perp)^2] = 4\sqrt{2}\pi G^2\rho_\mathrm{b}\left[\frac{m_\mathrm{eff}\log\Lambda_\mathrm{FDM}}{\sigma_\mathrm{eff}}\frac{(X_\mathrm{eff})-\mathbb{G}(X_\mathrm{eff})}{X_\mathrm{eff}} + \frac{m_\mathrm{b}\log\Lambda_\mathrm{soft}}{\sigma}\frac{(X)-\mathbb{G}(X)}{X}\right], \tag{A.70}$$

where $\Lambda_\mathrm{FDM} = 2b_\mathrm{max}/(_\sigma)$, $\Lambda_\mathrm{soft} = b_\mathrm{max}/\varepsilon$, m_eff is given by equation (4.22), the effective velocity dispersion is $\sigma_\mathrm{eff} = \sigma/\sqrt{2}$, and $X = v/\sqrt{2}\sigma$, $X_\mathrm{eff} = v/\sqrt{2}\sigma_\mathrm{eff} = v/\sigma$.

From the diffusion coefficients in equations (A.68)–(A.70), we can see that in the limit $m_\mathrm{b} \ll m_\mathrm{eff}$ ($m_\mathrm{b} \ll m_\mathrm{s}$, with m_s defined in equation (A.61)), the FDM dominates the relaxation. When $m_\mathrm{eff} \ll m_\mathrm{b} \ll m_\mathrm{c}$, with m_c defined in equation (A.62), the relaxation is dominated by the "classical" component, although the system is not a classical system since the size of the wavepackets associated with each particle is larger than the inter-particle separation, $\varepsilon \gg d$. In this regime, the wave nature of the particles affects the relaxation only through the Coulomb logarithm $\Lambda_\mathrm{soft} = b_\mathrm{max}/\varepsilon$. Finally, when $m_\mathrm{b} \gg m_\mathrm{c}$, the system is in the classical limit, and ε should be interpreted as the size of the (softened) particle (Bar-Or et al., 2019).

A.6 Solving the Integral in the Time Evolution of the Wigner Function

To solve the integral, we are going to use the following relation

$$\int d\mathbf{s} f' g = fg|_{\text{Surface}} - \int d\mathbf{s} f g'$$

In our case

$$\begin{cases} g = \psi^* \left(\mathbf{r}_-\right) e^{-i\mathbf{v}.\mathbf{s}} \rightarrow g' = e^{-i\mathbf{v}.\mathbf{s}} \left(-i\mathbf{v}\psi^* \left(\mathbf{r}_-\right) + \dfrac{\partial}{\partial s}\psi^*(\mathbf{r}_-)\right) \\ f = \nabla\psi(\mathbf{r}_+) \end{cases} \tag{A.71}$$

Now let's consider the first integral of the kinetic term and call it I,

$$\begin{aligned} I &= \int d\mathbf{s} e^{-i\mathbf{v}\cdot\mathbf{s}} \left(\psi^* \left(\mathbf{r}_-\right) \frac{\partial}{\partial s} \left[\nabla\psi \left(\mathbf{r}_+\right)\right]\right) \\ &= e^{-i\mathbf{v}\cdot\mathbf{s}}\psi^* \left(\mathbf{r}_-\right) \nabla\psi \left(\mathbf{r}_+\right)|_{surface} - \int d\mathbf{s} e^{-i\mathbf{v}\cdot\mathbf{s}} \nabla\psi \left(\mathbf{r}_+\right) \left(-i\mathbf{v}\psi^*(\mathbf{r}_-) + \frac{\partial}{\partial s}\psi^*(\mathbf{r}_-)\right) \end{aligned} \tag{A.72}$$

The first term vanishes since the integral is over all $\mathbf{s}$. To solve the second integral in the second term, we need to repeat the process of integration by parts.

$$\begin{cases} g = e^{-i\mathbf{v}.\mathbf{s}}\nabla\psi \left(\mathbf{r}_+\right) \rightarrow g' = e^{-i\mathbf{v}.\mathbf{s}} \left(-i\mathbf{v}\nabla\psi \left(\mathbf{r}_+\right) + \dfrac{\partial}{\partial s}\nabla\psi(\mathbf{r}_+)\right) \\ f = \psi^*(\mathbf{r}_-) \end{cases} \tag{A.73}$$

Now we can write the integral having neglected the fg term which vanishes

$$\int d\mathbf{s} e^{-i\mathbf{v}\cdot\mathbf{s}}\nabla\psi \left(\mathbf{r}_+\right) \left(\frac{\partial}{\partial s}\psi^*(\mathbf{r}_-)\right) = \int d\mathbf{s} e^{-i\mathbf{v}\cdot\mathbf{s}}\psi^*(r_-) \left(-i\mathbf{v}\nabla\psi \left(\mathbf{r}_+\right) + \frac{\partial}{\partial s}\nabla\psi(\mathbf{r}_+)\right) \tag{A.74}$$

Substituting these results in I will give

$$\begin{aligned} I &= \int d\mathbf{s} e^{-i\mathbf{v}\cdot\mathbf{s}} \left(\psi^* \left(\mathbf{r}_-\right) \frac{\partial}{\partial s} \left[\nabla\psi \left(\mathbf{r}_+\right)\right]\right) \\ &= \int d\mathbf{s} e^{-i\mathbf{v}\cdot\mathbf{s}}\nabla\psi \left(\mathbf{r}_+\right) \left(-i\mathbf{v}\psi^*(\mathbf{r}_-)\right) - \int d\mathbf{s} e^{-i\mathbf{v}\cdot\mathbf{s}}\psi^*(r_-) \left(-i\mathbf{v}\nabla\psi \left(\mathbf{r}_+\right) + \frac{\partial}{\partial s}\nabla\psi(\mathbf{r}_+)\right) \end{aligned} \tag{A.75}$$

After some rearrangement we will obtain

$$\int d\mathbf{s} e^{-i\mathbf{v}\cdot\mathbf{s}} \left(\psi^* \left(\mathbf{r}_-\right) \frac{\partial}{\partial s} \left[\nabla\psi \left(\mathbf{r}_+\right)\right]\right) = i \int d\mathbf{s} e^{-i\mathbf{v}\cdot\mathbf{s}}\nabla\psi \left(\mathbf{r}_+\right) \left(\mathbf{v}\psi^*(\mathbf{r}_-)\right) \tag{A.76}$$

So equation (5.25) will become

$$\begin{aligned} & i\int \frac{d\mathbf{s}}{(2\pi)^3} e^{-i\mathbf{v}\cdot\mathbf{s}} \left(\psi^*(\mathbf{r}_-)\frac{\partial}{\partial s}\cdot\left[\nabla\psi(\mathbf{r}_+)\right] + \psi(\mathbf{r}_+)\frac{\partial}{\partial s}\cdot\left[\nabla\psi^*(\mathbf{r}_-)\right]\right) \\ &= -\mathbf{v}\int \frac{d\mathbf{s}}{(2\pi)^3} e^{-i\mathbf{v}\cdot\mathbf{s}} \left(\nabla\psi \left(\mathbf{r}_+\right) \psi^*(\mathbf{r}_-) + \psi \left(\mathbf{r}_+\right) \nabla\psi^*(\mathbf{r}_-)\right) \\ &= -\mathbf{v}\cdot\nabla W \end{aligned} \tag{A.77}$$

A.7 Computing the Correlations of Potential Fluctuations

In Chapter 3, we showed that the evolution of the FDM halo distribution function is sourced by the correlations of the initial fluctuations in the system. These correlations are described by the function $\widehat{C}(\mathbf{k}, \mathbf{v})$, the Fourier transform of the correlation function, as defined in equation (5.57). Let us now explicitly compute this correlation.

In order to introduce that calculation, let us start by considering the classical case. In that regime, the system's discrete DF is given by

$$F_{\mathrm{d}}(\mathbf{r}, \mathbf{v}, t) = m_{\mathrm{b}} \sum_{i=1}^{N} \delta_{\mathrm{D}}[\mathbf{r} - \mathbf{r}_i(t)]\, \delta_{\mathrm{D}}[\mathbf{v} - \mathbf{v}_i(t)], \tag{A.78}$$

where at the initial time, the phase-space positions and velocities of the particles are drawn independently from another, uniformly in space, and according to the DF $F_{\mathrm{b}}(\mathbf{v})$ for their velocities. Similarly to equation (5.33), the instantaneous fluctuations in the system's DF are given by $f = -F_{\mathrm{b}}$. At the initial time, we can then write

$$\big\langle f_0(\mathbf{r}, \mathbf{v})\, f_0(\mathbf{r}', \mathbf{v}') \big\rangle = m_{\mathrm{b}}^2 \sum_{i,j} \big\langle \delta_{\mathrm{D}}(\mathbf{r}-\mathbf{r}_i)\, \delta_{\mathrm{D}}(\mathbf{v}-\mathbf{v}_i)\, \delta_{\mathrm{D}}(\mathbf{r}'-\mathbf{r}_j)\, \delta_{\mathrm{D}}(\mathbf{v}'-\mathbf{v}_j) \big\rangle - F_{\mathrm{b}}(\mathbf{v})\, F_{\mathrm{b}}(\mathbf{v}'), \tag{A.79}$$

where we dropped the time dependence ($t = 0$) to shorten the notation. As the particles are chosen independently, there are two types of terms in the double sum, depending on whether $i = j$ or $i \neq j$. We then get

$$\begin{aligned} \big\langle f_0(\mathbf{r}, \mathbf{v})\, f_0(\mathbf{r}', \mathbf{v}') \big\rangle = {} & m_{\mathrm{b}}^2\, \delta_{\mathrm{D}}(\mathbf{r}-\mathbf{r}')\, \delta_{\mathrm{D}}(\mathbf{v}-\mathbf{v}') \sum_i \big\langle \delta_{\mathrm{D}}(\mathbf{r}-\mathbf{r}_i)\, \delta_{\mathrm{D}}(\mathbf{v}-\mathbf{v}_i) \big\rangle \\ & + m_{\mathrm{b}}^2 \sum_{i \neq j} \big\langle \delta_{\mathrm{D}}(\mathbf{r}-\mathbf{r}_i)\, \delta_{\mathrm{D}}(\mathbf{v}-\mathbf{v}_i) \big\rangle \big\langle \delta_{\mathrm{D}}(\mathbf{r}'-\mathbf{r}_j)\, \delta_{\mathrm{D}}(\mathbf{v}'-\mathbf{v}_j) \big\rangle \\ & - F_{\mathrm{b}}(\mathbf{v})\, F_{\mathrm{b}}(\mathbf{v}'). \end{aligned} \tag{A.80}$$

Since F_{b} obeys the normalisation convention $\int \mathrm{d}\mathbf{v} F_{\mathrm{b}}(\mathbf{v}) = \rho_0$, we have

$$\big\langle \delta_{\mathrm{D}}(\mathbf{r}-\mathbf{r}_i)\, \delta_{\mathrm{D}}(\mathbf{v}-\mathbf{v}_i) \big\rangle = \frac{1}{N m_{\mathrm{b}}}\, F_{\mathrm{b}}(\mathbf{v}). \tag{A.81}$$

As a consequence, in the limit $N \gg 1$, the last two terms in equation (A.80) cancel and we have

$$\big\langle f_0(\mathbf{r}, \mathbf{v})\, f_0(\mathbf{r}', \mathbf{v}') \big\rangle = m_{\mathrm{b}} F_{\mathrm{b}}(\mathbf{v})\, \delta_{\mathrm{D}}(\mathbf{r}-\mathbf{r}')\, \delta_{\mathrm{D}}(\mathbf{v}-\mathbf{v}'). \tag{A.82}$$

Following the convention from equation (5.29), this can be rewritten in Fourier space as

$$\big\langle \widehat{f}_0(\mathbf{k}, \mathbf{v})\, \widehat{f}_0(\mathbf{k}', \mathbf{v}') \big\rangle = \frac{1}{(2\pi)^3}\, m_{\mathrm{b}}\, F_{\mathrm{b}}(\mathbf{v})\, \delta_{\mathrm{D}}(\mathbf{k}+\mathbf{k}')\, \delta_{\mathrm{D}}(\mathbf{v}-\mathbf{v}'), \tag{A.83}$$

and the needed correlation function from equation (5.57) is then

$$\widehat{C}(\mathbf{k}, \mathbf{v}) = \frac{1}{(2\pi)^3}\, m_{\mathrm{b}}\, F_{\mathrm{b}}(\mathbf{v}). \tag{A.84}$$

We note that this correlation function is independent of $\mathbf{k}$, a consequence of our assumption that the initial positions of the particles are chosen independently from a homogeneous distribution.

Let us now adapt this calculation to the FDM case and compute the statistics of the persistent fluctuations present in the Wigner distribution function of the halo. We consider the following wavefunction

$$\psi(\mathbf{r},t) = \int \mathrm{d}\mathbf{k}\, \varphi(\mathbf{k})\, \mathrm{e}^{\mathrm{i}[\mathbf{k}\cdot\mathbf{r}-\omega(k)t]}. \tag{A.85}$$

In the limit where the potential fluctuations $\Phi(\mathbf{r},t)$ vanish, this wavefunction is a solution of the free Schrödinger equation provided that it satisfies the dispersion relation

$$\omega(k) = \frac{\hbar k^2}{2m_{\mathrm{b}}}. \tag{A.86}$$

Let us now assume that the wavefunction in $\mathbf{k}$–space, $\varphi(\mathbf{k})$, is the sum of Gaussian wavepackets of the form

$$\varphi(\mathbf{k}) = A \sum_{i=1}^{N} \mathrm{e}^{\mathrm{i}\phi_i}\, \mathrm{e}^{-\mathrm{i}\mathbf{k}\cdot\mathbf{r}_i}\, \mathrm{e}^{-|\mathbf{k}-m_{\mathrm{b}}\mathbf{v}_i/\hbar|^2\varepsilon^2}. \tag{A.87}$$

In that expression, $\{\mathbf{r}_i,\mathbf{v}_i\}$ are random positions and velocities drawn independently from the DF $F_{\mathrm{b}}(\mathbf{v})$, and $\{\phi_i\}$ are independent random phases. In addition, ε is an ad hoc parameter, so that ε and $\hbar/(2m_{\mathrm{b}}\varepsilon)$ are respectively the initial uncertainties in the positions and velocities. This parameter will prove to be useful in managing our asymptotic developments. In equation (A.87), we also introduced the prefactor A that is tuned to satisfy the normalisation condition stemming from equation (5.43), namely that $\langle|\psi(\mathbf{r},t)|^2\rangle = \rho_0$.

Let us now determine the value of A. Starting from equation (A.85), we write

$$\big\langle|\psi(\mathbf{r},t)|^2\big\rangle = \int \mathrm{d}\mathbf{k}\mathrm{d}\mathbf{k}'\, \langle\varphi(\mathbf{k})\,\varphi^*(\mathbf{k}')\rangle\, \mathrm{e}^{\mathrm{i}(\mathbf{k}-\mathbf{k}')\cdot\mathbf{r}}\, \mathrm{e}^{-\mathrm{i}t[\omega(k)-\omega(k')]}. \tag{A.88}$$

The two-point correlation function of $\varphi(\mathbf{k})$ is

$$\begin{aligned}
\big\langle\varphi(\mathbf{k})\,\varphi^*(\mathbf{k}')\big\rangle &= A^2 \sum_{i,j} \big\langle \mathrm{e}^{\mathrm{i}(\phi_i-\phi_j)}\, \mathrm{e}^{-\mathrm{i}\mathbf{k}\cdot\mathbf{r}_i}\, \mathrm{e}^{\mathrm{i}\mathbf{k}'\cdot\mathbf{r}_j}\, \mathrm{e}^{-|\mathbf{k}-m_{\mathrm{b}}\mathbf{v}_i/\hbar|^2\varepsilon^2}\, \mathrm{e}^{-|\mathbf{k}'-m_{\mathrm{b}}\mathbf{v}_j/\hbar|^2\varepsilon^2}\big\rangle \\
&= A^2 \sum_{i} \big\langle \mathrm{e}^{-\mathrm{i}(\mathbf{k}-\mathbf{k}')\cdot\mathbf{r}_i}\, \mathrm{e}^{-|\mathbf{k}-m_{\mathrm{b}}\mathbf{v}_i/\hbar|^2\varepsilon^2}\, \mathrm{e}^{-|\mathbf{k}'-m_{\mathrm{b}}\mathbf{v}_i/\hbar|^2\varepsilon^2}\big\rangle \\
&= A^2 \sum_{i} \int \mathrm{d}\mathbf{r}\mathrm{d}\mathbf{v}\, \big\langle\delta_{\mathrm{D}}(\mathbf{r}-\mathbf{r}_i)\,\delta_{\mathrm{D}}(\mathbf{v}-\mathbf{v}_i)\big\rangle\, \mathrm{e}^{-\mathrm{i}(\mathbf{k}-\mathbf{k}')\cdot\mathbf{r}}\, \mathrm{e}^{-|\mathbf{k}-m_{\mathrm{b}}\mathbf{v}/\hbar|^2\varepsilon^2}\, \mathrm{e}^{-|\mathbf{k}'-m_{\mathrm{b}}\mathbf{v}/\hbar|^2\varepsilon^2}.
\end{aligned} \tag{A.89}$$

To get the second line we noted that $\langle \mathrm{e}^{\mathrm{i}(\phi_i-\phi_j)}\rangle$ is non-zero only for $i=j$. Using equation (A.81), one can write

$$\begin{aligned}
\big\langle\varphi(\mathbf{k})\,\varphi^*(\mathbf{k}')\big\rangle &= \frac{A^2}{m_{\mathrm{b}}} \int \mathrm{d}\mathbf{r}\mathrm{d}\mathbf{v}\, F_{\mathrm{b}}(\mathbf{v})\, \mathrm{e}^{-\mathrm{i}(\mathbf{k}-\mathbf{k}')\cdot\mathbf{r}}\, \mathrm{e}^{-|\mathbf{k}-m_{\mathrm{b}}\mathbf{v}/\hbar|^2\varepsilon^2}\, \mathrm{e}^{-|\mathbf{k}'-m_{\mathrm{b}}\mathbf{v}/\hbar|^2\varepsilon^2} \\
&= \frac{(2\pi)^3 A^2}{m_{\mathrm{b}}} \delta_{\mathrm{D}}(\mathbf{k}-\mathbf{k}') \int \mathrm{d}\mathbf{v}\, F_{\mathrm{b}}(\mathbf{v})\, \mathrm{e}^{-2|\mathbf{k}-m_{\mathrm{b}}\mathbf{v}/\hbar|^2\varepsilon^2}.
\end{aligned} \tag{A.90}$$

We can now use this result to pursue the simplification of equation (A.88). We have

$$\big\langle|\psi(\mathbf{r},t)|^2\big\rangle = \frac{(2\pi)^3 A^2}{m_{\mathrm{b}}} \int \mathrm{d}\mathbf{k}\mathrm{d}\mathbf{v}\, F_{\mathrm{b}}(\mathbf{v})\, \mathrm{e}^{-2|\mathbf{k}-m_{\mathrm{b}}\mathbf{v}/\hbar|^2\varepsilon^2} = \frac{2^{3/2}\pi^{9/2} A^2}{\varepsilon^3\, m_{\mathrm{b}}} \int \mathrm{d}\mathbf{v}\, F_{\mathrm{b}}(\mathbf{v}). \tag{A.91}$$

Recalling from equation (5.43) that $\int\!\mathrm{d}\mathbf{v}\, F_\mathrm{b}(\mathbf{v}) = \rho_0$, we obtain the value of A as

$$A = \frac{\varepsilon^{3/2}\, m_\mathrm{b}^{1/2}}{2^{3/4}\pi^{9/4}}. \tag{A.92}$$

Relying on the definition from equation (5.19), we can now compute the Wigner function $W(\mathbf{r},\mathbf{v},t)$ associated with equation (A.85). Following some cumbersome calculations, it takes the form

$$\begin{aligned}
W(\mathbf{r},\mathbf{v},t) &= \int \frac{\mathrm{d}\mathbf{s}}{(2\pi)^3}\, \mathrm{e}^{-\mathrm{i}\mathbf{v}\cdot\mathbf{s}}\, \psi\big(\mathbf{r}+\hbar\mathbf{s}/m_\mathrm{b},t\big)\, \psi^*(\mathbf{r}-\hbar\mathbf{s}/m_\mathrm{b},t) \\
&= \bigg(\frac{2m_\mathrm{b}}{\hbar}\bigg)^3 \int \mathrm{d}\mathbf{k}_1 \mathrm{d}\mathbf{k}_2\, \varphi(\mathbf{k}_1)\, \varphi^*(\mathbf{k}_2)\, \delta_\mathrm{D}\bigg(\mathbf{k}_1 + \mathbf{k}_2 - \frac{2m_\mathrm{b}}{\hbar}\mathbf{v}\bigg)\, \mathrm{e}^{\mathrm{i}(\mathbf{k}_1-\mathbf{k}_2)\cdot(\mathbf{r}-\mathbf{v}t)} \\
&= m_\mathrm{b} \bigg(\frac{m_\mathrm{b}}{\pi\hbar}\bigg)^3 \sum_{i,j} \mathrm{e}^{\mathrm{i}(\phi_i-\phi_j)}\, \exp\!\big[-\tfrac{2\varepsilon^2 m_\mathrm{b}^2}{\hbar^2}|(\mathbf{v}_i+\mathbf{v}_j)-\mathbf{v}|^2\big]\, \exp\!\big[-\tfrac{1}{2\varepsilon^2}|(\mathbf{r}_i+\mathbf{r}_j)-\mathbf{r}+\mathbf{v}t|^2\big] \\
&\qquad \times \exp\!\big\{-\mathrm{i}\tfrac{m_\mathrm{b}}{\hbar}\big[(\mathbf{r}_i-\mathbf{r}_j)\cdot\mathbf{v} + \big[(\mathbf{r}_i+\mathbf{r}_j)-\mathbf{r}+\mathbf{v}t\big]\cdot(\mathbf{v}_i-\mathbf{v}_j)\big]\big\}.
\end{aligned} \tag{A.93}$$

In the second line we have used the relation $\omega(k_2)-\omega(k_1) = (\hbar/m_\mathrm{b})(k_2^2-k_1^2) = (\hbar/m_\mathrm{b})(\mathbf{k}_2+\mathbf{k}_1)\cdot(\mathbf{k}_2-\mathbf{k}_1)$; when multiplied by the delta function in that equation this reduces to $\mathbf{v}\cdot(\mathbf{k}_2-\mathbf{k}_1)$.

In order to check these calculations, let us now follow the same method as in equation (A.89) to compute the ensemble-averaged Wigner function. Owing to the presence of the factor $\mathrm{e}^{\mathrm{i}(\phi_i-\phi_j)}$ in equation (A.93), only the contributions with $i=j$ remain. All in all, we obtain

$$\begin{aligned}
\overline{W}(\mathbf{r},\mathbf{v},t) &= \bigg(\frac{m_\mathrm{b}}{\pi\hbar}\bigg)^3 \int \mathrm{d}\mathbf{r}'\, \mathrm{d}\mathbf{v}'\, F_\mathrm{b}(\mathbf{v}')\, \exp\!\big[-\tfrac{2\varepsilon^2 m_\mathrm{b}^2}{\hbar^2}|\mathbf{v}'-\mathbf{v}|^2\big]\, \exp\!\big[-\tfrac{1}{2\varepsilon^2}|\mathbf{r}'-\mathbf{r}+\mathbf{v}t|^2\big] \\
&\simeq F_\mathrm{b}(\mathbf{v}),
\end{aligned} \tag{A.94}$$

To get the last line, we assumed that $\varepsilon \gg_\sigma = \hbar/(m_\mathrm{b}\sigma)$, with σ the system's typical velocity; physically, this means that the size of the wavepacket is much larger than the typical de Broglie wavelength. In that limit, we can then use the replacement

$$\mathrm{e}^{-\alpha|\mathbf{v}|^2/\sigma^2} \xrightarrow[\alpha\gg 1]{} \frac{\pi^{3/2}}{\alpha^{3/2}}\, \delta_\mathrm{D}(\mathbf{v}/\sigma), \tag{A.95}$$

with $\alpha^{-1} = \hbar^2/(2\varepsilon^2 m_\mathrm{b}^2\sigma^2)$ our small parameter. Thus, we have recovered in equation (A.94) the known result that the ensemble-averaged Wigner function is the same as the distribution function.

Having computed the Wigner distribution in equation (A.93), we can now find the correlation of its fluctuations at the initial time, as required by equation (5.57). Following equation (5.33), we write

$$\big\langle f_0(\mathbf{r},\mathbf{v})\, f_0(\mathbf{r}',\mathbf{v}')\big\rangle = \big\langle W(\mathbf{r},\mathbf{v})\, W(\mathbf{r}',\mathbf{v}')\big\rangle - \overline{W}(\mathbf{r},\mathbf{v})\, \overline{W}(\mathbf{r}',\mathbf{v}'), \tag{A.96}$$

where all the functions are evaluated at the initial time. Glancing back at equation (A.93), we note that the Wigner function can be rewritten in the shorter form

$$W(\mathbf{r},\mathbf{v}) = \sum_{i,j} \mathrm{e}^{\mathrm{i}(\phi_i-\phi_j)}\, g_{ij}(\mathbf{r},\mathbf{v}), \tag{A.97}$$

where the expression for the function $g_{ij}(\mathbf{r},\mathbf{v})$ naturally follows from equation (A.93). As a result, the ensemble average in the r.h.s. of equation (A.96) takes the form

$$\big\langle W(\mathbf{r},\mathbf{v})\, W(\mathbf{r}',\mathbf{v}')\big\rangle = \sum_{\substack{i,j\\k,l}} \big\langle \mathrm{e}^{\mathrm{i}(\phi_i-\phi_j+\phi_k-\phi_l)}\, g_{ij}(\mathbf{r},\mathbf{v})\, g_{kl}(\mathbf{r}',\mathbf{v}')\big\rangle \tag{A.98}$$

Because the wavepackets are drawn independently, the phase term $\langle \mathrm{e}^{\mathrm{i}(\phi_i-\phi_j+\phi_k-\phi_l)}\rangle$ is non-zero only in three cases, namely (i) $i{=}j{=}k{=}l$; (ii) $i{=}j$ and $k{=}l$ with $i{\neq}k$; (iii) $i{=}l$ and $j{=}k$ with $i{\neq}k$. In the limit $N \gg 1$, we can then rewrite equation (A.98) as

$$\big\langle W(\mathbf{r},\mathbf{v})\, W(\mathbf{r}',\mathbf{v}')\big\rangle = N\,\big\langle g_{ii}(\mathbf{r},\mathbf{v})\, g_{ii}(\mathbf{r}',\mathbf{v}')\big\rangle + N^2\big\langle g_{ii}(\mathbf{r},\mathbf{v})\, g_{kk}(\mathbf{r}',\mathbf{v}')\big\rangle + N^2\big\langle g_{ik}(\mathbf{r},\mathbf{v})\, g_{ki}(\mathbf{r}',\mathbf{v}')\big\rangle, \tag{A.99}$$

where, in the last two terms, it is understood that $\{\mathbf{r}_i,\mathbf{v}_i\}$ and $\{\mathbf{r}_k,\mathbf{v}_k\}$ are two independent sets of random variables. Let us now compute in turn each of the terms appearing in equation (A.99). We can first write

$$\begin{aligned}
N\big\langle g_{ii}(\mathbf{r},\mathbf{v})\, g_{ii}(\mathbf{r}',\mathbf{v}')\big\rangle &= m_\mathrm{b}\bigg(\frac{m_\mathrm{b}}{\pi\hbar}\bigg)^6 \!\int\!\mathrm{d}\mathbf{v}_i\, F_\mathrm{b}(\mathbf{v}_i)\, \exp\!\big[-\tfrac{2\varepsilon^2 m_\mathrm{b}^2}{\hbar^2}\big(|\mathbf{v}_i-\mathbf{v}|^2+|\mathbf{v}_i-\mathbf{v}'|^2\big)\big] \\
&\qquad\qquad \times\!\int\!\mathrm{d}\mathbf{r}_i \exp\!\big[-\tfrac{1}{2\varepsilon^2}\big(|\mathbf{r}_i-\mathbf{r}|^2+|\mathbf{r}_i-\mathbf{r}'|^2\big)\big] \\
&= m_\mathrm{b}\bigg(\frac{m_\mathrm{b}}{\pi\hbar}\bigg)^6 \exp\!\big[-\tfrac{\varepsilon^2 m_\mathrm{b}^2}{\hbar^2}|\mathbf{v}-\mathbf{v}'|^2\big]\!\int\!\mathrm{d}\mathbf{v}_i\, F_\mathrm{b}(\mathbf{v}_i)\, \exp\!\big[-\tfrac{4\varepsilon^2 m_\mathrm{b}^2}{\hbar^2}|\mathbf{v}_i-(\mathbf{v}+\mathbf{v}')|^2\big] \\
&\qquad\qquad \times \exp\!\big[-\tfrac{1}{4\varepsilon^2}|\mathbf{r}-\mathbf{r}'|^2\big]\!\int\!\mathrm{d}\mathbf{r}_i\, \exp\!\big[-\tfrac{1}{\varepsilon^2}|\mathbf{r}_i-(\mathbf{r}+\mathbf{r}')|^2\big] \\
&\simeq m_\mathrm{b}\, \delta_\mathrm{D}(\mathbf{r}{-}\mathbf{r}')\, \delta_\mathrm{D}(\mathbf{v}{-}\mathbf{v}')\, \overline{W}(\mathbf{v}),
\end{aligned} \tag{A.100}$$

where to get the last line, we assumed once again that $\varepsilon \gg_\sigma$, and used the asymptotic replacement from equation (A.95). The second term from equation (A.99) reads

$$\begin{aligned}
N^2\big\langle g_{ii}(\mathbf{r},\mathbf{v})\, g_{kk}(\mathbf{r}',\mathbf{v}')\big\rangle &= \bigg(\frac{m_\mathrm{b}}{\pi\hbar}\bigg)^3\!\int\!\mathrm{d}\mathbf{r}_i\mathrm{d}\mathbf{v}_i\, F_\mathrm{b}(\mathbf{v}_i)\, \exp\!\big[-\tfrac{2\varepsilon^2 m_\mathrm{b}^2}{\hbar^2}|\mathbf{v}_i-\mathbf{v}|^2\big]\, \exp\!\big[-\tfrac{1}{2\varepsilon^2}|\mathbf{r}_i-\mathbf{r}|^2\big] \\
&\quad \times \bigg(\frac{m_\mathrm{b}}{\pi\hbar}\bigg)^3\!\int\!\mathrm{d}\mathbf{r}_k\mathrm{d}\mathbf{v}_k\, F_\mathrm{b}(\mathbf{v}_k)\, \exp\!\big[-\tfrac{2\varepsilon^2 m_\mathrm{b}^2}{\hbar^2}|\mathbf{v}_k-\mathbf{v}'|^2\big]\, \exp\!\big[-\tfrac{1}{2\varepsilon^2}|\mathbf{r}_k-\mathbf{r}'|^2\big] \\
&= \overline{W}(\mathbf{r},\mathbf{v})\, \overline{W}(\mathbf{r}',\mathbf{v}'),
\end{aligned} \tag{A.101}$$

where we used the result from equation (A.94). The last term from equation (A.99) then reads

$$
\begin{aligned}
N^2\big\langle g_{ik}(\mathbf{r},\mathbf{v})\, g_{ki}(\mathbf{r}',\mathbf{v}')\big\rangle = & \left(\frac{m_{\mathrm{b}}}{\pi\hbar}\right)^{6}\!\int\! \mathrm{d}\mathbf{r}_i \mathrm{d}\mathbf{v}_i \mathrm{d}\mathbf{r}_k \mathrm{d}\mathbf{v}_k \, F_{\mathrm{b}}(\mathbf{v}_i)\, F_{\mathrm{b}}(\mathbf{v}_k) \\
& \times \exp\!\big[-\tfrac{2\varepsilon^2 m_{\mathrm{b}}^2}{\hbar^2}\big(|(\mathbf{v}_i+\mathbf{v}_k)-\mathbf{v}|^2 + |(\mathbf{v}_i+\mathbf{v}_k)-\mathbf{v}'|^2\big)\big] \\
& \times \exp\!\big[-\tfrac{1}{2\varepsilon^2}\big(|(\mathbf{r}_i+\mathbf{r}_k)-\mathbf{r}|^2 + |(\mathbf{r}_i+\mathbf{r}_k)-\mathbf{r}'|^2\big)\big] \\
& \times \exp\!\big\{-\mathrm{i}\tfrac{m_{\mathrm{b}}}{\hbar}\big[(\mathbf{r}_i-\mathbf{r}_k)\cdot(\mathbf{v}-\mathbf{v}')-(\mathbf{r}-\mathbf{r}')\cdot(\mathbf{v}_i-\mathbf{v}_k)\big]\big\} \\
= & \left(\frac{m_{\mathrm{b}}}{\pi\hbar}\right)^{6} \exp\!\big[-\tfrac{\varepsilon^2 m_{\mathrm{b}}^2}{\hbar^2}|\mathbf{v}-\mathbf{v}'|^2\big]\, \exp\!\big[-\tfrac{1}{4\varepsilon^2}|\mathbf{r}-\mathbf{r}'|^2\big] \\
& \times\!\int\! \mathrm{d}\mathbf{r}_i \mathrm{d}\mathbf{v}_i \mathrm{d}\mathbf{r}_k \mathrm{d}\mathbf{v}_k \, F_{\mathrm{b}}(\mathbf{v}_i)\, F_{\mathrm{b}}(\mathbf{v}_k)\, \exp\!\big[-\tfrac{4\varepsilon^2 m_{\mathrm{b}}^2}{\hbar^2}|(\mathbf{v}_i+\mathbf{v}_k)-(\mathbf{v}+\mathbf{v}')|^2\big] \\
& \times \exp\!\big[-\tfrac{1}{\varepsilon^2}|(\mathbf{r}_i+\mathbf{r}_k)-(\mathbf{r}+\mathbf{r}')|^2\big] \\
& \times \exp\!\big\{-\mathrm{i}\tfrac{m_{\mathrm{b}}}{\hbar}\big[(\mathbf{r}_i-\mathbf{r}_k)\cdot(\mathbf{v}-\mathbf{v}')-(\mathbf{r}-\mathbf{r}')\cdot(\mathbf{v}_i-\mathbf{v}_k)\big]\big\}.
\end{aligned}
\tag{A.102}
$$

At this stage, the asymptotic formula from equation (A.95) has to be used carefully, because the complex exponential from equation (A.102) is rapidly fluctuating. To clarify this calculation, let us perform the change of variables

$$
\begin{cases} \mathbf{r} = (\mathbf{r}_i+\mathbf{r}_k), \\ \mathbf{r} = \mathbf{r}_i - \mathbf{r}_k, \end{cases} \quad ; \quad \begin{cases} \mathbf{v} = (\mathbf{v}_i+\mathbf{v}_k), \\ \mathbf{v} = \mathbf{v}_i - \mathbf{v}_k. \end{cases}
\tag{A.103}
$$

Equation (A.102) becomes

$$
\begin{aligned}
N^2\big\langle g_{ik}(\mathbf{r},\mathbf{v})\, g_{ki}(\mathbf{r}',\mathbf{v}')\big\rangle = & \left(\frac{m_{\mathrm{b}}}{\pi\hbar}\right)^{6} \exp\!\big[-\tfrac{\varepsilon^2 m_{\mathrm{b}}^2}{\hbar}|\mathbf{v}-\mathbf{v}'|^2\big]\, \exp\!\big[-\tfrac{1}{4\varepsilon^2}|\mathbf{r}-\mathbf{r}'|^2\big] \\
& \times\!\int\! \mathrm{d}_{\mathbf{v}}\mathrm{d}_{\mathbf{v}}\, F_{\mathrm{b}}(\mathbf{v}{+}\mathbf{v})\, F_{\mathrm{b}}(\mathbf{v}{-}\mathbf{v})\, \exp\!\big[-\tfrac{4\varepsilon^2 m_{\mathrm{b}}^2}{\hbar^2}|\mathbf{v}-(\mathbf{v}+\mathbf{v}')|^2\big]\, \exp\!\big[-\mathrm{i}\tfrac{m_{\mathrm{b}}}{\hbar}(\mathbf{r}-\mathbf{r}')\cdot\mathbf{v}\big] \\
& \times\!\int\! \mathrm{d}_{\mathbf{r}}\mathrm{d}_{\mathbf{r}}\, \exp\!\big[-\tfrac{1}{\varepsilon^2}|\mathbf{r}-(\mathbf{r}+\mathbf{r}')|^2\big]\, \exp\!\big[-\mathrm{i}\tfrac{m_{\mathrm{b}}}{\hbar}\mathbf{r}\cdot(\mathbf{v}-\mathbf{v}')\big].
\end{aligned}
\tag{A.104}
$$

In this expression, we note that the exponential factor $\exp[-\frac{1}{4\varepsilon^2}|\mathbf{r}-\mathbf{r}'|^2]$ is nearly zero unless $|\mathbf{r}-\mathbf{r}'| \lesssim \varepsilon$. In that regime, the complex exponential $\exp[-\mathrm{i}\frac{m_{\mathrm{b}}}{\hbar}(\mathbf{r}-\mathbf{r}')\cdot\mathbf{v}]$ will average to nearly zero unless $|\mathbf{v}| \lesssim \hbar/(\varepsilon m_{\mathrm{b}}) = \sigma_\sigma/\epsilon$. Given our assumption that $\varepsilon \gg_\sigma$, we conclude that the dominant contribution to the integral comes from $|\mathbf{v}| \ll \sigma$. We recall that the typical variance of $F_{\mathrm{b}}(\mathbf{v})$ is σ, so in equation (A.104) we may perform the replacement $F_{\mathrm{b}}(\mathbf{v}{+}\mathbf{v})F_{\mathrm{b}}(\mathbf{v}{-}\mathbf{v}) \to F_{\mathrm{b}}^2(\mathbf{v})$. We get

$$
\begin{aligned}
N^2\big\langle g_{ik}(\mathbf{r},\mathbf{v})\, g_{ki}(\mathbf{r}',\mathbf{v}')\big\rangle & \simeq 2^6\, \delta_{\mathrm{D}}(\mathbf{r}-\mathbf{r}')\, \delta_{\mathrm{D}}(\mathbf{v}-\mathbf{v}')\!\int\! \mathrm{d}_{\mathbf{r}}\mathrm{d}_{\mathbf{v}}\, \exp\!\big[-\tfrac{1}{\varepsilon^2}|\mathbf{r}-\mathbf{r}|^2\big]\, F_{\mathrm{b}}^2(\mathbf{v})\, \exp\!\big[-\tfrac{4\varepsilon^2 m_{\mathrm{b}}^2}{\hbar^2}|\mathbf{v}-\mathbf{v}|^2\big] \\
& \simeq \frac{h^3}{m_{\mathrm{b}}^3}\, \delta_{\mathrm{D}}(\mathbf{r}-\mathbf{r}')\, \delta_{\mathrm{D}}(\mathbf{v}-\mathbf{v}')\, \overline{W}^2(\mathbf{v}),
\end{aligned}
\tag{A.105}
$$

Gathering together equation (A.100), A.101, and A.104, we can now rewrite the correlation from equation (A.96) to obtain

$$
\big\langle f_0(\mathbf{r},\mathbf{v})\, f_0(\mathbf{r}',\mathbf{v}')\big\rangle = \left[m_{\mathrm{b}} + \frac{h^3}{m_{\mathrm{b}}^3}\,\overline{W}(\mathbf{v})\right] \overline{W}(\mathbf{v})\, \delta_{\mathrm{D}}(\mathbf{r}-\mathbf{r}')\, \delta_{\mathrm{D}}(\mathbf{v}-\mathbf{v}').
\tag{A.106}
$$

Following equation (5.29) and 5.57, we finally obtain the needed correlation function as

$$\widehat{C}(\mathbf{k},\mathbf{v}) = \frac{1}{(2\pi)^3}\left[m_{\mathrm{b}} + \frac{h^3}{m_{\mathrm{b}}^3}\overline{W}(\mathbf{v})\right]\overline{W}(\mathbf{v}), \tag{A.107}$$

which reduces to the classical correlation function (A.84) as $h \to 0$.

A.8 Specific Energy Flow in the Orbit of a Massive Object

Flow of specific energy into the orbits of the massive objects in an FDM halo due to the combined effects of stochastic fluctuations in the gravitational potential and dynamical friction is

$$\begin{aligned}\langle \dot{E}\rangle &= \frac{1}{\rho_{\mathrm{t}}}\int \mathrm{d}\mathbf{v}_{\mathrm{t}} F_{\mathrm{t}}\left(\mathbf{v}_{\mathrm{t}}\right) D[\Delta E] \\ &= \frac{1}{\rho_t}\frac{\rho_t}{(2\pi\sigma_t^2)^{3/2}}\frac{8\sqrt{\pi}G^2\rho_b m_{\mathrm{eff}}\log\Lambda_{FDM}}{\sigma}\int d\mathbf{v}_t e^{-\frac{v_t^2}{2\sigma_t^2}} e^{-\frac{v_t^2}{\sigma^2}}\left[1-\mu_{\mathrm{eff}}K(v_t/\sigma)\right]\end{aligned} \tag{A.108}$$

The first term of the integral is

$$\int d\mathbf{v}_t e^{-a v_t^2} = \left(\frac{2\pi\sigma_t^2}{1+\frac{2\sigma_t^2}{\sigma^2}}\right)^{3/2}, \quad a = \frac{1}{2\sigma_t^2} + \frac{1}{\sigma^2} = \frac{1+\frac{2\sigma_t^2}{\sigma^2}}{2\sigma_t^2} \tag{A.109}$$

Using the definition of $K(x)$ the second term of the integral is

$$-\mu_{\mathrm{eff}}\int d\mathbf{v}_t e^{-\frac{v_t^2}{2\sigma_t^2}-\frac{v_t^2}{\sigma^2}}\left(\frac{\sqrt{\pi}}{v_t/\sigma}e^{\frac{v_t^2}{\sigma^2}}\,\mathrm{erf}\left(\frac{v_t}{\sqrt{2}\sigma}\right) - \sqrt{2}e^{\frac{v_t^2}{2\sigma^2}}\right) \tag{A.110}$$

We can rewrite the first term if the above relation in the form below

$$-\mu_{\mathrm{eff}}\,\sigma\sqrt{\pi}\int d\mathbf{v}_t \frac{e^{-\frac{v_t^2}{2\sigma_t^2}}\,\mathrm{erf}\left(\frac{v_t}{\sqrt{2}\sigma}\right)}{v_t} = 0 \tag{A.111}$$

Using the fact that the above function is odd, its integral over any symmetric interval will be zero. Therefore equation (A.110) becomes

$$\begin{aligned}&-\mu_{\mathrm{eff}}\int d\mathbf{v}_t e^{-\frac{v_t^2}{2\sigma_t^2}-\frac{v_t^2}{\sigma^2}}\left(-\sqrt{2}e^{\frac{v_t^2}{2\sigma^2}}\right) \\ &= \mu_{\mathrm{eff}}\sqrt{2}\int d\mathbf{v}_t e^{-b v_t^2}, \quad b = \frac{1}{2\sigma^2} + \frac{1}{2\sigma_t^2} = \frac{1+(\sigma_t^2/\sigma^2)}{2\sigma_t^2}\end{aligned} \tag{A.112}$$

which is another Gaussian integral and becomes

$$\mu_{\mathrm{eff}}\sqrt{2}\left(\frac{2\pi\sigma_t^2}{1+(\sigma_t^2/\sigma^2)}\right)^{3/2} \tag{A.113}$$

Putting together these results, we can write A.108 as the following

$$\langle \dot{E} \rangle = \frac{(2\pi\sigma_t^2)^{3/2}}{(2\pi\sigma_t^2)^{3/2}} \frac{8\sqrt{\pi}G^2\rho_b m_{\text{eff}} \log\Lambda_{FDM}}{\sigma} \left(\left(\frac{1}{1+\frac{2\sigma_t^2}{\sigma^2}} \right)^{3/2} - \mu_{\text{eff}}\sqrt{2} \left(\frac{1}{1+(\sigma_t^2/\sigma^2)} \right)^{3/2} \right)$$
$$= \frac{8\sqrt{\pi}G^2\rho_b m_{\text{eff}} \log\Lambda_{\text{FDM}}}{\sigma\,(1+2\sigma_t^2/\sigma^2)^{3/2}} \left(1 - \mu_{\text{eff}}\sqrt{2} \left(\frac{1+(2\sigma_t^2/\sigma^2)}{1+(\sigma_t^2/\sigma^2)} \right)^{3/2} \right) \tag{A.114}$$

A.9 Computing the Inverse Laplace Transforms

This section is adapted from Bar-Or et al. (2021): We compute explicitly the Laplace transforms from equation (5.58). The approach we follow is very similar to the one from Schekochihin (2017).

Let us first start with the inverse Laplace transforms appearing in the expression for $F_1(\mathbf{v})$ in equation (5.58). We want to evaluate

$$I(\mathbf{k},\mathbf{v}) = \int \frac{\mathrm{d}\omega}{2\pi}\frac{\mathrm{d}\omega'}{2\pi} \frac{1}{\epsilon(-\mathbf{k},\omega')} \frac{\mathrm{e}^{-\mathrm{i}(\omega+\omega')t}}{(\omega-\mathbf{k}\cdot\mathbf{v})(\omega'+\mathbf{k}\cdot\mathbf{v})}. \tag{A.115}$$

Recall that each integral is along a Bromwich contour $\mathcal{B}$, a horizontal contour that passes above all the poles of the integrands. We assume that the system is linearly stable, so the function $\omega \to 1/\epsilon(\mathbf{k},\omega)$ has no poles in the upper half of the complex plane. We carry out the integrals by lowering the integration contours to very negative imaginary values, so that $\mathrm{e}^{-\mathrm{i}(\omega+\omega')t}$ vanishes. Assuming that t is large enough for the transients associated with the system's damped modes (i.e., the contributions from the poles of the dielectric functions) to be negligible, only the contributions from the poles on the real axis $\omega = \mathbf{k}\cdot\mathbf{v}$ and $\omega' = -\mathbf{k}\cdot\mathbf{v}$ remain. Paying careful attention to the direction of integration, we note that these poles each contribute $-2\pi\mathrm{i}$ times the associated residue. Using these arguments, we obtain

$$I(\mathbf{k},\mathbf{v}) = -\frac{\epsilon(\mathbf{k},\mathbf{k}\cdot\mathbf{v})}{|\epsilon(\mathbf{k},\mathbf{k}\cdot\mathbf{v})|^2}. \tag{A.116}$$

Here we have used the symmetry relation

$$\epsilon(-\mathbf{k},-\omega_{\mathrm{R}}) = \epsilon^*(\mathbf{k},\omega_{\mathrm{R}}), \tag{A.117}$$

for $\omega_{\mathrm{R}} \in \mathbb{R}$, which directly follows from equation (5.49).

The second integral to compute appears in the expression for $F_2(\mathbf{v})$ in equation (5.58). We must evaluate

$$J(\mathbf{k},\mathbf{v},\mathbf{v}') = \int \frac{\mathrm{d}\omega}{2\pi}\frac{\mathrm{d}\omega'}{2\pi} \frac{1}{\epsilon(\mathbf{k},\omega)\,\epsilon(-\mathbf{k},\omega')} \frac{\mathrm{e}^{-\mathrm{i}(\omega+\omega')t}}{(\omega-\mathbf{k}\cdot\mathbf{v})(\omega-\mathbf{k}\cdot\mathbf{v}')(\omega'+\mathbf{k}\cdot\mathbf{v}')}. \tag{A.118}$$

Using the same approach as in equation (A.115), we first perform the integral over ω', noting that it involves a single pole along the real axis at $\omega' = -\mathbf{k}\cdot\mathbf{v}'$, the other poles being damped. equation (A.118) then becomes

$$J(\mathbf{k},\mathbf{v},\mathbf{v}') = -\mathrm{i}\frac{\mathrm{e}^{\mathrm{i}\mathbf{k}\cdot\mathbf{v}'t}}{\epsilon^*(\mathbf{k},\mathbf{k}\cdot\mathbf{v}')} \int \frac{\mathrm{d}\omega}{2\pi} \frac{1}{\epsilon(\mathbf{k},\omega)} \frac{\mathrm{e}^{-\mathrm{i}\omega t}}{(\omega-\mathbf{k}\cdot\mathbf{v})(\omega-\mathbf{k}\cdot\mathbf{v}')} \tag{A.119}$$

For the remaining integral there are two poles on the real axis, which each contribute $-2\pi\mathrm{i}$ times the associated residue. We obtain

$$\begin{aligned} J(\mathbf{k},\mathbf{v},\mathbf{v}') &= -\frac{\mathrm{e}^{\mathrm{i}\mathbf{k}\cdot\mathbf{v}'t}}{\epsilon^*(\mathbf{k},\mathbf{k}\cdot\mathbf{v}')}\left[\frac{1}{\epsilon(\mathbf{k},\mathbf{k}\cdot\mathbf{v})}\,\frac{\mathrm{e}^{-\mathrm{i}\mathbf{k}\cdot\mathbf{v}t}}{\mathbf{k}\cdot(\mathbf{v}-\mathbf{v}')}+\frac{1}{\epsilon(\mathbf{k},\mathbf{k}\cdot\mathbf{v}')}\,\frac{\mathrm{e}^{-\mathrm{i}\mathbf{k}\cdot\mathbf{v}'t}}{\mathbf{k}\cdot(\mathbf{v}'-\mathbf{v})}\right] \\ &= \frac{1}{|\epsilon(\mathbf{k},\mathbf{k}\cdot\mathbf{v}')|^2}\,\frac{1}{\mathbf{k}\cdot(\mathbf{v}-\mathbf{v}')}\left[1-\frac{\epsilon(\mathbf{k},\mathbf{k}\cdot\mathbf{v}')}{\epsilon(\mathbf{k},\mathbf{k}\cdot\mathbf{v})}\mathrm{e}^{-\mathrm{i}\mathbf{k}\cdot(\mathbf{v}-\mathbf{v}')t}\right]. \end{aligned} \tag{A.120}$$

Relying on our assumption of timescale separation, i.e., the assumption that the fluctuations evolve on timescales much faster than the mean system, we can take the limit $t\to\infty$ of equation (A.120). We then use the identity

$$\lim_{t\to\infty}\frac{\mathrm{e}^{-\mathrm{i}xt}}{x} = -\mathrm{i}\pi\delta_{\mathrm{D}}(x) \tag{A.121}$$

to simplify equation (A.120) to

$$J(\mathbf{k},\mathbf{v},\mathbf{v}') = \frac{1}{|\epsilon(\mathbf{k},\mathbf{k}\cdot\mathbf{v}')|^2}\left\{\mathcal{P}\left[\frac{1}{\mathbf{k}\cdot(\mathbf{v}-\mathbf{v}')}\right]+\mathrm{i}\pi\delta_{\mathrm{D}}[\mathbf{k}\cdot(\mathbf{v}-\mathbf{v}')]\right\}. \tag{A.122}$$

References

Abazajian, K., Fuller, G. M., and Patwardhan, A. (2001). Sterile neutrinos as dark matter. *Physical Review D*, 64(2):023504.

Aja, B., Arguedas Cuendis, S., Arregui, I., Artal, E., Barreiro, R. B., Casas, F. J., de Ory, M. C., Díaz-Morcillo, A., de la Fuente, L., Gallego, J. D., García-Barceló, J. M., Gimeno, B., Gomez, A., Granados, D., Kavanagh, B. J., Laso, M. A., Lopetegi, T., Lozano-Guerrero, A. J., Magaz, M. T., Martín-Pintado, J., Martínez-González, E., Miralda-Escudé, J., Monzó-Cabrera, J., Najarro de la Parra, F., Navarro-Madrid, J. R., Nuñez Chico, A. B., Pascual, J. P., Pelegrin, J., Peña Garay, C., Rodriguez, D., Socuéllamos, J. M., Teberio, F., Teniente, J., Vielva, P., Vila, I., Vilar, R., and Villa, E. (2022). The canfranc axion detection experiment (cadex): search for axions at 90 ghz with kinetic inductance detectors. *Journal of Cosmology and Astroparticle Physics*, 2022(11):044.

Alam, S. and others (eBOSS Collaboration) (2021). The completed sdss-iv extended baryon oscillation spectroscopic survey: Cosmological implications from two decades of spectroscopic surveys at the apache point observatory. *Physical Review D*, 103:083533.

Alcock, C., Allsman, R. A., Alves, D. R., et al. (2000). The macho project: Microlensing results from 5.7 years of lmc observations. *The Astrophysical Journal*, 542(1):281.

Alexander, T. (2017). Resonant relaxation and the onset of mass segregation around massive black holes. *Annual Review of Astronomy and Astrophysics*, 55:17–57.

Amin, M. A. and Mocz, P. (2019). Formation, gravitational clustering, and interactions of nonrelativistic solitons in an expanding universe. *Physical Review D*, 100:063507.

Armengaud, E., Palanque-Delabrouille, N., Yèche, C., Marsh, D. J. E., and Baur, J. (2017). Constraining the free-streaming of warm dark matter with the lyman-$\alpha forest. Monthly Notices of the Royal Astronomical Society, 471 : 4606 - -4617$.

Arvanitaki, A., Dimopoulos, S., Dubovsky, S., Kaloper, N., and March-Russell, J. (2010). Cosmological and astrophysical constraints on the axion and axion-like particles. *Phys. Rev. D*, 81:123530.

Bachlechner, T. C., Eckerle, K., Janssen, O., and Kleban, M. (2019). Axion-like particles and gravitational waves from cosmological sources. *JCAP*, 1909:062.

Ballesteros, G., Serpico, P. D., Taoso, M., and Urbano, A. (2020). Cosmological constraints on light primordial black holes. *Journal of Cosmology and Astroparticle Physics*, 2020(10):024.

Bar-Or, B., Fouvry, J.-B., and Tremaine, S. (2019). Relaxation in a fuzzy dark matter halo. *The Astrophysical Journal*, 871(1):28. Published January 18, 2019.

Bar-Or, B., Fouvry, J.-B., and Tremaine, S. (2021). Relaxation in a fuzzy dark matter halo. ii. self-consistent kinetic equations. *The Astrophysical Journal*, 915(1):27.

Baumgardt, H. and Makino, J. (2003). Dynamical evolution of star clusters in tidal fields. *Monthly Notices of the Royal Astronomical Society*, 340:227–246.

Begelman, M. C. and Rees, M. J. (1980). The formation of supermassive black holes. *Nature*, 287(5785):307–310.

Binney, J. and Tremaine, S. (1987). *Galactic Dynamics*. Princeton University Press, Princeton, NJ.

Binney, J. and Tremaine, S. (2008). *Galactic Dynamics*. Princeton University Press, Princeton, NJ, 2nd edition.

Bird, S., Cholis, I., Muñoz, J. B., Ali-Haïmoud, Y., Kamionkowski, M., et al. (2016). Did ligo detect dark matter? *Physical Review Letters*, 116:201301.

Bohm, D. (1952). A suggested interpretation of the quantum theory in terms of "hidden" variables. i. *Physical Review*, 85(2):166.

Bullock, J. S. and Boylan-Kolchin, M. (2017). Small-scale challenges to the Λcdm paradigm. *Annual Review of Astronomy and Astrophysics*, 55:343–387.

Cardoso, V., P., F., W., and Lemos, J. P. S. (2016). Black holes, bosonic stars, and the implications of the axion. *Phys. Rev. D*, 94.

Carr, B. and Hawking, S. W. (1974). Black holes in the early universe. *Monthly Notices of the Royal Astronomical Society*, 168:399–420.

Carr, B. J., Kohri, K., Sendouda, Y., and Yokoyama, J. (2010). New cosmological constraints on primordial black holes. *Physical Review D*, 81(10):104019.

Chandrasekhar, S. (1943). Stochastic problems in physics and astronomy. *Rev. Mod. Phys.*, 15:1–89.

Chavanis, P.-H. (2011). Mass-radius relation of newtonian self-gravitating bose-einstein condensates with short-range interactions. i. analytical results. *Physical Review D*, 84(4).

Chavanis, P.-H. (2013). Title of the 2013 paper. *European Physical Journal Plus*, 128:126.

Clowe, D., Gonzalez, A., and Markevitch, M. (2004). Weak-lensing mass reconstruction of the interacting cluster 1e 0657–558: Direct evidence for the existence of dark matter. *The Astrophysical Journal*, 604:596.

Cohen, L. (1975). Dynamics of stellar systems. In *IAU Symposium 69, ed. A. Hayli*, page 33. Reidel, Dordrecht.

Coles, P. and Spencer, K. (2002). Mnras. *MNRAS*, 342:176.

Eisenstein, D. J. et al. (2005). Detection of the baryon acoustic peak in the large-scale correlation function of sdss luminous red galaxies. *Astrophysical Journal*, 633:560–574.

Erdős, L., Salmhofer, M., and Yau, H.-T. (2004). J. stat. phys. *J. Stat. Phys.*, 116:367.

Ershkovich, A. I. (2011). Arxiv e-prints. *arXiv:astro-ph/1108.5519*. arXiv:astro-ph/1108.5519.

Escrivà, A., Kühnel, F., and Tada, Y. (2024). *Primordial black holes*, page 261–377. Elsevier.

Falco, M., Hansen, S. H., Wojtak, R., and Mamon, G. A. (2013). Why does the jeans swindle work? *Monthly Notices of the Royal Astronomical Society: Letters*, 431(1):L6–L9.

Famaey, B. and McGaugh, S. S. (2012). The core-cusp problem: A review of the evidence for core profiles in dark matter haloes. *Living Reviews in Relativity*, 15:10.

Fregeau, J. M., C. P. P. Z. S. F. R. F. A. (2004). Stellar collisions and binary formation in dense star clusters. *Monthly Notices of the Royal Astronomical Society*, 352:1–19.

Fried, B. D. and Conte, S. D. (1961). *The Plasma Dispersion Function.* Academic Press.

G. Bertone, D. H. and Silk, J. (2005). Particle dark matter: Evidence, candidates and constraints. *Physics Reports*, 405:279–390.

G. Jungman, M. K. and Griest, K. (1996). Supersymmetric dark matter. *Physics Reports*, 267:195–373.

Garcia-Bellido, J. and Morales, E. R. (2017). Primordial black holes from single field models of inflation. *Physics of the Dark Universe*, 18:47–54.

Giersz, M., H. D. C. H. J. R. (2008). Monte carlo simulations of star clusters - iv. the globular cluster ngc 6397. *Monthly Notices of the Royal Astronomical Society*, 388:429–438.

Gnedin, O. Y., L. H. M. O. J. P. (1999). Effects of tidal shocks on the evolution of globular clusters. *Astrophysical Journal*, 522:935–949.

Goodman, J. (1983). Apj. *ApJ*, 270:700.

Graham, P. W., Irastorza, I. G., Lamoreaux, S. K., Lindner, A., and van Bibber, K. A. (2015). Axion searches with cold matter. *Ann. Rev. Nucl. Part. Sci.*, 65:485–514.

Griest, K., Cieplak, A. M., and Lehner, M. J. (2014). New limits on primordial black hole dark matter from an analysis of kepler source microlensing data. *The Astrophysical Journal*, 786(2):158.

Halverson, J., Long, C., and Nath, P. (2017). Axion dark matter and the hubble tension. *Phys. Rev. D*, 96:056025.

Hamilton, C. and Fouvry, J.-B. (2024). Kinetic theory of stellar systems: A tutorial.

Heggie, D. C. (1975). Binary evolution in stellar dynamics. *Monthly Notices of the Royal Astronomical Society*, 173:729–787.

Hlozek, R., Grin, D., Marsh, D. J. E., and Ferreira, P. G. (2015). The effect of warm dark matter on the matter power spectrum: A study of sterile neutrinos and the lyman-$\alpha forest. Physical Review D, 91(10) : 103512$.

HongSheng Zhao, S. M. M. (2000). Dynamical friction in dark matter halos and its effect on galactic evolution. *Monthly Notices of the Royal Astronomical Society*, 319:300–316.

Hu, W., Barkana, R., and Gruzinov, A. (2000). Fuzzy cold dark matter: The wave equation. *Physical Review Letters*, 85(22):1158–1161.

Hui, L. (2021). Wave dark matter. *Annual Review of Astronomy and Astrophysics*, 59(1):247–289.

Hui, L., Ostriker, J. P., Tremaine, S., and Witten, E. (2017). Ultralight scalars as cosmological dark matter. *Phys. Rev. D*, 95(4):043541.

Hénon, M. (1961). The monte carlo method. ii. application to the study of stellar dynamics. *Annales d'Astrophysique*, 24:369.

Irsìc, V., Viel, M., Haehnelt, M. G., Bolton, J. S., and Becker, G. D. (2017). First constraints on the free-streaming of sterile neutrinos from lyman-$\alpha forestdata. PhysicalReviewLetters, 119(3) : 031302$.

Jeans, J. H. (1929). *The Universe Around Us*. Cambridge University Press, Cambridge, UK.

Jedamzik, K. (2020). Primordial black hole dark matter and the ligo/virgo observations. *Journal of Cosmology and Astroparticle Physics*, 2020(09):022.

Katz, A., Kopp, J., Sibiryakov, S., and Xue, W. (2018). Femtolensing by dark matter revisited. *Journal of Cosmology and Astroparticle Physics*, 2018(12):005.

Kawai, H. and Meneghetti, M. (2024). Galaxy-galaxy strong lensing cross-section with fuzzy dark matter model.

Klypin, A., Kravtsov, A. V., Valenzuela, O., and Prada, F. (1999). Where are the missing galactic satellites? *The Astrophysical Journal*, 522:82–92.

Klypin, A. A., Trujillo-Gomez, S., and Primack, J. (2011). Dark matter halos in the standard cosmological model: Results from the bolshoi simulation. *The Astrophysical Journal*, 740:102.

Kobayashi, T., Murgia, R., Simone, A. D., Irsìc, V., and Viel, M. (2017). Constraining the warm dark matter particle mass from the lyman-$\alpha forest. PhysicalReviewD, 96(12) :$ 123514.

Kolb, E. W. and Turner, M. S. (1990). *The Early Universe*. Addison-Wesley.

Kormendy, J. and Bender, R. (2013). The scaling relations of dark matter halos with galaxy luminosity and mass. *Annual Review of Astronomy and Astrophysics*, 51:511–653.

Lancaster, L. and Challinor, A. (2020). Dynamical friction in fuzzy dark matter. *Journal of Cosmology and Astroparticle Physics*, 01:001.

Landau, L. (1936). The transport equation in the case of coulomb interactions. *Phys. Z. Sowjetunion*, 10:154.

Landau, L. D. and Lifshitz, E. M. (1980). *Statistical Physics (Volume 5 of Course of Theoretical Physics)*. Pergamon Press, Oxford.

Leong, K.-H., Schive, H.-Y., Zhang, U.-H., and Chiueh, T. (2018). Non-linear evolution of fuzzy dark matter halos from 3d simulations.

Levkov, D. G., Panin, A. G., and Tkachev, I. I. (2018). Gravitational bose-einstein condensation in the kinetic regime. *Physical Review Letters*, 121:151301.

Lynden-Bell, D. (1967). Statistical mechanics of violent relaxation in stellar systems. *Monthly Notices of the Royal Astronomical Society*, 136:101.

Madelung, E. (1926). Z. phys. *Z. Phys.*, 40:322.

Marsh, D. J. E. (2016). Axion cosmology. *Phys. Rept.*, 643:1–79.

Merritt, D. (2013). *Dynamics and Evolution of Galactic Nuclei*. Princeton University Press.

Mo, H. J., van den Bosch, F. C., and White, S. D. M. (2010). *Galaxy Formation and Evolution*. Cambridge University Press.

Mocz, P., Lancaster, L., Fialkov, A., Becerra, F., and Chavanis, P.-H. (2018). Gravitational cooling and bose-einstein condensation in binary wave dark matter halos. *Physical Review D*, 97:083519.

Moore, B., Ghigna, S., Governato, F., Lake, G., Quinn, T., and Stadel, J. (1999). Dark matter density profiles and the core-cusp problem. *Astrophysical Journal*, 524(1):L19–L22.

Navarro, J. F., Frenk, C. S., and White, S. D. M. (1997a). The structure of cdm halos. *Astrophysical Journal*, 490(2):493–508.

Navarro, J. F., Frenk, C. S., and White, S. D. M. (1997b). A universal density profile from hierarchical clustering. *The Astrophysical Journal*, 490:493–508.

Niikura, H., Takada, M., Yokoyama, S., et al. (2019). Microlensing constraints on primordial black holes with subaru/hsc. *Nature Astronomy*, 3(6):524–534.

Nordheim, L. W. (1928). Proc. r. soc. lond. a. *Proc. R. Soc. Lond. A*, 119:689.

Nori, M., Baldi, M., Viel, M., Menci, N., and Schneider, A. (2021). Lyman-α forest and cosmic microwave background constraints on ultralight scalar dark matter. *Monthly Notices of the Royal Astronomical Society*, 505:6138–6154.

Nori, M., Murgia, R., Irsìc, V., Baldi, M., and Viel, M. (2019). Reconstructing the warm dark matter particle mass with the lyman-$\alpha forest : acombinedanalysisofthe3dfluxpowerspectrumandfluxskewness.MonthlyNoticesoftheRoyalAstrono$ $3227 - -3240$.

Pandey, S., Hall, E. D., and Evans, M. (2024). First results from the axion dark-matter birefringent cavity (adbc) experiment.

Peccei, R. D. and Quinn, H. R. (1977). Cp conservation in the presence of pseudoparticles. *Physical Review Letters*, 38:1440.

Peebles, P. J. E. (1980). *The Large-Scale Structure of the Universe*. Princeton University Press.

Peebles, P. J. E. (1982). Large-scale structure of the universe. *Princeton University Press*.

Planck Collaboration, Aghanim, N., et al. (2020). Planck 2018 results. vi. cosmological parameters. *Astronomy & Astrophysics*, 641:A6.

Raffelt, G. (1996). Astrophysical axion bounds. *Physics Reports*, 333:575–603.

Rauch, K. P. and Tremaine, S. (1996). Resonant relaxation in stellar systems. *New Astronomy*, 1:149–170.

Risken, H. (1996). *The Fokker-Planck Equation*. Springer Series in Synergetics. Springer Berlin, Heidelberg, 2 edition. Springer Book Archive, Published: 17 September 1996 (Softcover), 06 December 2012 (eBook).

Rosenbluth, M. N., MacDonald, W. M., and Judd, D. L. (1957). Fokker-planck equation for an inverse-square force. *Physical Review*, 107:1.

Rubin, V. C. and Ford, W. K. (1970). Rotation of the andromeda nebula from a spectroscopic survey of emission regions. *The Astrophysical Journal*, 159:379–403.

Rubin, V. C., Thonnard, N., and Ford, W. K. J. (1980). Rotational properties of 21 sc galaxies with a large range of luminosities and radii, from ngc 4605 (r = 4 kpc) to ugc 2885 (r = 122 kpc). *The Astrophysical Journal*, 238:471.

Ruffini, R. and Bonazzola, S. (1969). Systems of self-gravitating particles in general relativity and the concept of an equation of state. *Physical Review*, 187:1767–1783.

Sasaki, M., Suyama, T., Tanaka, T., and Yokoyama, S. (2018). Primordial black hole scenario for the gravitational-wave event gw170817. *Classical and Quantum Gravity*, 35:063001.

Schekochihin, A. A. (2017). *Lecture Notes on Kinetic Theory and Magnetohydrodynamics of Plasmas*. Available at http://www-thphys.physics.ox.ac.uk/people/AlexanderSchekochihin/lectures.html.

Schive, H., Tsai, Y., Chiueh, T., and Broadhurst, T. (2014a). The core-cusp problem in fuzzy dark matter: A resolution with fuzzy dark matter halo simulations. *Nature Physics*, 10:283–286.

Schive, H.-Y., Chiueh, T., and Broadhurst, T. (2014b). Cosmic structure as the quantum interference of a coherent dark wave. *Nature Physics*, 10:496.

Schneider, A., Niemeyer, J. C., and Mota, D. F. (2020). Effects of quantum pressure on galaxy formation. *Monthly Notices of the Royal Astronomical Society*, 495(1):1–10.

Seife, C., Murgia, R., and Chavanis, P. H. (2020). Stability of fuzzy dark matter halos in simulations: The role of quantum pressure. *Physics of the Dark Universe*, 29:100616.

Sikivie, P. (2009). The interaction of axion quasiparticles with electromagnetic fields. *Physics Reports*, 323:121–137.

Sikivie, P. (2020). The axion as a dark matter candidate. *arXiv:2003.02206*.

Spergel, D. N. and Steinhardt, P. J. (2000). Observational evidence for self-interacting dark matter. *Phys. Rev. Lett.*, 84:3760–3763.

Spergel, D. N., Verde, L., Peiris, H. V., et al. (2003). First-year wilkinson microwave anisotropy probe (wmap) observations: Determination of cosmological parameters. *The Astrophysical Journal Supplement Series*, 148:175.

Spitzer, L. (1969). Equipartition and the formation of compact nuclei in spherical stellar systems. *Astrophysical Journal*, 158:L139.

Springel, V., White, S. D. M., Tormen, G., and Kauffmann, G. (2001). The history of galaxy formation: A simulation perspective. *Monthly Notices of the Royal Astronomical Society*, 328:726–736.

Stefano Ruffo, Luigi Frachebourg, e. a. (2017). *Dynamics of Star Clusters and Stellar Systems*. Cambridge University Press.

Svrcek, P. and Witten, E. (2006). Axions and quantum gravity. *JHEP*, 06:051.

Tavio, H., Cuesta, A. J., Prada, F., Klypin, A. A., and Sanchez-Conde, M. A. (2008). Arxiv e-prints. *arXiv:astro-ph/0807.3027*. arXiv:astro-ph/0807.3027.

Tegmark, M. and others (SDSS Collaboration), . (2004). Cosmological parameters from sdss and wmap. *Physical Review D*, 69:103501.

Tisserand, P., Le Guillou, L., Afonso, C., Albert, J. N., Andersen, J., Ansari, R., et al. (2007). Limits on the macho content of the galactic halo from the eros-2 survey. *Astronomy Astrophysics*, 469:387–404.

Tremaine, S. and Gunn, J. E. (1979). Dynamical evolution of dense stellar systems. *Phys. Rev. Lett.*, 42(6):407–410.

Tremaine, S. and Weinberg, M. D. (1975). Dynamical friction in a system of stars. *Astrophysical Journal*, 200:1–12.

Trenti, M. and van der Marel, R. P. (2013). No evidence for equipartition in two- and three-component star clusters. *Monthly Notices of the Royal Astronomical Society*, 435:3272–3282.

Uehling, E. A. and Uhlenbeck, G. E. (1933). Phys. rev. *Phys. Rev.*, 43:552.

Viel, M., Becker, G. D., Bolton, J. S., and Haehnelt, M. G. (2013). The effect of uv background fluctuations on the lyman-$\alpha forest. Physical Review D, 88(4):043502$.

Vogelsberger, M., Genel, S., Springel, V., and et al. (2014). Introducing the illustris project: Simulating the universe in a box. *Monthly Notices of the Royal Astronomical Society*, 444(2):1518–1545.

Weinberg, D. H., Bullock, J. S., Governato, F., Kuzio de Naray, R., and Peter, A. H. G. (2015). Cold dark matter: controversies on small scales. *Proceedings of the National Academy of Sciences*, 112(40):12249–12255.

Weinberg, S. (1978). New light bosons as a possible source of cosmic dark matter. *Physical Review Letters*, 40:223–226.

Widrow, L. M. and Kaiser, N. (1993). Apj. *ApJ*, 416:L71.

Wigner, E. (1932). On the quantum correction for thermodynamic equilibrium. *Phys. Rev.*, 40:749–759.

Y. Farhi, H. Schive, e. a. (2020). Heating of stellar systems by fuzzy dark matter quasiparticles. *The Astrophysical Journal*, 892:26.

Yavetz, T. D., Li, X., and Hui, L. (2022). Construction of wave dark matter halos: Numerical algorithm and analytical constraints. *Physical Review D*, 105(2).

Yifan Liu, Weiguang Li, e. a. (2020). Numerical simulation of fuzzy dark matter halo dynamics. *Astrophysical Journal*, 894:54.

Zeldovich, Y. B. and Novikov, I. D. (1971). *Relativistic Astrophysics. Vol. 1: Stars and Relativity*. University of Chicago Press, Chicago, IL.

Zwicky, F. (1937). On the masses of nebulae and of clusters of nebulae. *The Astrophysical Journal*, 86:217.